ASPECTS OF ORGANIC PETROGRAPHY AND GEOCHEMISTRY OF MAASTRICHTIAN COALS AND SHALES AT GOMBE, GONGOLA BASIN, NIGERIA

BY

JIMOH, YUSUF AYOOLA
B.Sc. (ILORIN), M.Sc. (IBADAN)
MATRIC NO: 03/55EA055

A PH.D THESIS SUBMITTED IN PARTIAL FULFILLMENT OF THE REQUIREMENTS FOR THE AWARD OF DOCTOR OF PHILOSOPHY DEGREE IN THE DEPARTMENT OF GEOLOGY AND MINERAL SCIENCES, FACULTY OF PHYSICAL SCIENCES, UNIVERSITY OF ILORIN, ILORIN NIGERIA.

October, 2019

DEDICATION

This research work is dedicated to Almighty Allah, for his love, protection, grace and mercies to complete this program, and to my late father, Mr. JIMOH NURUDEEN. I also dedicate this work to my entire family. May God bless you all (Amin).

CERTIFICATION

This is to certify that JIMOH, Yusuf Ayoola (03/55EA055) carried out this research under my supervision and has been read and approved as meeting the requirements for the award of PhD degree in Geology.

Name	Signature	Date
……..	……	……
External Examiner		
Dr. O. A. Omotoso		
……..	……	……
Head of Department and Chief Examiner		
Dr. O. S. Oguntoye		
……..	……	……
Internal Examiner from a Related Department in the University (Name of Dept: Department of Chemistry)		
Prof. S. O. Akande		
……..	……	……
Supervisor and Internal Examiner		
Dr. O. A. Adekeye		
……..	……	……
Departmental Postgraduate Programme Coordinator and Internal Examiner		

ACKNOWLEDGEMENTS

Firstly, I am deeply and sincerely grateful to Almighty Allah, The Lord of incomparable majesty, The Merciful, The Provider and The Master of the day of Judgement who lavishly gave me the endurance, resilience, foresight and thoughtfulness to undertake this project.

I wish to specially thank my supervisor, Prof. Olusola Johnson Ojo for his motivations, supports, contributions and inputs to make this work a reality. I acknowledge your efforts and sincerely you inspired me tremendously to pursue this research with my utmost zeal and I say thank you sir. I equally appreciate and thank our father of Geology, the erudite professor, Prof. S.O Akande for your contributions. I thank all my lecturers' right from my undergraduate days till present for imparting knowledge required to succeed in all ramification. Appreciation goes to KWASU managements, academic and non academic staff of Geology department for their support and contributions. I thank all members of the academic and non-academic staff of the Department of Geology, University of Ilorin, starting from the Head of Department, Dr.O.O. Ige, Prof. Ogunsanwo, Prof. J.I.D Adekeye, Prof. R.B. Bale. It is a great pleasure and honour to be trained under your tutelage, academic impartation and influence.

Let me also use this opportunity to thank Dr. Bisi Adekeye, Dr. Adedoyin and Dr. Omotosho and other academic staffs for their positive influence and academic supports.

Most importantly, let me deeply and sincerely appreciate my family. To my late father, Mr. JIMOH NURUDEEN for his sacrifice he made and discipline he imparted in me, your memory still lingers on. I am very grateful to my Mother, Mrs Zainab Iyabo JIMOH for all the love, care and supports in prayer, cash, concern and most importantly encouragement that you have showed me during my studies. Your parental presence has been so overwhelming. Your deep concern is unequalled and I really thank God for giving me such a wonderful mother like you. May God in his infinite mercies bless and reward you abundantly; you will

reap the fruits of your labour (Amin). Special appreciation to my darling wife Tijjani Oluwakemi Aminah for her perseverance and love and to my lovely boy Jimoh Abdulhaleem. My brother Jimoh Abdulgafar, wonderful siblings, Hauwa, Idris, Tomiwa, Wale, Bilikis and Shukrat, you are all wonderful. Thank you for your concern and care that kept me going. I love you and may God bless you all.

Acknowledgements to my colleagues and friends in the person of Engr. Akinpelu Mutiu, Adepoju Suraju, Sa'ad Abdullahi, Onimago Yakub, Officer Bolaji, Dr. Ibrahim Omore, Dr. Aras and a host of others for the significant role they played in one way or the other in ensuring the success of my program, I am indeed very grateful.

Once again, to God Almighty, who is the beginning and the end, the present, the past, and the future. I say (Alhamdullilah).

TABLE OF CONTENTS

TITLE PAGE i

DEDICATION ii

CERTIFICATION iii

ACKNOWLEDGEMENTS iii

TABLE OF CONTENTS vi

LIST OF FIGURES xi

LIST OF TABLES xvi

ABSTRACT xviii

CHAPTER ONE 1

INTRODUCTION 1

1.1 General Statement 1

1.2 Scientific Background 2

1.2.1 Source Rocks 2

1.2.1.1 Coal 4

1.2.1.2 Shale 5

1.2.2 Petroleum Generation from Shale and Coaly Source Rocks 6

1.3 Location and Accessibility of the Study Area 10

1.3.1 Relief and Drainage 10

1.3.2 Climate and Vegetation 13

1.4 Previous Work 13

1.5 Definition of Research Problem 20

1.6 Aim and Objectives 21

1.7 Research Significance 21

CHAPTER TWO 23

GEOLOGIC SETTING AND STRATIGRAPHY OF NORTHERN BENUE TROUGH 23

2.1 Geologic Settings of Northern Benue Trough 23

2.1.1 Origin and Structural Setting 23

2.2 Regional Stratigraphy of Northern Benue Trough 24

2.2.1 Bima Formation 27

2.2.2 Yolde Formation 27

2.2.3 Pindiga Formation 27

2.2.4 Gombe Formation 28

2.2.5 Kerri Kerri Formation 28

CHAPTER THREE 30

METHODOLOGY 30

3.1 General Statement 30

3.2 Field Study 30

3.3 Laboratory Studies 43

3.3.1 Soxhlet Extraction 43

3.3.2 Total Organic Carbon (TOC) 43

3.3.3 Rock Eval Pyrolysis 46

3.3.4 Source Rock Kinetics 48

3.3.5 Medium Performance Liquid Chromatography 48

3.3.6 Gas Chromatography (GC) 49

3.3.7 Gas Chromatography – Mass Spectroscopy (GC-MS) 50

3.3.8 Gas Chromatography – Isotope Ratio-Mass Spectroscopy (GC-IRMS) 53

3.3.9 Organic Petrology (Maceral Analysis) 53

3.4 Organic Petrology (Vitrinite Reflectance, Visual kerogen and Palynology) 54

3.4.1 Proximate Analysis 55

3.4.2 Elemental Analysis 56

CHAPTER FOUR 58

RESULTS AND DISCUSSION 58

4.1. Lithostratigraphy and Sedimentology of the Gombe Formation 58

4.1.1 Lithologic Description at Maiganga 58

4.1.1.1 Sandstone 58

4.1.1.2 Clayey Siltstone 58

4.1.1.3 Coaly Shale- Shale 64

4.1.1.4 Coal 64

4.1.2 Lithologic Description at Zange 64

4.1.3 Lithologic Description at Liji 65

4.1.4 Lithologic Description at Mallam Inna 65

4.1.5 Lithologic Description at Riman 65

4.1.6 Lithologic Description at Maiduku 65

4.1.7 Lithologic Description at Bobona 65

4.1.8 Lithologic Description at Garin Magaji 66

4.2 Lithofacies Description and Depositional Environments 80

4.2.1 Fluvial Channel Facies 81

4.2.2 Nonmarine Swamp/Overbank Facies 81

4.3 Organic Geochemical Evaluation 82

4.3.1 Organic Matter Richness 82

4.3.2 Organic Matter Type / Kerogen Quality 82

4.3.3 Hydrocarbon Potential 83

4.3.4 Thermal Maturity 90

4.4 Source Rock Kinetics 91

4.4.1 Activation Energy Distribution 94

4.4.2 Hydrocarbon Potential 94
4.5 Biomarker Geochemistry (Saturate and Aromatic) 106
4.5.1 Source and Depositional Environments 109
4.5.2 Thermal Maturity and Rank 112
4.5.3 Age 113
4.6 Compound Specific Isotope Analysis (CSIA) 133
4.7 Organic Petrography 136
4.7.1 Maceral Composition and Hydrocarbon Potential 136
4.7.2 Thermal Maturity 137
4.7.3 Depositional Environments 140
4.8 Palynology 149
4.8.1 Palynostratigraphic Zonation and Age 156
4.8.2 Palynofacies, Paleoecology and Paleoclimate 164
4.9 Coal Quality and Rank 170
4.9.1 Major Element Geochemistry 175
4.9.2 Trace Element Geochemistry 177
4.9.3 Rare Earth Element Geochemistry 183
CHAPTER FIVE 188
CONCLUSIONS AND RECOMMENDATION 188
5.1 Conclusions 188
5.2 Recommendations 193
REFERENCES 194
APPENDIX I 212
APPENDIX II 219
APPENDIX III 226

APPENDIX IV 240

LIST OF FIGURES

Figure 1.1: Geological map of Nigeria showing the basement rocks and sedimentary basins with coal occurrences
Error! Bookmark not defined.

Figure 1.2: Map of Nigeria showing coal occurrences in Nigeria
Error! Bookmark not defined.

Figure 1.3: Location map of the study areas.
Error! Bookmark not defined.

Figure 2.1: Schematic Break-up of Africa and South-America during Late Mesozoic
Error! Bookmark not defined.

Figure 2.2: Geological map of the Benue Trough. The traces of the Equatorial Fracture Zones are indicated
Error! Bookmark not defined.

Figure 2.3: Stratigraphy of Northern Benue Trough
Error! Bookmark not defined.

Figure 3.1: Methodology Flow chart.
Error! Bookmark not defined.

Figure 3.2: a and b, distance view of coal seams with shale interbed at Phase I
Error! Bookmark not defined.

Figure 3.3: Distance view of coal seams with shale interbed at Phase II
Error! Bookmark not defined.

Figure 3.4: Illustrative picture showing preparation steps in TOC Analysis.
Error! Bookmark not defined.

Figure 3.5: LECO C230 Machine
Error! Bookmark not defined.

Figure 3.6: Cycle of analysis and example of record obtained by the pyrolysis method.
Error! Bookmark not defined.

Figure 3.7: Illustrative picture of RE-6.
Error! Bookmark not defined.

Figure 3.8: Illustrative picture of Medium Pressure Liquid Chromatography (MPLC)
Error! Bookmark not defined.

Figure 3.9: a) Illustrative picture of Agilent 6890N GC system/Agilent 7683B series Injector and b) Hewlett Packard (HP) 6890 Series GC

System/ (HP) 6890 series injector.
Error! Bookmark not defined.

Figure 3.10: Saturate GC-MS.
Error! Bookmark not defined.

Figure 3.11: Aromatic GC-MS.
Error! Bookmark not defined.

Figure 4.1: Lithologic succession of Gombe Formation exposed at the Maiganga mine.
Error! Bookmark not defined.

Figure 4.2: Lithologic succession of Gombe Formation at the Maiganga mine.
Error! Bookmark not defined.

Figure 4.3: Litholog of Borehole 15 at Maiganga.
Error! Bookmark not defined.

Figure 4.4: Coarse-grained and weakly laminated Ferruginised sandstone at Maiganga.
Error! Bookmark not defined.

Figure 4.5: Friable, whitish to brownish colour weakly laminated (localized) clayey siltstone at Maiganga
Error! Bookmark not defined.

Figure 4.6: The clayey siltstone interbedded with the shale at Maiganga.
Error! Bookmark not defined.

Figure 4.7: Grayish well compacted carbonaceous shale at Maiganga
Error! Bookmark not defined.

Figure 4.8: Shale interbedded with coal at Maiganga
Error! Bookmark not defined.

Figure 4.9: Panoramic view of Maiganga mine.
Error! Bookmark not defined.

Figure 4.10: Seam B coal, dull in luster having cleat (fracture)
Error! Bookmark not defined.

Figure 4.11: Lithologic section of the Gombe Formation exposed at Zange village
Error! Bookmark not defined.

Figure 4.12: Field photograph of thinly laminated brownish clayey siltstone at Zange village
Error! Bookmark not defined.

Figure 4.13: Field Photograph of grayish mudstone at Zange village
Error! Bookmark not defined.

Figure 4.14: Lithologic section of Gombe Formation exposed at Liji village.
Error! Bookmark not defined.

Figure 4.15: Lithologic section of Gombe Formation exposed at Mallam Inna.
Error! Bookmark not defined.

Figure 4.16: Lithologic section of Gombe Formation exposed at Riman village.
Error! Bookmark not defined.

Figure 4.17: Lithogic section of Gombe Formation exposed at Maiduku village.
Error! Bookmark not defined.

Figure 4.18: Field photograph showing thinly laminated clayey siltstone unit, grayey shale and the fine grained sandstone unit at Maiduku village
Error! Bookmark not defined.

Figure 4.19: Lithologic section of Gombe Formation exposed at Bobona village.
Error! Bookmark not defined.

Figure 4.20: Field photograph of thinly laminated clayey siltstone exposed at Bobona
Error! Bookmark not defined.

Figure 4.21: Field photograph of shale exposed at Bobona
Error! Bookmark not defined.

Figure 4.22: Lithologic section of Gombe Formation exposed at Garin Magaji.
Error! Bookmark not defined.

Figure 4.23: Field photograph showing parallel stratified clayey siltstone/shale at Garin Magaji village.
Error! Bookmark not defined.

Figure 4.24: Plot of S2 versus TOC for coal and shale samples of Maiganga, Gongola Basin.
Error! Bookmark not defined.

Figure 4.25: Plot of HI versus OI for the typing of kerogen (1- 1V).
Error! Bookmark not defined.

Figure 4.26: Plot of Hydrogen index (HI) against Tmax of coal, coaly shale and shale samples from Maiganga, Gongola Basin.
Error! Bookmark not defined.

Figure 4.27: Plot of hydrogen index (HI) against vitrinite reflectance of coal and shale samples from Maiganga, Gongola Basin.
Error! Bookmark not defined.

Figure 4.28: Plot of production index (PI) against Tmax of coal, coaly shale and shale samples from Maiganga, Gongola Basin.
Error! Bookmark not defined.

Figure 4.29: Plot of production index (PI) against vitrinite reflectance of coal and shale samples from Maiganga, Gongola Basin.
Error! Bookmark not defined.

Figure 4.30: (a-h): Pyrogram (reaction rate vs temperature)
Error! Bookmark not defined.

Figure 4.31: (a-h): Bulk kinetics showing the activation energies of coal and shale samples of Gombe Formation.
Error! Bookmark not defined.

Figure 4.32: (a-h) and 4.32 (a'-h'): Bar charts indicates the percentage reaction vs activation energy for coal and shale samples of Gombe Formation.
Error! Bookmark not defined.

Figure 4.33: Bar chart showing the proportion of the extracted sample into saturate, aromatic, resins and asphaltenes.
Error! Bookmark not defined.

Figure 4.34: Ternary diagram showing the proportion of saturated hydrocarbons, aromatic hydrocarbons and polar (NSO+Asphaltenes) in extracts of coal, shale and coaly shale source rocks of maiganga, Gombe Formation.
Error! Bookmark not defined.

Figure 4.35: Plot of Pr/n-C_{17} vs Ph/n-C_{18} of coal and shale samples of Maiganga, Gombe Formation.
Error! Bookmark not defined.

Figure 4.36: Plot of dibenzothiophene/phenanthrene (DBT/PH) vs. pristane/phytane (Pr/Ph) of coaly and shaly source rocks of Maiganga, Gombe Formation
Error! Bookmark not defined.

Figure 4.37: Ternary diagram of the distribution of C_{27}, C_{28}, C_{29} steranes in Maiganga coal and shale, Gombe Formation.
Error! Bookmark not defined.

Figure 4.38: Ternary diagram of the distribution of C_{27}, C_{28}, C_{29} monoaromatic steroid in Maiganga coal, shale and coaly shale, Gombe Formation.
Error! Bookmark not defined.

Figure 4.39: Organic matter source discrimination of Maiganga samples
Error! Bookmark not defined.

Figure 4.40: Plot of total Sulphur vs. dibenzothiophene/phenanthrene (DBT/PHEN) for Maiganga coal
Error! Bookmark not defined.

Figure 4.41: Cross plot of total Sulphur vs methyldibenzothiophene/ methylphenanthrene (MDBT/MPHEN) of Maiganga coal
Error! Bookmark not defined.

Figure 4.42: Plots of 22S/22S+22R C32 homohopanes against C29αββ/αββ+ααα steranes
Error! Bookmark not defined.

Figure 4.43: Correlation of MethylPhenanthrene index (MPI-1) with Vitrinite reflectance (Ro) of Maiganga coal and shale of Gombe Formation.
Error! Bookmark not defined.

Figure 4.44: Correlation of vitrinite relectance with proximate parameters.
Error! Bookmark not defined.

Figure 4.45: Chromatograms of sample MG1G showing *n*-Alkanes distribution.
Error! Bookmark not defined.

Figure 4.46: Chromatograms of sample MG2H showing *n*-Alkanes distribution.
Error! Bookmark not defined.

Figure 4.47: Chromatograms of sample MG2O showing *n*-Alkanes distribution.
Error! Bookmark not defined.

Figure 4.48: Chromatograms of sample MG3S showing *n*-Alkanes distribution.
Error! Bookmark not defined.

Figure 4.49: Chromatograms of sample MG4D showing *n*-Alkanes distribution.
Error! Bookmark not defined.

Figure 4.50: Chromatograms of sample MG4K showing *n*-Alkanes distribution.
Error! Bookmark not defined.

Figure 4.51: Chromatograms of sample BH15B showing *n*-Alkanes distribution.
Error! Bookmark not defined.

Figure 4.52: Plot of $\delta^{13}C$ saturate against $\delta^{13}C$ aromatic. The coal and shale plotted in terrigenous source
Error! Bookmark not defined.

Figure 4.53: Ternary plot indicating the proportion of the vitrinite, inertinite and liptinite and the corresponding hydrocarbon
Error! Bookmark not defined.

Figure 4.54: (a-i): Pie charts indicating the percentages composition of the macerals for coal and shale samples
Error! Bookmark not defined.

Figure 4.55: Photomicrographs of Palynomorphs observed in sample MG2L
Error! Bookmark not defined.

Figure 4.56: Photomicrographs of Palynomorphs observed in sample MG2R
Error! Bookmark not defined.

Figure 4.57: Photomicrographs of Palynomorphs observed in sample MG3D
Error! Bookmark not defined.

Figure 4.58: Photomicrographs of Palynomorphs observed in sample MG3Z
Error! Bookmark not defined.

Figure 4.59: Photomicrographs of Palynomorphs observed in sample MG4D
Error! Bookmark not defined.

Figure 4.60: Photomicrographs of Palynomorphs observed in sample BH15A
Error! Bookmark not defined.

Figure 4.61: Photomicrograph of coal sample a) MG1D, b) MG1W and c) MG2H
Error! Bookmark not defined.

Figure 4.62: Lithologic succession of Gombe Formation exposed at the Maiganga mine
Error! Bookmark not defined.

Figure 4.63: Lithologic succession of Gombe Formation exposed at the Maiganga mine
Error! Bookmark not defined.

Figure 4.64: Litholog of Borehole (15) sampled at Maiganga.
Error! Bookmark not defined.

Figure 4.65: Palynomorph distribution charts of selected outcrop samples of Gombe Formation
Error! Bookmark not defined.

Figure 4.66: Highlight of key biomarker events at some depth from phase I and II.
Error! Bookmark not defined.

Figure 4.67: Bar chart showing the percentage of moisture, ash, volatile matter and fixed carbon of the coal samples (as received).
Error! Bookmark not defined.

Figure 4.68: Bar chart showing the percentage of volatile matter, ash and fixed carbon of the coal samples (dry).
Error! Bookmark not defined.

Figure 4.69: Correlation between stratigraphic depth and fixed carbon.
Error! Bookmark not defined.

Figure 4.70: Al_2O_3 - (K_2O+CaO+MgO) - (Fe_2O_3+MgO) [AKF] Ternary plot of Maiganga coal samples.
Error! Bookmark not defined.

Figure 4.71: A-CNK-FM plot for the Maiganga coal samples which indicates low proportion of base neutralizing cation.
Error! Bookmark not defined.

Figure 4.72: Plot of Hafnium (Hf) against Zirconium (Zr).
Error! Bookmark not defined.

Figure 4.73: Plot of Vanadium (V) against Ash.
Error! Bookmark not defined.

Figure 4.74: Rare earth elements (REE) Pattern for the coal samples.
Error! Bookmark not defined.

LIST OF TABLES

Table 3.1: Sample codes and analyses carried out for each sample
Error! Bookmark not defined.

Table 4.1: TOC, Rock eval Pyrolysis and Vitrinite reflectance data of Maiganga Coal and Shale sample of Gombe Formation
Error! Bookmark not defined.

Table 4.2: Bulk Kinetics data for Coal and Shale Samples of Maiganga, Gombe Formation
Error! Bookmark not defined.

Table 4.3: Extract Parameters obtained from the Gas Chromatography
Error! Bookmark not defined.

Table 4.4: n-Alkanes, isoprenoids parameters and percentage composition of the extracts from coal and shale of Maiganga, Gombe Formation.
Error! Bookmark not defined.

Table 4.5: Selected Saturate biomarker source and depositional indices
Error! Bookmark not defined.

Table 4.6: Selected Aromatic biomarker source and depositional indices
Error! Bookmark not defined.

Table 4.7: Selected saturate biomarker maturity indices
Error! Bookmark not defined.

Table 4.8: Saturate biomarker ratio, thermal equilibrium value and vitrinite reflectance of the samples.
Error! Bookmark not defined.

Table 4.9: Selected Aromatic biomarker Maturity indices
Error! Bookmark not defined.

Table 4.10: Isotope data for coal and shale samples of Maiganga, Gombe Formation
Error! Bookmark not defined.

Table 4.11: Visual Kerogen Data for Coal and Shale samples of Maiganga, Gombe Formation
Error! Bookmark not defined.

Table 4.12: Maceral and vitrinite reflectance data for Coal samples of Maiganga, Gombe Formation
Error! Bookmark not defined.

Table 4.13: List of Palynomorphs, abundance and count obtained from coal and shale samples of Gombe Formation
Error! Bookmark not defined.

Table 4.14: Dominant palynomorphs in the the coal and shale samples of Gombe Formation
Error! Bookmark not defined.

Table 4.15: Results of Proximate analysis and the Calorific values of Maiganga coal
Error! Bookmark not defined.

Table 4.16: Trace elements of Maiganga coal, Gombe Formation
Error! Bookmark not defined.

Table 4.17: Major elements of Maiganga coal, Gombe Formation
Error! Bookmark not defined.

Table 4.18: Rare earth elements of Maiganga coal, Gombe Formation
Error! Bookmark not defined.

Table 4.19: Average concentration of some trace elements in Maiganga coal compared with average world coals.
Error! Bookmark not defined.

Table 4.20: Chondrite Normalized Values, Europium and Cerium Anomalies of Maiganga coal samples
Error! Bookmark not defined.

Table 4.21: Ce anomalies with corresponding plant forming coal
Error! Bookmark not defined.

ABSTRACT

The investigated source rock interval of the Maastrichtian Gombe Formation is located at the Maiganga coal mine, near Gombe, Gongola Basin, Nigeria. Samples were collected from a borehole and the exposed part of the mine (Phase I and II). The sections at Maiganga coarsen upward with the basal part made up of coal and shale interbeds while the upper part consists of siltstone, ironstone and sandstone. The coals and interbedded shales appear most prospective source rock facies in the formation and were evaluated with respect to their hydrocarbon source rock potential including the kinetics, paleodepositional environments, source, type and maturity of the organic matter in the organofacies. Geochemical techniques employed includes TOC, Rock-Eval Pyrolysis, Soxhlet Extraction, Gas Chromatography, Medium Performance Liquid Chromatography, Gas Chromatography - Mass Spectroscopy, Isotope Ratio – Mass Spectroscopy, Palynological technique, Maceral and Visual kerogen analysis were employed in this study. Inorganic study includes Elemental and Proximate analysis.

The log motif of the sections at Maiganga mine and other outcrop sections at Zange, Liji, Mallam Inna, Maiduku and Garin Magaji revealed coarsening upward sequence. Field observations in these locations indicate fluvial depositional settings. The poorly sorted sandstones with sub angular to angular grains observed in the locations represent channel facies while the fine grained clayey siltstones and shale represent overbank deposits reflecting low energy condition. The occurrence of coal at Maiganga suggests development of incoaling condition in a deltaic setting.

The studied samples (coal, shale and coaly shale) were rich in organic carbon, the TOC of the coals and shale range between (32.40-65.29wt %) and (0.64-4.84 wt %) with an average of 38.03wt% and 3.14 wt% respectively while the coaly shale has an average of 12.1wt%. The average Genetic potential (GP) value for the coals, shales and coaly shales are 70.7mg/g, 5.04mg/g and 12.6mg/g respectively indicating an excellent source potential. HIs is less than 200mgHC/gTOC for all the samples. The organic matter in the coaly source rocks suggests Type III kerogen and plant contributions from terrestrial sources probably from plant (*Vicia villossa*), peat vegetation (*Sphagnum L*) or mangrove. This is corroborated by broad activation energy (Ea) distribution (41-65kcal/mol) reflecting heterogeneous composition. Consequently, gaseous hydrocarbon potential is exhibited in the source beds.

The major phase and peak of hydrocarbon generation occurs at 460 – 465^{o}C for the coal and shale facies corresponding to Ea (54-55kcal/mol) defining up to 70% of the petroleum potential.

The coals and the shales were characterized by high molecular weight n-alkanes which range from C_{10}-C_{41} for the coal facies and C_9- C_{41} in the shaly facies. The n-alkanes were the dominant component of the aliphatic hydrocarbon fraction and they show variation in quantity and distribution. The extracts were characterized by predominance of polar compounds indicating low maturity level of kerogen cracking. Saturated fractions comprises of tricyclic and pentacyclic terpanes, steranes, diasteranes and tetracyclic polyprenoids while aromatic fractions comprises mono, triaromatic steroids and triaromatic methylsteroids.

The *n*-alkanes distributions in the coaly source rocks maximizes at C_{29}. This pattern indicates organic matter derived mainly from terrestrial organic matter while the shaly facies maximizes at C_{16} and C_{29} indicating mixed source. Pr/Ph ratio for the coaly facies ranges from 2.15-3.51 (avg. 2.79) while the shaly facies ranges between 0.95-2.37 (avg. 1.82) indicating fluvio-deltaic depositional environment in sub-oxic to oxic setting. The predominance of Pristane (n-C_{17}) over Phytane (n-C_{18}) suggests humic origin of the organic matter for the coaly source rocks in a mixed/transitional depositional environment.

The coals were rich in C_{29} steranes (> 50%) and (~40%) calculated from isosterane αββS and ααα R configuration. This is an indication of significant land plant contribution as evidenced from the very low C_{27} steranes. This is corroborated by the long chain length and isotopic value of -27.7 δ^{13}‰ PDB and -31.0 δ^{13}‰ PDB for the coal and shale respectively. The shale also have high C_{29} steranes but with appreciable quantity of C_{27} and C_{28} αββS sterane (26% and 29%) and (34% and 24%) in C_{27}, C_{28}ααα R sterane confirming probable marine contribution for the organic matter. The sterane/hopane ratio values range from 0.06-0.35 (<0.6) suggesting incorporation of high level of bacterial inputs commonly associated with terrigenous organic matter in coals. The dibenzothiophene/phenanthrene (DBT/PH) ratio range from 0.03 to 0.19 for the coal and 0.08-0.14 for the shaly source rocks respectively indicating appreciable quantity of terrestrial organic matter.

The average Tmax for the coal and shaly facies were less than 435^{o}C, and the vitrinite reflectance less than 0.55Ro. The carbon preference index (CPI) is greater than unity and in conjunctions with other saturate and aromatic maturity indices indicates that the samples were immature to low maturity status. Petrographic examination revealed vitrinite is the most abundant maceral followed by inertinite and liptinite, although there were absence of alginate and amorphous organic matter. The organic matter in the organic facies consists of opaque to non opaque biostructured phytoclasts and cuticles associated with common amounts of spores and pollen such as *Arecidites sp., Ephedripites sp., Monocolpites marginatus, Cyathidites sp., Foveotriletes margaritae, Longapertites marginatus, Longapertites vaneendenburgi, Proxapertites cursus, Proxapertites operculatus, Cingulatisporites ornatus Constructipollenites ineffectus, Retibrevitricolpites triangulatus, Echitriporites trianguliformis, Nyssapollenites sp., Araucariadites australis, and Fovoetriletes margaritae.* The coal and shales facies were dated Early- Late Maastrichtian and assemblage zone of *Arecipites – Dictyophyllidites harrisii* were assigned.

The proximate analysis of the coals revealed sub-bituminous rank, non-coking but suitable for fuelling, combustion and power generation due to high calorific value, high volatiles and low ash content. The average concentrations of the trace elements are lower when compared to world coals and indicate lesser negative impact to the environments, plants, animals and humans. The positive correlations of the trace elements such (Na, Ba, Th, and Co) with SiO_2 and Al_2O_3 in the coals suggests primarily aluminosilicate affinities.

In conclusion, the Maastrichtian coal and shale of Gombe Formation, Gongola Basin constitute good to excellent source rocks with potential to generate mainly gas and will generate oil if higher thermal maturity level is attained. Also, the coal facies were formed from organic matter derived from mainly terrestrial/terrigenous organic matter under oxidizing condition and deposited in the fluvial/deltaic environments, while the shaly facies were from mixed sources deposited under reducing lacustrine environments.

CHAPTER ONE

INTRODUCTION

1.1 General Statement

Recognizing sedimentary units favorable for petroleum formation is essential in petroleum prospecting. Source rocks (shale and coal) are capable of generating petroleum although there were controversies on the potentiality of coal to generate hydrocarbon despite advanced knowledge of the processes involved. The generation and expulsion of liquid hydrocarbon in coal source rocks has been widely debated in some studies and reviews (Hunt, 1991; Killops et al., 1994; Boreham et al., 1999; Sykes et al., 2014).

Coal is a carbonaceous combustible organic sedimentary rock formed by the alteration of plant remains (peat) through different processes compaction and dehydration and peatification (Schopf, 1956). Source rocks including coals and shales containing significant amount of organic matter have received much focus in generating commercial quantity of petroleum (oil and gas) in many basins around the world (Petersen et al., 2000; Boreham et al., 2003).

Coal has both organic and inorganic composition. Primarily, it is composed of carbon, hydrogen and oxygen, with less nitrogen and sulfur. The inorganic composition consists of a various ash-forming compounds such as quartz, clay and feldspar distributed in the coal. Different properties of coal include chemical (volatile matter, moisture content, ash, mineral matter and fixed carbon), physical (specific gravity, density, specific heat and porosity), thermal and plastic properties (caking and free swelling index) are often analyzed for various economic and technological applications. The major period of coal deposits was formed in (Upper Carboniferous period) about 350 to 270 million years ago with largest deposit of coal formed durng late Carboniferous and Permian and lesser amounts in the Jurassic through the Tertiary (Kotarba et al., 2002).

Coal deposit exist in many parts of the world namely United States of America, United Kingdom, Canada, Germany, China, Australia, India, Indonesia, and South Africa. In Nigeria, coal deposits occur in Anambra basin, Bida basin and the Benue Trough in the following areas; Enugu, Benue, Nasarawa, Kogi, Sokoto and Gombe (Figures 1.1 and 1.2). Coal deposits have been found in localities such as Kumo, Doho, Warji and Haman Gari in Gombe state, while some supposedly higher rank coals occur at Lamja and Chikila (Jauro et al., 2007) (Figure 1.2).

1.2 Scientific Background

1.2.1 Source Rocks

A source rock (shale and coal) is defined as any fine grained organic sedimentary rock capable of generating hydrocarbon with sufficient exposure to pressure and heat. The hydrocarbon generation potential of source rocks is primarily related to volume, organic richness and thermal maturity (Tissot and Welte, 1984). The oil source capacity of a possible source rock is dependent on four parameters i.e the amount of organic matter, quality, thermal maturity of kerogen and expulsion efficiency of the source sequence (Waples, 1979).

The organic contents of sediment depend on accumulation and degradation of organic matter, the environment that preserve large amount of organic matter are large, stagnant water areas and silled basins. Basically the organic matter content of recent sediment can be attributed to rate of organic deposition versus mineral deposition, availability of oxygen and level of biological activity. The critical factor related to the organic matter preservation in the sub aquatic sediment is the development of anoxicity (Demaison and Moore, 1980).

The organic source richness as measured by the Total Organic Carbon content (TOC) is mostly used as the the basic quantitative parameter when determining the hydrocarbon generation potential of a stratigraphic unit. However, the quantity of organic matter in sediments is usually estimated by the determination of organic carbon, the limiting element in

the petroleum forming reaction is not carbon but hydrogen. The reason for analyzing carbon, however, is that only the hydrogen bonded in organic molecules is active in the petroleum forming processes. The organic content of sediments which eventually becomes a source bed of petroleum generally ranges between 0.5 and 5.0% with a mean around 1.5% (Tissot and Welte, 1984)

The amount of organic hydrogen is determined by the type of organic matter present in the sediment, and thus, the kerogen can be broadly classified in four (Types I, II, III, and IV) depending on the relative content of organic hydrogen. There are four kerogen types that correspond to distinct biological source materials.

Type I kerogen is derived from algal debris (Tasmanites in marine waters and Botryoccocus in fresh water). The H/C ratio of Type I kerogen is the highest for all types of kerogens and, thus, this kerogen has the highest petroleum generation potential, even though higher levels of thermal maturation are needed for the formation of hydrocarbons from type I kerogen than from the other three types of kerogen.

Type II kerogen is derived from phytoplanktons which is marine organic matter. This type of kerogen is far more common than Type I and is known as the typical "oil" source kerogen.

Type III kerogen is terrestrial organic matter derived from higher land plants. It is rich in lignin and cellulose. Type III kerogen normally yields gas unless the plant remains are enriched in cuticles, sporomorphs or resinite to produce waxy oil from terrestrial organic matter. (Barker, 1974) has stated Type III kerogen may dominate marine shale despite its terrestrial origin.

The fourth type (Type IV) of organic matter contains the lowest H/C level and has been defined after Pennsylvanian coal. Type IV kerogen consists mainly of black, opaque debris of angular shape which are sourced from lignin precursors, i.e altered woody materials,

that have been oxidized. Type IV kerogen corresponds to inertinite and is sometimes refered to as "dead-carbon" and it has no potential to generate hydrocarbon i.e inert. The Hydrogen Index (HI) is a very important geochemical parameter used in determining the organic matter quality. Hydrogen Index for gas-prone organic matter is between 50-200 mg/g TOC, oil and gas prone organic matter is between 200-300 mg/g TOC, while oil-prone organic matter is ranged between 300-600 mg/g TOC (Tissot and Welte, 1984).

Not only the amount and quality of organic matter are important for the generation of hydrocarbons but also the level of thermal maturation. Only dry gas and possibly heavy oil will be found in the immature source rocks; oil and wet gas in the mature source rocks; and only dry gas in the metamorphosed facies. The matuartion of organic matter in the rock involves continous process or stages that are irreversible (Barker, 1979). The thermal maturation of organic matter is controlled by the duration of exposure to various heat and temperatures.

The generation of hydrocarbons from organic matter (mainly kerogen) during burial is a part of the process of thermal alteration of organic matter and is often referred to as "organic metamorphism" (Hood et al., 1975). This process has also been called "thermal alteration" (Staplin, 1969). There are many scales such as those based on coal rank (Suggate, 1959), pollen and spore (Staplin, 1969), elemental composition and colour of kerogen (Tissot et al., 1974), vitrinite reflectance (Mccartney and Teichmüller, 1972; Shibaoka et al., 1973), electron spin resonance (Pusey, 1973a, 1973b), and chemical maturity indicators (Tissot et al., 1974) which reflect irreversible effects of organic metamorphism.

1.2.1.1 Coal

Organic metamorphism or coalification i.e alteration of plants material during burial which consists of five successive overlapping stages; peatification, dehydration, bituminization, debituminization and graphitization (Levine, 1993). According to Tissot and

Welte (1984), the evolutionary stages of peatification and dehydration corresponds to diagenesis, bituminization and debituminization to catagenesis, and graphitization to metagenesis. Plants undergo transformation from peat to lignite, lignite to sub-bituminous coal, sub-ituminous coal to bituminous coal, bituminous coal to anthracite and anthracite to pure graphite. These stages represent different level of coalification/rank of the coal.

During alteration, temperature and pressure are the main controlling factor and as the carbon content increases there is a corresponding decrease in oxygen. The amount of hydrogen remains constant at early stage but later it begins to decrease with increasing rate at the highest level of maturity. The physical and chemical stage of alteration is initiated and maintained by deep post-depositional subsidence of the coal seam which increases the pressure and temperature in response to the geothermal energy, local heat flow and increasing thickness of overburden according to (Dissel et al., 1992). Time and temperature controls the coalification processes, while pressure decreases the rate of chemical reactions during coalification and enhances certain physical changes such as the porosity and alignment of structural units (Stach et al., 1982; Taylor et al., 1998). Increasing temperature with depth causes increase in chemical rank.

1.2.1.2 Shale

For many years shale source rocks have generated hydrocarbon in many basins across the world unlike coal source rocks. Little knowledge about the generation and expulsion of hydrocarbon just of recent has started gaining a lot of attention. Assessment of hydrocarbon accumulation in a petroleum system is subject to accurate characterization of the oil source potential inferred through various analytical techniques such as pyrolysis, fluorescence, infrared (IR) spectroscopy, or bulk techniques such as elemental analysis and 13C NMR spectroscopy.

1.2.2 Petroleum Generation from Shale and Coaly Source Rocks

Several oil accumulations have been explored and exploited in many coal basins across the world e.g Taranaki basin in New Zealand, Cooper – Eromanga basin in Australia, Ardjuna – Kutai basin in Indonesia. However, ability of coal charging an oilfield has generated argument and debate that coals can effectively source oil and the ability to geochemically differentiate between oil generated from coals and associated shales tends to be difficult even with a similar land-plant geochemical signature (Sun et al., 2000). Hunt (1991) and Sakurovs et al. (2012) stated that the distribution of the pore size and the adsorptive capacity of coals are limiting factors for efficient expulsion of oil and gas especially for hydrogen-rich coals.

The types of petroleum generated from coaly source rocks are basically dependent on the availability of hydrogen (Hunt, 1996; Petersen and Nytoft, 2006). The broad physico-chemical heterogeneity of coals controlled by the maceral composition as well as the depositional environments results in variable potential for oil generation (Sykes, 2001). Coals enriched in perhydrous maceral with high paraffinicity are suggested to have oil generating potential (Bertrand, 1984; Isasken et al., 1998; Killops et al., 1998). The relative proportion of coal macerals suggest the type of hydrocarbon it can generate because difference in the proportion of macerals results to different hydrogen content which is a limiting factor controlling the hydrocarbon generation from sedimentary organic matter (Hunt, 1991; Mukhopadhyay et al., 1991; Boreham and Powell, 1993).

A minimum of 15-20% liptinitic maceral in a coal is considered as important for source rock (Mukhopadhyay and Hatcher, 1993). The higher the liptinic maceral, the greater its ability to generate long chain aliphatic components resulting in higher potential in generating and expelling liquid hydrocarbon during maturation (Hunt, 1996; Isasken et al.,

1998; Petersen and Nytoft, 2006). The inertinite maceral reduces the hydrocarbon potential due to pre – sedimentary oxidation and diagenetic alteration of the organic matter.

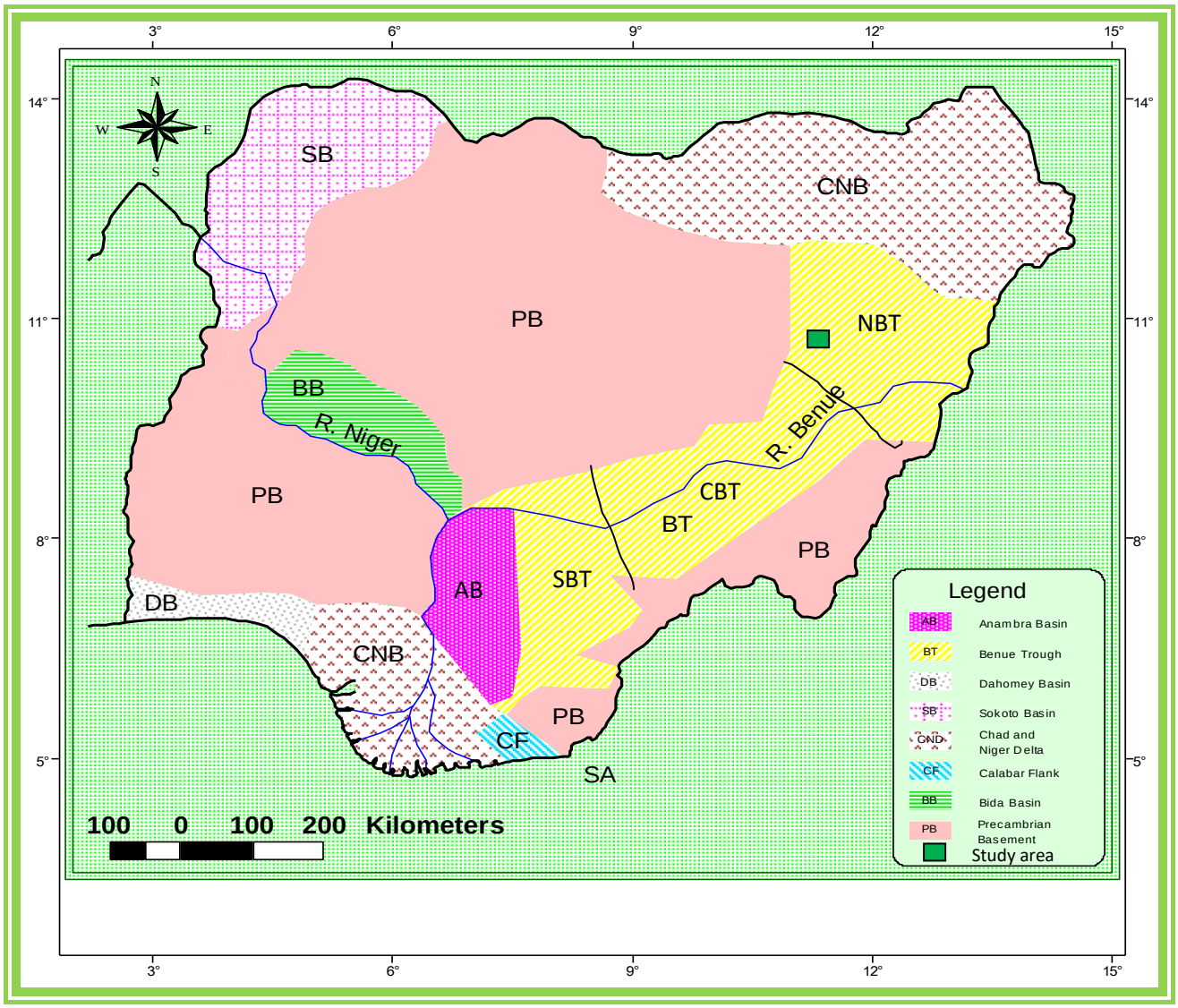


Figure 1.1: Geological map of Nigeria showing the basement rocks and sedimentary basins with coal occurrences (Modified after Obaje 2004). NBT- Northern Benue Trough, CBT- Central Benue Trough, SBT- Southern Benue Trough.

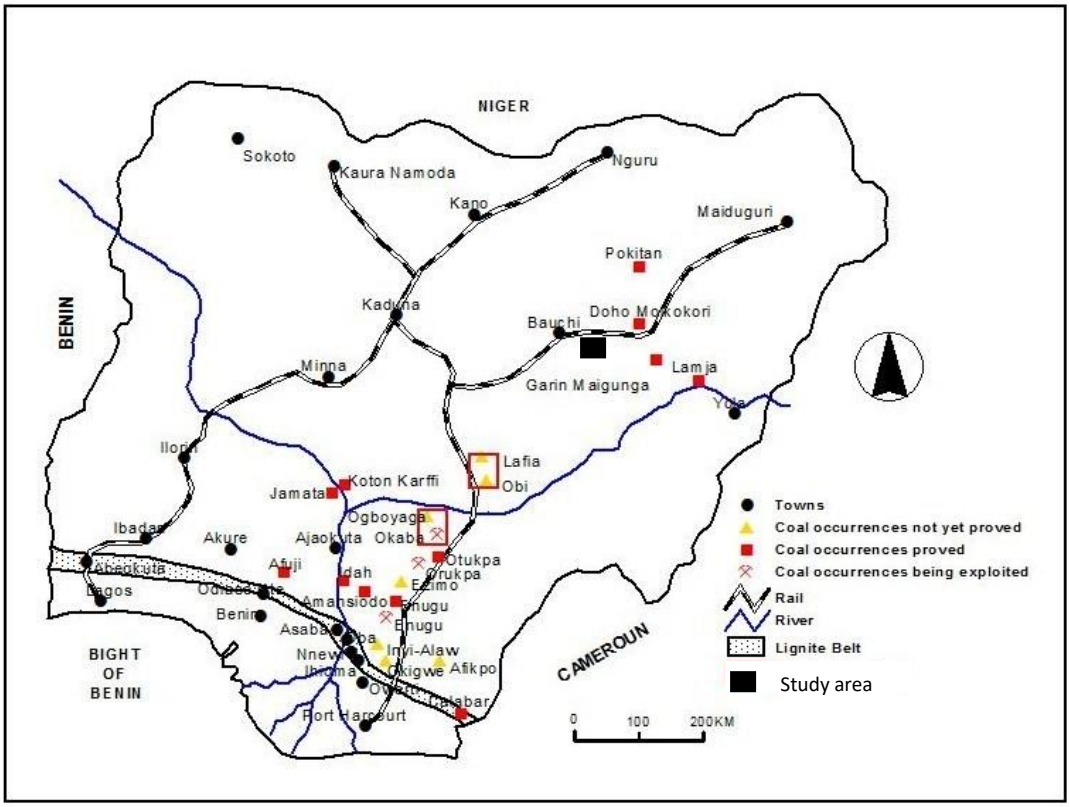


Figure 1.2: Map of Nigeria showing coal occurrences in Nigeria (modified after Elizabeth and Obaje, 2012).

1.3 Location and Accessibility of the Study Area

The study area covers eight localities Zange, Maiduku, Bobona, Liji, Mallam Inna, Riman, Garin Magaji and Maiganga coal mine near Kumo, Gongola basin, Northern Benue Trough covering latitude $10^0\ 02^I$N-$10^0\ 22^I$N and longitude $11^0\ 07^I$-$11^0\ 15^I$N. Zange, Maiduku, Riman, Garin Magaji and Maiganga are located in the Gombe sheet map 152 SW while Bobona, Liji and Mallam Inna are located in the sheet 152 NW (Figure 1.3). The locations were accessible by road (major and minor) as well as footpath.

The Maiganga coal mine is an open pit mine situated in Maiganga village southwest of Kumo town, in Akko Local Government area of Gombe state. It is about 9 km from Kumo town, off Gombe-Yola road and about 50 km from Gombe. The Maiganga mine occupies an area of about 4 km^2 and was quite accessible through minor roads and footpaths. The coal mine was logged from bottom at different phases of the mine where lithologies were exposed. Each of the localities where outcrop exposures were seen was also logged.

1.3.1 Relief and Drainage

Gombe state is considered to be on Nigeria highlands; however, the flat landscapes in northern and southern part of the state have isolated hills. The elevation of the plain is at about 600m above the sea-level. River Gongola runs North-South towards the River Benue with principal tributaries draining from the west to the east into River Gongola. Gombe state lies mostly within the poor ground water provinces in the Gombe Sandstones Formation, the Pindiga shale; Kerri-kerri Formation of Tertiary age and the isolated hills region of the northern, central and southern parts. Ground water is found between 180m depth on the sandstones. Because of the Cretaceous sandstones and shale, ground water is generally scarce and meagre. Dams from surface drainage systems could be more economically viable than ground water and bore-holes as source of water for domestic, agricultural and industrial uses in the state. The only river that traverses the state in the north and east through Dukul, Nafada

and all the eastern local government areas is River Gongola and join the River-Benue at Numan.

Gongola River is the sixth longest river in Nigeria, about 530 km, It has many tributaries and smaller streams in the state including rivers Dukul and Ruhu in the north Dukul Local Government Area. In the west central part, there are tributaries of River Guji, and in the southern part of the state including Kaltungo, Balanga, Billiri and Shongore. The headwaters of minor tributaries of River Benue characterize the landscape; which includes Dadin kowa and Rivers Balanga. Thus, the state lies within the wider Benue drainage basin which is dominated by the western part of the Gongola sub-basin.

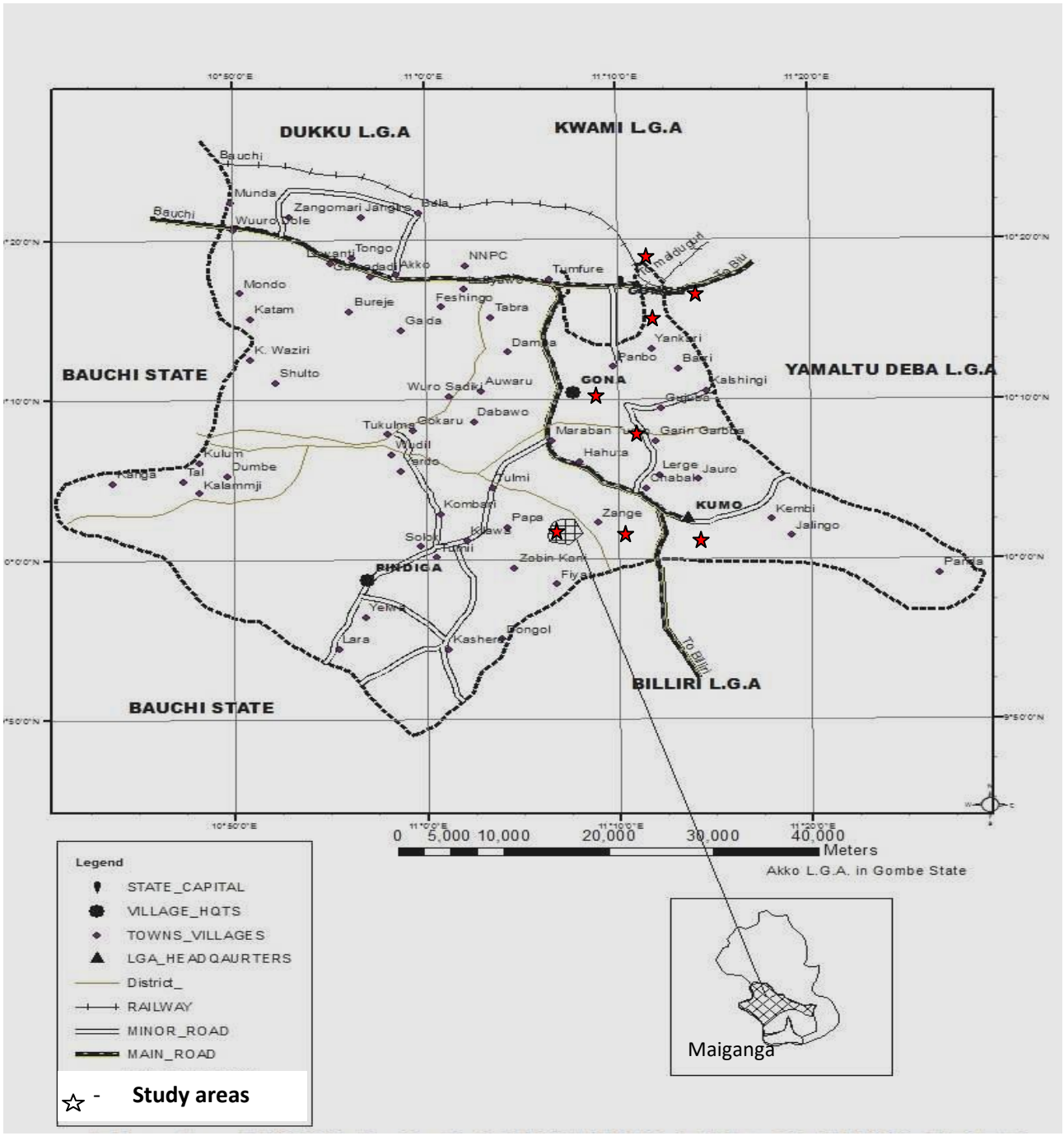


Figure 1.3: Location map of the study areas.

1.3.2 Climate and Vegetation

Gombe state is characterized by two major climates, the dry season between (November-March) and the rainy season (April-October) with an average rain fall of 835mm (Balzerek et al., 2003). Gombe is generally a guinea savannah grass land with concentration of wood lands in the southeastern and southwestern part of the state (Yahaya and Adamu 2016). The climate in Gombe influence the soil and vegetation; hence over half of the state (central part) underlain by the kerri-kerri Formation has impoverished soil with sand loams on iron pan. Soils in the eastern part of Gombe state consist of loamy, sandy clay, loam and vertisols with cracking clays that have weathered from shale. The wooded shrub land dominates the vegetation.

1.4 Previous Work

There is no doubt a lots of research has been carried out on the potentiality of coals to generate hydrocarbon in many coal basins around the world. While several information on the processes involved has been revealed, more attention and investigation on coal is needed to confirm the hydrocarbon generation and expulsion from coal.

Makeen et al., (2015) investigated hydrocarbon potential of Abu Gabra Formation of the Muglad basin. 34 ditch cuttings from two oil field in sudan were analysed by TOC, Bulk kinetics, Pyrolysis (SRA), Pyrolysis GC, Elemental analysis and Kerogen Microscopy. Incident light microscopy showed that liptinitic maceral, amorphous organic matter (AOM) dominated the organic matter with some mineral matter. Type I kerogen (alginite) was dominant followed by Type II kerogen which shows intense fluorescence suggesting early stage of oil generation with vitrinite reflectance value ranging from 0.59Ro to 0.76Ro. The Abu Gabra sediments were confirmed to have good source potential based on the TOC and S_2 values of the pyrolysis. The HI characterizes the organic matter to Type I and II and grades into mixed Type II-III. Pyrolysis – GC was further used to reveal and authenticate the type of

kerogen and the type of hydrocarbon to be generated. The bulk kinetics showed narrow activation energies and confirms contributions from algae (Type I kerogen).

Peterson and Nytoft (2006) investigated the relative proportions of aliphatic CH_2, CH_3, aliphatic hydrogen (H_{ali}) to determine the oil generation capacity of coal based on age. The aliphatic chain length of Carboniferous, Permian, Jurassic and Cenozoic humic coals was deduced by FTIR and ruthenium tetroxide catalysed oxidation (RTCO) followed by GC–MS analysis of the n-monocarboxylic acids (esterified) to determine the potential to generate oil. The samples used were low rank coals and humic which contain vitrinite as dominant maceral (>70%). Carboniferous coals showed a dominance of chain lengths $<C_{19}$ which indicate principal gas and condensate generative potential (light oil). However, the study revealed that all the coals have aliphatic chains in the range $C_{16–18}$, which indicates a general ability to generate light oil.

Adegoke et al., (2017) employed organic geochemical and palynofacies studies on eighty four (84) ditch cuttings obtained from four exploratory wells to deduce the paleoenvironments and source of the organic matter of Fika sediments in the Bornu basin. The focus of their research emanated from the little understanding of the evolution of the subsurface lithology, paleodepositional condition of the organic matter and the source rock potential which has led to unsuccessful exploration in the Chad (Bornu) Basin. Analytical methods used in the study include advanced (GC-IRMS), (GC-MS), and (CSIA).

The TOC values range from 0.41 and 2.37 wt%, hydrogen index (HI) values are less than and oxygen 200 mg HC/gTOC. The Tmax value is between 429–465 °C and PI (0.03–0.37). High n- alkane and isoprenoid distribution were obtained from the m/z 85 mass chromatograms. Unimodal and bimodal n-alkane distribution was observed in the chromatogram with an abundance of C_{13} to C_{24} chain n-alkanes. High phytane over pristane

and low terrigenous/aquatic ratios (TAR) and presence of high amount of waxy alkanes (+n-C_{25}) were observed in many of the samples.

The Fika sediments comprise of Amorphous Organic matter (AOM), Phytoclast and palynomorphs. The phytoclast (woody debris and cuticles) are predominant whereas there was low occurrence of spores and pollen. The organic matter was dominated by Type III and Type IV deposited in transitional environments and sourced from both terrigenous and marine input.

Akande et al., (2015) investigated the source rocks of Ogwashi –Asaba Formation in Anambra basin for hydrocarbon potential using hydrous pyrolysis, Organic petrology and Rock eval Pyrolysis. The source rocks have high TOC values indicating excellent source potential. The lignite and coaly shale have an average of 426 mg HC/g TOC and 222 mg HC/g TOC respectively. The Tmax and the vitrinite values indicate the samples are immature.

The maceral analyses indicate huminite as the dominant maceral (60 and 70%) in the lignite and coaly shale respectively. Sequential hydrous pyrolysis was conducted on two samples and the result indicated that the lignite with higher percentage of liptinite (38.0%), TOC (63.46 wt. %), and HI values (481 mgHC/g TOC) generates and expels more oil than the adjacent coaly shale. The oil expelled from the lignite is characterized by high Pr/Ph ratio with abundant molecular weight n-alkanes indicative of source rock derived from terrestrial source. It was concluded that the source rocks intervals within the Ogwashi - Asaba Formation and its subsurface equivalent, the Agbada Formation, at maturity could be responsible for the generation of hydrocarbon in the Niger Delta.

Akande et al., (2012) carried out geochemical characterisation of Cenomanian – Coniacian and Campanian - Maastrichtian source rocks intervals in the Lower Benue and Midle Benue Trough to determine the hydrocarbon potential of the sediments. Samples from

potential source rocks were obtained in outcrop exposures and boreholes on specific traverses. Analytical methods includes Total Organic Carbon (TOC), Rock Eval Pyrolysis, Organic Petrology and Biomarker analysis. Their result revealed that total organic carbon contents ranged from 0.24 to 5.47% in Eze- aku and Awgu shale. Shales of the Enugu / Nkporo Formation in the Anambra basin indicate TOC contents between 0.54 and 3.0% and 60.97 to 77.01% in the Lower Maastrichtian Mamu Formation. In the Middle Benue Basin, TOC contents range from 0.12 to 0.31% in the Asu River Shales, 0.3 to 1.93 % in the Awe Shales and ranged from 0.1 to 0.19% in the Keana shale facies. Kerogen classification of Awe, Asu River and Awgu shales in the Middle Benue Basin indicate Type III kerogen which shows substantial contribution from terrestrial sources.

Varying levels of maturity was obtained in the Abakaliki and Anambra Basins with values of Tmax of at least 430^{o}C and Vitrinite reflectance (VRom) values between 0.6 and 1.3%. Eze-Aku Shale (0.71 to 0.93%), the Lokpanta shales with Tmax varying from 424 to 430^{o}C and VRom between 0.43 to 0.55%, Awgu Shale with Tmax from 434 to 467^{o}C and VRom between 0.81 to 1.07%.

Sub-bituminous coals in the Anambra Basin were notably immature to marginally mature on the basis of the Tmax values ranging from 417^{o}C to 428^{o}C and VRom between 0.41 to 0.63%. Obvious odd – even predominance and dominance of long chain aliphatics in Anambra coal suggest high input of terrigenous organic matter deposited in an oxic conditions. The high pristane / phytane ratios and nC_{29} sterane components indicate a considerable input from terrestrial organic matter. Finally, the coals and the interbedded shales of the Awgu Formation showed dominance of nC_{29} regular steranes with no obvious odd over even predominance suggesting the organic matter was contributed from both algal Type II and terrigenous Type III organic matter.

Sonibare et al., (2008) studied three outcrop section from Lower Benue (Enugu) and Middle Benue (Lafia/Obi) Trough to determine the hydrocarbon potential of the coal in the basin through Rock Eval pyrolysis and Gas Chromatography/Mass Spectrometry (GC-MS). The result showed that Total Organic Carbon contents (TOC) ranges from 45.2 to 70.7wt.%. The genetic potential (GP), S1+S2 for the coals ranged from 99.0 to 202.8 mgHC/g, suggesting that the samples have excellent potential to generate hydrocarbons. C_{27} – C_{29} regular steranes and diasteranes were reported to be present in the samples indicating the coals were derived from mixed sources (marine and terrestrial) and have the capacity to generate both oil and gas. Also, Ts/Ts+Tm, βα/αβ of C_{29} sterane and βα/αβ of C_{30} sterane values for the coal range from 0.03-0.09, 0.15 – 0.60 and 0.18 – 0.53 respectively while 22S/22S+22R C_{32} hopane ratios in the coal ranges from 0.47 to 0.60. These values indicate that the coals are of very low maturity.

Akande et al., (2007) carried out organic petrography on coals from Onyeama, Owukpa and Okaba mine, Mamu Formation in Lower Benue Trough. Their results showed that huminite (detrohuminite) is the dominant maceral at the base of the mines with varying amount of liptinite (sporinite, resinite, cutinite) and inertinite (fusinite, inertodetrinite and sclerotinite). The TOC content of the coal samples ranges from 60.8 to 77wt% and HI values all exceed 200 mgHC/ TOC classifying the kerogen in the coal as Type III. The Vitrinite reflectance (0.44-0.6Ro) and Tmax (417-419^{o}C) suggest the coals are thermally immature to marginally mature. Significant increase in S1 yield, Production Index (PI) and decrease in Bituminen Index and HI during maturation was observed at Tmax of 453^{o}C suggesting efficient oil expulsion.

Akande et al., (1992) investigated outcrop and borehole samples of coals from five localities namely (Enugu, Orukpa, Okaba, Ihioma and Ogwashi-Asaba) and obtained mean random vitrinite reflectance ranging from 0.54% - 0.63% for Enugu coal (Onyeama mine)

indicating a sub-bituminous A coalification stage. Orukpa coal and Okaba were classified as sub-bituminous B to A and sub-bituminous C to B respectively. The Ihioma and and Ogwashi-Asaba coal are lignite. The Ihioma and Azagba-Ogwashi lignites were interpreted as reed swamp depositional environment, concentration of large amount of liptinite in the Orukpa mine were interpreted to be of wet condition of reed swamp environment whereas large amount of inertinite in Onyeama and Okaba seam indicate shift to drier condition possibly forest swamp facies.

Previous work on Maastrichtian source rock of Gombe Formation include the determination of the source rock potential and depositional setting of the Cretaceous coals and mudstones of the Maiganga and Yayi –Ngari, Gombe Formation by Ayinla et al., (2017) using analytical techniques such as TOC, Rock Eval Pyrolysis and biomarker analyses of outcrop samples obtained from the mine. However, problems yet to be addressed in his research include inability to provide valuable information on the kerogen composition and structure as it relates to the generation and expulsion of hydrocarbon in the organic facies, the source rock kinetics to reveal the oil generation potential and to precisely date the coaly and shaly unit of the Formation.

The result indicated that Maiganga coal have relatively high TOC values ranging from 50.3 to 80.0 wt. % compared to the shale samples (from 3.8 to 24.3 wt. %), (S_2) from pyrolysis is between 0.24 to 158.84 mg HC/g rock. A fairly moderate value was observed for the Yaya-Ngari shale (0.24 to 0.37 mg HC/g rock). Tmax is generally less than 435^{o}C, whereas, Yaya-Ngari shale samples have Tmax between 447 to 450°C. Hydrogen Index (mgHC/gTOC) for Maiganga coal is between 41 to 234 mg HC/g TOC, 57 to 185 mg HC/g TOC for the shale and 24 to 107 mg HC/g TOC for the mudstone, however low HI was obtained for Yaya-Ngari (25 to 33 mg HC/g TOC).

Organic matter indicated Type II-III kerogen from the HI values which suggest generation of mainly gas and limited amount of liquid hydrocarbon. The mass chromatogram also confirm high amount of C_{29} sterane compared to other sterane which also supported terrestrial sources for the sediments. The depositional condition of the sediments was oxic for the coaly source rocks in a mixed environment while that of the mudstone and shale revealed suboxic-oxic settings.

Organic petrography showed that huminite was the dominant maceral. It was suggested that the Upper Cretaceous petroleum system constitute a good source rock with potential to generate gas with limited amount of liquid hydrocarbon.

Onoduku and Okosun (2014) also deduced the paleoenvironment and palynostratigraphy of sediments exposed at the Maiganga mine. A total of 174 core samples from three boreholes (BH-7, BH-16 and BH-17) that penetrated Gombe Formation were studied for their palynofloral contents and the results were used to date, zone and interprete the paleoclimatic conditions of the studied area. Two biozones were erected in the studied boreholes i.e Assemblage Zone I (*Proteacidites sigalii – Echitriporites trianguliformis* Assemblage Zone). This zone was dated Early Maastrichtian defined by the basal and abundant occurrence of *Echitriporites trianguliformis, Proteacidites sigalii and Retidiporites magdalensis* in the following borehole intervals: 47 – 23.22 m (BH-7), 57 – 22 m (BH-16) and 46 - 21 m (BH-17). Assemblage Zone II (*Cyathidites sp Laevigatosporites haardtii* Assemblage Zone) was dated Late Maastrichtian and characterized by the presence of *Cyathidites sp* and other palynoforms that ranged from the lower zone such as *Acrostichumaureum, Proxapertites cursus, Laevigatosporites sp and Inaperturopollenites sp* at intervals: 23.22 – 4 m (BH-7), 22 – 1.0m (BH-16) and 21 – 1.0m (BH-17). The Paleoclimatic deductions from pollen/spores data indicate Late Cretaceous Palmae Province and a tropical climatic condition for the deposition of Gombe Formation.

Onoduku et al., (2013) investigated core samples (shales and coal) from three boreholes around Maiganga coal mine to characterise the source rock potential using preliminary screening methods such as TOC and Rock Eval Pyrolysis. Their results showed that TOC value range from 2.00-4.27wt% for the shales and 47-47.10wt% for coal indicating good to excellent source potential, the S2 and the (S1+S2) also corroborate the moderately good hydrocarbon potential, The Hydrogen Index was used to constrain the type of organic matter and results revealed that the organic matter are mainly Type III kerogen as indicated from the HI values not eexceeding 200 mg/HC/TOC. The value confirms terrestrial sources for the organic matter. The maturity of the organic matter was deduced from the Tmax obtained from the rock eval pyrolysis and was generally less than 435^{o}C. It was concluded that samples constitute good source rock, but are thermally immature.

1.5 Definition of Research Problem

Many of the previous work applied routine and preliminary screening methods in the study area. The existing data therefore could not sufficiently characterize the source rock potential and kinetics of the organofacies. Hence, advanced geochemical techniques are required to characterize the source rocks with respect to hydrocarbon potential and kinetics as it is been employed in other coal basins. Valuable information on the kerogen composition and structure as it relates to the generation and expulsion of hydrocarbon in the organic facies is yet to be established.

As at now, the data on biomarker characterization of the coal and shaly source rocks with respect to paleodepositional condition, source, type and maturity of the organic matter is limited. Also, the stratigraphy of Gombe Formation needs to be more refined, particularly the recently discovered Maiganga coal and its associated shaly units needs to be precisely dated.

1.6 Aim and Objectives

The aim of this research is to evaluate and characterize the hydrocarbon potential of the source rocks of Gombe Formation by examining the molecular composition of the hydrocarbon generated from the kerogen through geochemical techniques. The following are the objectives of the study:

1. To determine the oil generation potential of the coal and shale by assessing the aliphatic component/chain length of the kerogen and source rock kinetics.
2. To determine the thermal maturity of the organic matter in the organic facies based on vitrinite reflectance (%Rm), Tmax, thermal alteration index (TAI), spore coloration, saturate and aromatic biomarker parameters.
3. To determine the kerogen type, source, paleodepositional environments of the organic matter from biomarker distribution.
4. To determine the percentage composition of the kerogen extract for saturate, aromatic and polar fractions.
5. To determine the age and paleoenvironments of the coals and shales based on palynological investigation.
6. To determine the quality of the coal with respect to cokability, power generation, combustion and the environmental impact on its utilization.
7. To infer the vegetation type that formed the coal based on elemental compositions.

1.7 Research Significance

As the world's hydrocarbon reserves continue to deplete, there is need for alternative energy to complements the conventional sources. This has led to keen interest in investigating the Cretaceous basin in Nigeria particularly the frontier (inland) sedimentary basins. Nigeria has the 10th largest hydrocarbon reserve and the 12^{th} largest producer of oil & gas in the world contributing approximately 3% to Global production. The nation holds an estimated

36.5 billion barrels of crude oil & condensates and 180.4 trillion standard cubic feet of gas reserves mostly domiciled in the Niger-Delta. Consequently, the reserve can be improved by exploring the inland sedimentary basins in Nigeria of which Benue Trough is an important part. It is also pertinent to note that most of the samples from the Bima, Yolde, Pindiga, and Gongila Formations yielded poor source rock quality and most of the samples falls have no hydrocarbon potential (Mukhtar and Congjiao, 2012).

The Total world reserves of coal are estimated to be about 1083 billion tons (EIA, International Energy Annual 2001) with Nigeria having 209 million tons. The coals are mined in various part of the country for power generation and in steel production and a lot of these coal reserve are yet to be exploited. Part of the significance of this study is that the potential of Gombe coal in terms of hydrocarbon and electricity generation with be unraveled and these will have implication for increasing the GDP of Nigeria's economy and consequently generating employments

CHAPTER TWO

GEOLOGIC SETTING AND STRATIGRAPHY OF NORTHERN BENUE TROUGH

2.1 Geologic Settings of Northern Benue Trough

2.1.1 Origin and Structural Setting

The opening of the Atlantic ocean which was inititated during the separation of South America from Africa in the Late Jurassic through the process of Sea floor spreading consequent to continental updoming and rifting has been linked to the evolution of the Benue Trough (Wright, 1968) (Figure 2.1). The spreading of ridges was also proposed by Olade (1975) and applied the Y-shaped triple rift junction model (R-R-R) to the seperation of South American and African plates in which two arms of the radial triple rift continue to spread while the spreading in the third arm was aborted. Based on this model, the three radial rift systems became active during the Early Cretaceous and met at (R-R-R) triple junction in the Gulf of Guinea. The Gulf of Guinea, the South Atlantic and the Benue Trough represent rift arms of this triple junction. Benkhelil, (1989) also suggested that the evolution of the trough could be the effect of tension that resulted in a rift or wrench related fault basin in which magmatism accompanied the tectonic rift as it spread all over the trough (Coulon et al., 1996), a magmatic old rift was also suggested for the Gongola Basin (Shemang et al., 2001).

The Cretaceous Benue Trough of Nigeria is a rift basin in central West Africa that trends NNE-SSW direction. It length is 800 km and 150 km in width (Figure 1.1). The Trough has up to 6000 m of Cretaceous–Tertiary sediments of which those pre-dating the mid-Santonian have been compressionally deformed compressionally, uplifted in several places and faulted. The mid-Santonian tectonic episode affected the whole of Benue Trough producing series of compressional folding which was quite intense such as 100 anticlines and synclines (Benkhelil, 1989). Consequently, the mid-Santonian tectonism and magmatism displaced the depositional axis in the Benue Trough westward and resulted in subsidence of

the Anambra Basin which is believed to be part of Southern Benue Trough. The Anambra Basin in the Benue Trough is a related structure that developed after the compressional episode (Akande and Erdtmann, 1998). The sediments fill is Campano-Maastrichtian to Eocene in age.

The Benue Trough is subdivided into a Southern, Central and Northern portion (Figure 1.1). Review on the geology and stratigraphic successions including formations, lateral extensions, bed thicknesses and stratigraphic locations in the Benue Trough have been given by several workers e.g Carter et al. (1963), Offodile (1976), Petters (1982), Petters and Ekweozor (1982), Obaje (1994) amongst others. The Northern Benue Trough is subdivided into the east–west trending Yola Basin (or "Arm") and the north–south trending Gongola Basin. A third basin, the Lau-Gombe Basin is also been recognized by Akande et al., (1998).

2.2 Regional Stratigraphy of Northern Benue Trough

The study area lies within the northern part of Benue Trough. The Northern Benue Trough consists of the Precambrian-Paleozoic basement gneissses and granite which occur as inlier, example is the Kaltungo inlier which is shown in Figure 2.2. The stratigraphy consists of the basement rocks as the oldest, the Albian -Turonian Bima Formation, the Cenomanian Yolde Formation, the Turonian-Coniacian Pindiga Formation, the Masstrichtian Gombe Formation, the Tertiary Kerri Kerri Formation and the Alluvium (Figure 2.3).

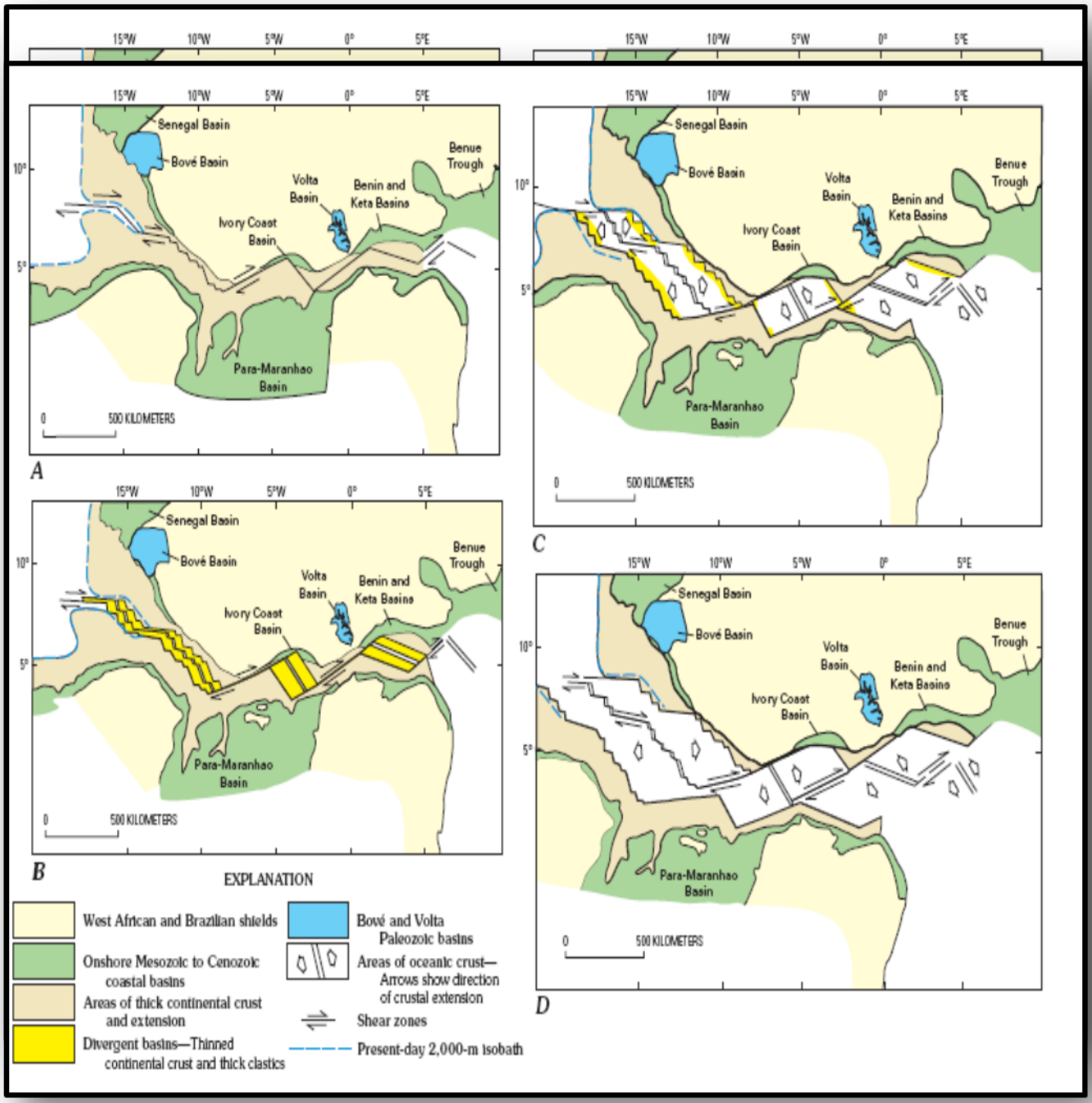


Figure 2.1: Schematic Break-up of Africa and South-America during Late Mesozoic (after Genik, 1993).

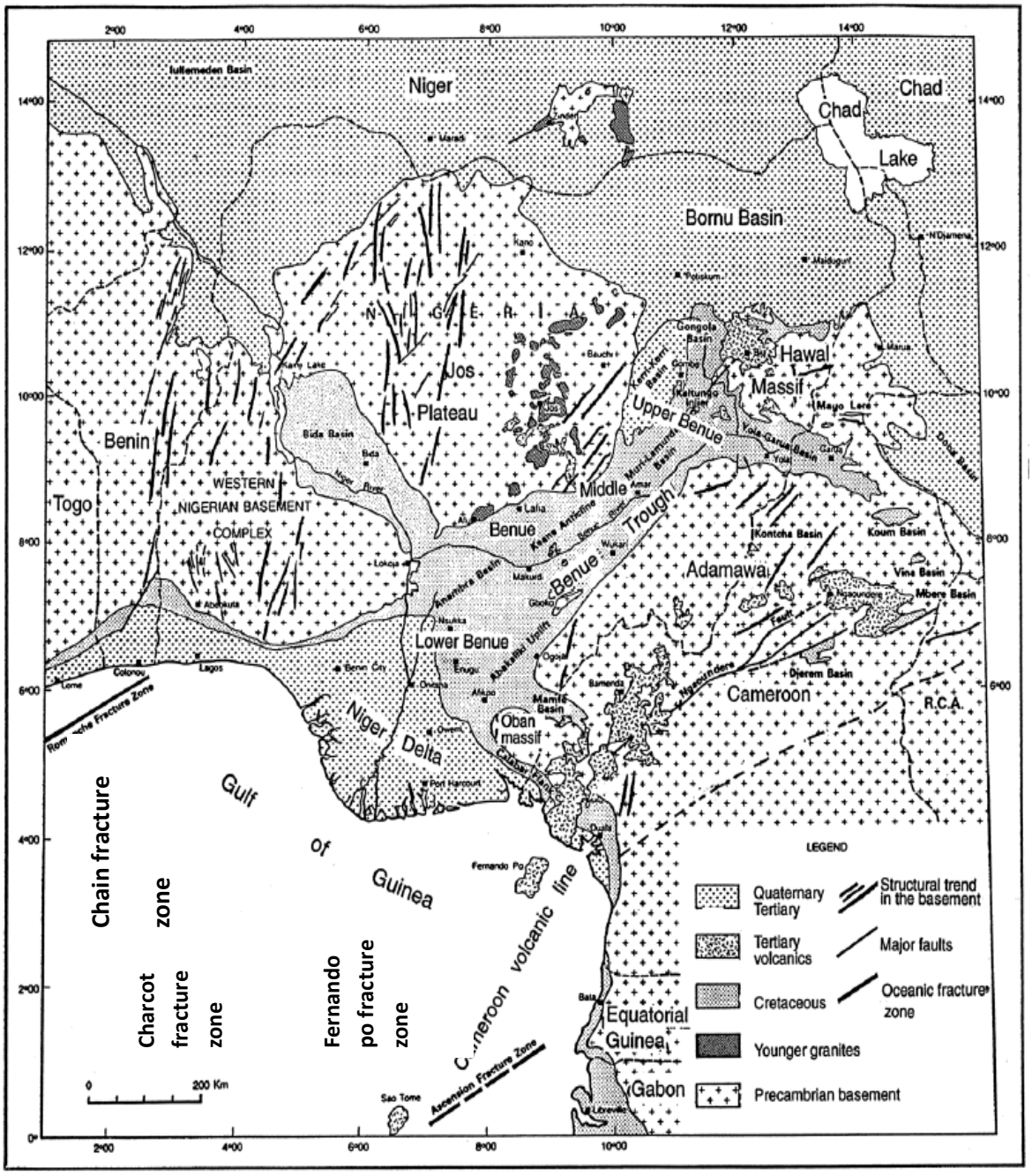


Figure 2.2: Geological map of the Benue Trough. The traces of the Equatorial Fracture Zones are indicated (after Odebode, 2010).

2.2.1 Bima Formation

The Bima Formation is the most extensive, oldest and thickest of the Cretaceous sedimentary Formations in northeastern Nigeria. It is covered and lies directly on the Precambrian Basement Complex. The sandstones of Bima Formation are yellow-brown, massive cross-bedded feldspathic with thickness of 3500m. The sandstones were derived from the granitic basement complex. (Guiraud, 1990) subdivided the sandstone into three members namely; the Upper Bima (B3), the Middle Bima (B2) and the Lower Bima (B1). The age of the Formation is uncertain, however, various researchers indicate Upper Albian to Lower Turonian (Carter et al, 1963). The Basement Complex includes all the Pre-Mesozoic rocks and is thus the oldest formation of the Nigerian stratigraphic series.

2.2.2 Yolde Formation

The Yolde Formation conformably overlies the massive coarse sandstones of the Bima Formation (Albian- Cenomanian) and is conformably overlie the marine shale of the Pindiga Formation. The Yolde Formation constitutes the transition facies between continental and marine sedimentation. This Formation consists of a variable sequence of shales and sandstones with thickness of about 200m. The sandstones are thin-bedded at the base, and overlain by alternations of shelly limestone and sandy mudstones (Whiteman, 1982).

2.2.3 Pindiga Formation

The Pindiga Formation succeeds the Yolde Formation; an unconformity separates the Pindiga from the overlying Maastrichtian Gombe Formation. The Pindiga Formation consists of marine, blue-black shale with interbedded fossiliferous limestone at the base with thickness up to 240m (Carter et al, 1963). The Formation was depoisted under marine conditions that prevailed during the early – late Turonian and Coniacian times. The Gongila and the Fika Formations are the lateral equivalents of the Pindiga Formation (Zaborski et al, 1997).

2.2.4 Gombe Formation

The Maastrichtian Gombe Formation is a heterogenous sequence consisting of sandstone, shale, siltstones and ironstones and coal seams with maximum thickness of 600m. This sequence was divided into two parts: the upper 223m consisting of sandstones and the lower part consists of shale and ironstones layers up to 200m thick (Carter et al, 1963). The Gombe Formation is located below the Kerri-Kerri Formation in the Gongola Basin. It has equivalence to Ajali/Owerri/Mamu Formation of Anambra (Southern Benue Trough), Lafia Formation of the Central Benue Trough, and Lokoja Formation in the Bida Basin. It extends into the southeastern part of the Bornu Basin.

2.2.5 Kerri Kerri Formation

The Paleogene Kerri-Kerri Formation was deposited in a continental environments ranging from lacustrine to deltaic settings. It lies unconformably on the Gombe Formation with maximum thickness about 320m (Carter et al, 1963). In the western part of the plateau, which coincides with the western edge of the area, the Kerri-Kerri Formation overlies the basement complex, but the contact is almost completely filled with abundant alluvial deposits. The Formation has the lowest fracture density compared to other formations because it has not been tectonised simply because it was laid down after the main tectonic episode.

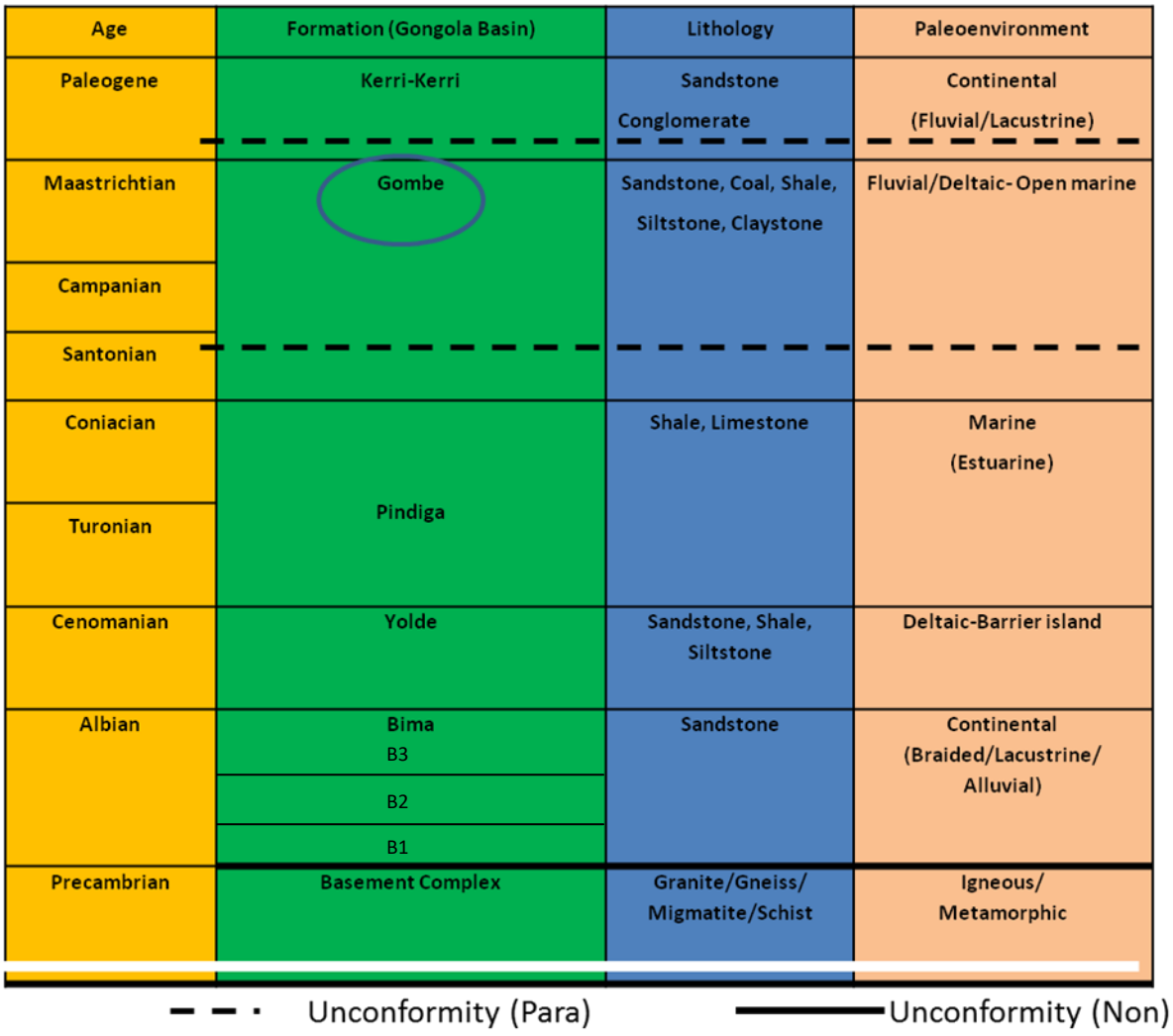


Figure 2.3: Stratigraphy of Northern Benue Trough (Modified after Abubakar et al, 2006).

CHAPTER THREE

METHODOLOGY

3.1 General Statement

The method employed in this research involves field mapping and laboratory analysis. Analytical techniques include both the organic and inorganic geochemical techniques. The organic techniques include Soxhlet Extraction, Total Organic Carbon (TOC), Rock-Eval Pyrolysis, Maceral and Visual Kerogen analysis, Medium Performance Liquid Chromatography, Gas Chromatography, Gas Chromatography – Mass Spectroscopy, Gas Chromatography – Isotope-Ratio Mass Spectroscopy and Palynological analyses. The inorganic analytical techniques used are proximate and whole rock elemental analyses. Figure 3.1 shows the flow chart of the methodology.

3.2 Field Study

Field study was carried out on Gombe map sheet 152 SW and NW on a scale of 1:50,000 in the following localities Riman, Mallam inna, Liji, Bobona, Garin Magaji, Maiduku, Zange and Maiganga coal mine for the purpose of logging and collection of samples for laboratory analyses. Two phases of the open pit mine at Maiganga (Phase I and II) were logged and samples collected. Phase I (Figures 3.2 and 4.1) of the mine is about 35m thick section consisting of shale, coal, sandstone, siltstone and intercalations of ironstone concretions while phase II of the mine is 25m thick section (Figures 3.3 and 4.2) with same lithologies observed in phase I. The sections were logged from the base to the top in each phase as there were obvious changes in the lithologic units during logging which shows different lithological changes such as colour, texture, mineralogy, structure and geometry. There are two coal seams (A and B) in the mine which occurs at the base and grades upward into shale, claystone, siltstone and sandstone unit. A total of Twenty six (26) surface cuttings were obtained from the phases (sections). Measurements were taken and samples were

collected at intervals depending on the vertical variation in the properties of the bed sequence. The coal seams were sampled at interval of 0.5m, shale at 0.3m, siltstone at 0.4m and sandstone at 0.5m while paying attention to weathered surfaces. Fresh samples were collected and carefully labeled and stored in different labeled sample bags. Three (3) borehole samples were also obtained from borehole 15. The samples were taken to the Geology Laboratory in the Geology Department, University of Ilorin for lithologic description and sample preparation.

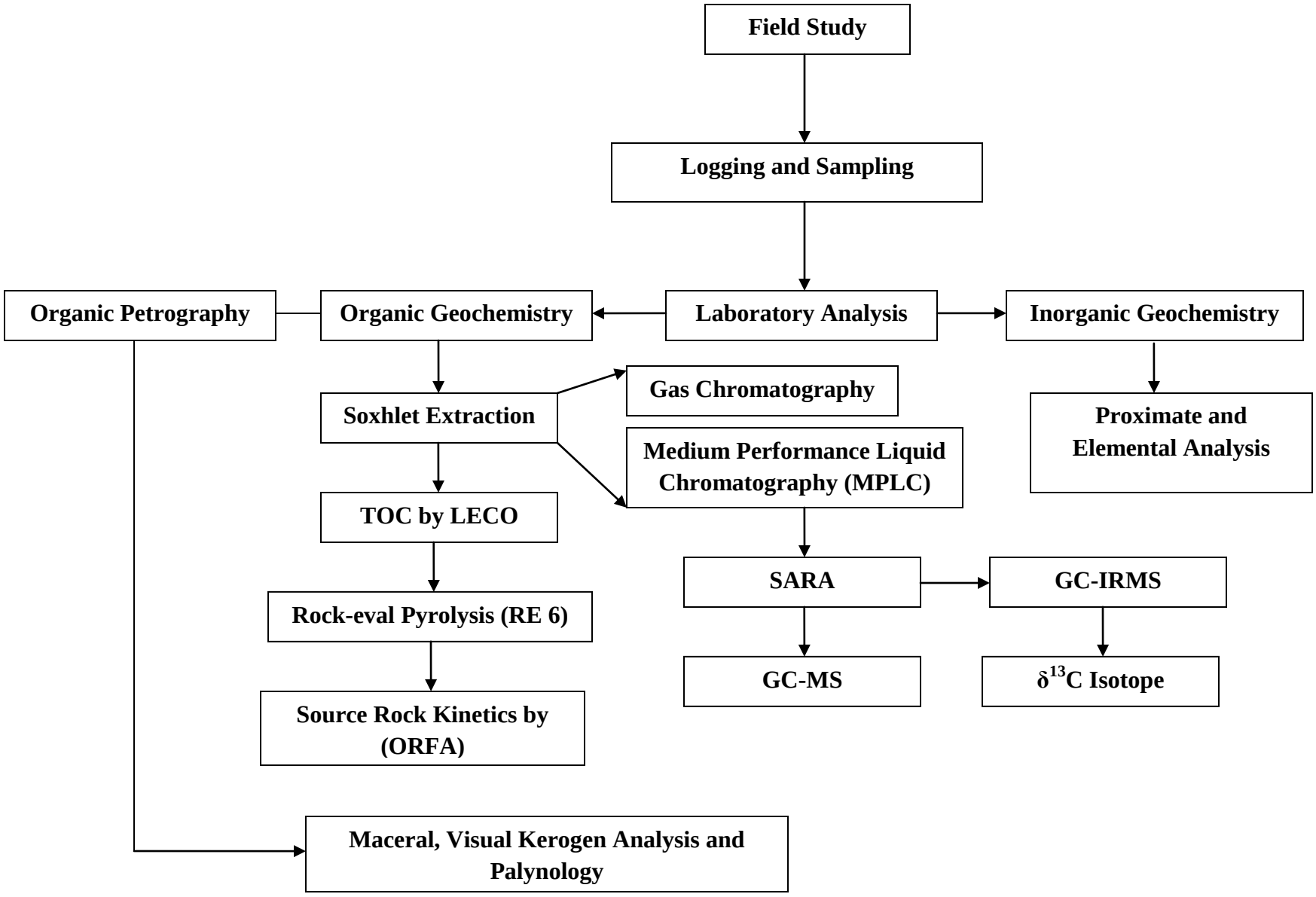


Figure 3.1: Methodology Flow chart. (SARA: Saturate, Aromatic, Resin and Asphaltene, ORFA: One Run Fixed A).

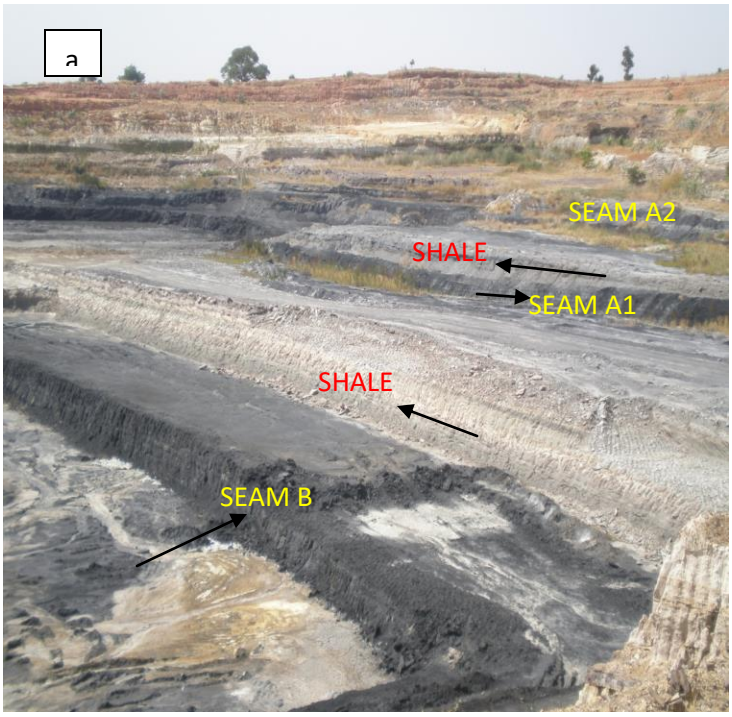




Figure 3.2: a and b, distance view of coal seams with shale interbed at Phase I (10^0 02' 39"N, 11^0 12' 17"E).



Figure 3.3: Distance view of coal seams with shale interbed at Phase II (10^0 04' 46"N, 11^0 12' 23"E).

Table 3.1: Sample codes and analyses carried out for each sample

S/N	SAMPLE CODE	LITHOLOGY	TOC	ROCK EVAL	KINETICS	MPLC	GC	GC-MS	GC-IRMS	ORGANIC PETROLOGY	PALYNOLOGY	PROXIMATE ANALYSIS	ELEMENTAL ANALYSIS
1	MG1A	Coal	✓	✓								✓	✓
2	MG1D	Coal	✓	✓						✓			
3	MG1F	Coal	✓	✓									
4	MG1G	Coal	✓	✓		✓	✓	✓				✓	
5	MG1H	Coal	✓	✓							✓		
6	MG1W	Coal	✓	✓						✓		✓	✓
7	MG1X	Coal	✓	✓									
8	MG2H	Coal	✓	✓		✓	✓	✓	✓	✓		✓	✓
9	MG2O	Coal	✓	✓		✓	✓	✓					
10	MG3D	Coal	✓	✓	✓					✓	✓		
11	MG3Z	Coal	✓	✓	✓				✓	✓			
12	MG4K	Coal	✓	✓	✓	✓	✓	✓			✓		
13	MG2K	C. Shale	✓	✓									
14	MG3S	C. Shale	✓	✓	✓	✓	✓	✓			✓		
15	MG1I	Shale	✓	✓									
16	MG1J	Shale	✓	✓									
17	MG1L	Shale	✓	✓								✓	
18	MG1O	Shale	✓	✓							✓		
19	MG1Q	Shale	✓	✓									
20	MG1R	Shale	✓	✓									
21	MG1Z	Shale	✓	✓							✓		
22	MG2C	Shale	✓	✓									
23	MG2F	Shale	✓	✓							✓		
24	MG2L	Shale	✓	✓						✓			
25	MG2R	Shale	✓	✓					✓	✓	✓		
26	MG4D	Shale	✓	✓	✓	✓	✓	✓		✓	✓		
27	BH15A	Shale	✓	✓	✓					✓	✓		
28	BH15B	Shale	✓	✓	✓	✓	✓	✓	✓		✓		
29	BH15C	Shale	✓	✓	✓						✓		

3.3 Laboratory Studies

Twenty nine (29) samples comprising of coals, coaly shales and shales were selected for various geochemical analyses listed above (Table 3.1). TOC and Rock Eval Pyrolysis were carried out at Weatherford laboratory Houston, Texas, USA and Stratochem Laboratory in Cairo, Egypt. GC, MPLC, GC-MS, GC-IRMS, Source Rock Kinetics, Visual Kerogen Studies were also carried out at Stratochem Laboratory in Cairo, Egypt, Maceral analysis was done at Pearson Coal Petrography in South Holland, Illinois, (USA), while Proximate and Elemental analysis was carried out at Actlab, Ancaster, Ontario Canada. The palynology was carried out at University of Ibadan, Ibadan Nigeria.

3.3.1 Soxhlet Extraction

Extraction was done by dissolving the soluble hydrocarbons from the rock sample by repeatedly flushing the sample with an appropriate solvent. Obvious contaminants were picked from the sample, pulverized and passed through a 40-Mesh sieve. The samples were weighed and placed in a thimble. Dichloromethane was added into a 100ml empty flask. The thimble was placed in the Soxhlet apparatus while the water tap was opened through the condenser. The sample was extracted for at least 16 hours. After extraction, the solvent was evaporated and the flask reweighed to get the extract weight. The extract was subjected to further analysis.

3.3.2 Total Organic Carbon (TOC)

The LECO C230 carbon analyzer (Fig. 3.5) is a microprocessor-based, software-driven instrument for measurement of carbon content. The LECO C230 uses an induction furnace and measures carbon by infrared absorption. The analysis began by weighing out a sample into a ceramic crucible on a balance. The crucible was placed on the loading pedestal. Furnace closure was performed automatically, and then the combustion chamber purged with

oxygen to drive off residual atmospheric gases. After purging, oxygen flow through the system was restored and the induction furnace turned on.

The analytical procedure began by pulverizing and weighing out a sample (Figure 3.4) into a ceramic crucible on a balance and hydrochloric acid was added and placed on a hot plate. The sample was filtered using ashless microfiber filter paper with suction (Buchner system) and placed on a LECO crucible and oven dried.



Figure 3.4: Illustrative picture showing preparation steps in TOC Analysis.



Figure 3.5: LECO C230 Machine (Source- Stratochem Lab)

3.3.3 Rock Eval Pyrolysis

Pyrolysis is the decomposition of the organic matter by heating the sample in the absence of oxygen in RE-6 machine (Figure 3.7). Obvious contaminant was picked from the sample. Each pre-cleaned samples were crushed in mortal using pestle and weighed accurately (100 mg approx.) into the sample holder. The samples are poured into the RE-6 Crucible using a funnel and capped. The crucible was placed in the RE-6 Carousel and the samples analyzed according to the instrument manual. The procedure involved the transfer of each sample into the furnace where it was heated initially at 300^{o}C for three minutes in an atmosphere of helium to release the free hydrocarbons (S_1). Pyrolysis of the bound hydrocarbons to give S_2 peak followed immediately as the oven temperature was increased rapidly to 550^{o}C at the rate of 25^{o}C/min. Both the S_1 and S_2 hydrocarbon peaks were measured using a Flame Ionization Detector (FID). A splitting arrangement permitted the measurement of S_3 peak (carbon dioxide) by means of a thermal conductivity detector (TCD). The following parameters were generated.

S1: The amount of free hydrocarbons in the sample recorded in (mg HC/g Rock). **S2:** The amount of the hydrocarbons generated by thermal cracking of the kerogen in (mg HC/g Rock). **S3:** The amount of CO2 that is produced during the heating of the organic matter (mg CO2/g Rock). **Tmax:** The temperature at which the decomposition rate of kerogen reaches its maximum (Figure 3.6).

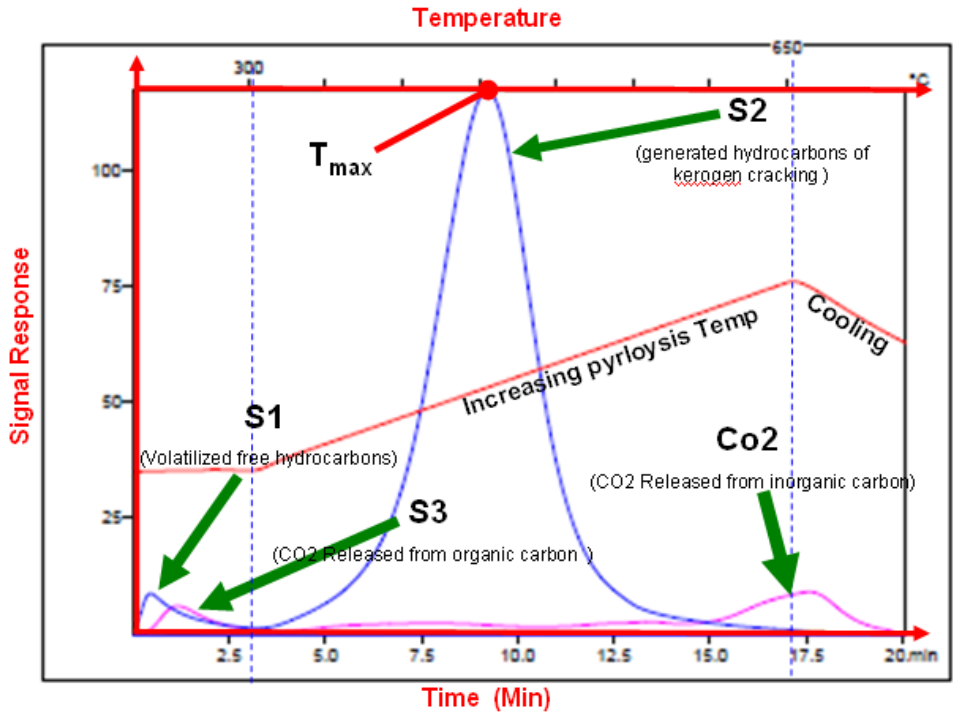


Figure 3.6: Cycle of analysis and example of record obtained by the pyrolysis method.



Figure 3.7: Illustrative picture of RE-6 (Source- Stratochem Lab).

3.3.4 Source Rock Kinetics

The theory of operation is by cracking or breakdown of kerogen molecules by overcoming the barrier of the Activation Energy (Ea). Each kerogen type has its own activation energy range, depending on how many types of organic matter contributed to the kerogen composition and according to its generated hydrocarbons, which is related to its maturity. Kinetics is measured by the Rock-Eval 6 by heating the sample in an inert atmosphere at a specific heating rate where the kerogen decomposes by bond cleavage and releases hydrocarbons that are detected in bulk by Flame Ionization Detector (FID). This method measures activation energy distribution versus the relative abundance of each activation energy. It also employs personalized kinetics i.e analysed by one heating rate which is 25^{o}C/min with initial temperature of 300^{o}C to a final 650^{o}C. The analytical procedure is as follows:

1. The pre-extracted rock free of obvious contaminants was pulverized.
2. The sample was weighed in a Rock-Eval crucible and placed on the RE-6 Carousel.
3. The heating rate was selected and the sample weight recorded by inputting it in the RE-6 software.
4. Once the analysis is completed, the sample was processed using kinetics software (Kinetics 05 or ORFA).

Note: Before running samples, the instrument must be calibrated using IFP standard on the usual pyrolysis method (Bulk Rock) to ensure that the Tmax calculation is correct.

3.3.5 Medium Performance Liquid Chromatography

Medium Pressure Liquid Chromatography (MPLC) is an analytical column chromatographic technique. This method is used for separating the saturate, aromatic and polar fractions of a crude oil or an extract through a pre-column, containing thermally deactivated silica, and a main column of activated silica as the stationary phase with *n*-hexane

as the mobile phase (Figure 3.8). Oil and extracts are first deasphaltened by adding *n*-pentane to the oil or extract (*n*-pentane dissolves the maltene fraction (Saturates, Aromatics and NSO), then agitated well and centrifuged to make sure that all the maltene is dissolved in the *n*-pentane and the asphaltenes precipitated forming a dark layer at the bottom of the vial.

The maltene samples passes through the pre-column and the main column. The aromatics are retained near the head of the main column, while the saturate are eluted from the column and collected. Then, a back flush occurs, reversing the flow of *n*-hexane in the main column and the aromatics are eluted and collected. Resins (NSO compounds) are adsorbed by the pre-column silica and subsequently removed by a mixture of dichloromethane and methanol.

Analytical procedures are stated below:

1- The extract was weighed in an 8 ml vial; *n*-pentane was added, and placed in the ultrasonic bath, then in the centrifuge.

2- Maltene fraction was filtered from the asphaltenes through a glass wool-containing pipette.

3- Weights of the asphaltene and maltene fractions were recorded

4- Maltene fraction was injected into the MPLC.

5- Saturate, Aromatic and NSO fractions were labeled into collection tubes.

6- The saturate, aromatic and NSO was evaporated to a minimum solvent volume using a turbo vap, and then transferred into pre-weighed 4 ml vials.

7- The vials were evaporated on the nitrogen evaporator carefully to remove all solvent and the fraction weight recorded to get their percentages

3.3.6 Gas Chromatography (GC)

Quantitative and qualitative analyses are performed on crude oils and extracts by injecting microliter volumes of the whole oil or extract into a split/splitless injector of a gas chromatograph (GC). A capillary column is used to provide separation of the hydrocarbon

compounds in the *n*-C4 to *n*-C42 carbon range for detection by a flame ionization detector (FID).

The procedures followed include; a 2ml auto sampler vials were used to transfer the extracts from the flask, the extract was then injected into the GC (Figure 3.9) after selecting the appropriate GC method.

3.3.7 Gas Chromatography – Mass Spectroscopy (GC-MS)

Theory of operation is by performing quantitative and qualitative analyses on saturate and aromatic fractions by injecting microliter volumes into a split/splitless injector. A capillary GC column was used to provide hydrocarbons separation. A mass selective detector provides ionization, fragmentation, filtration, and detection of biomarkers. The procedures followed for the saturate fractions include; A 2 ml auto sampler vial was placed and inserted, the saturate fraction was weighed and cholane was added as internal standard. Cyclohexane was added and the fraction injected into the GC-MS (Figures 3.10 and 3.11) after selecting the method. For aromatic, OTP (Orthoterphenyl) was added to serve as internal standard before cyclohexane was added.



Figure 3.8: Illustrative picture of Medium Pressure Liquid Chromatography (MPLC)



Figure 3.9: a) Illustrative picture of Agilent 6890N GC system/Agilent 7683B series Injector and b) Hewlett Packard (HP) 6890 Series GC System/ (HP) 6890 series injector. (Source- Stratochem Lab).



Figure 3.10: Saturate GC-MS. (Source- Stratochem Lab).



Figure 3.11: Aromatic GC-MS. (Source- Stratochem Lab).

3.3.8 Gas Chromatography – Isotope Ratio-Mass Spectroscopy (GC-IRMS)

Isotope-ratio mass spectrometry (IRMS) is a aspect of mass spectrometry, in which mass spectrometric methods are used to measure the relative abundance of stable (non-radioactive) isotopes in a given sample. Coupled with the Flash 2000 HT Plus and ConFlo IV, the Delta V Advantage Isotope Ratio MS can measure the isotopic ratios of a complex mixture of gases after they have been separated and then converted into simple gases. For carbon/sulfur isotopic analysis, the analysis requires the bulk combustion of the sample followed by separation of products, which are then sent to the isotope ratio mass spectrometer for ionization, separation, and detection. The samples are weighed in a tin capsule and squashed until it becomes a cube and no air is present inside. It is then placed into auto sampler and analyze.

3.3.9 Organic Petrology (Maceral Analysis)

The analysis focused on coal macerals and was determined by reflected light microscopy on polished specimens made from crushed samples mounted in epoxy resin. The polished briquettes were prepared from crushed 1 mm-size samples and mounted in epoxy resin. Ordinary white reflected light from a tungsten lamp and violet-blue light from a high-pressure mercury lamp was used to initiate fluorescence. Maceral observation was carried out on a Leitz MPV-2 photomicroscope. The composition of maceral was determined by means of a swift automatic point counter; each composition was based on at least 500 counts. The preparation and polishing of the specimens were done in accordance with Standard Association of Australia (1977). The methods used in estimating the organic abundance of organic matter and maceral composition were outlined in Cook & Kantsler (1982), Sappal (1986) and Struckmeyer & Felton (1990). The results were expressed as semi quantitative volumetric percentages of the various microscopically recognizable macerals including mineral matter of the coal, which was defined by their colour and morphology.

3.4 Organic Petrology (Vitrinite Reflectance, Visual kerogen and Palynology)

The term “kerogen” refers to the fossil organic matter in sedimentary rocks that is insoluble in common organic solvents (Durand, 1980). Palynological and Petrographic examination of kerogen is commonly done after separating the organic matter from the rock matrix using HF and HCL acids. The kerogen sample was prepared by cleaning 20-40g of the sample to eliminate any contamination and then crushed to fragments. The crushed samples were first treated with HCL acid to remove carbonates and HF acid to remove silicates. A heavy liquid ($ZnCl_2$) was added to concentrate the kerogen. After decantation, the organic residue was sieved at 10µm (micron mesh) sieve, and a portion of the retained material strew was mounted on glass slide for kerogen and fluorescence studies using transmitted and fluorescence Microscopy. Techniques of microscopic examinations (Transmitted, UV fluorescence and Light reflectance) were applied to the isolated kerogen. For palynological analysis, the microscopic studies was performed on strew slides of kerogen concentrate sample using transmitted white light and UV fluorescence mode. The organic matter type was identified using the translucency and shape of particles, and in some cases their fluorescence.

For ultraviolet light microscopy (fluorescence), each slide in this study was examined under incident blue light fluorescence using a Zeiss Axio-A1 Scope at X50 magnification. This was primarily to determine the preservation state of palynomorphs and amorphous organic matter present, according to the fluorescence preservation of Tyson (1995).

For reflected light microscopy, the kerogen macerals were mounted in small plastic plugs mixed with resin and hardener (epoxy) after the separation from the whole rock sample using standard palynological technique. The plugs were polished using 4 grades (320 grit, 600 grit, 1000 grit & 4000 grit), followed by polishing by alumina suspension and microcloths. Polished plug was mounted on the microscopic stage and drop of oil was placed

on the surface of the plug for reflectance analysis (vitrinite reflectance measurements). Petrological observation and vitrinite reflectance measurements were made on a Zeiss Axio-1 Scope (linked to Spectra Vision software for data acquisition) and using an X50 oil objective. Vitrinite reflectance data was gathered by measuring the random reflectance of up to 48-50 individual particles of vitrinite macerals. The data were stored and exported as histogram (Appendix IV).

3.4.1 Proximate Analysis

Proximate analysis of five coal samples (MG1A, MG1G, MG1W, MG2H and MG2P) was carried out to determine the moisture content, volatile matter, ash, fixed carbon and calorific value.

Moisture

The procedure for determining the moisture was done out by placing a sample of powdered raw coal of size 200-micron size in an uncovered crucible and placed in the oven at 108 ± 2^0C along with the lid. The sample was allowed to cool to room temperature and weighed again. The loss in weight represents moisture. Mathematically, % Moisture = % M = (Y-Z/Y-X) *100.

Where X represent the weight of crucibles in gms,

Y represents the weight of coal + crucibles in gms (before heating)

Z represents the weight of coal + crucibles in gms (After heating).

Volatile Matter

Fresh coal sample was crushed and weighed, placed in a covered crucible, and heated in a furnace at 900 ± 15^0C. The sample was cooled and weighed. Loss of weight represents moisture and volatile matter. The residue is the coke (fixed carbon and ash). Mathematically,

% V.M = (Y-Z/Y-X)*100

Where X represents weight of crucibles in gms

Y represents weight of coal + crucibles in gms (before heating)

Z represents weight of coal + crucibles in gms (after heating)

Fixed carbon, % C= 100-(%M+%V.M+%Ash)

Fixed Carbon and Ash

The cover from the crucible used in the last test was removed and the crucible was heated over the Bunsen burner until all the carbon burned. The residue was weighed, which is the incombustible ash. The difference in weight from the previous weighing is the fixed carbon. In actual practice, fixed carbon can be derived by subtracting from 100 the value of moisture, volatile matter and ash.

% Ash = (Z-X/Y-X)*100

Where X represents weight of crucibles in gms

Y represents weight of coal + crucibles in gms (before heating)

Z represents weight of coal + crucibles in gms (After heating)

3.4.2 Elemental Analysis

Three coal samples (MG1A, MG1W and MG2H) was analysed by Inductively Coupled Plasma-Mass Spectroscopy (ICP-MS) with data being acquired for 10 major elements (Si, Na, K, Al, Ti, Fe, Mg, Ca P, and Mn), 30 trace elements, (Ba, Be, Ta, Th, U, Co, W, Zr, Ge, Mo, Br Cs, Ga, Hf, Nb, Rb, Sn, Sr, V, Y, In, Tl, Au, As, Cl, Cr, Sb, Sc, and Se) and 14 rare-earth elements (La, Ce, Pr, Nd, Sm, Eu, Gd, Tb, Dy, Ho, Er, Tm, Yb and Lu) according to the following procedures: Each sample was dried at (60°C) and sieved to -80 mesh. About 250g aliquot was riffle splitted and pulverized to 85% passing 200 meshes (75 µm) in a mild-steel and puck mill.

A 0.2 g aliquot was weighed into a crucible and mixed with 1.5g of lithium metaborate/tetraborate flux ($LiBO_2/Li_2B_4O_7$). The crucibles was placed in an oven and heated to 980°C for 30 minutes. The cooled bead was dissolved in 5% (HNO_3). Reagent blanks and

calibration standards was added to the sample sequence. To avoid contamination, all samples were washed thoroughly using deionised water prior to preparation for ICP analyses. Loss on ignition (LOI) was determined by igniting a 1g sample split at 950°C for 90 minutes then measuring the weight loss.

CHAPTER FOUR

RESULTS AND DISCUSSION

4.1. Lithostratigraphy and Sedimentology of the Gombe Formation

Seven (7) stratigraphic sections in the following localities were studied (Zange, Liji, Mallam inna, Riman, Maiduku, Bobona and Garin Magaji. (Phase I and II) and one borehole at Maiganga mine were also studied to establish facies variation and depositional environments.

4.1.1 Lithologic Description at Maiganga

The lithologic units of Gombe Formation in Maiganga were exposed due to mining activities. The lithologic units at Maiganga coal mine comprises of coal seams, shales, siltstones, sandstones and intercalation of ironstones (Figures 4.1, 4.2 and 4.3).

4.1.1.1 Sandstone

This facies occur in the upper part of the Maiganga section directly below the overburden (Figure 4.4). The thickness is about three meters (3m). The sandstones are reddish in color, poorly sorted and thinly laminated internally. The quartz grains are sub-angular to angular. The sandstone bed coarsens upward suggesting fluctuation in energy of transporting medium. Sedimentary structures that were visible include bioturbation and weak parallel lamination (Figure 4.4). The sandstones are immature due to high feldspar content. Clay clasts were observed and may be due to dissolution of the feldspar grains.

4.1.1.2 Clayey Siltstone

The clayey siltstones at Maiganga underlie the sandstone unit with thickness of 9.8m (Figure 4.5). The siltstones are friable, clayey, and whitish to brownish yellow in colour. This unit also occurs as interbeds within the underlying shale and coal sequences. The clayey siltstone bed has parallel lamination and makes sharp contact with the underlying shale (Figure 4.6). In some part, burrows were observed.

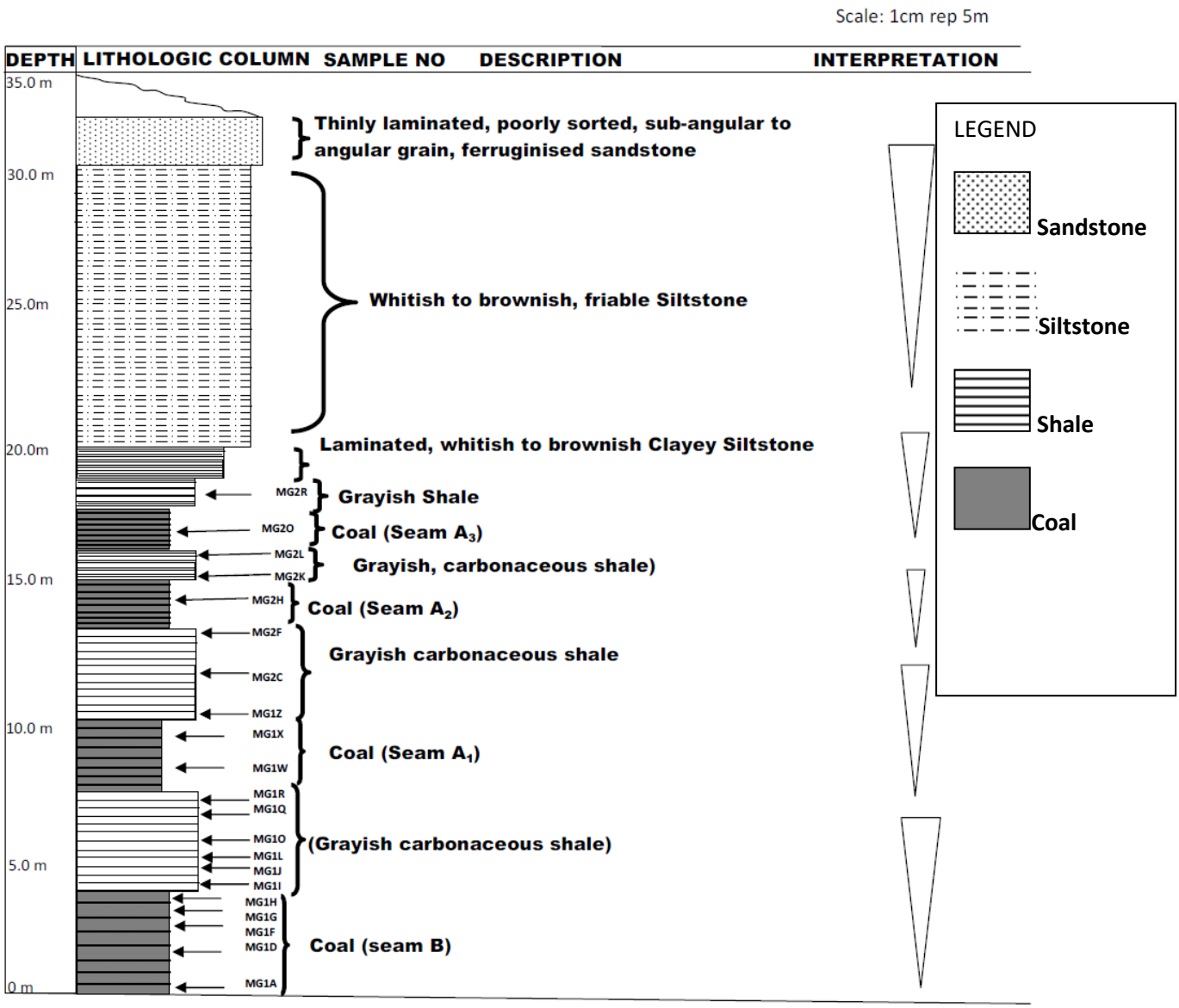


Figure 4.1: Lithologic succession of Gombe Formation exposed at the Maiganga mine. The coarse upward sequence from the base begins with coal, shale, siltstone to sandstone. The arrows indicate the selected samples. Phase 1, Coordinates: (10^0 02' 39"N, 11^0 12' 17"E).

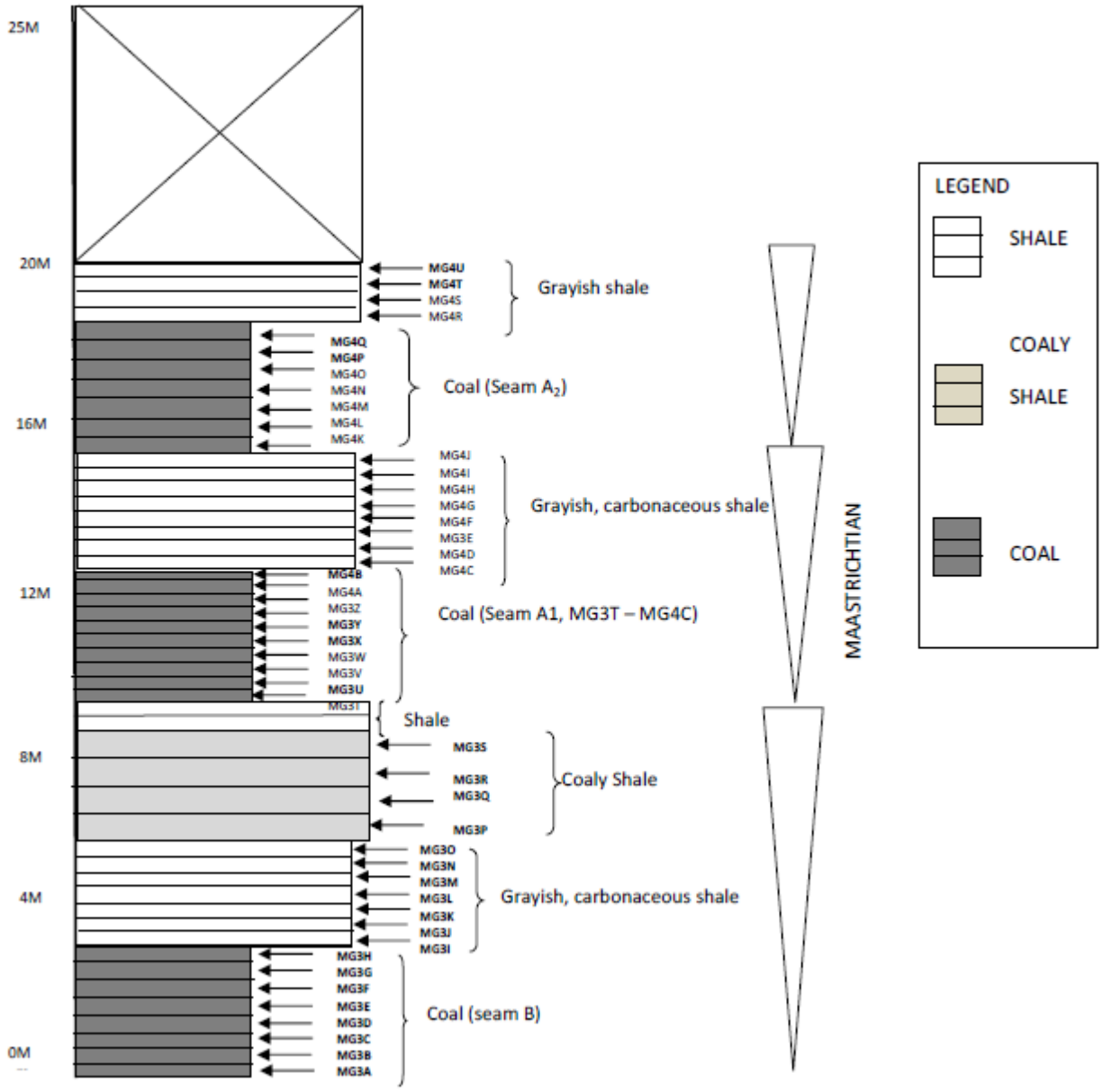


Figure 4.2: Lithologic succession of Gombe Formation at the Maiganga mine. The coarse upward sequence from the base begins with coal, shale, coaly shale. The star symbol indicates the selected samples. Phase 2, Coordinates: (10^0 04' 46"N, 11^0 12' 23"E).

meters			Lithology	Lithological description	
Depth from	Depth To	Thickness			
0.00	0.30	0.30		Top soil	
0.30	3.00	2.70		Clay reddish brown Sandstone	
3.00	6.50	3.50		Clayey Siltstone	
6.50	6.70	0.20		Indurated Ironstone	
6.70	9.00	2.30		Carbonaceous shale	
9.00	9.50	0.50		Indurated Ironstone	
9.50	12.00	2.50		Carbonaceous shale	→ BH15A
12.00	12.50	0.50		Indurated Ironstone	
12.50	20.00	7.50		Carbonaceous shale	→ BH15B
20.00	20.20	0.20		Well indurated Ironstone	
20.20	23.50	3.30		Yellowish Clayey siltstone	
23.50	27.00	3.50		Ironstone	
27.00	42.00	15.00		whitish-yellowish laminated friable siltstone	
42.00	50.00	8.00		grayish, well compacted carbonaceous shale	→ BH15C

Figure 4.3: Litholog of Borehole 15 at Maiganga. GPS: x = 734251, y = 1105749, z = 458. Arrow indicates selected samples. The log shows shale, siltstone and ironstone intercalation.



Figure 4.4: Coarse-grained and weakly laminated Ferruginised sandstone at Maiganga. The sandstones are bioturbated and immature due to high feldspar content and presence of clay clast (10^0 02' 39"N, 11^0 12' 17"E).



Figure 4.5: Friable, whitish to brownish colour weakly laminated (localized) clayey siltstone at Maiganga (10^0 02' 39"N, 11^0 12' 17"E).

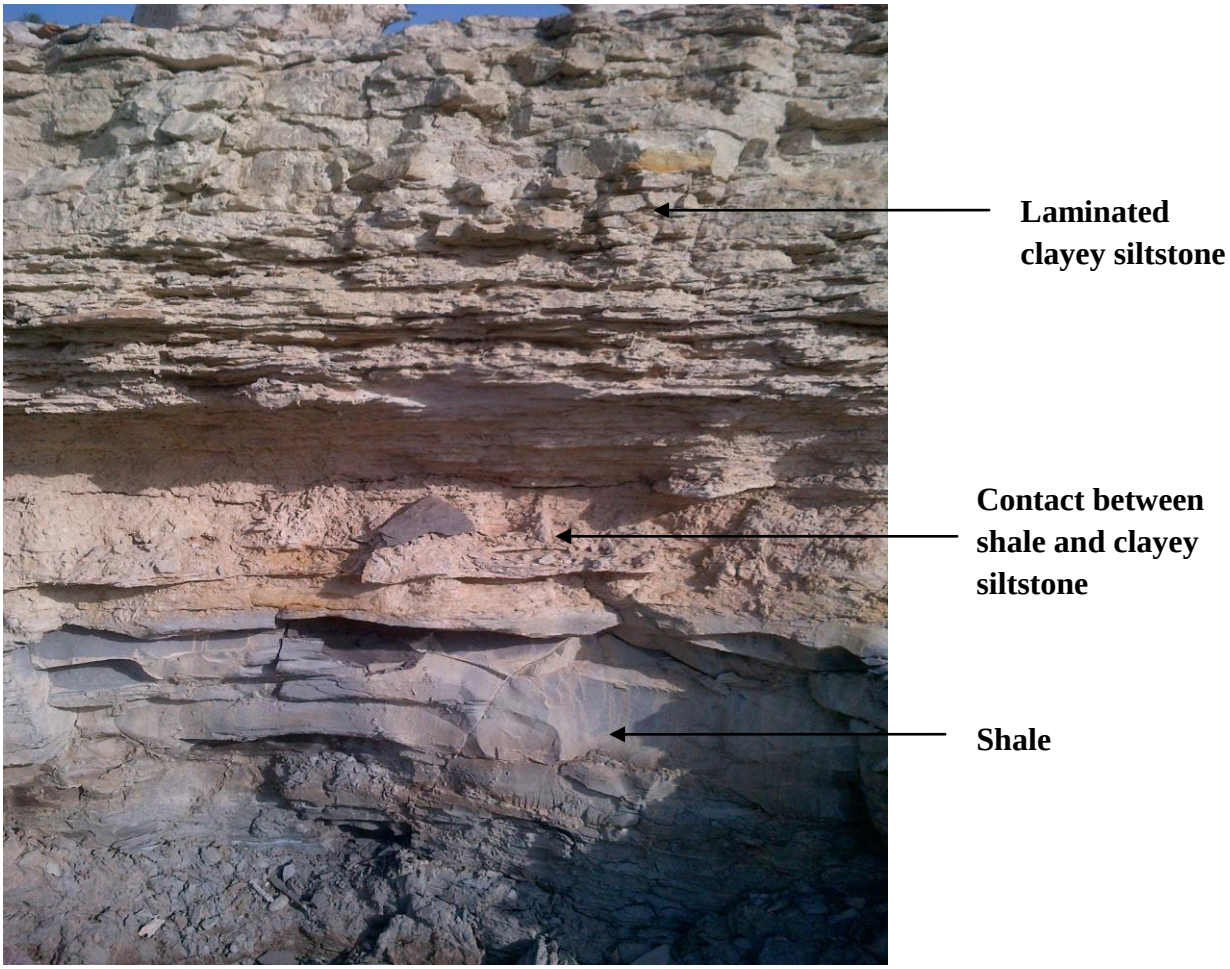


Figure 4.6: The clayey siltstone interbedded with the shale at Maiganga. The contact between shale and clayey siltstone were noticeable (10^0 02' 39"N, 11^0 12' 17"E).

4.1.1.3 Coaly Shale- Shale

The shale facies at Maiganga underlie the clayey siltstone. The shales are very compacted and flaggy (Figure 4.7). It is grayish in color, carbonaceous and has imprint of plant fossil preserved. It also occurs as interbed within the coal unit (Figure 4.8). The maximum thickness of the shaly unit in the succession is 6m. Specks of phytoclasts (dark patches of preserved plants debris) were observed in the lower part of the bed.

4.1.1.4 Coal

The Maiganga coal is made up of two seams, namely seam A and B. Seam B occurs at the base of the section (Figure 4.1 and 4.2). The coal is the first bed with thickness of 4.3m (seam B) in phase I, (Figure 4.1, 4.9) and about 3m in phase II (Figure 4.2). It is overlain by shale and clayey siltstone unit. Seam A has three sub-seams namely seam A_1, seam A_2 and seam A_3 with thickness of 2.4, 1.8 and 1.4 meters respectively (Figure 4.8). The coal seams have interbeds of shale. In hand specimen, the coals has a dull lustre and dark in colour. Cleat and partitions were observed in the seams probably from dehydration, stresses in the upper crust during coalification or devolatilization (Figure 4.10). These coal seams occur between the depth of 17 to 32m (Figures 4.1 and 4.2).

4.1.2 Lithologic Description at Zange

At Zange, the thickness of the exposure is about 2.35m (Figure 4.11). Lithologies observed include light grayish mudstone, brownish clayey siltstone, thinly laminated ferruginised siltstone and fine grained massive sandstone units. The mudstone has thickness of 0.2m (Figure 4.13) and is suceeded by milky to brownish color clayey siltstone which has a thickness of 1m with parallel lamination (Figure 4.12). It grades upward into a fine grained sandstone of 0.5m.

4.1.3 Lithologic Description at Liji

The lithologic units seen at Liji are shale and siltstones. The exposure is 3.2m thick (Figure 4.14). The shale is grayish and fissile with thickness of 0.8m. This is succeeded by whitish, parallel laminated to massive clayey siltstone of 0.6m and 1m thick respectively.

4.1.4 Lithologic Description at Mallam Inna

The channel exposure is 3.8m thick consisting of siltstone and sandstone (Figure 4.15). The siltstone is whitish in colour and it is parallel stratified with thickness of 1.2m. This is succeeded by whitish massive siltstone with thickness of 1.1m and finally grades into brownish, massive poorly sorted sandstone unit of about 1.5m.

4.1.5 Lithologic Description at Riman

The lithogic succession in this location consist mainly of siltstones. The thickness of the section is 5.8m (Figure 4.16). The siltstones are whitish, brownish-yellowish in colour, and ranges from parallel stratified to massive siltstone.

4.1.6 Lithologic Description at Maiduku

The thickness of this surface exposure is 2m (Figure 4.17). The lithologic succession consist of shale, clayey siltstone and sandstone. The siltstones are whitish-brownish in colour, friable and parallel stratified. The clayey siltstones are interbedded and it is suceeded by light grey fissile shale. The upper part of this section has the sandstone which are brownish, massive and fine grained (Figure 4.18).

4.1.7 Lithologic Description at Bobona

Lithologies unit seen at Bobona are mainly clayey siltstone and shale. The thickness of this section is 2.7m (Figure 4.19). The clayey siltstones are brownish- reddish in colour (Figure 4.20) and are laminated occuring at the lower part and upper part section. The shale are light grey and weakly laminated (Figure 4.21).

4.1.8 Lithologic Description at Garin Magaji

The thickness of this section is 2.4m (Figure 4.22). Lithologies seen are mainly clayey siltstone/shale intercalation intercalation. The siltstone are parallel stratified (Figure 4.23), it has brownish – milky colour. The sandstone are reddish and medium grained at the upper part of the section.



Figure 4.7: Grayish well compacted carbonaceous shale at Maiganga (10^0 02' 39"N, 11^0 12' 17"E).



Figure 4.8: Shale interbedded with coal at Maiganga (10^0 02' 39"N, 11^0 12' 17"E).



Figure 4.9: Panoramic view of Maiganga mine. Coal seams at the base grades into shale, siltstone and sandstone indicating coarsening upward sequence (10^0 02' 39"N, 11^0 12' 17"E).



Figure 4.10: Seam B coal, dull in luster having cleat (fracture) probably from dehydration or stresses in the upper crust during coalification (10^0 02' 39"N, 11^0 12' 17"E).

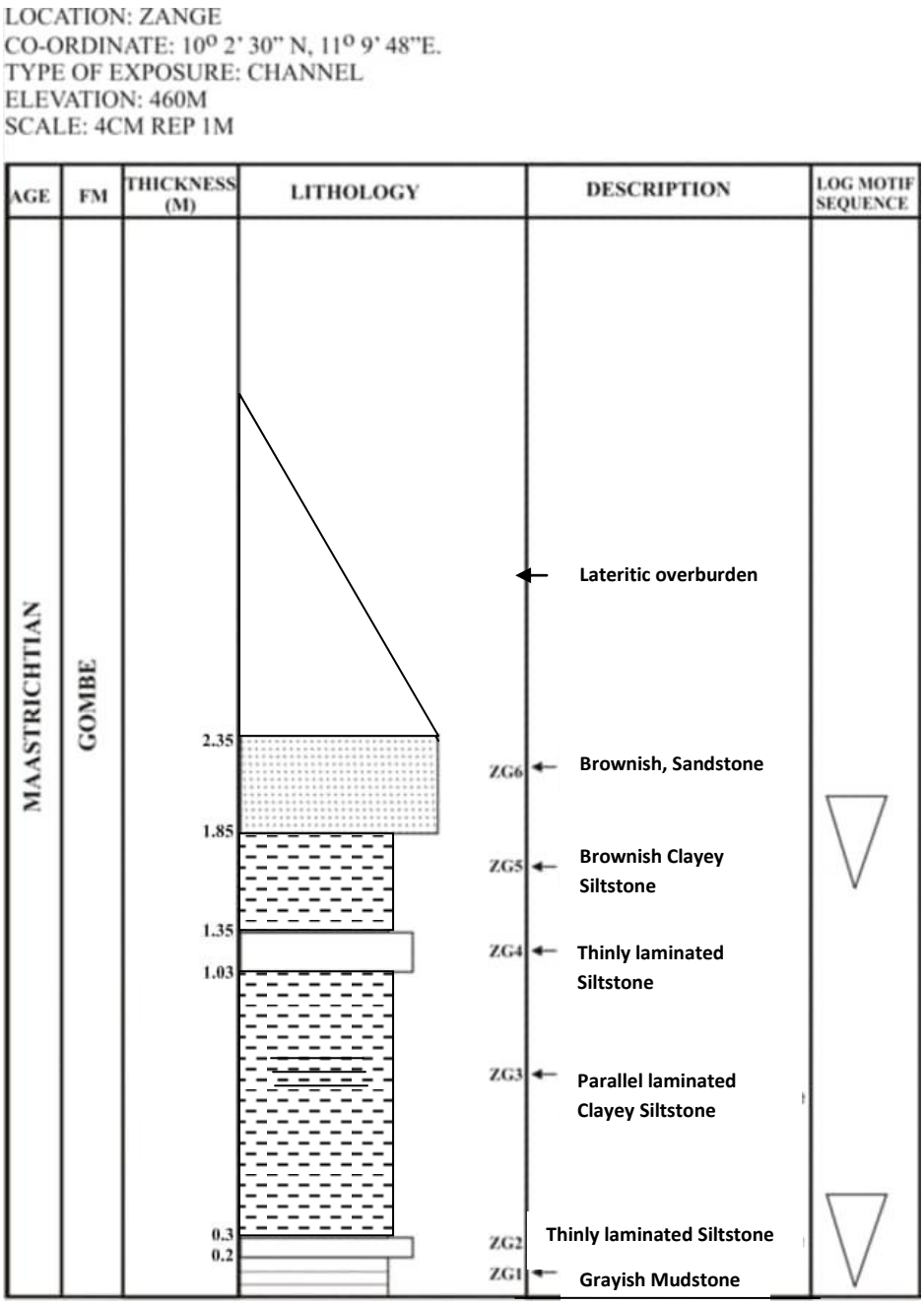


Figure 4.11: Lithologic section of the Gombe Formation exposed at Zange village (10^{o} 2^{I} 30^{II}N, 11^{o} 9^{I} 48^{II}E).



Figure 4.12: Field photograph of thinly laminated brownish clayey siltstone at Zange village (10^{o} 2^{I} 30^{II}N, 11^{o} 9^{I} 48^{II}E).



Figure 4.13: Field Photograph of grayish mudstone at Zange village (10^{o} 2^{I} 30^{II}N, 11^{o} 9^{I} 48^{II}E). Mudcrack indicate the presence of clay.

LOCATION: LIJI
CO-ORDINATE: 10° 16' 33" N, 11° 14' 16"E.
TYPE OF EXPOSURE: ROAD CUT
ELEVATION: 400M
SCALE: 4CM REP 1M

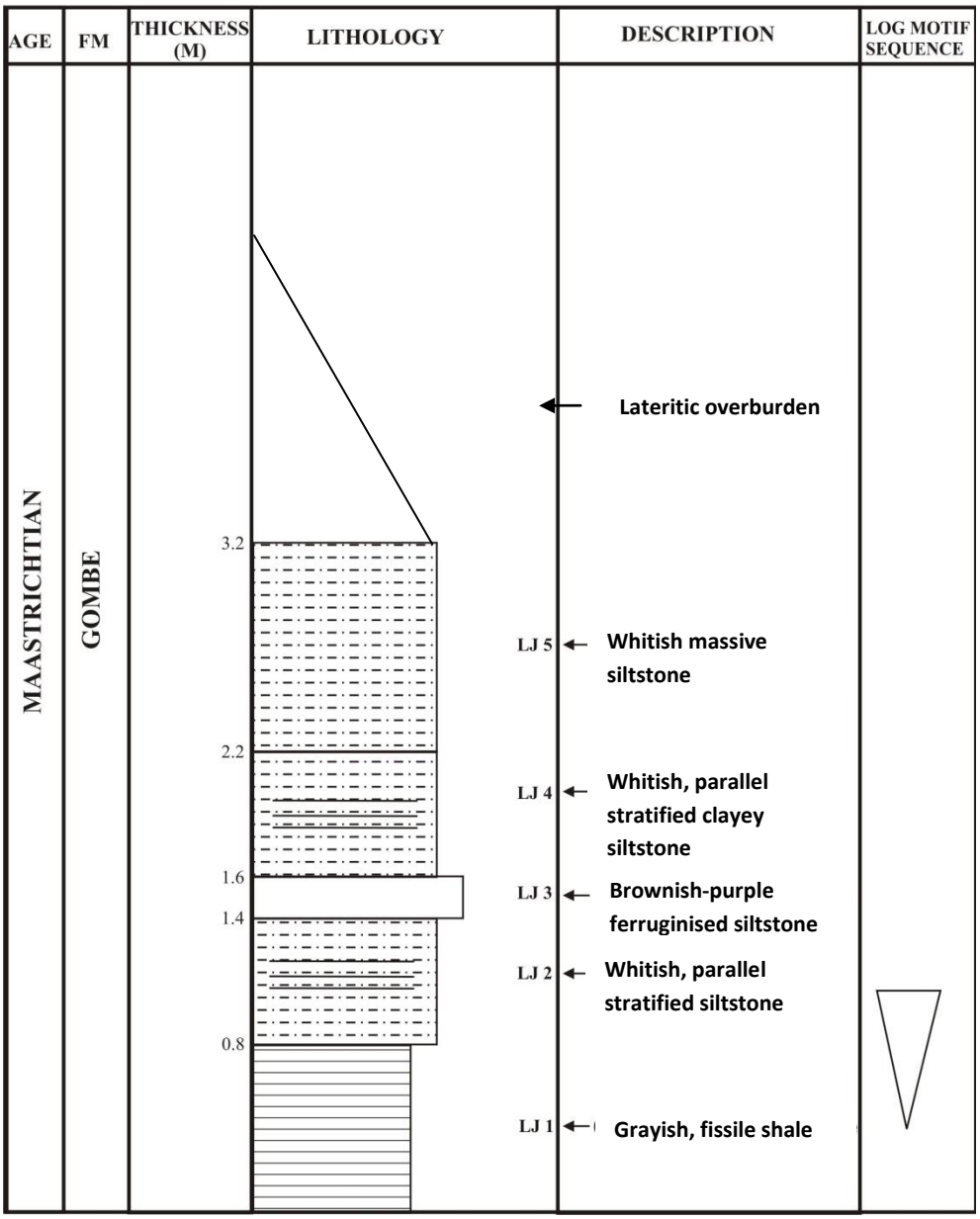


Figure 4.14: Lithologic section of Gombe Formation exposed at Liji village.

LOCATION: MALLAM INNA
CO-ORDINATE: 10° 18' 17" N, 11° 11' 09"E.
ELEVATION: 420M
SCALE: 4CM REP 1M

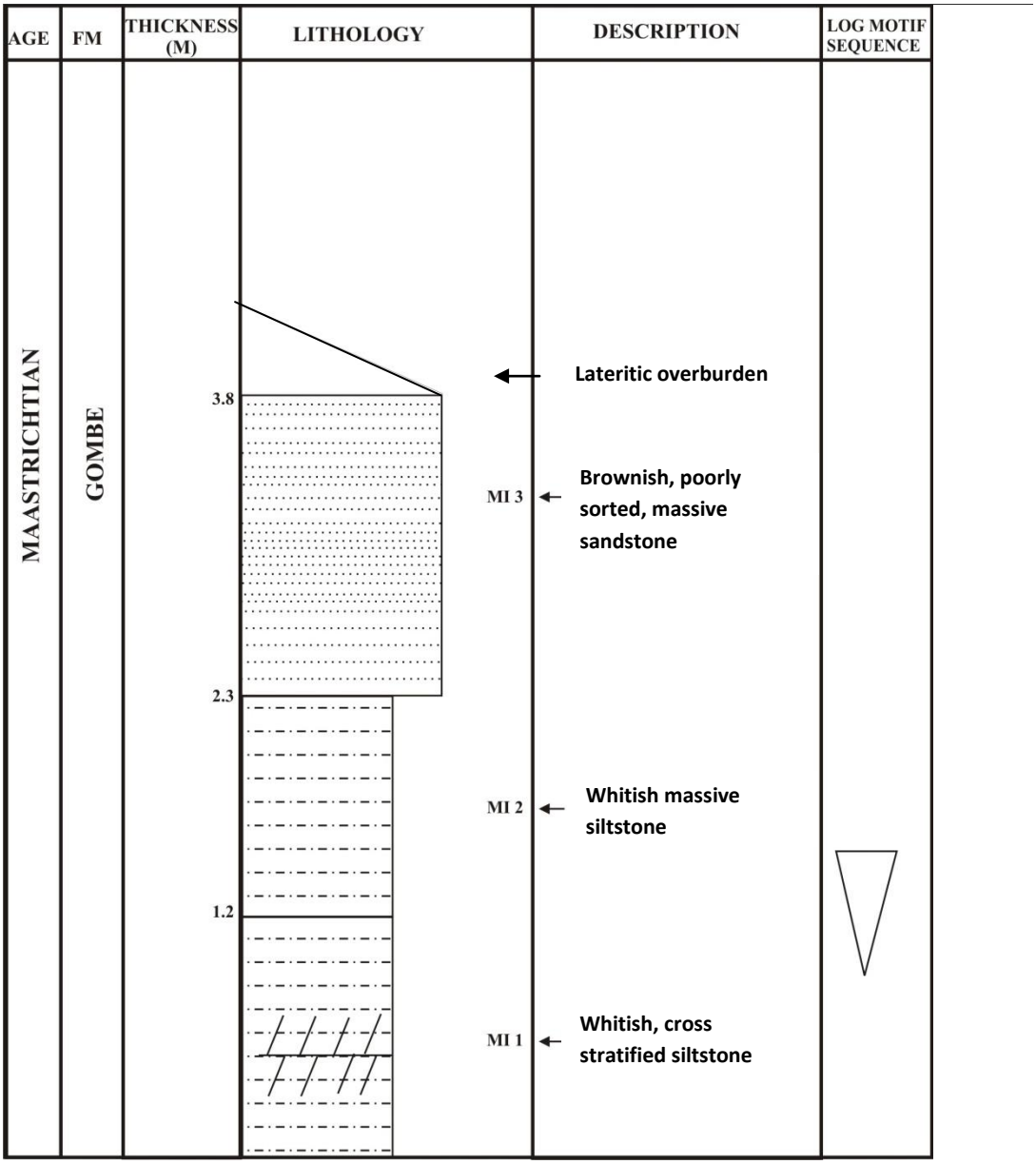


Figure 4.15: Lithologic section of Gombe Formation exposed at Mallam Inna.

LOCATION: RIMAN
CO-ORDINATE: 10° 10' 10" N, 11° 09' 35"E.
TYPE OF EXPOSURE: RIVER CHANNEL
ELEVATION: 516M
SCALE: 2CM REP 1M

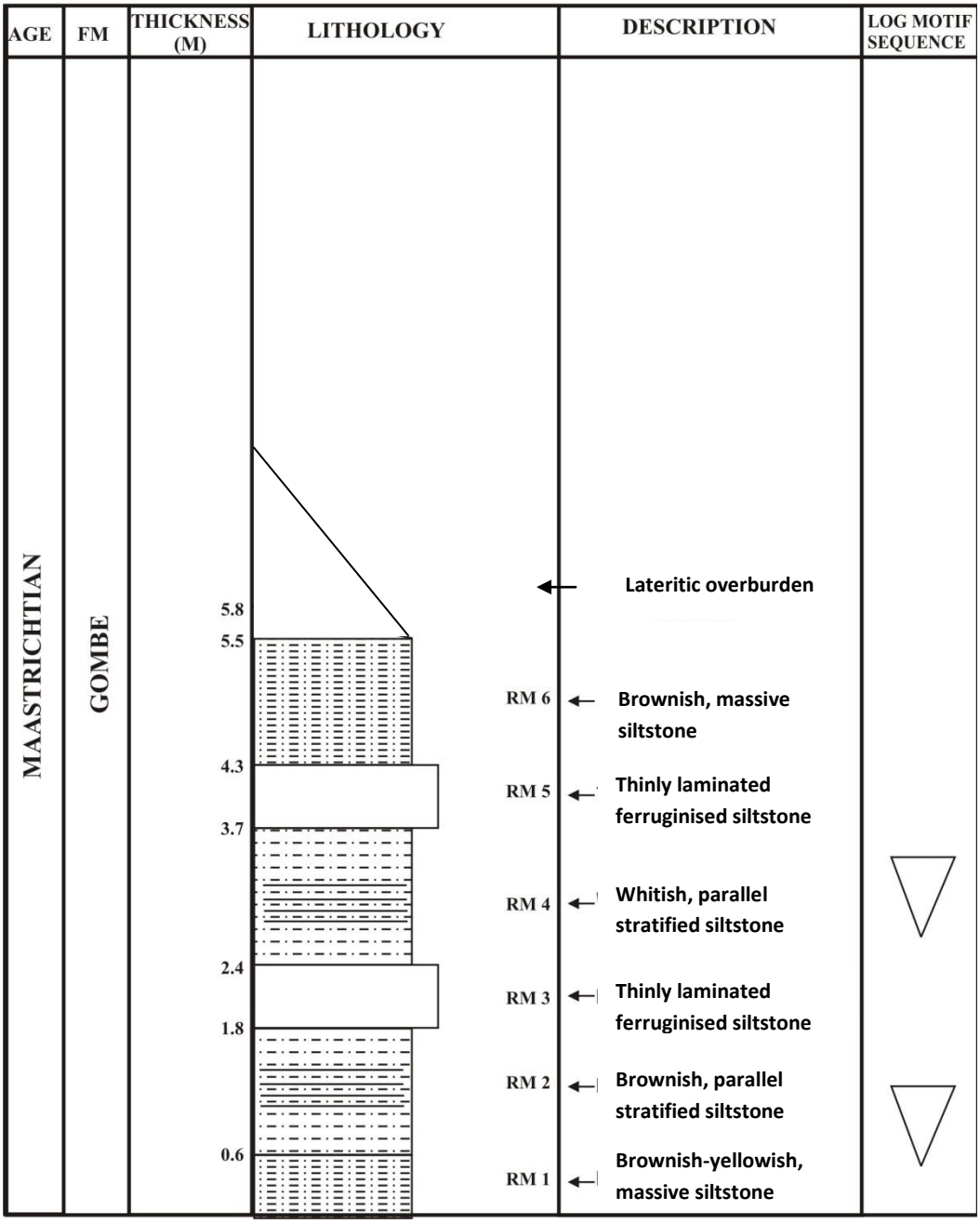


Figure 4.16: Lithologic section of Gombe Formation exposed at Riman village.

LOCATION: MAIDUKU
CO-ORDINATE: 10^{O} 08' 26" N, 11^{O} 11' 23"E.
TYPE OF EXPOSURE: OPEN PIT
ELEVATION: 442M
SCALE: 4CM REP 1M

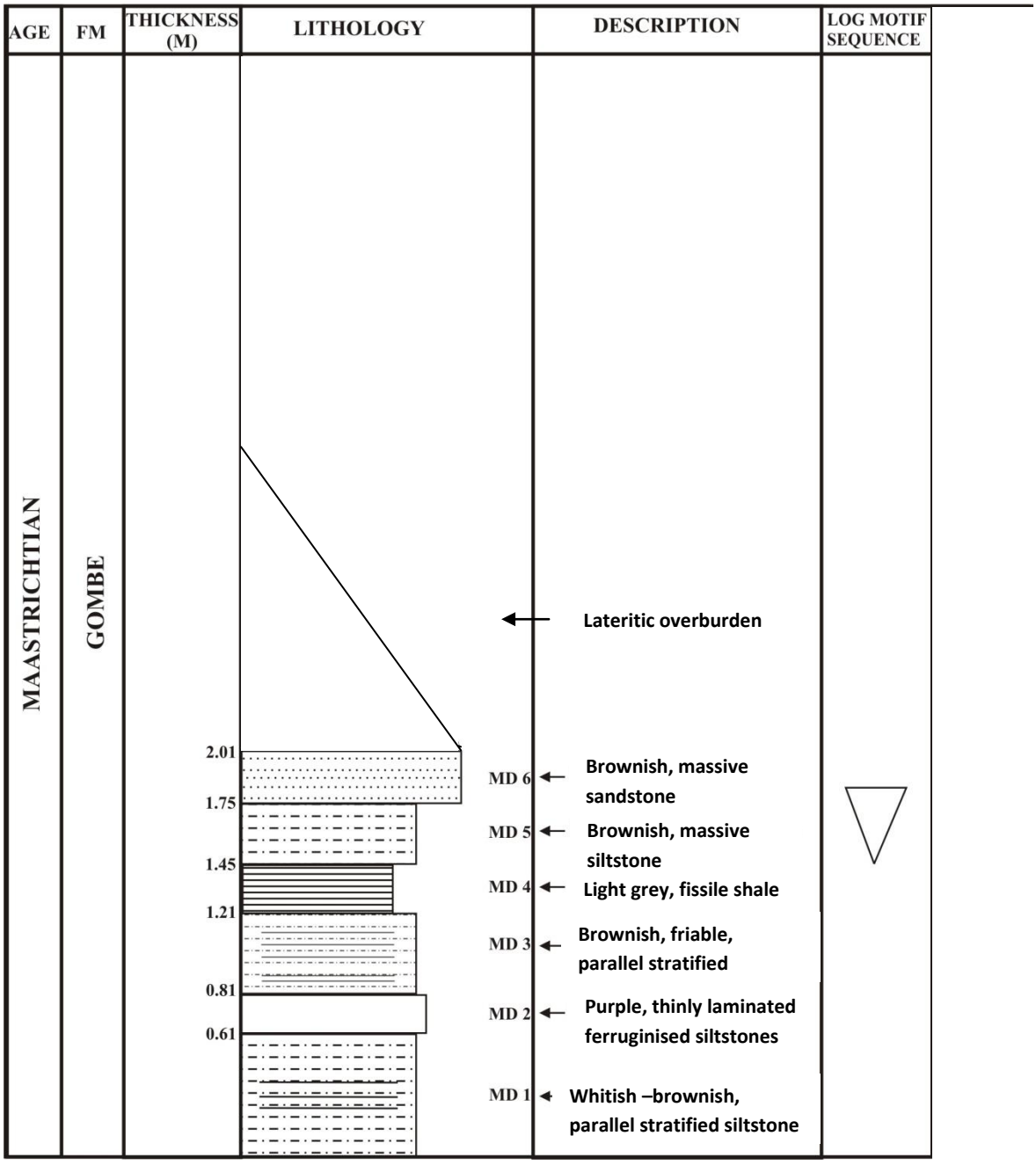


Figure 4.17: Lithogic section of Gombe Formation exposed at Maiduku village. It shows thinly laminated clayey siltstone at the base, shale at the middle section and siltstone and sandstone at the top.

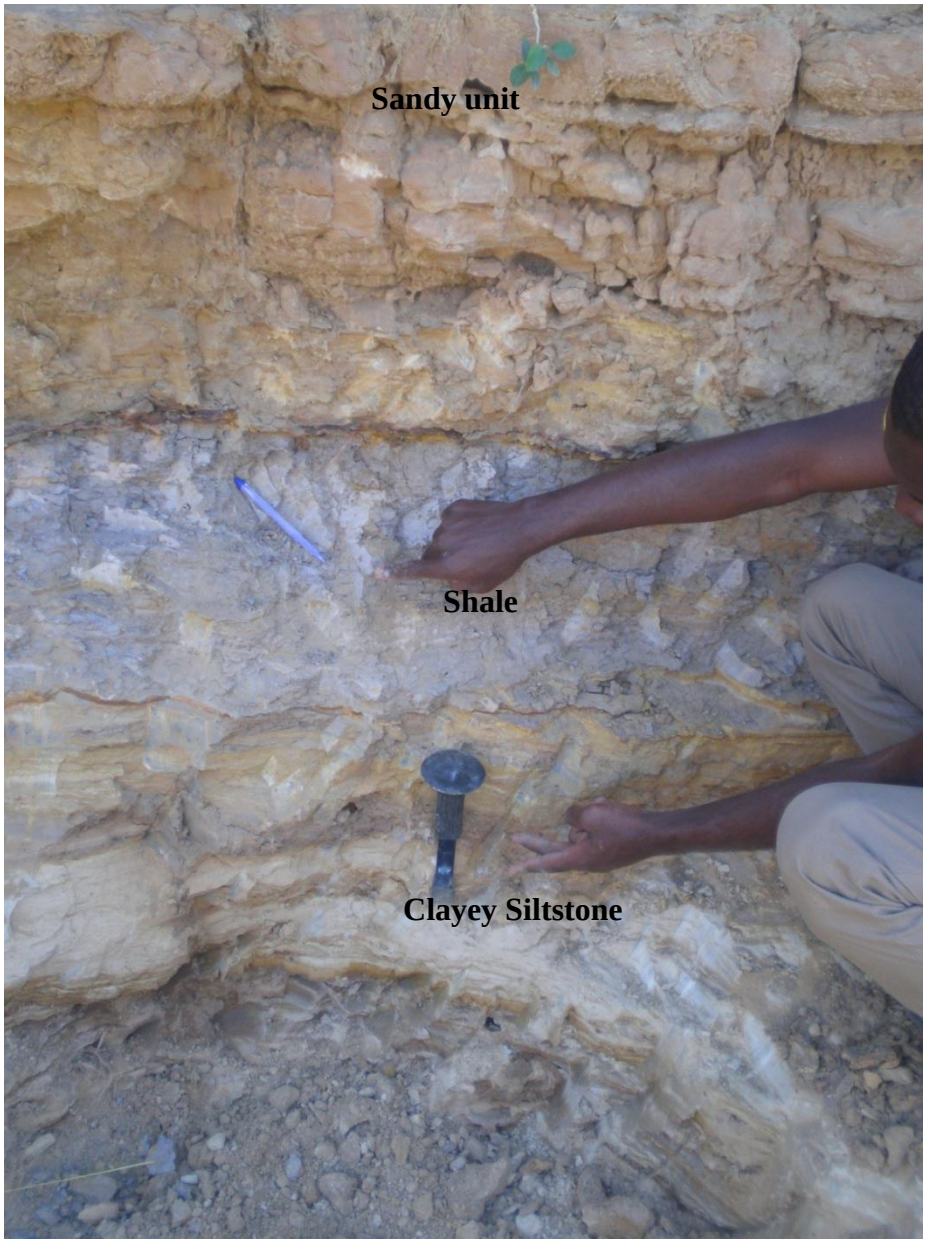


Figure 4.18: Field photograph showing thinly laminated clayey siltstone unit, grayey shale and the fine grained sandstone unit at Maiduku village (10^{o} 08^{I} 26^{II}N, 11^{o} 11^{I} 23^{II}E).

LOCATION: BOBONA
CO-ORDINATE: 10^{O} 15' 02" N, 11^{O} 12' 03"E.
ELEVATION: 443M
SCALE: 4CM REP 1M

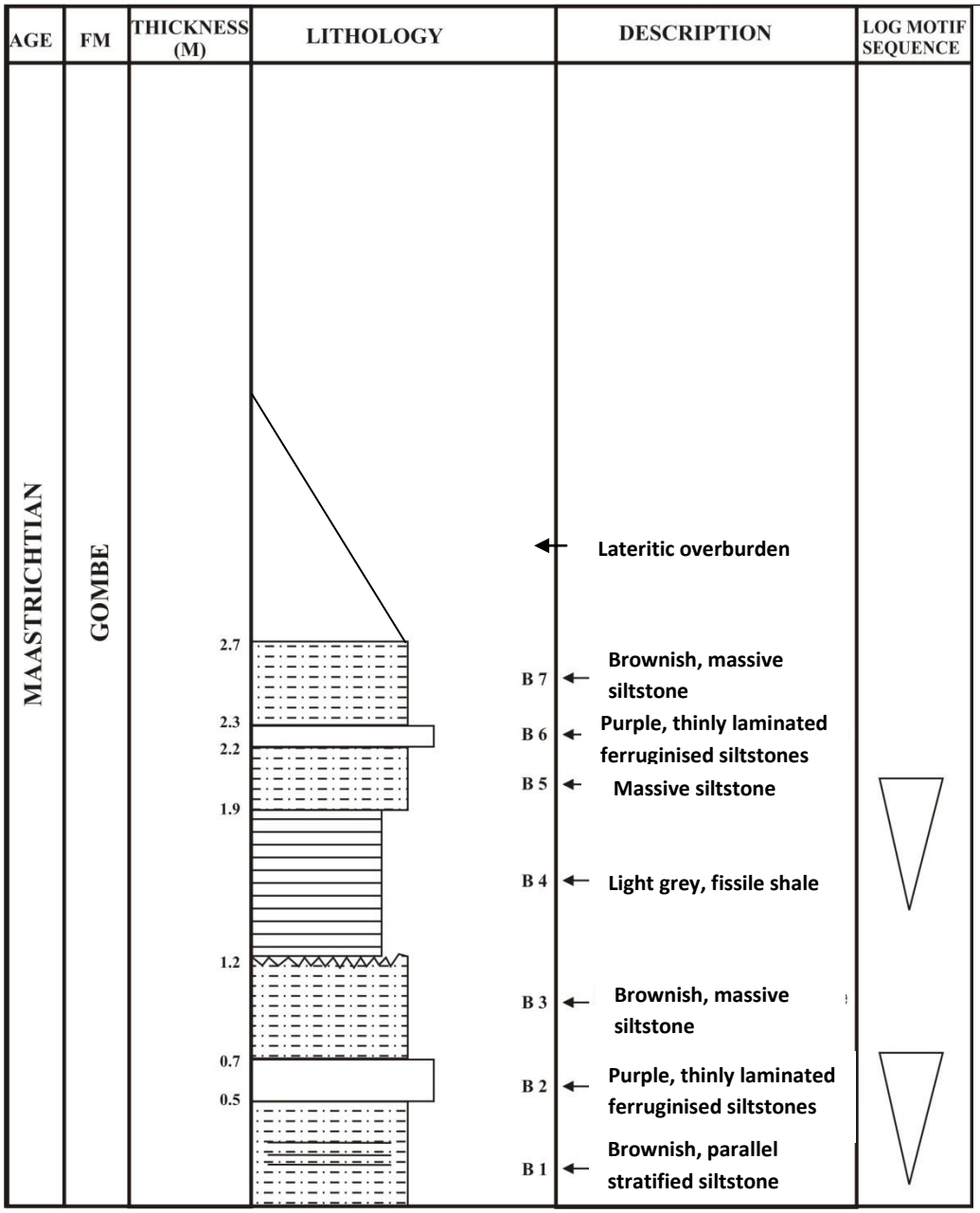


Figure 4.19: Lithologic section of Gombe Formation exposed at Bobona village.



Figure 4.20: Field photograph of thinly laminated clayey siltstone exposed at Bobona (10^{o} 15^{I} 02^{II}N, 11^{o} 12^{I} 03^{II}E).



Figure 4.21: Field photograph of shale exposed at Bobona (10^{o} 15^{I} 02^{II}N, 11^{o} 12^{I} 03^{II}E).

LOCATION: GARIN MAGAJI
CO-ORDINATE: 10^{O} 11' 32" N, 11^{O} 14' 18"E.
TYPE OF EXPOSURE: ROAD CUT
ELEVATION: 410M
SCALE: 4CM REP 1M

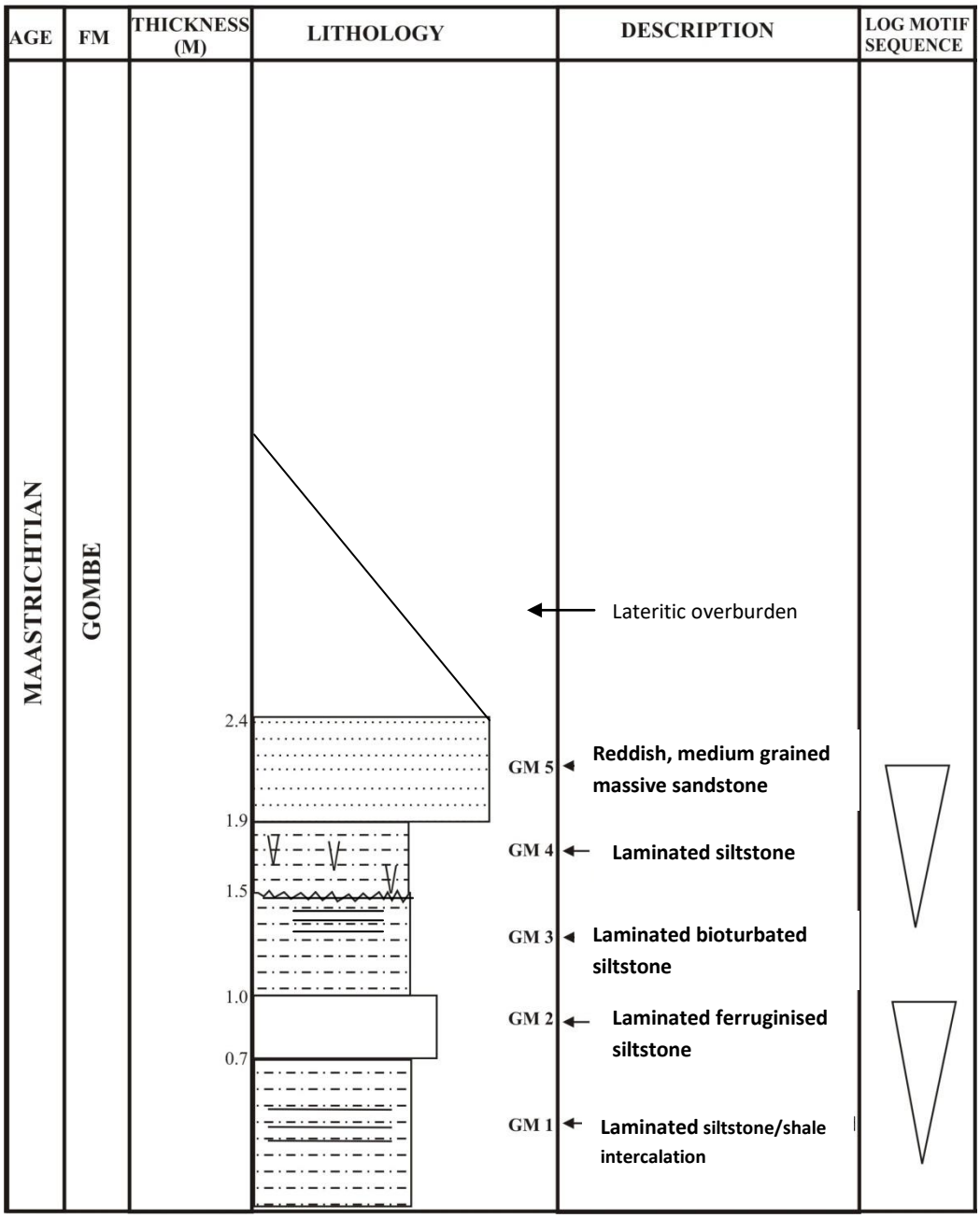


Figure 4.22: Lithologic section of Gombe Formation exposed at Garin Magaji.



Figure 4.23: Field photograph showing parallel stratified clayey siltstone/shale at Garin Magaji village. Note the shaly partings defining the bedding planes.

4.2 Lithofacies Description and Depositional Environments

The lithologic variability of Gombe Formation is recognized in stream sections, road cut, open pit and borehole section at different localities; Maiganga (Figures 4.1, 4.2 and 4.3), Zange (Figures 4.11, 4.12 and 4.13), Liji (Figure 4.14), Mallam Inna (Figure 4.15), Riman (Figure 4.16), Maiduku (Figures 4.17, 4.18), Bobona (Figures 4.19, 4.20 and 4.21) and Garin Magaji (Figures 4.22 and 4.23). Description of measured outcrops sections indicated that Gombe Formation was deposited in various sub environments of fluvial and deltaic settings. Zaborski et al., (1997) distinguished three main lithofacies in the Gombe Formation in a type section located in the Kware River at the southern outskirt of Gombe town which is in proximity to where the sections mentioned above were logged.

According to Zaborski et al., (1997), the lower section of Gombe Formation consists of series of alternating fine to medium grained sandstone and thin beds of silty shales with ironstone intercalation. The next lithofacies is the bedded facies which consist of fine to medium grained sandstone (quartz arenite with interbedded silts, clays and vesicular ironstones. The upper section of the formation consist of red sandstone facies consisting of planar cross bedded sandstone and interbedded purple and light grey shaly mudstones. It was also reported that there were coarse to very coarse cross bedded channel fill sandstones that were sporadically distributed. However, the facies observed in the sections logged corresponds to the upper part of the formation Zaborski, et al., (1997) interpretated.

The lithologic section (phase I and II) exposed at Maiganga mine of Gombe Formation is characterised by upward passage from a sequence of coal, interbedded shale, siltstone, sandstone and ironstone units indicating prograding deltaic sedimentation. The coal indicates developments of swamp in places during the Maastrichtian and have been reported by Dike (1993) and Ojo and Akande (2004). The following facies associations were observed in the sections logged.

4.2.1 Fluvial Channel Facies

This facies comprises of the fine grained and medium grained sandstone observed at Maiganga (Figures 4.1, 4.2, 4.3 and 4.4), Zange (Figures 4.11, 4.12 and 4.13), Mallam Inna (Figure 4.15), Maiduku (Figures 4.17, 4.18) and Garin Magaji (Figures 4.22 and 4.23). The sandstones are brownish to reddish in colour, massive and poorly sorted consisting of sub angular to angular grains of quartz and feldspar.

4.2.2 Nonmarine Swamp/Overbank Facies

This facies consist of clayey siltstone/mudstone and shale and is represented in most of the locations that were logged. The siltstones are whitish to brownish in colour, well sorted with parallel laminations. In some places, the siltstone appears to have some clay, friable and massive. The mudstone and shale are fine grained, grayish in colour and indurated. The fine grained facies suggest low energy environment (Ojo and Akande, 2009). The occurrence of coal and other associated lithologies in a coarsening upward sequence in the Maiganga sections (Figures 4.1 and 4.2) suggest progradation pattern reflecting deltaic sedimentation probably in the delta plain setting that favored the development of incoaling condition.

4.3 Organic Geochemical Evaluation

Twenty nine samples (coal, coaly shale and shale) from Maiganga coal mine were subjected to preliminary organic geochemical screening (TOC and Rock-Eval Pyrolysis) to determine the organic source richness, hydrocarbon generation potential, kerogen type and thermal maturity. The result of the TOC and Rock-Eval Pyrolysis are presented in (Table 4.1).

4.3.1 Organic Matter Richness

The quantity of organic matter as measured by the Total Organic Carbon content (TOC) is the primary quantitative parameter used in deducing the hydrocarbon generation potential of a stratigraphic unit. The organic carbon content of the coals ranges between (32.40-65.29 wt %) with an average of 38.03wt%, the shales ranges from (0.64-4.84 wt %) with an average of 3.14 wt% while coaly shales have an average of 12.1wt% (Table 4.1). The minmum TOC value defining a good source rock is 0.5wt% for shale, 0.3wt% for carbonate and 1wt% for clastic rock (Killops and Killops, 1993). Generally, the range of 1.5-2wt% has been generally accepted for good source rocks (Killops and Killops, 1993; Hunt, 1996). However, the TOC values in the coal, shale and shaly coal samples exceeded the acceptable minimum values required for a potential source rock (Hunt, 1996) and thus indicate good source potential. This is corroborated by the average genetic potential (GP) value for the coals, shales and coaly shales which are 70.7mg/g, 5.04mg/g and 12.6mg/g respectively. The genetic potential values are greater than 2 mg/g required for a potential source rock (Hunt, 1996; Peters et al. 2005) (Table 4.1).

4.3.2 Organic Matter Type / Kerogen Quality

The organic matter quality in the samples was evaluated from their Hydrogen Index (HI). The Hydrogen Index for the coal ranges from (57-189mgHC/gTOC), (29-172mgHC/gTOC) for the shale and (84-140mgHC/gTOC) for coaly shale. HI values in all the

samples are less than 200mgHC/gTOC (Table 4.1) suggesting Type III organic matter (Hunt, 1996). The plots of S2 vs. TOC (Figure 4.24) indicated gas prone kerogen i.e Type III organic matter). HI vs. OI (Van Krevelen diagram) (Figure 4.25) also confirm Type III kerogen for the coal, shale and coaly shale samples. However, there are few samples of shale samples that fall under Type IV kerogen. This is corroborated by plot of Tmax vs HI (Figure 4.26) and VR vs HI (Figure 4.27) indicating the organic matter is immature and mainly Type III kerogen capable of generating mainly gas. Similarly, some shale samples fall under type IV kerogen which is inert. The S2/S3 value ranges from (1.7-6.7), (1.9-7.4) and (0.5-3.5) for the coal, coaly shale and shale respectively also suggest Type III kerogen (Hunt, 1996).

4.3.3 Hydrocarbon Potential

The S2 yield range from (30.6-91.4mg/g) for the coals, (2.97-6.89mg/g) for the shales and (11.03- 13.73mg/g) for the coaly shale (Table 4.1). The average values of the S2 are (68.7mg/g), (4.92mg/g) and (12.4mg/g) respectively. These values indicate moderate to good source rock potential and it is comparable to what was observed in other hydrocarbon generating coal basins in the world such as Cooper- Eromanga Basin in Australia and Taranaki basin in New Zealand. This is further corroborated by the average genetic potential value greater than 2mg/g. The plot of PI vs Tmax (Figure 4.28) and PI vs VR (Figure 4.29) indicate that all the samples have low Production Index (PI) (less than 0.1) which also corresponds to low Tmax, indicating low level conversion.

Table 4.1: TOC, Rock eval Pyrolysis and Vitrinite reflectance data of Maiganga Coal and Shale sample of Gombe Formation

S/n	Sample no/code	Lithology	TOC wt%	S1	S2	S3	Tmax (^oC)	HI	OI	S2/S3	PI	S1/TOC* 100	GP (S1+S2)	V.R
1	MG1A	Coal	63.5	2.89	102.39	16.47	418	162	26	6.2	0.03	5	105.28	
2	MG1D	Coal	63.39	1.49	57.96	12.12	416	90	19	4.8	0.03	2	59.45	0.55
3	MG1F	Coal	60.67	2.31	75.59	11.40	421	125	19	6.6	0.03	4	77.9	
4	MG1G	Coal	65.29	2.09	71.02	12.87	413	109	20	5.5	0.03	3	73.11	
5	MG1H	Coal	62.46	3.81	103.21	15.35	420	165	25	6.7	0.04	6	107.02	
6	MG1W	Coal	64.22	3.51	88.63	20.99	418	138	33	4.2	0.04	5	92.14	0.49
7	MG1X	Coal	59.30	3.34	91.36	18.84	419	154	32	4.8	0.04	6	94.7	
8	MG2H	Coal	62.75	3.11	87.59	16.47	422	140	26	5.3	0.03	5	90.7	0.48
9	MG2O	Coal	37.71	4.11	71.16	20.42	417	189	54	3.5	0.05	11	75.27	
10	MG3D	Coal	53.4	0.49	30.58	17.56	429	57	33	1.7	0.02	1	31.07	0.50
11	MG3Z	Coal	55.80	0.97	73.15	27.26	435	131	49	2.7	0.01	2	74.12	0.46
12	MG4K	Coal	32.4	0.67	55.29	21.68	439	171	67	2.6	0.01	2	55.96	
13	MG2K	C. Shale	16.35	0.27	13.72	1.85	426	84	11	7.4	0.02	2	13.99	
14	MG3S	C. Shale	7.90	0.26	11.03	5.96	428	140	75	1.9	0.02	3	11.29	
15	MG1I	Shale	2.11	0.05	1.35	1.29	430	64	61	1.0	0.04	2	1.4	
16	MG1J	Shale	2.13	0.05	0.72	1.34	419	34	63	0.5	0.06	2	0.77	
17	MG1L	Shale	1.78	0.05	0.51	0.83	425	29	47	0.6	0.09	3	0.56	
18	MG1O	Shale	1.85	0.01	0.84	1.18	431	45	64	0.7	0.01	0.5	0.85	
19	MG1Q	Shale	1.19	0.05	0.92	0.63	430	77	53	1.5	0.05	4	0.97	
20	MG1R	Shale	2.15	0.06	2.48	1.03	426	115	48	2.4	0.02	3	2.54	
21	MG1Z	Shale	2.95	0.11	3.31	2.07	428	112	70	1.6	0.03	4	3.42	
22	MG2C	Shale	2.99	0.05	2.32	1.65	428	78	55	1.4	0.02	2	2.37	
23	MG2F	Shale	3.91	0.10	3.58	2.06	425	92	53	1.7	0.03	3	3.68	
24	MG2L	Shale	4.81	0.14	5.14	2.52	429	107	52	2.0	0.03	3	5.28	0.49
25	MG2R	Shale	3.84	0.17	6.22	1.79	430	162	47	3.5	0.03	4	6.39	0.50
26	MG4D	Shale	4.64	0.09	4.84	3.12	428	104	67	1.6	0.02	2	4.93	0.52
27	BH15A	Shale	1.95	0.16	2.97	1.19	428	152	61	2.5	0.05	8	3.13	0.49
28	BH15B	Shale	2.96	0.09	5.09	1.99	428	172	67	2.6	0.02	3	5.18	
29	BH15C	Shale	4.84	0.09	6.89	3.93	427	142	81	1.8	0.01	2	6.98	

TOC= Total Organic Carbon (wt.%) **S1**=Hydrocarbon already present in the sample which are mainly stripped at temperatures about 300^oC. **S2**= Hydrocarbons generated through thermal cracking of kerogen at temperatures in the range of 300-650^oC. **S3**= CO_2 that is generated from the kerogen at the same time the S2 hydrocarbons are being generated.
Tmax = Temperature of maximum generation of S2 peak. **HI**= (Hydrogen index). An important indicator of kerogen type - oil/gas proneness measured in (mgHC/gTOC), HI= S2*100/TOC. **OI**= (Oxygen index). An indicator of kerogen type measured in (mgCO_2/gTOC), OI= S3*100/TOC. **PI**= (Production index) (S1/(S1+S2), indicative of free petroleum content.
GP=Genetic Potential. **VR**=Vitrinite Reflectance.

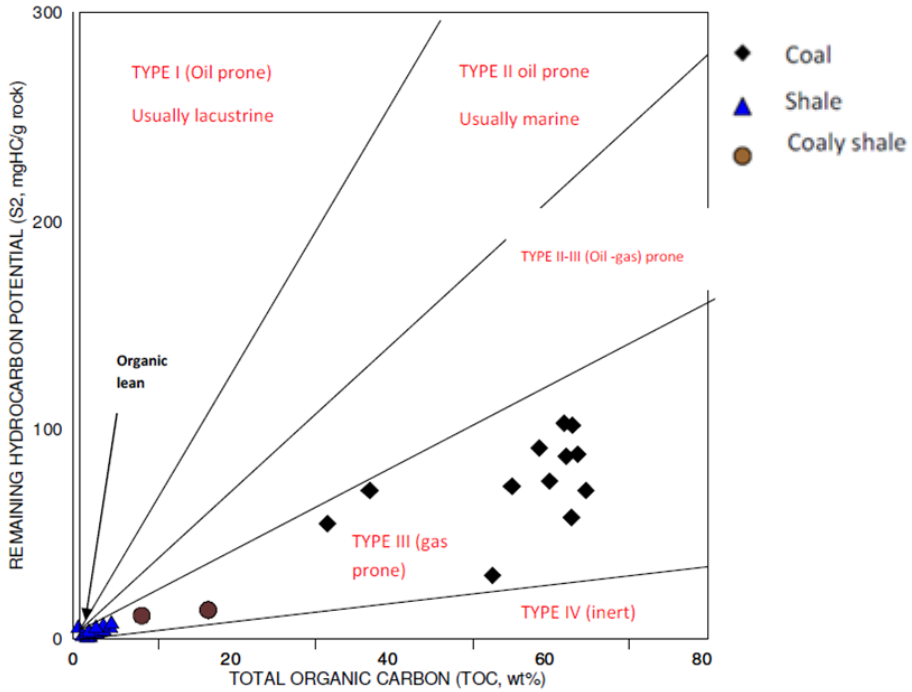


Figure 4.24: Plot of S2 versus TOC for coal and shale samples of Maiganga, Gongola Basin. The plot indicates Type III kerogen (gas prone) for the samples. The shale samples are organically lean (after Langford and Blanc-Valleron, 1990).

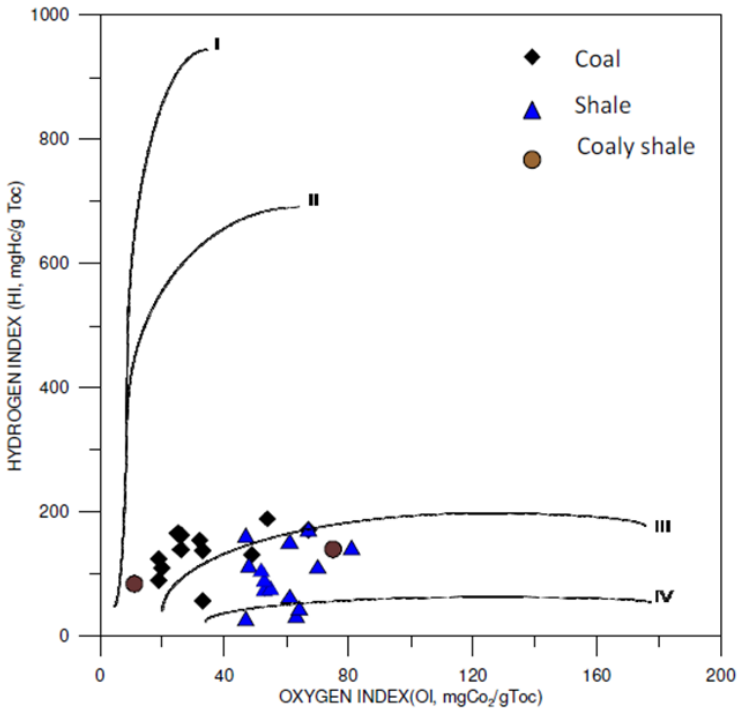


Figure 4.15: Plot of HI versus OI for the typing of kerogen (1- 1V). Most of the samples fall within Type III kerogen (gas prone) typical of terrestrial source organic matter (after Van Krevelen, 1961).

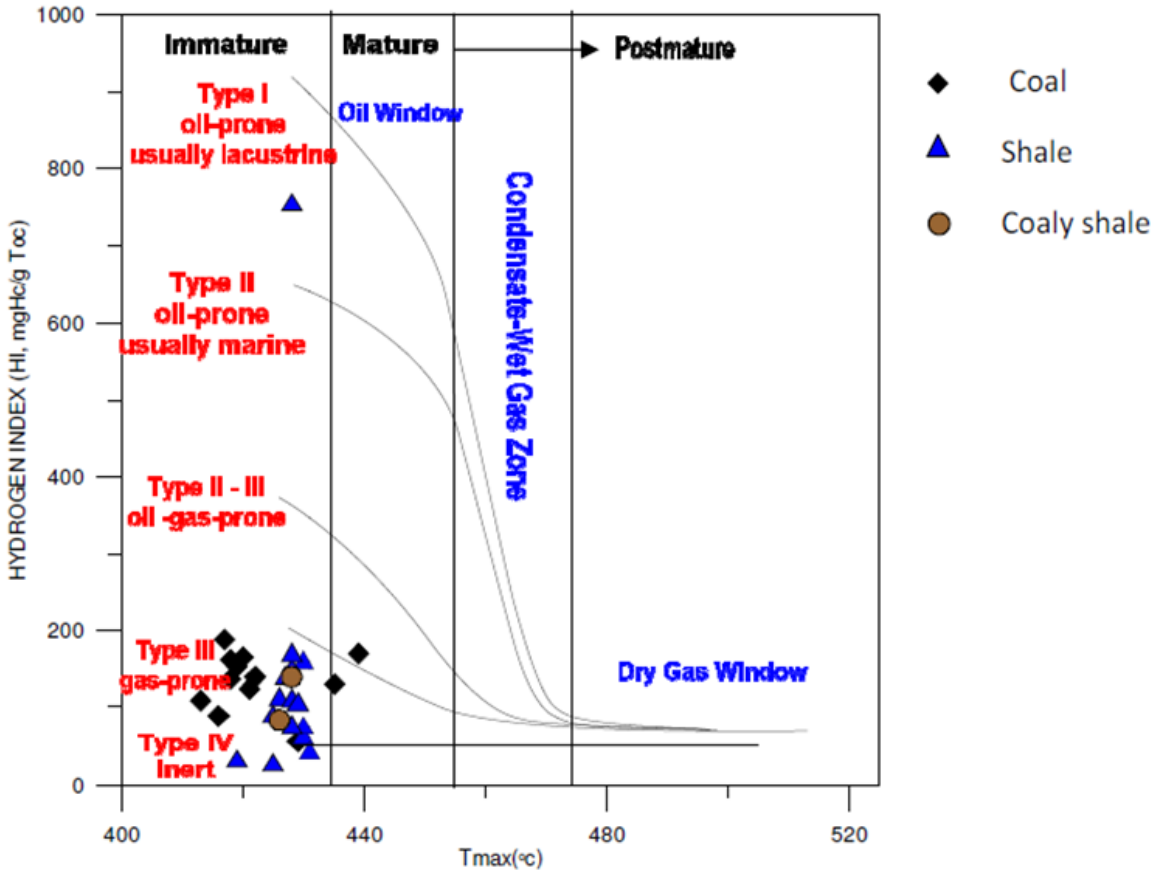


Figure 4.26: Plot of Hydrogen index (HI) against Tmax of coal, coaly shale and shale samples from Maiganga, Gongola Basin. Majority of the samples fall in immature zone and Type III kerogen (gas prone) typical of terrestrially sourced organic matter.

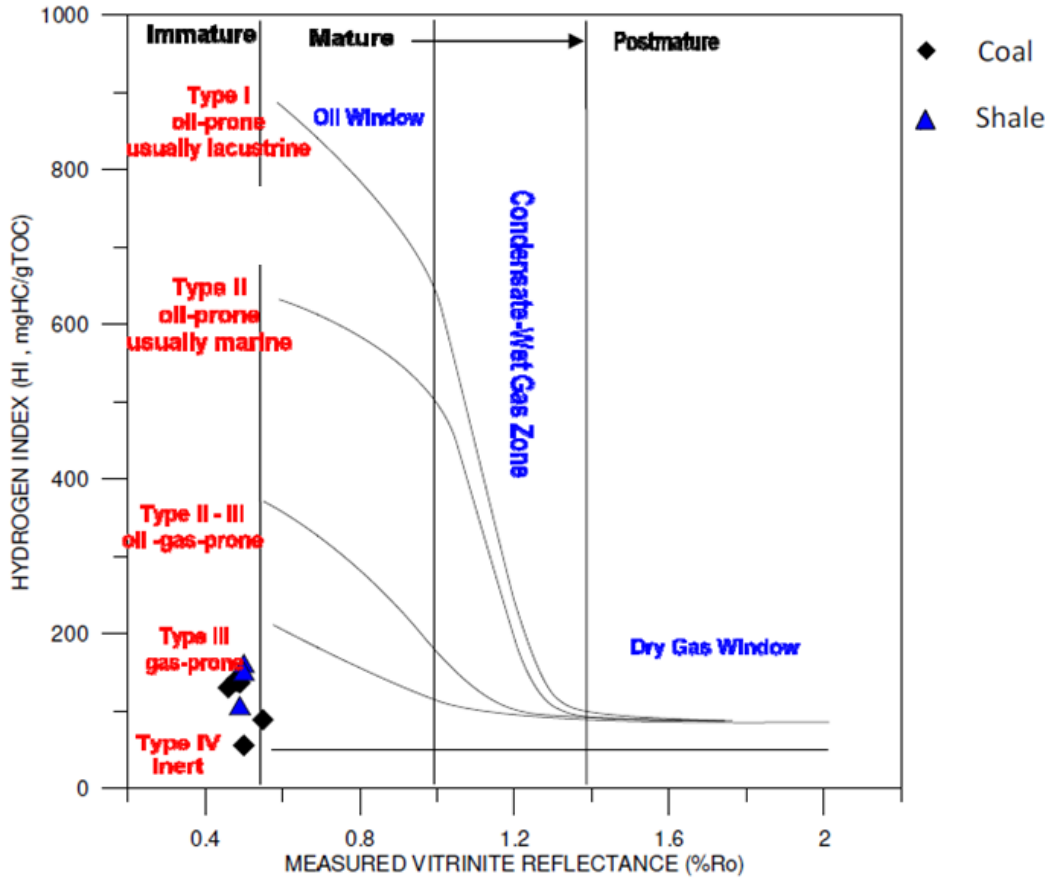


Figure 4.27: Plot of hydrogen index (HI) against vitrinite reflectance of coal and shale samples from Maiganga, Gongola Basin. The samples fall in immature zone and Type III kerogen (gas prone) typical of terrestrially sourced organic matter.

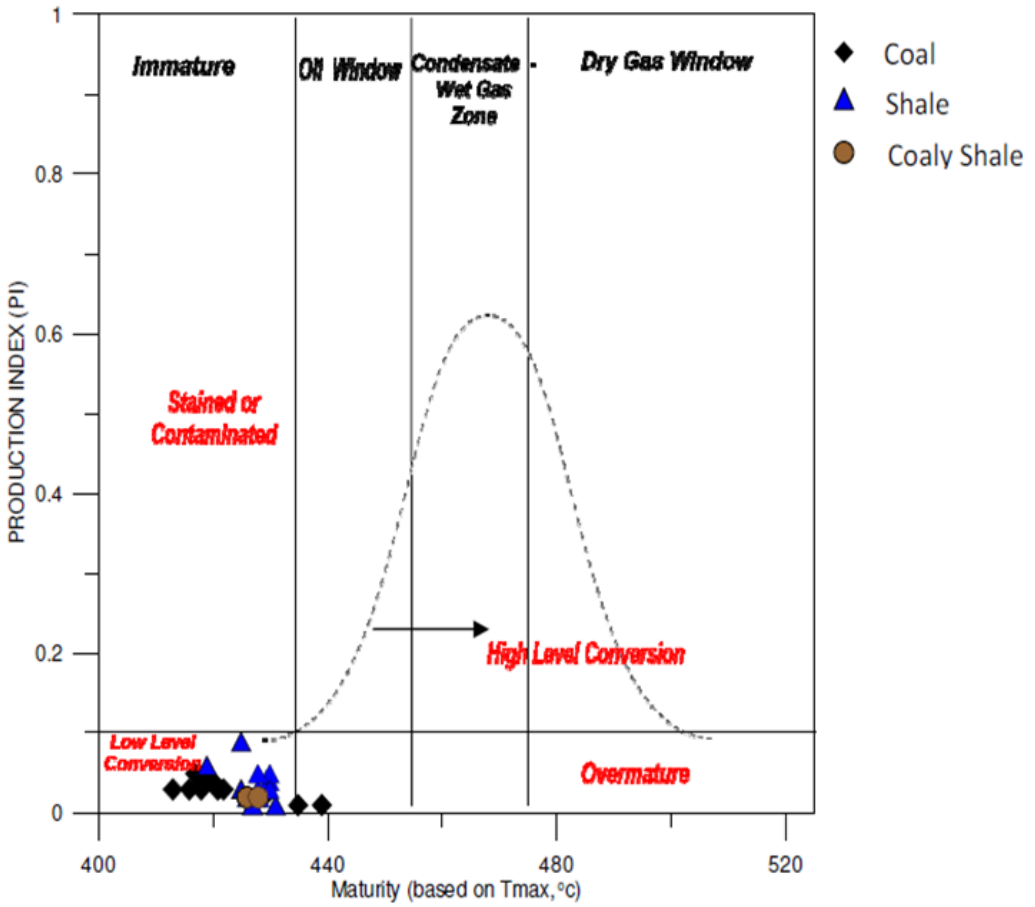


Figure 4.28: Plot of production index (PI) against Tmax of coal, coaly shale and shale samples from Maiganga, Gongola Basin. The samples are immature and have low level conversion of kerogen to oil.

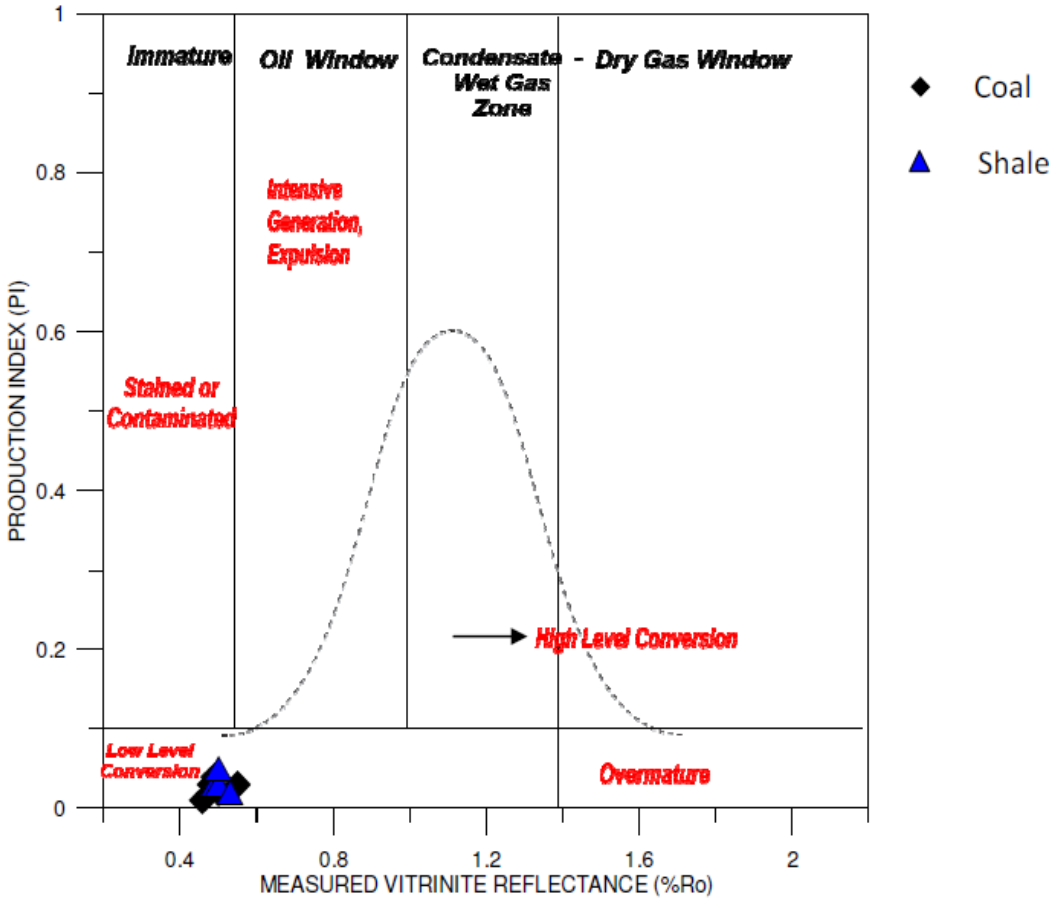


Figure 4.29: Plot of production index (PI) against vitrinite reflectance of coal and shale samples from Maiganga, Gongola Basin. The samples are immature and have low level conversion of kerogen to oil.

4.3.4 Thermal Maturity

The thermal maturity for all the samples is represented by Tmax of 413–439°C. The Tmax for the coals range between (413-439°C) with an average of 428°C, while the shales range between 419–431°C with average value of 427°C (Table 4.1).

The Tmax for the coaly shale is between 426-428°C, averaging 427°C. Table 4.1 shows that majority of the samples having Tmax less than 435°C with exception of two coal samples having 435°C and 439°C. The spiked Tmax of these two samples (MG3Z and MG4K) having the threshold values for maturity could probably arise from impurities or weathering of the samples or possibly human error as there are no conditions that could possibly increase the maturity at that stratigraphic interval. Consequently, (Clayton and King 1987; Lo and Cardott, 1995) has shown that weathering in outcropping source rocks has significant effect on the amount and quality of organic matter obtained by Rock Eval pyrolysis. This is also noted in the OI values for the two samples 49 $mgCO_2$/gTOC in MG3Z and 67 $mgCO_2$/gTOC for MG4K indicating the highest level of weathering in the sample package.

The samples are presently thermally immature because of the low average Tmax values an indication of late diagenetic stage of maturation and yet to reach oil window (Figure 4.44) (Killops and Killops, 1993; 2005). The low production index (PI) recorded for all the samples also indicate low maturity. Organic petrography (vitrinite reflectance) and visual kerogen analyses including (thermal alteration index and spore coloration) of the samples were also used to evaluate the maturity level of the organic matter. A total of nine (9) samples were analysed for vitrinite reflectance. The vitrinite reflectance of the coal ranges from (0.46-0.55Ro) averaging 0.5Ro while the shale ranges between (0.49-0.53Ro) with the average of 0.51Ro (Table 4.1). These values are less than 0.6Ro and thus confirm the low level of maturity and late diagenesis (Figure 4.44). The plot of HI vs Tmax (Figure 4.26), HI

vs VR (Figure 4.27), PI vs Tmax (Figure 4.28) and PI vs VR (Figure 4.29) all indicated that the samples are immature. The thermal alteration index (TAI) of the samples (coals and shales) falls between (2.4-2.6) also corroborate other maturity indices such as the spore coloration which fluoresce between pale yellow–yellow, yellow-orange and dark orange (Table 4.11) indicated low level maturity for the samples. Inputs from biomarker analysis also indicate that the organic matter is of low maturity. The biomarker maturity indices of saturate and aromatic hydrocarbon are summarized in (Table 4.7 and 4.9).

4.4 Source Rock Kinetics

Kerogen classification or organic matter typing is a function of the total hydrocarbon potential, hydrocarbon generation kinetics and oil chemistry according to (Van Krevelin, 1961; Rippen et al., 2013; Abbassi et al., 2014). Rock Eval Pyrolysis data for eight samples (3 core samples and 5 surface cuttings from phase II of the mine were analysed to study the bulk kinetic characteristics in order to evaluate the hydrocarbon generation of the kerogen.

The distribution of the kinetic parameters (Table 4.2) for cracking of the kerogen was obtained by processing the results of the Rock Eval 6 pyrolysis using kinetic software called ORFA (One Run Fixed A). The ORFA converts Rock-Eval pyrolysis data from a single run into a set of activation energies and break the bulk or total hydrocarbon kinetics into oil and gas generation, a method similar to that of Waples and Ramly (2001). Ideally, immature samples were used for kinetics analysis in order to elevate the maturity level and to reach the threshold required for hydrocarbon generation through simulation. However, Varma et al., (2015) have also used samples > 435^{o}C or very early – least mature samples, organic matter richness and quality were also taken into consideration for the kinetic analysis.

Tissot and Espitalie (1975), Schenk and Horsfield (1998) showed that the fractionation of kerogen into simpler hydrocarbon is a complex process and as such, the discrete bulk kinetic concepts is based primarily on Arrhenius law K(T) = A*exp(-E/(RT)

where K is the reaction rate parameter dependent on absolute temperature (T, in Kelvin); E is the activation energy of the reaction (J/mol) and R is the molar gas constant (J/mol/K); A is the exponential frequency factor/ Arrhenius constant (sec^{-1}). The value of the Arrhenius factor (A) are constrained by thermodynamics to be (10^{14} sec^{-1}) in this analysis. The Arrhenius law K (T) = A*exp (-E/ (RT) can also be expressed as dXi/dt =Aexp (-Ei/RT). Xi. Where dXi/dt is the hydrocarbon generation rate and Xi is the residual petroleum potential of the organic matter involved in reaction i. E is the activation energy related to reaction i (Tissot et al., 1987). Gas and pyrobitumen is the end product when the primary product (kerogen) breaks down into smaller molecules through secondary cracking processes as a result of increasing temperature.

Table 4.2: Bulk Kinetics data for Coal and Shale Samples of Maiganga, Gombe Formation

S/N	S. code	Lithology	Sample type	Depth (m)	TOC	SI	S2	Tmax (^{o}C)	HI	Ea Range	Mean (Ea)	Oil (%)
1	MG3D	Coal	Surface	23	53.40	0.49	30.58	429	57	41-65	57.64	64
2	MG3S	C. shale	Surface	17	7.90	0.26	11.03	428	140	41-65	56.19	70.8
3	MG3Z	Coal	Surface	12	55.80	0.97	73.15	435	131	41-65	57.35	70.3
4	MG4D	Shale	Surface	13	4.64	0.09	4.84	428	104	41-65	56.61	68.6
5	MG4K	Coal	Surface	9	32.40	0.67	55.29	439	171	41-65	57.49	72.3
6	BH15A	Shale	Core	44	1.95	0.16	2.97	428	152	41-65	56.17	71.5
7	BH15B	Shale	Core	46	2.96	0.09	5.09	428	172	41-65	56.66	72.4
8	BH15C	Shale	Core	48	4.84	0.09	6.89	427	142	41-65	56.85	70.9

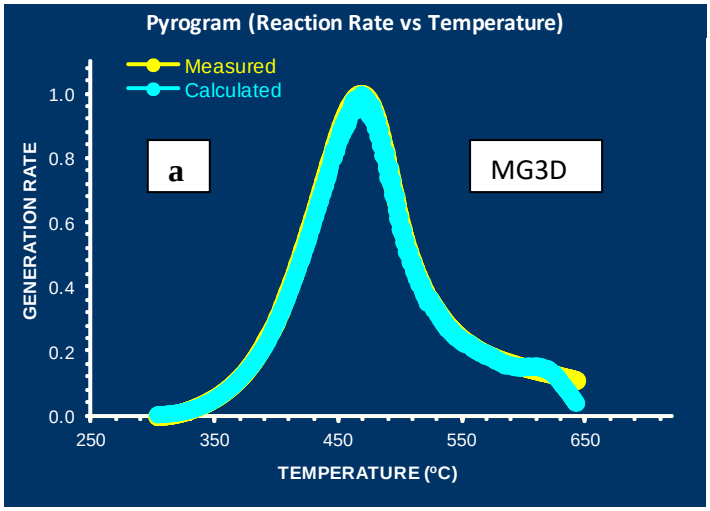
Note: **TOC**= Total organic carbon, **S1**=Hydrocarbon already present in the sample which are mainly stripped at temperatures about 300^{o}C. **S2**= Hydrocarbons generated through thermal cracking of kerogen at temperatures in the range of 300-650^{o}C. **Tmax** = Temperature of maximum generation of S2 peak. **HI**= (Hydrogen index). **Ea** = Activation energy.

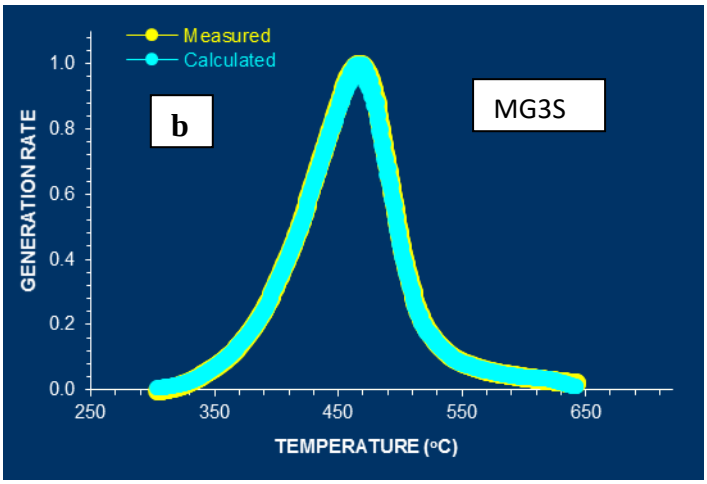
4.4.1 Activation Energy Distribution

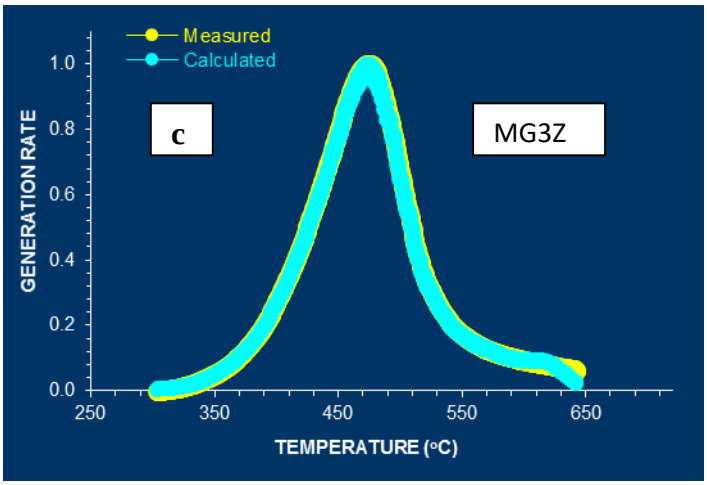
The best fit between the measured and calculated hydrocarbon generation rates were obtained with the distribution of activation energy (Ea) and single pre-exponential factor (A) for the coal and shale samples (Figures 4.30a-h). Generally, the activation energy distributions observed in the samples are broad, indicating heterogeneous compositions typical of terrigenous organic matter derived from higher land plants (Schenk et al., 1997; Mahlstedt and Horsfield, 2012). The activation energies (Ea) measured for the samples ranges from 41–65 kcal/mol, with associated fixed frequency factors of 2.00E+14/s. The coal facies are comparatively slightly matured than the shale facies and showed activation energies between (41-65 kcal/mol) with mean Ea of 57.49 kcal/mol. The peak energy for the hydrocarbon bond breaking is at 55 kcal/mol. The shale facies also have higher activation energies from (41-65kcal/mol) with mean Ea of 56.57 kcal/mol.

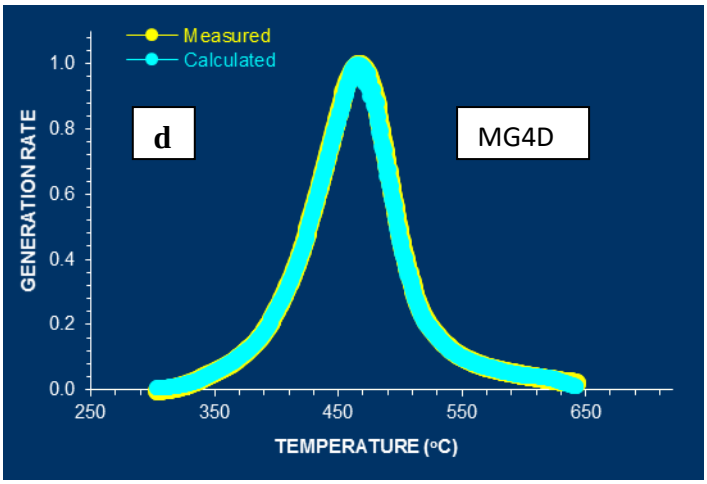
4.4.2 Hydrocarbon Potential

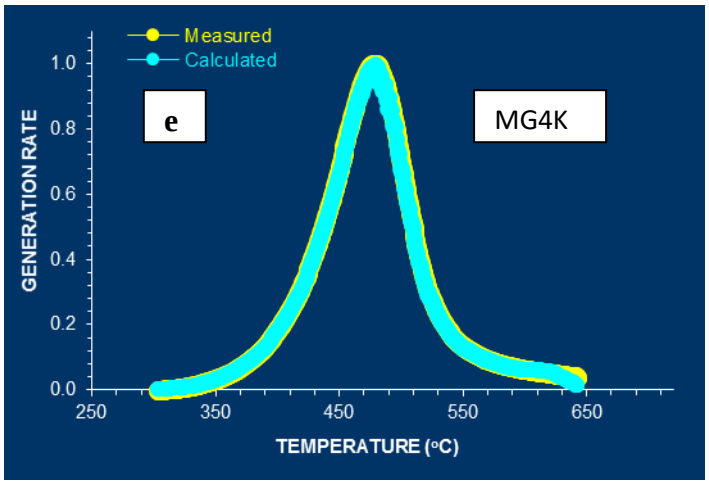
The frequency factor and the distribution of the activation energy is controlled by the organic matter type (Dieckmann, 2005). The distribution of the shale and coal samples analysed is indicative of heterogeneous compositions and bond types typical of Type III kerogen (HI = 57-172 mgHC/gTOC). Based on the kinetics, the coal and shale facies are in early- late mature oil and gas generating stages which probably have would have partially converted the kerogen to oil or gas as depicted by the broad range of activation energy. The major phase and peak of hydrocarbon generation occurs at 460 – 465^{o}C for the coal and shale facies with a constant heating rate of 25^{o}C/min (Figures 4.31a-h). The bar height from each activation energy signifies the generation potential for each sample (Figures 4.32a-h and 4.32 a'-h') with peak hydrocarbon bond breaking at 54 and 55 kcal/mol defining up to 70% of the petroleum potential in which most of the kerogen has been converted to oil. The percentage of oil generated from the HIs for the coal facies range from (64-72%) while the shale facies range from (68.6-72.4%) (Table 4.2).

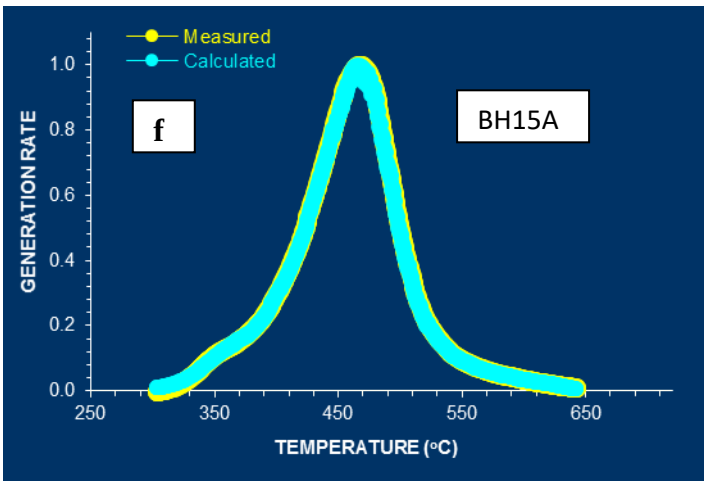

Pyrogram (Reaction Rate vs Temperature)
Measured
Calculated
a
MG3D
GENERATION RATE
1.0
0.8
0.6
0.4
0.2
0.0
250
350
450
550
650
TEMPERATURE (°C)

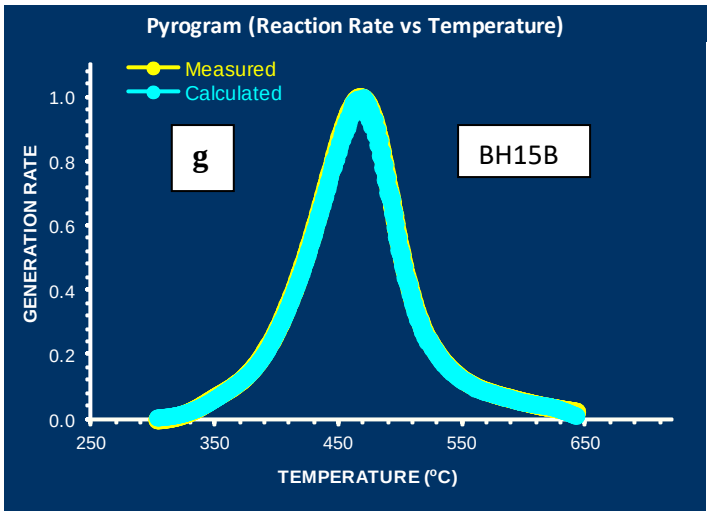

Measured
Calculated
b
MG3S
GENERATION RATE
1.0
0.8
0.6
0.4
0.2
0.0
250
350
450
550
650
TEMPERATURE (°C)


Measured
Calculated
c
MG3Z
GENERATION RATE
1.0
0.8
0.6
0.4
0.2
0.0
250
350
450
550
650
TEMPERATURE (°C)


Measured
Calculated
d
MG4D
GENERATION RATE
1.0
0.8
0.6
0.4
0.2
0.0
250
350
450
550
650
TEMPERATURE (°C)


Measured
Calculated
e
MG4K
GENERATION RATE
1.0
0.8
0.6
0.4
0.2
0.0
250
350
450
550
650
TEMPERATURE (°C)


Measured
Calculated
f
BH15A
GENERATION RATE
1.0
0.8
0.6
0.4
0.2
0.0
250
350
450
550
650
TEMPERATURE (°C)



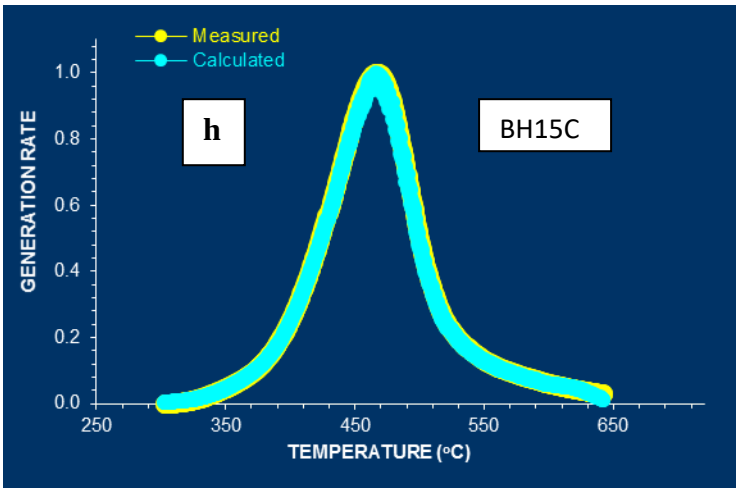
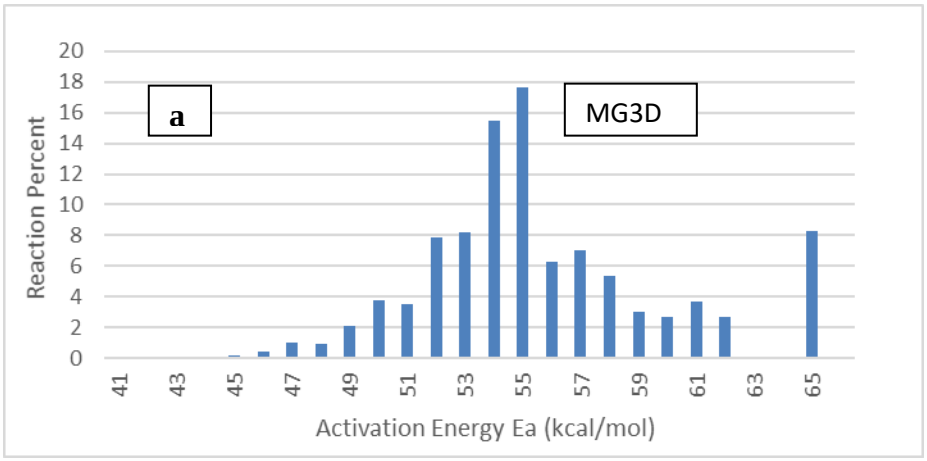
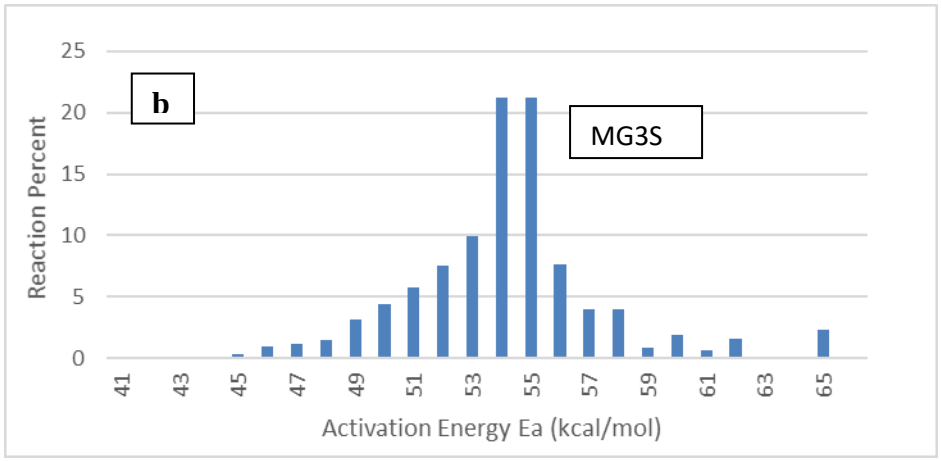
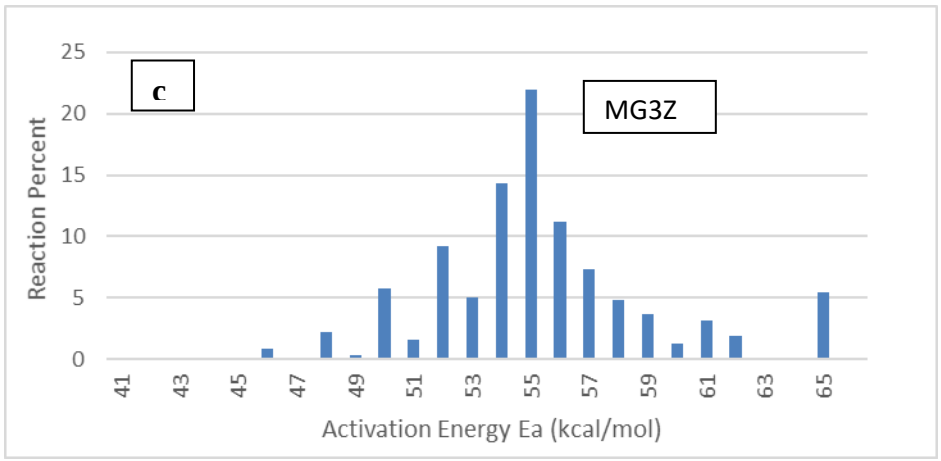
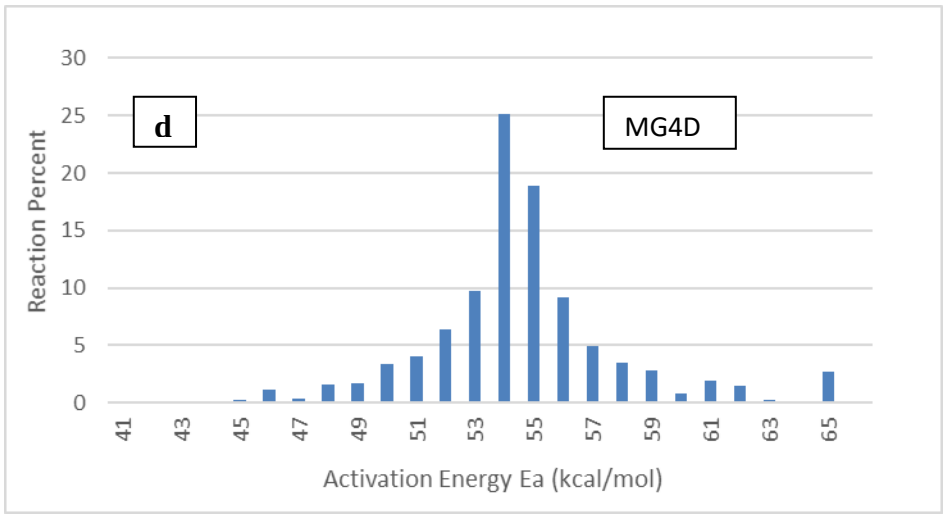


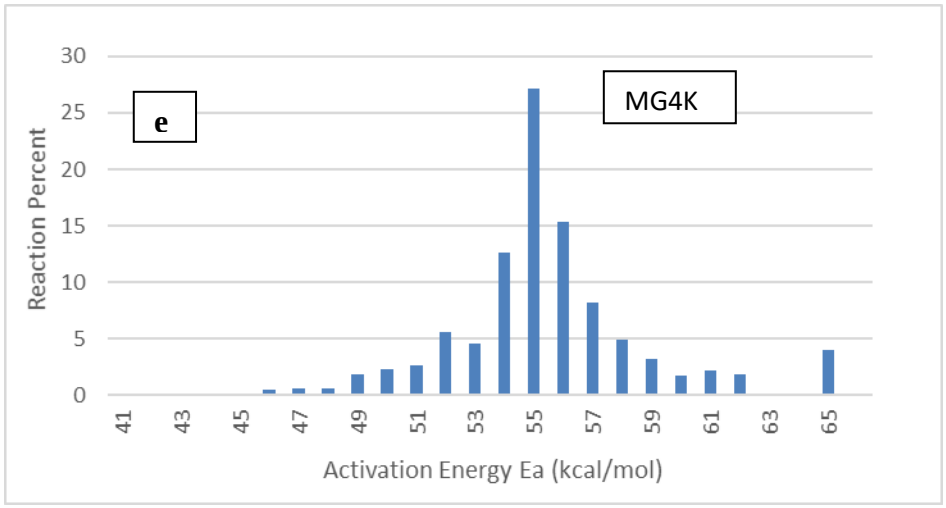
Figure 4.30 (a-h): Pyrogram (reaction rate vs temperature) showing calculated and measured hydrocarbon generation rate for coal and shale samples of Maiganga (Note: peak of hydrocarbon generation for the samples is between 460 – 465°C.

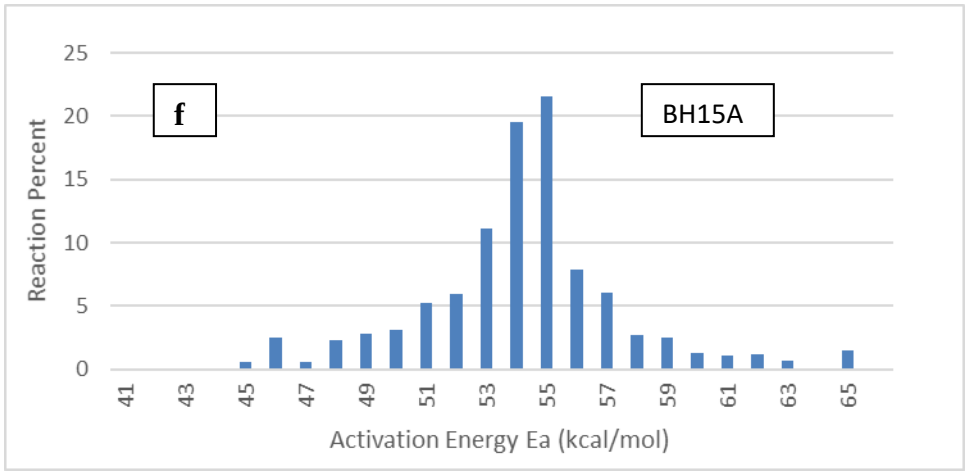


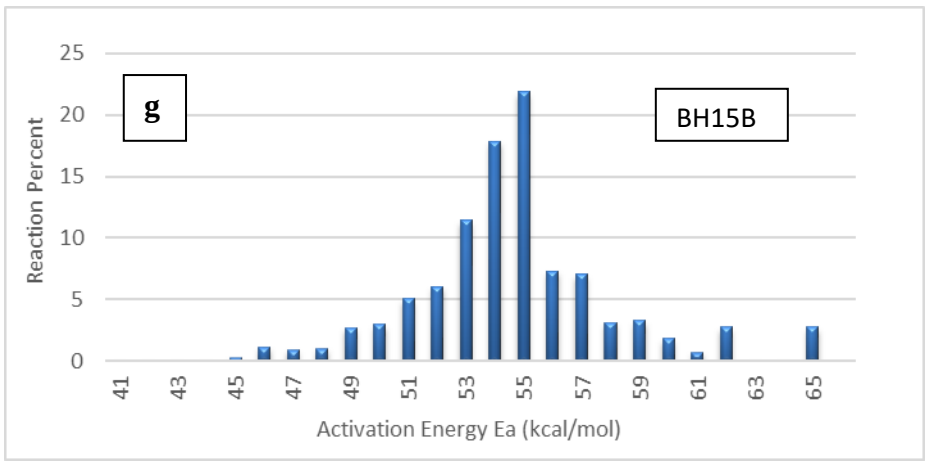

b
MG3S
Reaction Percent
0
5
10
15
20
25
41
43
45
47
49
51
53
55
57
59
61
63
65
Activation Energy Ea (kcal/mol)


c
MG3Z
Reaction Percent
0
5
10
15
20
25
41
43
45
47
49
51
53
55
57
59
61
63
65
Activation Energy Ea (kcal/mol)


d
MG4D
Reaction Percent
0
5
10
15
20
25
30
41
43
45
47
49
51
53
55
57
59
61
63
65
Activation Energy Ea (kcal/mol)


e
MG4K
Reaction Percent
30
25
20
15
10
5
0
41
43
45
47
49
51
53
55
57
59
61
63
65
Activation Energy Ea (kcal/mol)


f
BH15A
Reaction Percent
25
20
15
10
5
0
41
43
45
47
49
51
53
55
57
59
61
63
65
Activation Energy Ea (kcal/mol)


g
BH15B
Reaction Percent
25
20
15
10
5
0
41
43
45
47
49
51
53
55
57
59
61
63
65
Activation Energy Ea (kcal/mol)

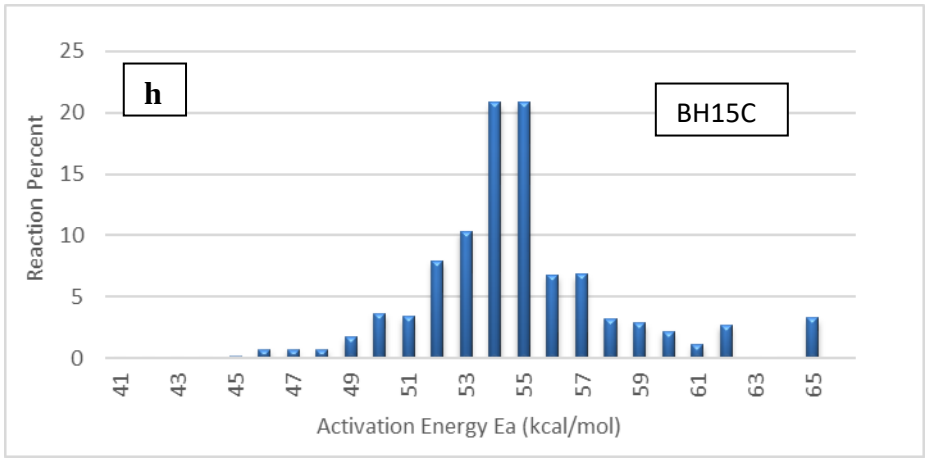
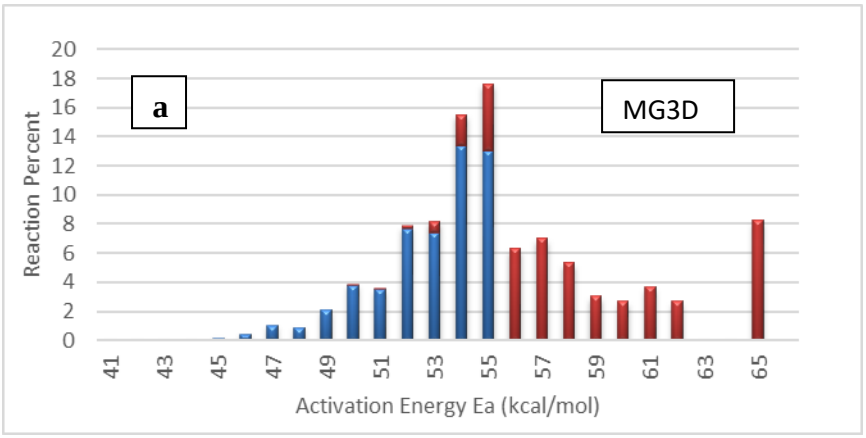
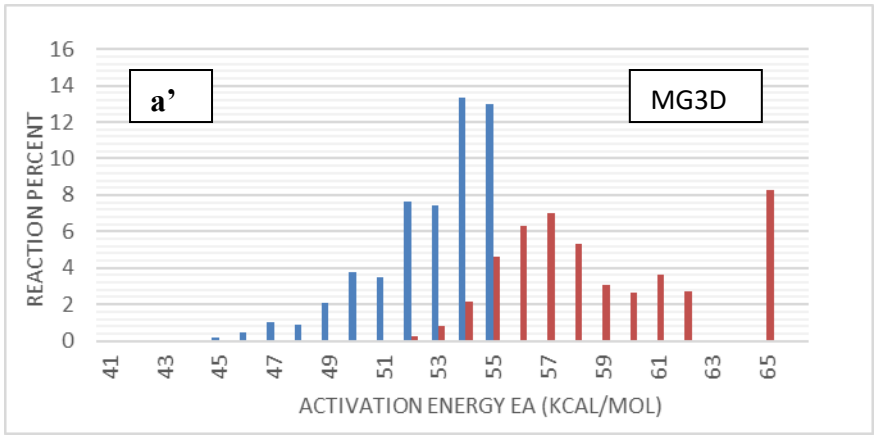
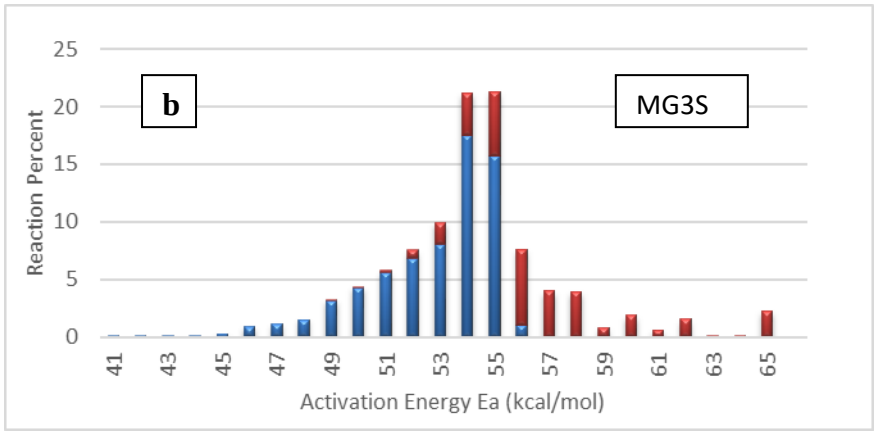
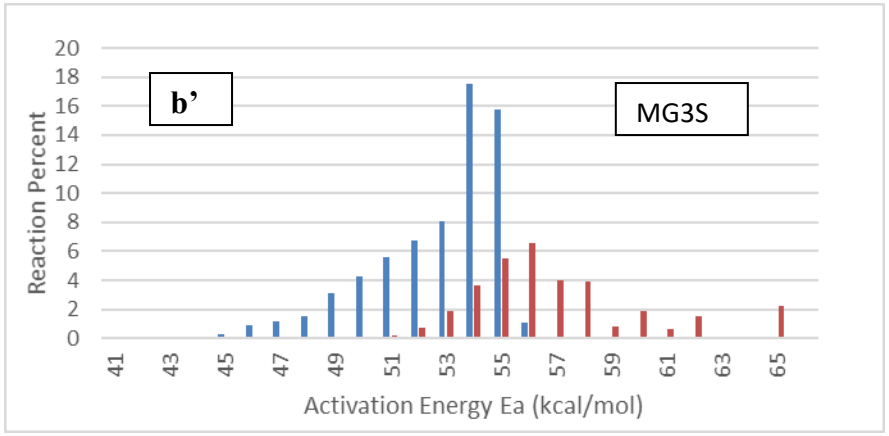


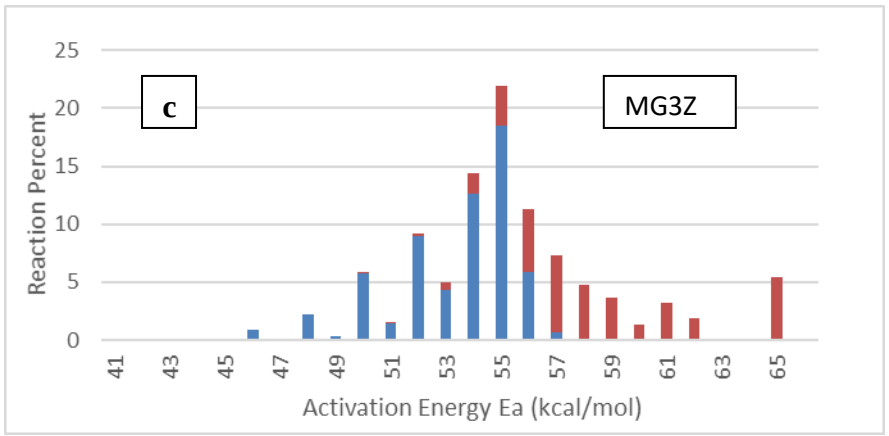
Figure 4.31(a-h): Bulk kinetics showing the activation energies of coal and shale samples of Gombe Formation. (Note: The bar height for each activation energy indicates generation potential and its highest at Ea-55 with exception of sample MG4D (Ea-54). Oil (Blue) and Gas (Red) Kinetics

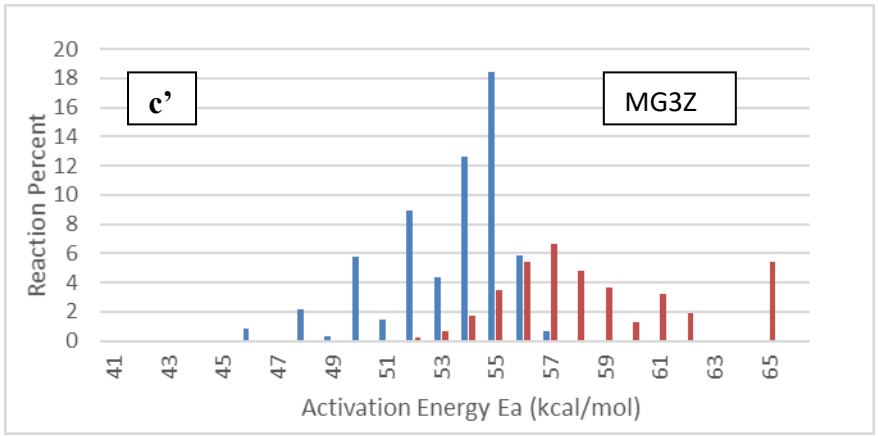


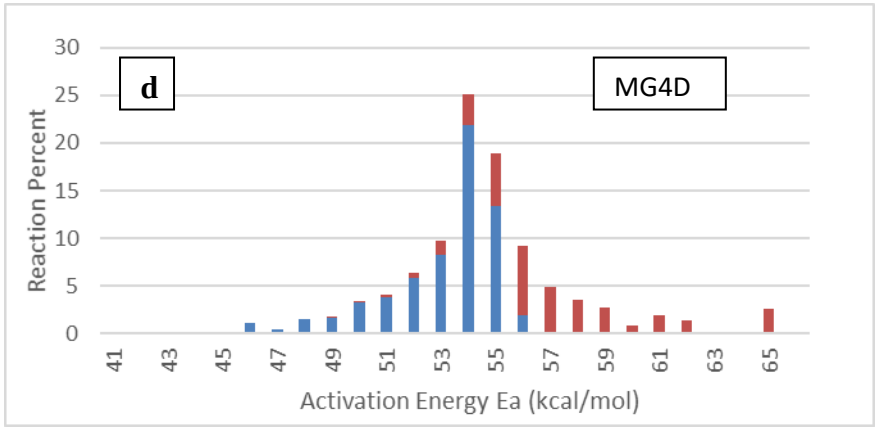


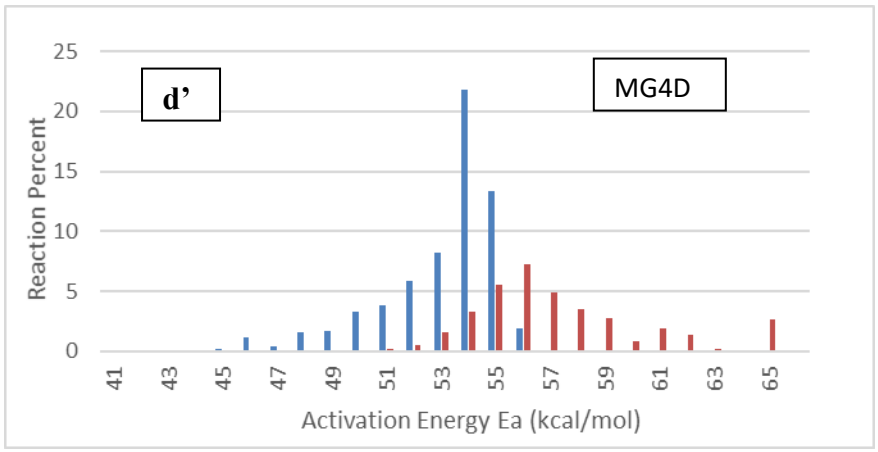

b
MG3S
Reaction Percent
Activation Energy Ea (kcal/mol)

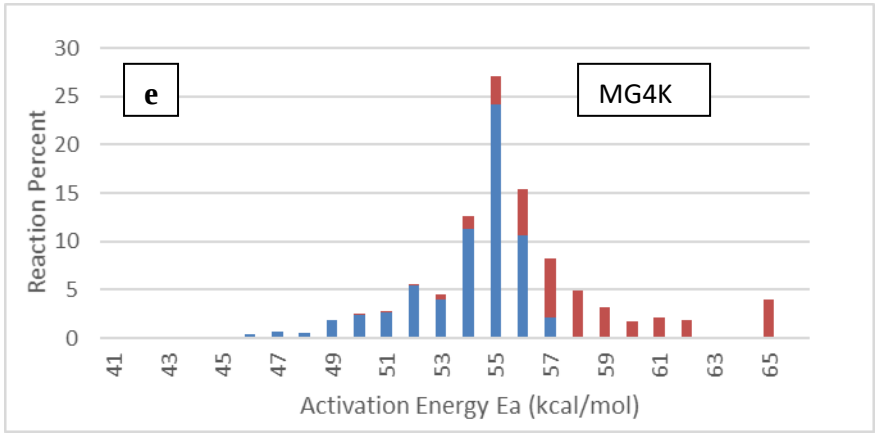

b'
MG3S
Reaction Percent
Activation Energy Ea (kcal/mol)

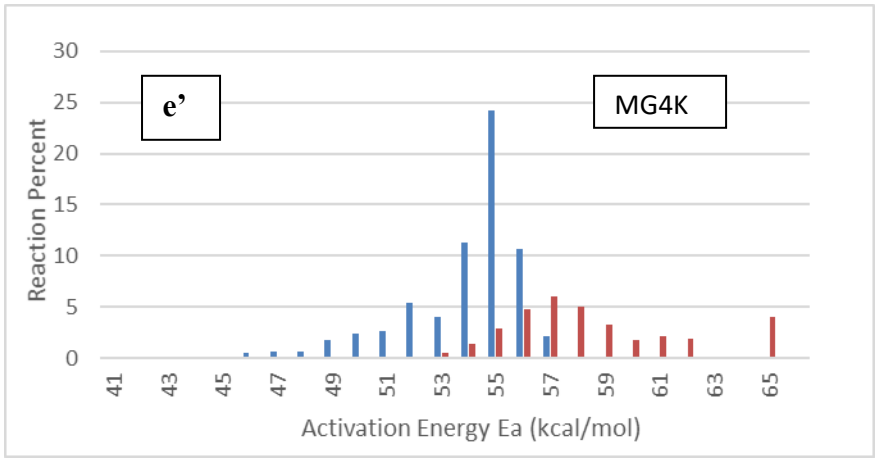

c
MG3Z
Reaction Percent
Activation Energy Ea (kcal/mol)

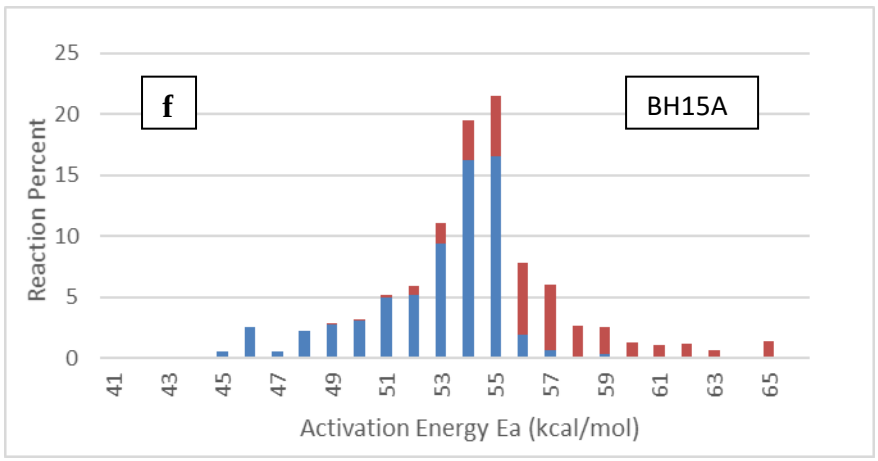

c'
MG3Z
Reaction Percent
Activation Energy Ea (kcal/mol)

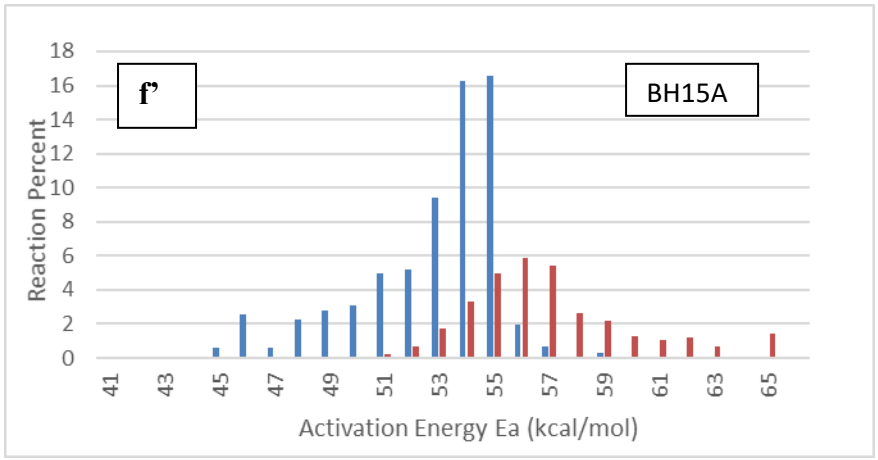

d
MG4D
Reaction Percent
30
25
20
15
10
5
0
41
43
45
47
49
51
53
55
57
59
61
63
65
Activation Energy Ea (kcal/mol)

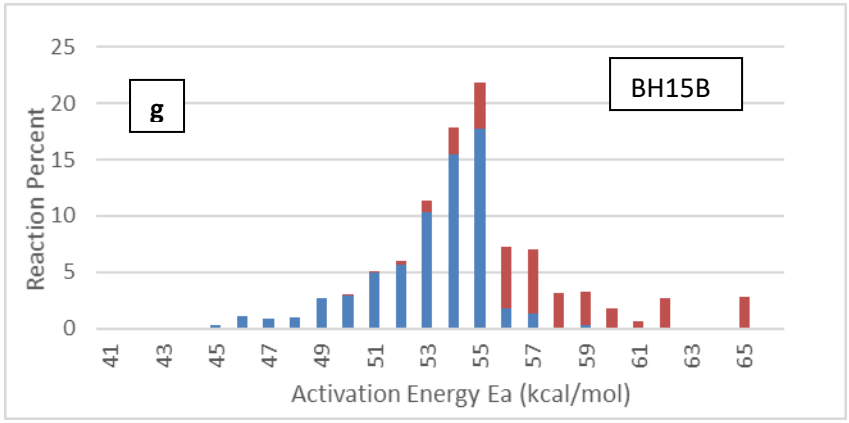

d'
MG4D
Reaction Percent
25
20
15
10
5
0
41
43
45
47
49
51
53
55
57
59
61
63
65
Activation Energy Ea (kcal/mol)

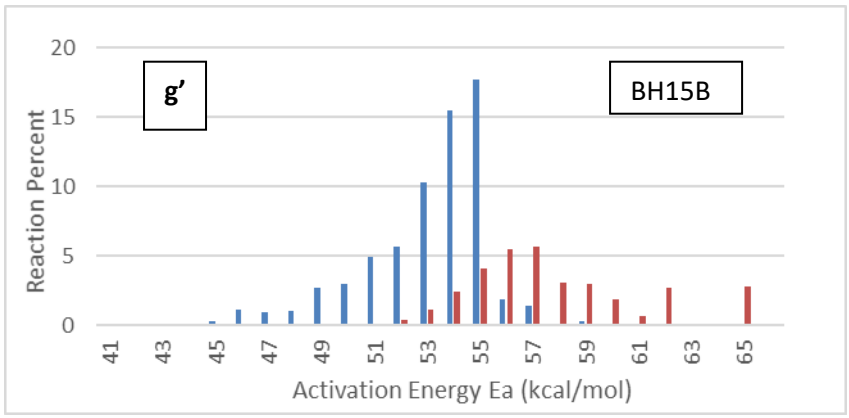

e
MG4K
Reaction Percent
30
25
20
15
10
5
0
41
43
45
47
49
51
53
55
57
59
61
63
65
Activation Energy Ea (kcal/mol)

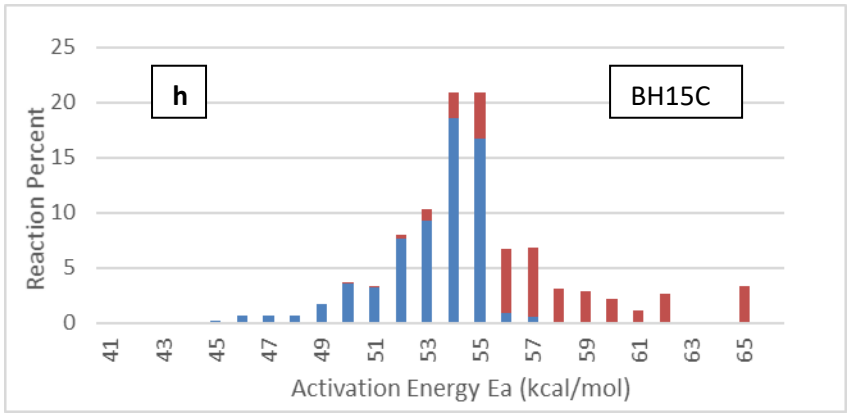

e'
MG4K
Reaction Percent
Activation Energy Ea (kcal/mol)


f
BH15A
Reaction Percent
Activation Energy Ea (kcal/mol)


f'
BH15A
Reaction Percent
Activation Energy Ea (kcal/mol)


g
BH15B
Reaction Percent
Activation Energy Ea (kcal/mol)


g'
BH15B
Reaction Percent
Activation Energy Ea (kcal/mol)


h
BH15C
Reaction Percent
Activation Energy Ea (kcal/mol)

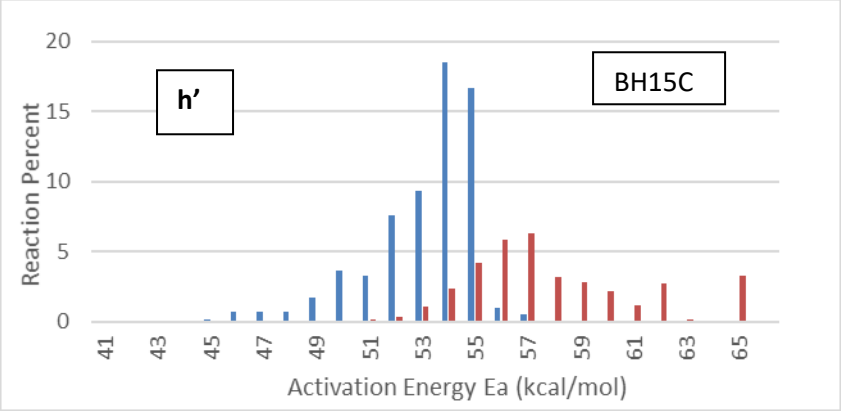


Figure 4.32:(a-h) and 4.32 (a'-h'): Bar charts indicates the percentage reaction vs activation energy for coal and shale samples of Gombe Formation. Note: Oil (Green) and Gas (Red) Kinetics. Peak hydrocarbon generation is at 55 (Ea) for majority of the samples.

4.5 Biomarker Geochemistry (Saturate and Aromatic)

Seven samples (four coals, two shales and coaly shale) were extracted and separated into saturate, aromatic, resins and asphaltenes by Medium Performance Liquid Chromatography. The polar compounds (Asphaltenes and NSO) dominate the extract followed by saturate. The aromatics represent small percentage of the composition of the extracts (Figures 4.33 and 4.34). Table 4.4 shows the percentage composition of the extract into saturate, aromatic, resins and asphaltenes.

The saturate and aromatic fractions were analyzed by Gas Chromatography and Mass Spectrometry**.** The extract from the Gas Chromatography were resolved into normal paraffin, isoprenoids and unknown components (Table 4.3). The n-alkane ion chromatograms of each sample extract are shown in (Figure 4.45 - Figure 4.51). The n-alkanes are the dominant component of the aliphatic hydrocarbon fraction and showed variation in quantity and distribution in the samples analysed. The biomarker peaks label and compounds name are presented in (Appendix II and III). The peak areas from the ion chromatogram were used to calculate the n-alkanes and isoprenoids parameters listed in (Table 4.4). The n-alkanes range from C_{10}-$_{41}$ for the coal samples and C_9-$_{41}$ in the shaly facies (Table 4.4). The samples are characterized by high molecular weight n-alkanes. The absence of low molecular weight n-alkanes could be probably due to evaporative ion during processing. Isoprenoids in the samples include C_{11}, C_{13}, C_{14}, C_{15}, C_{16}, C_{18}, C_{19} and C_{20}.

The ion fragmentograms of the saturate fractions obtained by Gas chromatography and Mass spectrometry were recorded in (m/z 191, m/z 217, m/z 218 and m/z 259) corresponding to tricyclic and pentacyclic terpanes, steranes, diasteranes, and tetracyclic polyprenoids while the aromatic fractions were recorded on the m/z 253, m/z 251 and m/z 245 corresponding to monoaromatic steroids, triaromatic steroids and triaromatic methylsteroids respectively (Appendix I). There are variations in the biomarker compounds

in each of the samples in terms of composition and their quantity. The coal samples (MG1G, MG2O and MG2H) are characterized by saturate compounds such as diamantane, C_{19}-C_{30} tricyclic terpane (excluding C_{27}), gammacerane, trisnorhopane, bisnorhopane, norneohopane, diahopane, C_{30}-C_{35}17αH (22R+22S) hopane, C_{27}-C_{29} βα (20S+20R) diasterane, C_{27}- C_{29} αα (20S+20R) sterane, C_{27}- C_{30} ββ (20S+20R) sterane and C_{30} tetracyclic polyprenoid while the shaly facies has imprint of diamantane, C_{19}-C_{26} terpane, bisnorhopane, norhopane, diahopane, C_{30}-C_{31}17αH (22R+22S) hopane and gammacerane.

In the same vein, the aromatic fractions for the coaly source rocks are dominated by compounds such as C_{27}-C_{29} methyltriaromatic steroid, triaromatic dinosteroids, C_{21}-C_{22} monoaromatic steroid, C_{29}-C_{30} secohopanoids. Other compounds include dimethyl, tri and tetramethyl naphthalene, phenanthrene, dibenzothiophene, C_{32}-C_{35} Benzohopane and Cadalene (Appendix III). Consequently, some of the compounds found in the coaly source rocks are absent in the shaly facies expecially the monoaromatic, triaromatic steroids and triaromatic dinosteroids. However, shale sample (BH15B) has similar aromatic compounds with that of coals (Appendix III). This is probably due to similar geochemical conditions such as nutrient level, physico-chemical conditions of the sedimentary environments (Pu et al., 1990).

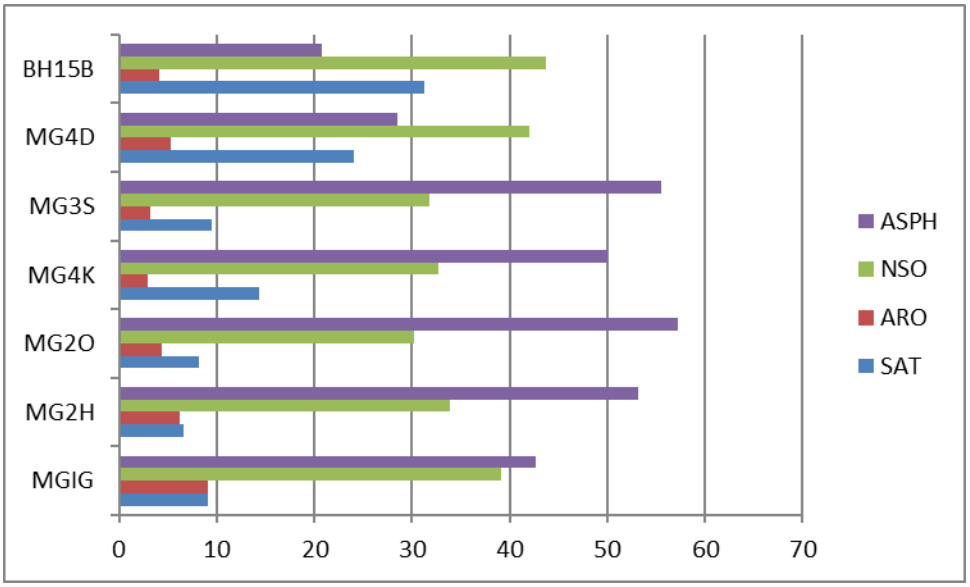


Figure 4.33: Bar chart showing the proportion of the extracted sample into saturate, aromatic, resins and asphaltenes.

Table 4.3: Extract Parameters obtained from the Gas Chromatography

S/n	Sample no/code	Sample type	Depth	Lithology /Rank	Resolved Components		
					Normal paraffin (%)	Isoprenoids %	Resolved Unknown %
1	MG1G	Surface	105	Coal (SB)	2.1	0.1	97.8
2	MG2H	Surface	62	Coal (SB)	1.6	0.1	98.3
3	MG2O	Surface	59	Coal (SB)	1.0	0.0	99
4	MG4K	Surface	14	Coal (SB)	0.7	0.0	99.2
5	MG3S	Surface	38	C. Shale	0.4	0.0	99.6
6	MG4D	Surface	23	Shale	1.0	0.1	98.9
7	BH15B	Core	157	Shale	1.1	0.1	98.9

4.5.1 Source and Depositional Environments

To infer the source of the organic matter and the environments of deposition, saturate and biomarker ratios and parameters were used (Tables 4.4, 4.5 and 4.6). The *n*-alkanes distributions in the coaly source rocks ranges from C_{10}-C_{41} maximizing at C_{29} (Table 4.4, Figures 4.45, 4.46, 4.47 4.48 and Appendix II). The pattern suggests organic matter derived mainly from terrestrial organic matter. The dominance of long chain C_{27}-C_{35} aliphatics relative to the total n-alkanes especially is typical of terrestrial higher plants (Tissot and Welte, 1984; Hunt, 1995; Miranda, et al., 1999). The n-alkanes for the shaly source rock ranges from C_9-C_{41} also maximizing at C_{16} and C_{29} (Table 4.4, Figures 4.48, 4.49, 4.51 and Appendix II) indicating mixed source. Pr/Ph ratio for the coaly facies ranges from 2.15-3.51 (avg. 2.79) while the shaly facies ranges between 0.95-2.37 (avg. 1.82) indicating coastal swamp and fluvio-deltaic depositional environment in sub-oxic to oxic setting (Killops and Killops, 2005; Peters et al., 2005).

The Pr/n-C_{17} ratios for the coals ranged from (0.71-3.63) with an average of 2.12 and (0.34-0.56) with an average of 0.45 for the shale. The Ph/n-C_{18} ranged from (0.26-0.92) averaging 0.57 for coaly source rock and (0.18-0.28) averaging 0.23 for the shale. The predominance of Pristane (n-C_{17}) over Phytane (n-C_{18}) support humic origin of the organic matter for the coaly source rocks deposited under oxidizing condition in fluvial-deltaic environments (Hughes et al. 1995, Peters et al., 2005) while the organic matter in the shaly source rocks were from mixed sources deposited under reducing condition in lacustrine setting (Figure 4.36, 4.37). The plot of Pr/n-C_{17} vs Ph/n-C_{18} (Figure 4.35) also confirms terrestrial and mixed sources for the organofacies corroborated by the high values of nC_{17}/*n*C_{29} over nC_{18}/*n*C_{19} (Table 4.4).

The saturate biomarker depositional indices used include C_{27}, $C_{28,}$ C_{29} αββS and ααα R sterane, gammacerane/hopane, diahopane/hopane and others (Table 4.5). The coals are rich in

C_{29} αββS steranes (> 50%) and C_{29} αααR sterane (~40%) calculated from isosterane αββS and αααR configuration from the m/z 218 and m/z 217 respectively. This is an indication of significant land plant contribution as evidenced from the very low C_{27} steranes. The shale also have high C_{29} steranes but with appreciable quantity of C_{27} and C_{28} αββS sterane (26% and 29%) and (34% and 24%) in C_{27}, C_{28}αααR sterane respectively confirming possible marine contribution for the shale source rocks (Table 4.5, Figures 4.36 and 4.37).

The minimal presence of C_{27} and C_{28} in the shale samples also reflects little contributions from phytoplankton; algae, diatoms, dinoflagellates (Volkman et al., 1998; Sari and Bahtiyar, 1999; Peters et al., 2005). This is in agreement with plot of Pr/n-C_{17} vs Ph/n-C_{18}, though there is absence of $C_{30,}$ 24 n-propyl cholestane (biomarker of chrysophyte algae to strengthen the marine algae contribution. However, the presence of C_{30} tetracyclic polyprenoids (TPP) a marker of lacustrine algae supports fresh water lacustrine depositional conditions (Holba et al., 2003).

The presence of gammacerane in the m/z 191 chromatogram also indicate stratified reducing water column (Sinninghe Damste et al, 1995). Diahopane/hopane ranges from 0.05-0.2 in the coals and 0.11-0.67 in the shale suggest suboxic to oxic condition because of presence of diahopane produced by aerobic bacteria in clay rich sediments accumulated in oxidizing and suboxidizing conditions (Moldowan et al., 1991; Peters et al., 2005). The ratios of homohopanes H35/H34 of < 1 in the coals and the predominance of pristane over phytane indicate that organic matter undergone intense oxidation transformations during diagenesis. The relatively low level of C_{23} tricyclic terpanes in m/z 191 of the coal compared to other tricyclic terpane distribution is consistent with the tricyclic distribution seen in terrestrial organic matter (Peters et al, 2005) this is backed up by the low average value of sterane/hopane for the coal (0.09) as sterane/hopane >1 indicate marine organic matter.

The C_{24}tetra/C_{30}hopane ratios also range from 0.08 to 0.12 (Table 4.5) in the coaly source rocks reflecting lacustrine and fluvial/deltaic environments (Peters et al., 2005). The C_{24}tetra/C_{26}tri(R+S) ratios range between 0.63-0.71 (avg, 0.68) for the coals probably reflects organic matter sourced from terrestrial plants (Philip and Gilbert, 1986).

The sterane/hopane ratio values range from 0.06-0.35 (Table 4.5). This ratio value (<0.6) suggest introduction of bacterial commonly associated with terrigenous organic matter in coals (non-marine organic matter) according to (Peters and Moldowan, 1993; Norgate et al., 1999). The presence of homohopanes (C_{31}-C_{35}) in all the samples, suggest that bacteriohopanetetrol and other C_{35} hopanoids associated with prokaryotic micro-organisms could be contributors to the source of the organic matter (Rohmer, 1987; Wang et al., 1996).

The aromatic biomarker depositional indices further corroborate the saturate indices and gives credence to the earlier interpretations. The dibenzothiophene/phenanthrene (DBT/PH) ratio range from 0.03 to 0.19 for the coal and 0.08-0.14 for the shaly source rocks respectively (Table 4.6). These values indicate contributions of terrestrial organic matter (Requejo, 1994). The low amounts of dibenzothiophene to phenanthrene (DBT/PH) (Table 4.6 and Figure 4.36, 4.40) indicate deposition of the organic matter predominantly in lacustrine and/or fluvial/deltaic environments (Hughes et al., 1995). There is also probable indication that the shales are sulphate poor because of a shale sample plotted between the boundary of zone 2 and zone 3 (Figure 4.40).

The % $C_{26,}$ C_{27}, $C_{28,}$ C_{29} TAS for the coals range from **(**1.3-2), (7.3-21.5), (3.9-6.4) and (72.6-86.8) respectively (Table 4.6). The predominance of C_{29} Triaromatic steroid (TAS) indicates a terrestrial source as evident from the ternary plot of C_{27}, $C_{28,}$ C_{29} Monoaromatic steroid (MAS) (Figure 4.38). There is appreciable amount of C_{27}, C_{28} MAS in the shale sample which may suggest mixed sources.

According to (Killops and Killops, 2005), the presence of 1, 2, 5- and 1, 2, 7-Trimethylnaphthalene (TMN) in the coal samples indicates both gymnosperms and angiosperm contribution to the organic matter. Also, the presence of 1,6-, 1,7-, and 2,6-Dimethynaphthalene (DMN) in all the samples indicates terrestrial organic matter input (Simoneit et al., 1986) as corroborated by the occurrence of 1,7-Dimethyphenanthrene DMP (pimanthrene) in the samples. In addition, the presence of 1, 2, 6-TMN also indicates microbial contribution to the biomass.

4.5.2 Thermal Maturity and Rank

Despite the confirmation of the maturity status of the samples analysed through the Tmax and vitrinite reflectance (Table 4.1) values indicating immature to marginally maturity level, biomarker maturity parameters (saturate and aromatic) was used to validate the maturity level. According to Sykes and Snowdon (2002), the minimum threshold for hydrocarbon generation for coaly source rock is 420^{o}C in which about half of the coals analysed reached the threshold.

The predominance of asphaltenes and NSO in the extracts (Fig. 4.34) also confirms that the bitumen originates from low maturity level of kerogen cracking (Clayton and Law, 1993). The Carbon Preference Index (CPI) which measures the odd/even predominance of the n-alkanes showed the samples to range from 2.74-3.76 (Table 4.4). These values are essentially greater than unity, qualifying them as immature (Peters and Moldowan, 1993). The high CPI (>1) and OEP values observed for the coals are characteristic of low rank coal i.e. subbituminous (Sabel et al., 2005; Stefanova et al., 2005).

Coal sample (MG4K) showed Tmax of 439^{o}C indicating maturity in the oil window; the spiked Tmax may possibly due to effect of weathering or impurities in the sample. However, the low S/(S+R)(C_{29} ααα) and ββS/(ββS+ ααR) (C_{29}) values (0.12-0.28) and (0.26-0.61) respectively (Table 4.7) for the coals indicates immature to marginally mature organic

matter, though the thermal equilibrium value (TEV) of the sterane ratios are 0.55 and 0.70 respectively which corresponds to approximate vitrinite reflectance (VR) values at which the thermal equilibrium value of the biomarker ratio (TEV) was reached.

According to (Seifert and Moldowan, 1986), C_{31}- or C_{32}-homohopanes can be used for calculations of the sterane 22S/(22S+22R) ratio which is also a maturity parameter and is always close to it thermal equilibrium value (TEV). However, considering the C_{32} homohopane ratios of the coal ranging from 0.28-0.53 and their TEV value of 0.6, the C_{32} homohopane ratios falls below the equilibrium range and thus indicates thermal maturity level has not been reached. Most of the saturate maturity parameters are lower compared to their corresponding TEV value indicating low maturity status (Table 4.8) and hence have not reach stage of oil generation (Mackenzie et al., 1980). The Moretane/Hopane and Ts/Ts + Tm ratios in the samples range from 0.42-0.68 and 0.07-0.12 respectively (Table 4.7). These values suggest low maturity status (Peters et al., 2005).

The aromatic maturity indices are presented in Table 4.9 to infer the maturity status of the organofacies. The calculated Methyl Phenanthrene index (MPI-1) and (MPI-2) values are close. The MPI-1and MPI-2 of the coal ranges from 0.23-0.31 and 0.31-0.50 respectively while the shaly source rock range from 0.33-0.51 and 0.45-0.56 respectively (Table 4.9). This suggest immature to marginally mature source rocks. The TAS/(MAS+TAS) ratio range from 0.19-0.39 suggest immature level. Other maturity parameters such as DNR, TDE and Rc also corroborate low maturity status for the samples (Table 4.9).

4.5.3 Age

The absence of oleanane peak in m/z 191 mass chromatogram confirms gymnosperm high plant input older than Late Cretaceous. The coals have appreciable quantity of C_{19} and C_{20} tricyclic terpane suggesting gymnosperm contribution. Though low aromatic compound such as C_{30} 8, 14 secohopanoid are present which are probably sourced from angiosperms.

The dinosteroid index and C4/C3+C4 mester of the coals range from 0.15-1.28 and 0.32-0.62 respectively suggesting Mesozoic age.

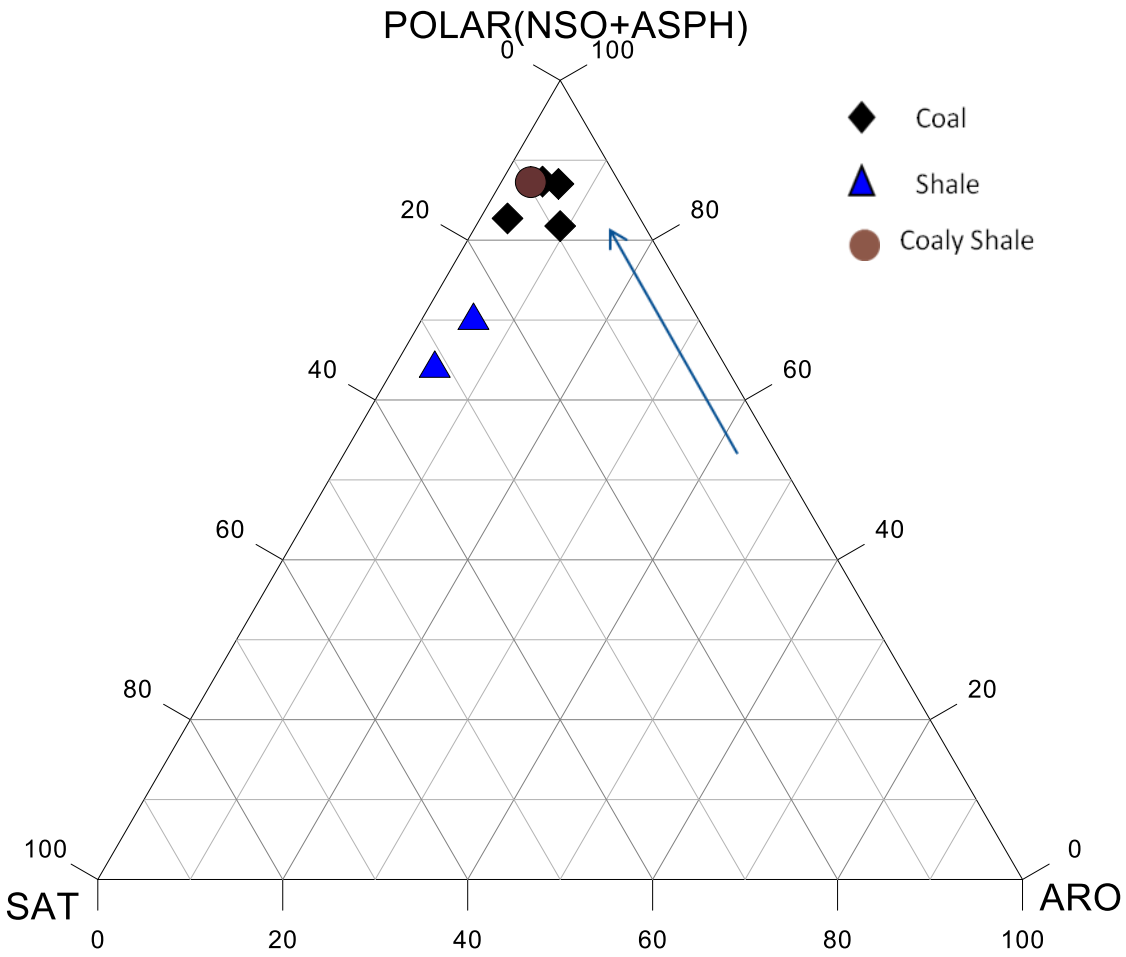


Figure 4.34: Ternary diagram showing the proportion of saturated hydrocarbons, aromatic hydrocarbons and polar (NSO+Asphaltenes) in extracts of coal, shale and coaly shale source rocks of maiganga, Gombe Formation. The samples have higher percentage of heterocompounds (after Clayton and Law, 1993).

Table 4.4: n-Alkanes, isoprenoids parameters and percentage composition of the extracts from coal and shale of Maiganga, Gombe Formation.

S/n	Sample no/code	Depth (ft)	Lithology/Rank	Ext (gm)	Ext (ppm)	Pr/Ph	Pr/n-C_{17}	Ph/n-C_{18}	nC_{17}/nC_{29}	nC_{18}/nC_{19}	C range	CPI	SAT %	ARO %	NSO %	ASPH %	Total Recov %
1	MG1G	105	Coal (SB)	42	6000	2.15	2.82	0.74	1.21	0.01	C_{11-41}	3.30	9.09	9.09	39.09	42.73	100
2	MG2H	62	Coal (SB)	50.6	7229	3.51	3.63	0.92	1.10	0.03	C_{10-41}	3.28	6.64	6.27	33.95	53.14	100
3	MG2O	59	Coal (SB)	63	9000	2.94	1.30	0.34	1.32	0.03	C_{11-41}	3.54	8.21	4.40	30.21	57.18	100
4	MG4K	14	Coal (SB)	891	15872	2.55	0.71	0.26	0.96	0.04	C_{11-41}	3.76	14.3	2.92	32.75	50.00	100
5	MG3S	38	C. Shale	190	27035	2.37	1.16	0.46	0.85	0.07	C_{11-35}	2.74	9.52	3.17	31.75	55.56	100
6	MG4D	23	Shale	19.9	2985	2.13	0.56	0.28	1.15	0.08	C_{11-41}	3.02	24.1	5.36	41.96	28.57	100
7	BH15B	157	Shale	60.9	7382	0.95	0.34	0.18	1.87	0.15	C_{9-39}	2.82	31.3	4.17	43.75	20.83	100

Pristane/Phytane = IP19/IP20
Pristane/nC17 = IP19/NC17
Phytane/nC18 = IP20/NC18
nC18/nC19 = NC18/NC19
nC17/nC29 = NC17/NC29
CPI Marzi[4] = ((NC23+NC25+NC27)+(NC25+NC27+NC29))/(2*(NC24+NC26+NC28))

Key: Ext-Extract (gm, ppm) SB- Sub-Bituminous, Pr- Pristane, Ph-Phytane, CPI- Carbon Preference Index, Sat- Saturate, Aro- Aromatic, NSO- Resin, ASPH- Asphaltene, Recov-Recovery.

Table 4.5: Selected Saturate biomarker source and depositional indices

S/n	Sample no/code	Depth (ft)	Lithology /Rank	$\%C_{27}\alpha\beta\beta S$	$\%C_{28}\alpha\beta\beta S$	$\%C_{29}\alpha\beta\beta S$	$\%C_{27}\alpha\alpha\alpha R$	$\%C_{28}\alpha\alpha\alpha R$	$\%C_{29}\alpha\alpha\alpha R$	Ga/Ho	D/Ho	H35/H34	C_{23}/C_{24} TT	St/Ho
1	MG1G	105	Coal (SB)	3.8	6.4	89.9	9.9	51.2	38.9	0.2	0.19	0.59	1.51	0.06
2	MG2H	62	Coal (SB)	3.4	4.4	92.2	22.0	38.0	40.0	0.25	0.10	0.64	1.46	0.10
3	MG2O	59	Coal (SB)	5.3	44.2	50.6	12.5	39.3	48.3	0.29	0.05	0.51	1.97	0.12
4	MG4K	14	Coal (SB)	-	-	-	-	-	-	0.23	0.2	-	-	-
5	MG3S	38	C. Shale	-	-	-	-	-	-	-	3.6	-	-	-
6	MG4D	23	Shale	-	-	-	-	-	-	0.12	0.67	-	1.72	-
7	BH15B	157	Shale	26.6	29.4	44.0	34.1	24.3	41.7	0.12	0.11	-	1.67	0.35

KEY: Ga= Gammacerane, Ho=Hopane, H = Homohopane, TT=Tricyclic terpane, St= Sterane
$\%C_{27}\alpha\beta\beta S$ = 100*C27ABBS/(C27ABBS+C28ABBS+C29ABBS), $\%C_{28}\alpha\beta\beta S$ = 100*C28ABBS/(C27ABBS+C28ABBS+C29ABBS)
$\%C_{29}\alpha\beta\beta S$ = 100*C29ABBS/(C27ABBS+C28ABBS+C29ABBS), $\%C_{27}\alpha\alpha\alpha R$ = 100*C27R/(C27R+C28R+C29R),
$\%C_{28}\alpha\alpha\alpha R$ = 100*C28R/(C27R+C28R+C29R) , $\%C_{29}\alpha\alpha\alpha R$ = 100*C29R/(C27R+C28R+C29R), Ga/Ho= GAM/H30
H35/H34= (H35R+H35S)/(H34R+H34S)
St/Ho=(DIA27S+DIA27R+DIA28SA+DIA28SB+DIA28RA+DIA28RB+C27S+BB_D29S+C27BBS+C27R+DIA29R+
C28S+C28BBR+C28BBS+C28R+C29S+C29BBR+C29BBS+C29R)/(TS+TM+H28+H29+C29TS+DH30+H30+
H31R+H31S+H32R+H32S+H33R+H33S+H34R+H34S+H35R+H35S)

Table 4.6: Selected Aromatic biomarker source and depositional indices

S/n	Sample no	Depth (ft)	Lithology	%26TAS	%27TAS	%28TAS	%29TAS	%27MAS	%28MAS	%29MAS	DBT/PH	MDBT/ MPHEN	9MP/ (9MP+1 MP)	Paq
1	MG1G	105	Coal (SB)	2	7.3	3.9	86.8	23.8	20.1	56.1	0.03	0.10	0.67	0.15
2	MG2H	62	Coal (SB)	1.3	21.5	4.6	72.6	17.3	25.3	57.4	0.04	0.09	0.40	0.06
3	MG2O	59	Coal (SB)	1.9	12.2	6.4	79.4	9.9	23.3	66.8	0.10	0.38	0.55	0.12
4	MG4K	14	Coal (SB)	-	-	-	-	10	19.3	70.7	0.19	0.33	0.49	0.10
5	MG3S	38	C. Shale	-	-	-	-	16.6	19.4	63.9	0.11	0.19	0.50	0.11
6	MG4D	23	Shale	-	-	-	-	14.2	25.8	60.0	0.08	0.25	0.50	0.16
7	BH15B	157	Shale	10	28.1	18.5	43.4	21.4	23.9	54.6	0.14	0.57	0.50	0.19

TAS = Triaromatic Steroids, MAS = Monoaromatic Steroids, DBT = Dibenzothiophene, PH = Phenanthrene, MPHEN-MethylPhenanthrene, MDBT-Methyldibenzothiophene, 9MP- 9-MethylPhenanthrene, 1MP- 1- MethylPhenanthrene, Paq= nC23 + nC25/ nC23 + nC25 + nC29 + nC31 – Alkanes.

Table 4.7: Selected saturate biomarker maturity indices

S/n	Sample no/code	Depth (ft)	Lithology /Rank	S/(S+R)(C_{29} ααα)	C_{29})ββS/(ββS+ ααR)	Ts/Ts+Tm	Mor/Hop	H32S/(R+S)	TT/Hop
1	MG1G	105	Coal(SB)	0.28	0.26	0.12	0.54	0.53	0.04
2	MG2H	62	Coal(SB)	0.28	0.61	0.08	0.62	0.40	0.03
3	MG2O	59	Coal(SB)	0.12	0.37	0.07	0.61	0.28	0.08
4	MG4K	14	Coal(SB)	-	-	-	0.63	-	-
5	MG3S	38	C. Shale	-	-	-	0.55	-	-
6	MG4D	23	Shale	-	-	-	0.68	-	0.09
7	BH15B	157	Shale	0.1	0.04	-	0.42	-	0.38

Note: Ts/Ts+Tm = Trisnorhopane, Mor/Hop = Moretane/Hopane, TT/Hop = Tricyclic terpane/ Hopane, H32S/(R+S) = Homohopanes, S/(S+R)(C_{29} ααα)= Sterane (217), C_{29})ββS/(ββS+ ααR) = Sterane (217).

Table 4.8: Saturate biomarker ratio, thermal equilibrium value and vitrinite reflectance of the samples.

S/n	Saturate Biomarker	Range	TEV	*VR (%)	Maturity
1	S/(S+R) (C_{29} ααα)	0.1-0.28	0.55	0.80	IM-LM
2	(C_{29}) ββS/(ββS+ ααR)	0.04-0.61	0.70	0.90	IM-LM
3	Diasterane/ C_{27} ααα sterane	0.17-1.01	1.00	1.40	IM-LM
4	Moretane/Hopane	0.42-0.68	0.05	0.70	IM-LM
5	Ts/(Ts+Tm)	0.07-0.12	1.00	1.40	IM
6	C_{32} Homohopane	0.28-0.53	0.60	0.60	IM-LM

Note: TEV = Thermal Equilibrium value of the biomarker ratio (Seifert and Moldowan, 1986) *VR = Approximate Vitrinite Reflectance value at which the TEV value was reached. IM = Immature and LM = Low maturity.

Table 4.9: Selected Aromatic biomarker Maturity indices

S/n	Sample no/code	Depth (ft)	Lithology/Rank	TAS/ (TAS+MAS)	MPI-1	MPI-2	DNR-1	DNR-2	MDR	MDR-1	TDE-1	TDE-2	Rc	VR
1	MG1G	105	Coal (SB)	0.27	0.31	0.50	2.70	1.31	0.66	1.15	5.10	0.27	0.56	0.55
2	MG2H	62	Coal (SB)	0.39	0.23	0.32	4.12	1.09	0.77	0.90	7.55	0.19	0.51	0.48
3	MG2O	59	Coal (SB)	0.19	0.23	0.31	4.11	1.88	0.42	1.64	9.44	0.40	0.51	-
4	MG4K	14	Coal (SB)	-	0.34	0.45	4.51	1.81	0.38	2.64	5.43	0.37	0.58	0.49
5	MG3S	38	C. Shale	-	0.37	0.50	2.99	1.55	0.67	1.12	8.21	0.26	0.59	-
6	MG4D	23	Shale	-	0.33	0.45	2.88	1.18	0.39	2.01	8.42	0.30	0.57	0.52
7	BH15B	157	Shale	0.20	0.51	0.56	3.40	1.94	0.81	0.83	4.79	0.38	0.68	0.49

Note: Methyl Phenanthrene index = (MPI-1) and (MPI-2), Mono= (MAS) and Triaromatic Steroids (TAS), DNR = Dimethylnaphthalene ratio, MDR = Methyldibenzothiophene ratio, Rc = Calculated Vitrinite Reflectance of the aromatic biomarker, VR=Vitrinite Reflectance of the sample. MPI-1=1.5(2MP+3MP)/(P+1MP+9MP) MPI-2=3(2MP)/(P+1MP+9MP), MDR=4MDBT/1MDBT, MDR-1=1MDBT/DBT, DNR 1=(2,6+2,7)/(1,5) DMN, Rc=0.6(MPI-1)+0.37.

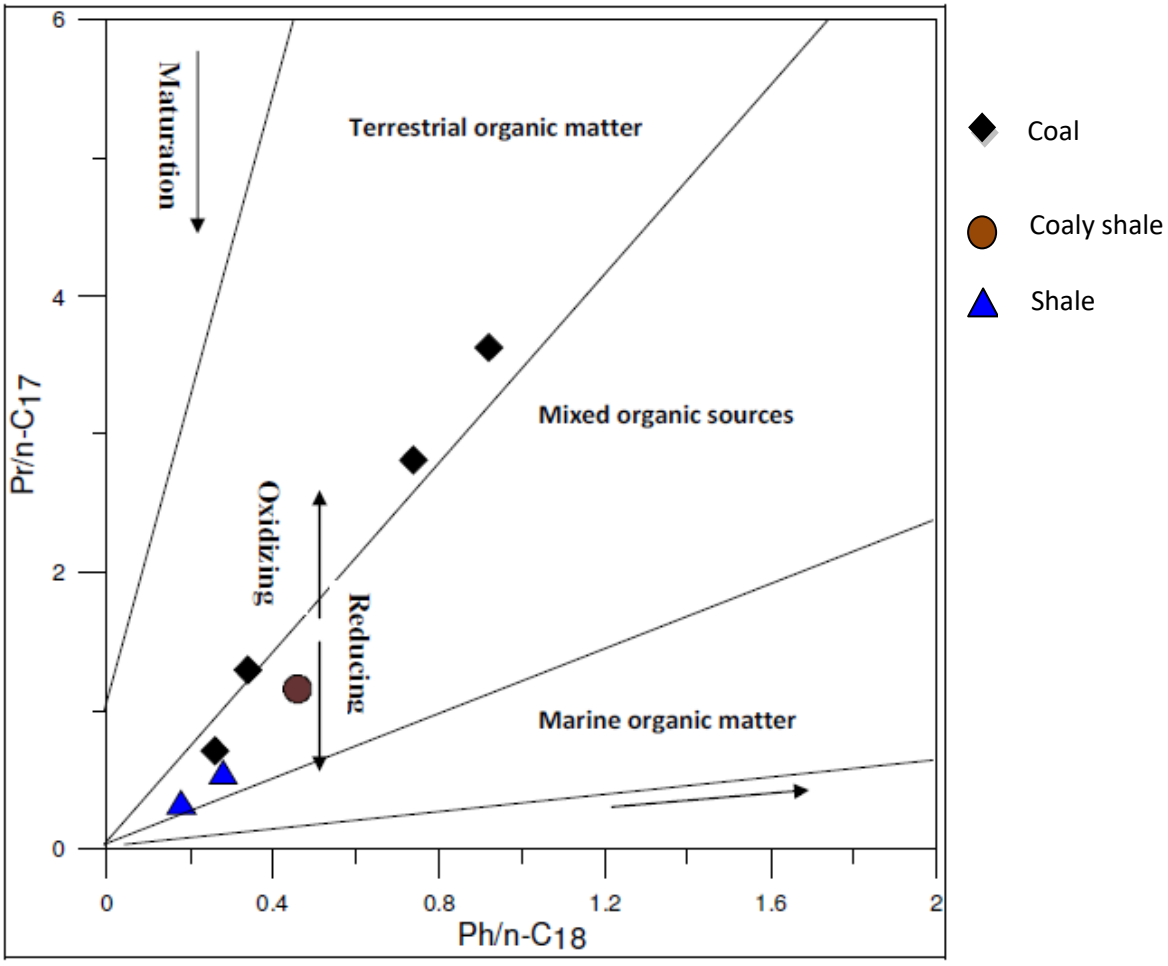


Figure 4.35: Plot of Pr/n-C_{17} vs Ph/n-C_{18} of coal and shale samples of Maiganga, Gombe Formation. The coals fall within the terrestrial sources in oxic depositional settings, shales plotted within the mixed sources (after Peters et al., 2005; Hunt, 1995).

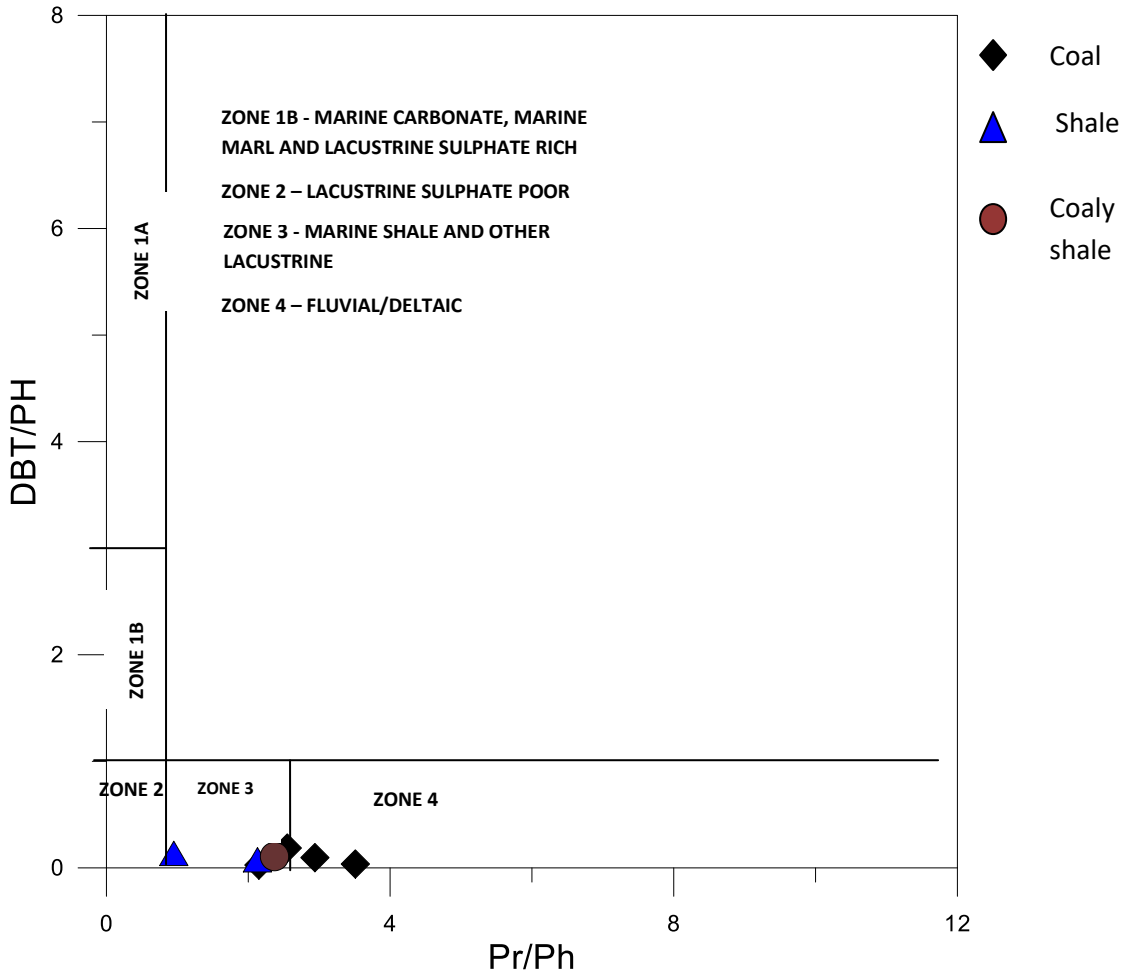


Figure 4.36: Plot of dibenzothiophene/phenanthrene (DBT/PH) vs. pristane/phytane (Pr/Ph) of coaly and shaly source rocks of Maiganga, Gombe Formation (Hughes et al., 1995). The coals, shale and coaly shale plotted in Zone 3 and 4 (Marine shale, lacustrine and fluvial/deltaic environment).

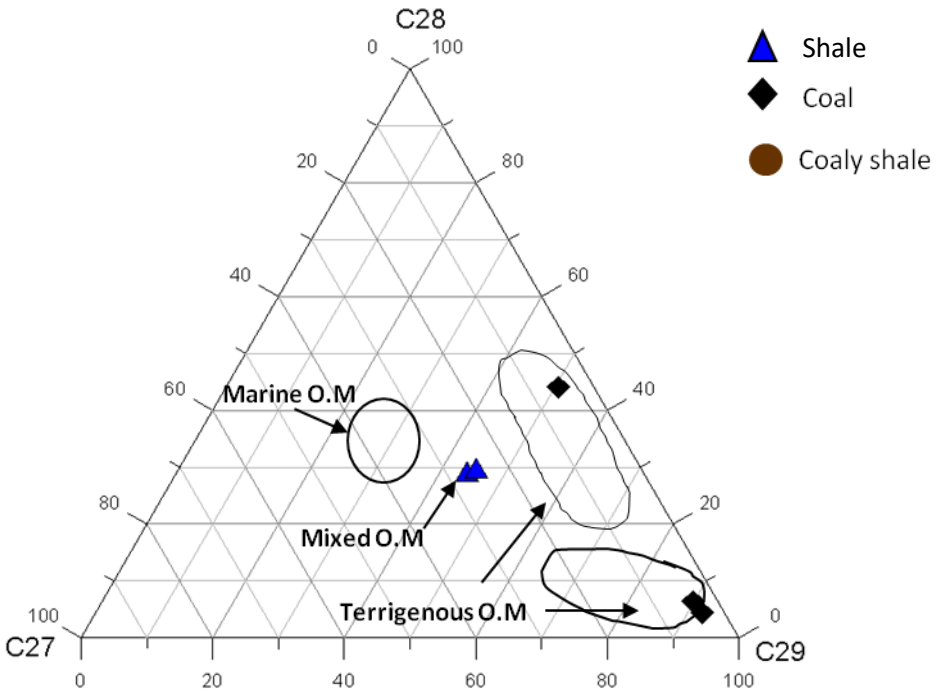


Figure 4.37: Ternary diagram of the distribution of C_{27}, C_{28}, C_{29} steranes in Maiganga coal and shale, Gombe Formation. The coals are plotted in terrigenous portion due to predominance of C_{29} (after Moldowan et al., 1985).

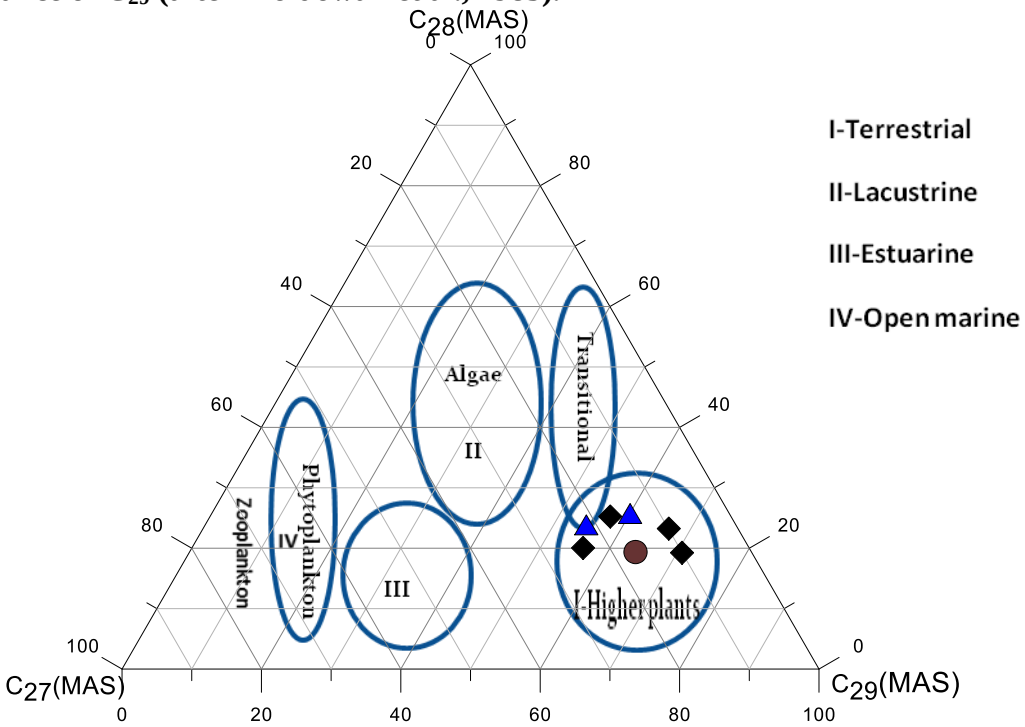


Figure 4.38: Ternary diagram of the distribution of C_{27}, C_{28}, C_{29} monoaromatic steroid in Maiganga coal, shale and coaly shale, Gombe Formation. The coals are plotted in terrigenous portion due to predominance of C_{29} MAS (after Moldowan et al., 1985).

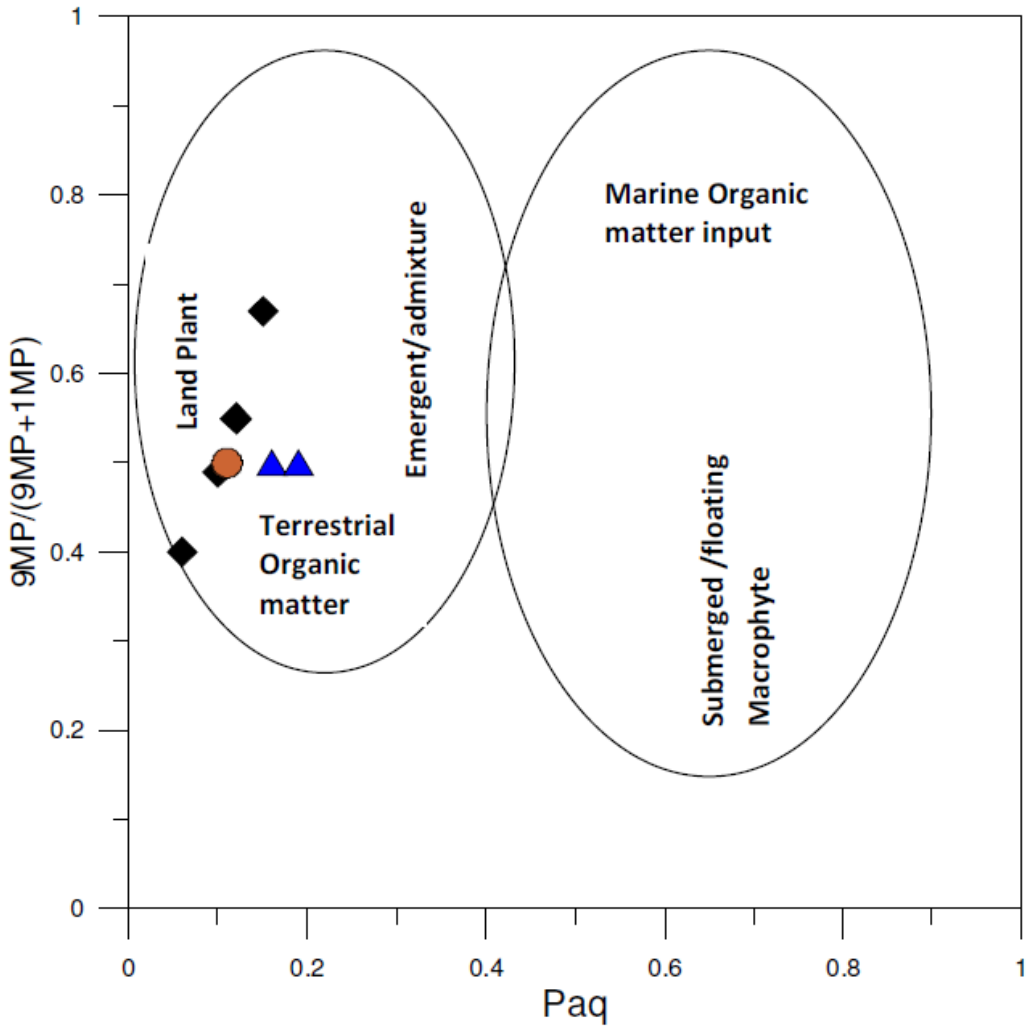


Figure 4.39: Organic matter source discrimination of Maiganga samples (After Ficken et al., 2000). The samples falls within the terrestrial source land plant.

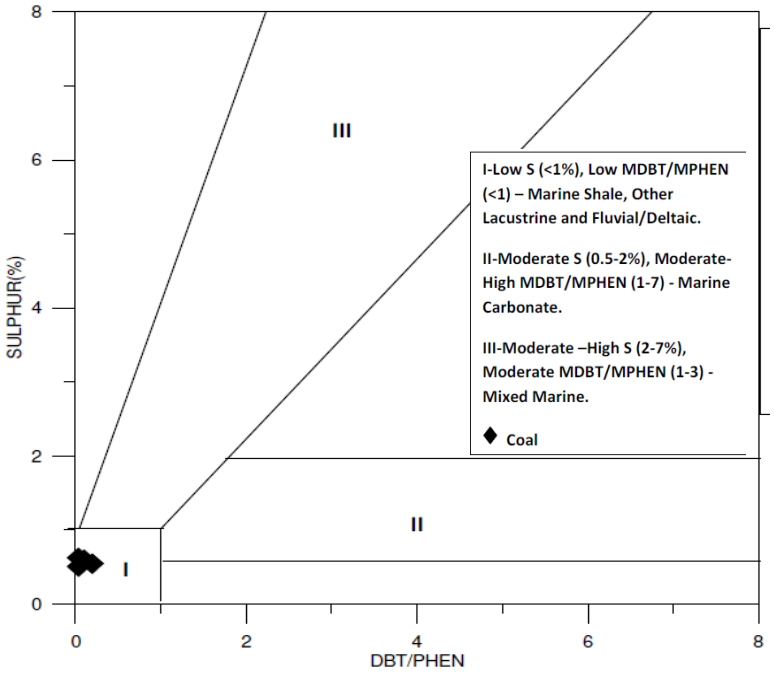


Figure 4.40: Plot of total Sulphur vs. dibenzothiophene/phenanthrene (DBT/PHEN) for Maiganga coal (after Hughes et al., 1995).

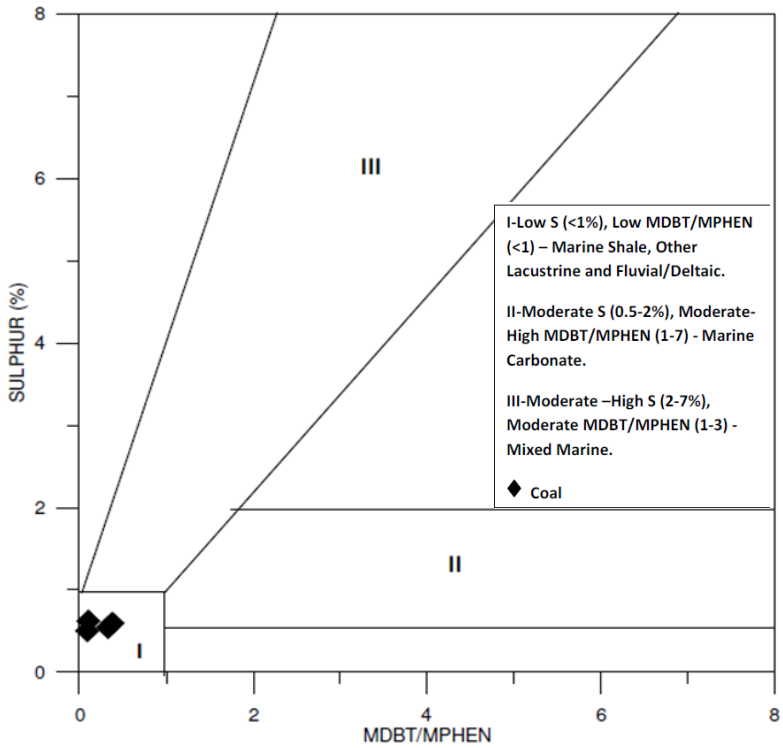


Figure 4.41: Cross plot of total Sulphur vsmethyldibenzothiophene/methylphenanthrene (MDBT/MPHEN) of Maiganga coal (after Hughes et al., 1995).

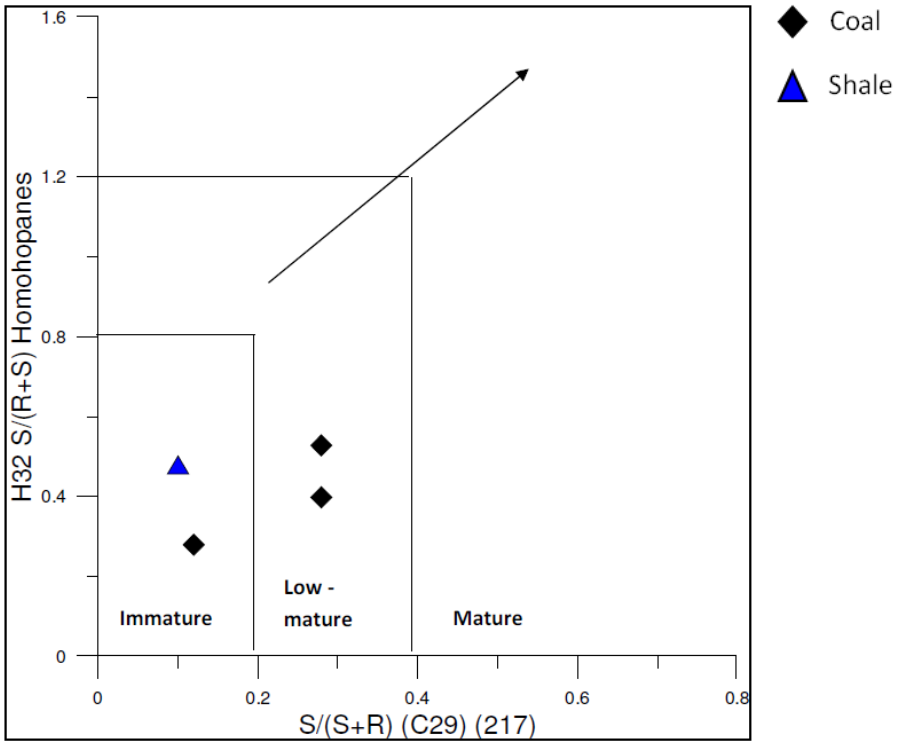


Figure 4.42: Plots of 22S/22S+22R C32 homohopanes against C29αββ/αββ+ααα steranes (After Inaba et al., 2001). The coal and shale samples are immature to low maturity.

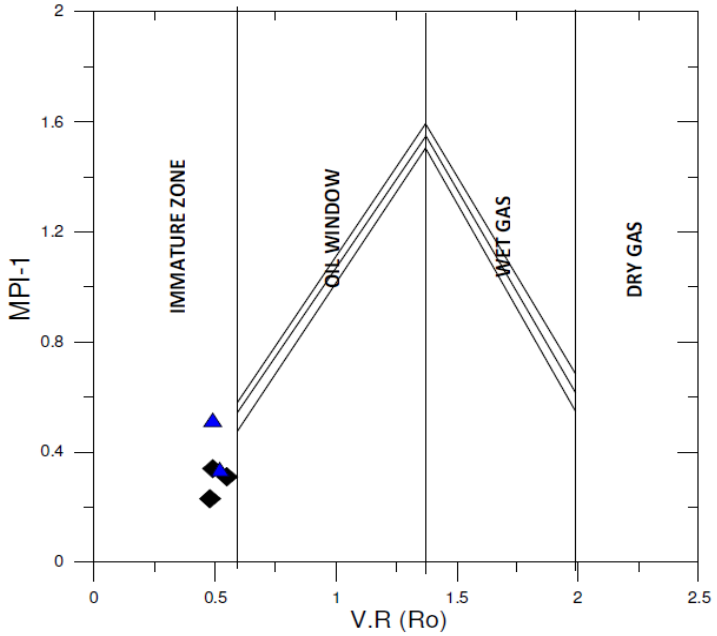


Figure 4.43: Correlation of MethylPhenanthrene index (MPI-1) with Vitrinite reflectance (Ro) of Maiganga coal and shale of Gombe Formation. The samples fall under immature zone.

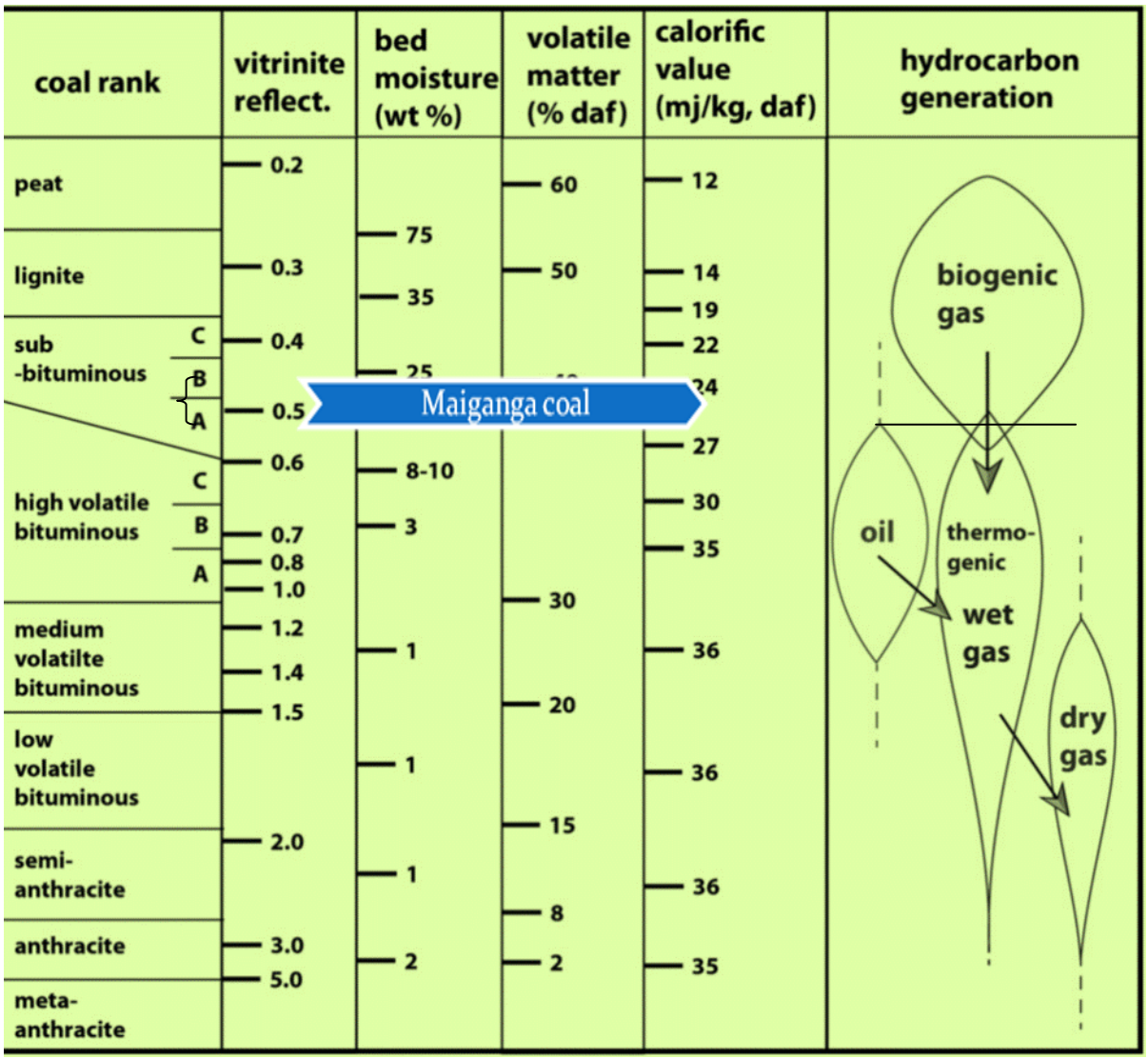


Figure 4.44: Correlation of vitrinite relectance with proximate parameters, the Romax value (0.48-0.55) shows coalification/rank of sub-bituminous B to A capable of generating biogenic gas.

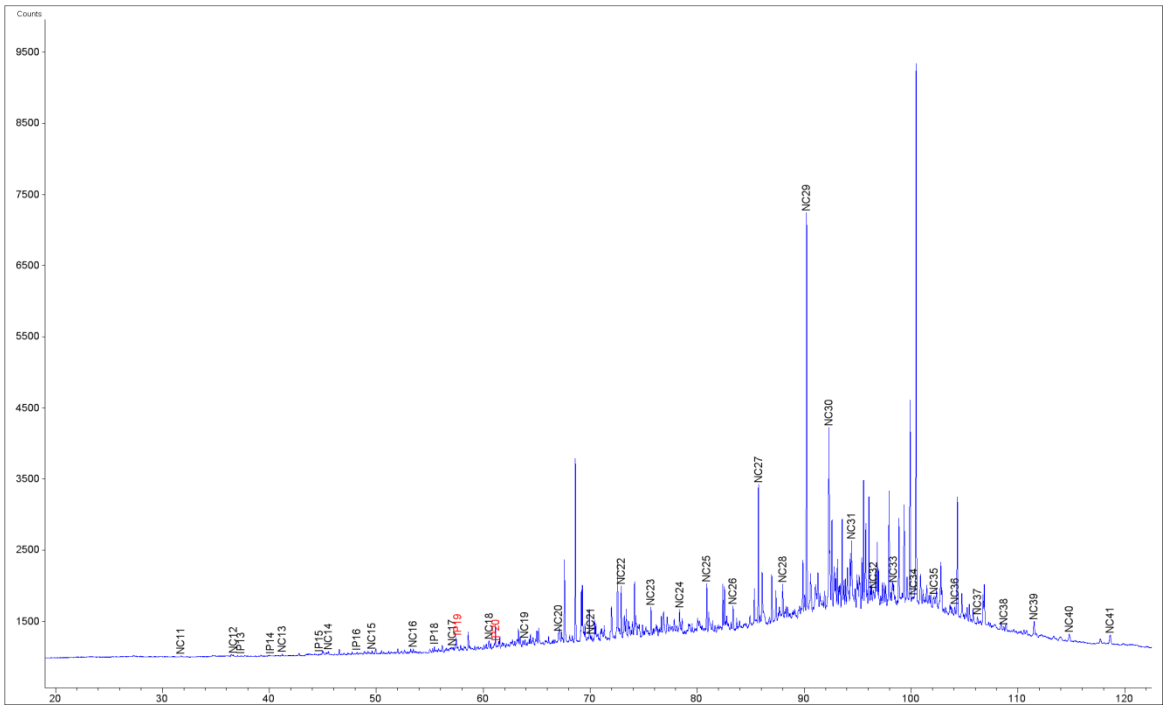


Figure 4.45: Chromatograms of sample MG1G showing *n*-Alkanes distribution.

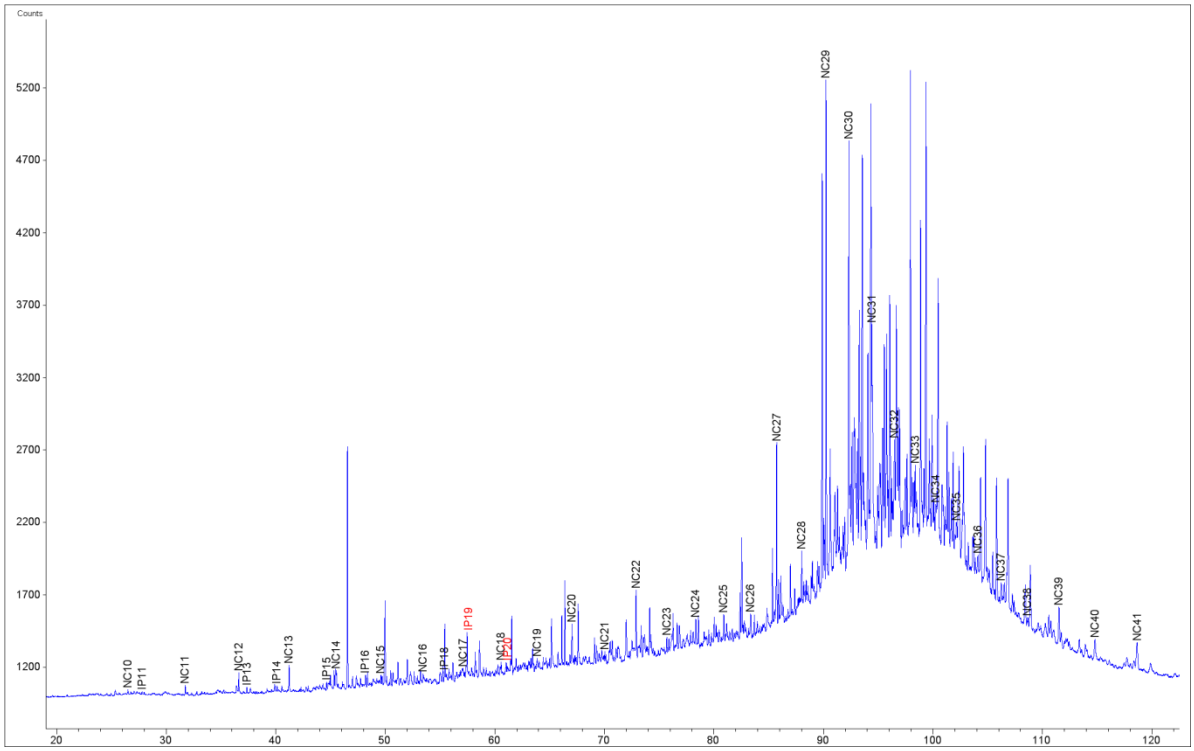


Figure 4.46: Chromatograms of sample MG2H showing *n*-Alkanes distribution.

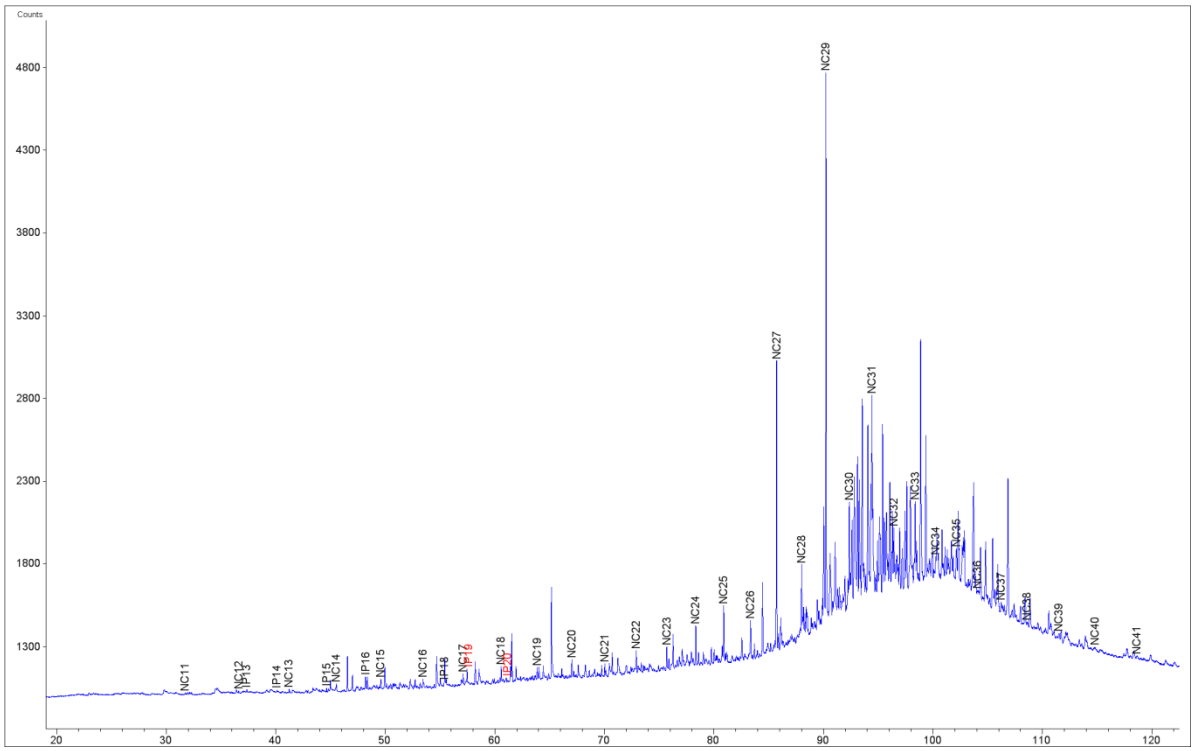


Figure 4.47: Chromatograms of sample MG2O showing *n*-Alkanes distribution.

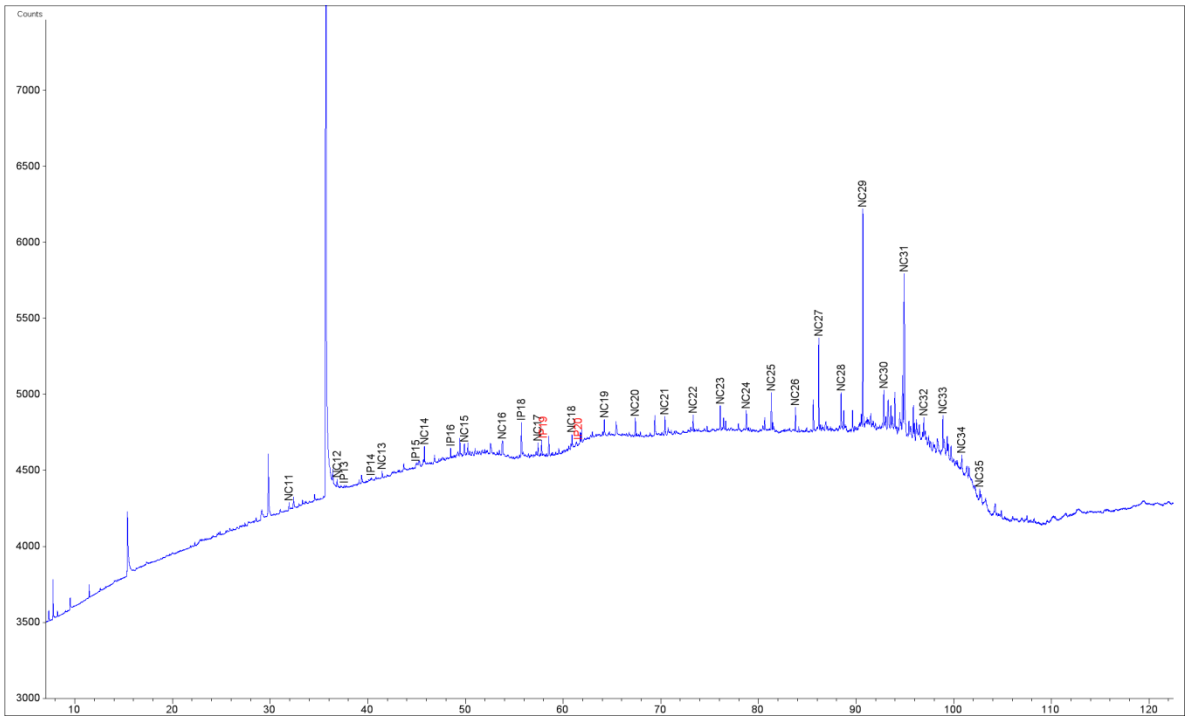


Figure 4.48: Chromatograms of sample MG3S showing *n*-Alkanes distribution.

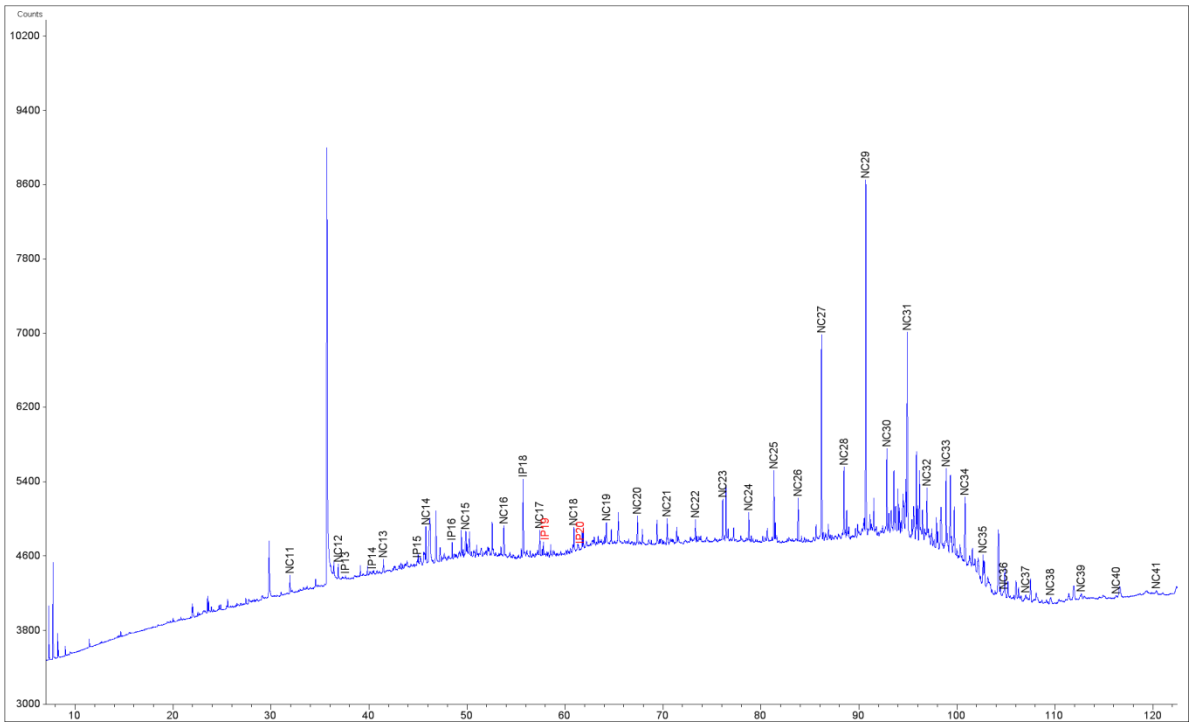


Figure 4.49: Chromatograms of sample MG4D showing *n*-Alkanes distribution.

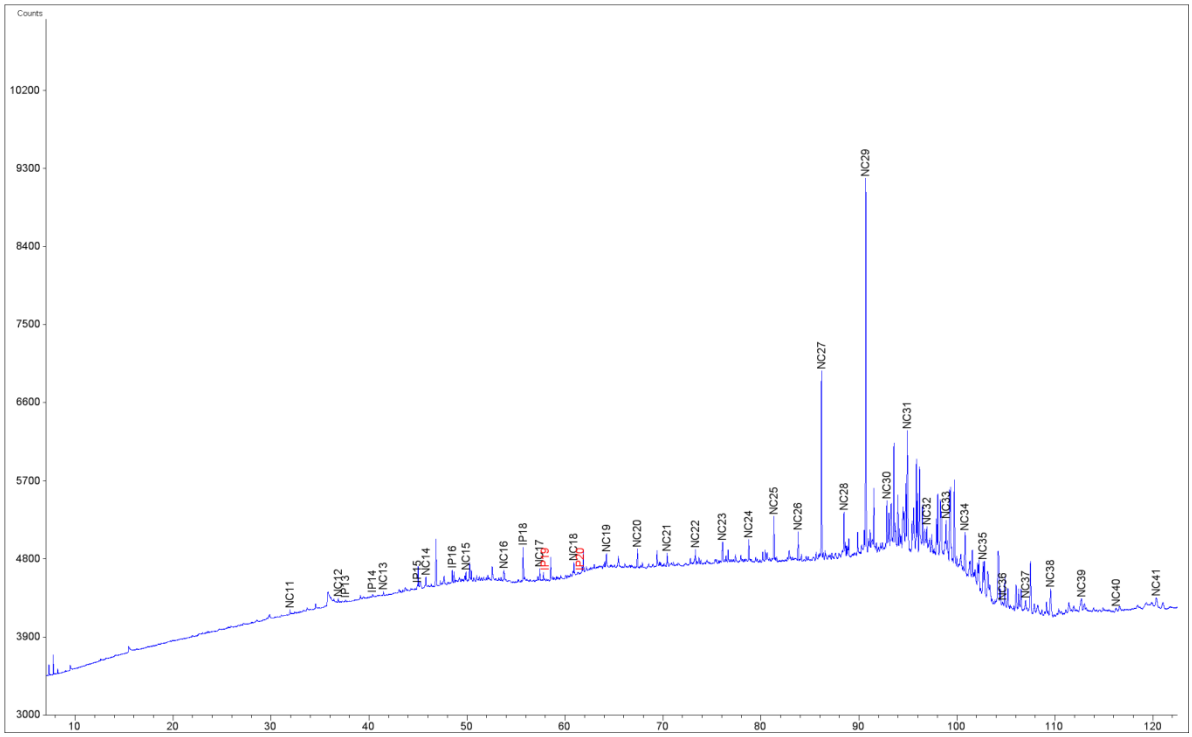


Figure 4.50: Chromatograms of sample MG4K showing *n*-Alkanes distribution.

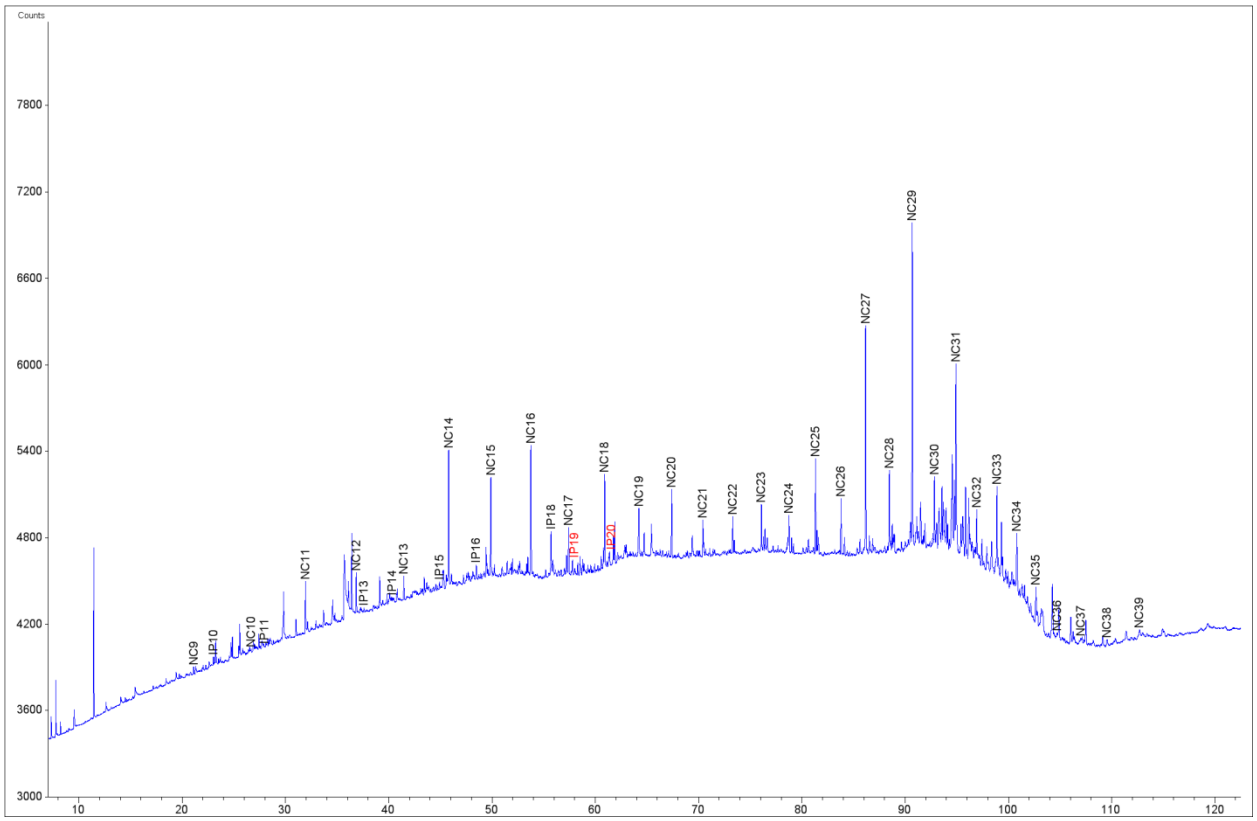


Figure 4.51: Chromatograms of sample BH15B showing *n*-Alkanes distribution.

4.6 Compound Specific Isotope Analysis (CSIA)

$\delta^{13}C$ of the kerogen, saturate and aromatic fraction of the coal extract are presented in (Table 4.10) to deduce the source and depositional condition of the organic matter in the organofacies. Chabbi et al., (2007) has shown that $\delta^{13}C$ composition in kerogen and n-alkane may indicate the chemical components of the organic material that came from the same vegetation type. Palaeoenvironmental indicator can also be deduced by assessing the distribution of ^{13}C among natural products (Hayes, 1993) which can provide information about ancient biogeochemical processes. ^{13}C isotopic composition has also been used in reconstructing global carbon cycle according to (Arens et al., 2000).

According to (Schouten et al., 2001; Yangming et al., 2005), the shape of *n*-alkane carbon isotopes can be used to distinguish terrestrial source from marine source. Terrestrial organic matter sourced from higher plants tends towards isotopically lighter values while a flat or positively sloping profile for *n*-alkane isotopes are usually recoeded for marine origin. The *n*-alkane carbon isotope profiles can be altered if there are materials from multiple sources because *n*-alkanes and their precursors are produced by various organisms (Collister et al., 1994).

The carbon isotopic composition of the saturate for coal sample MG2H is -27.7 δ^{13}‰ PDB while for shale sample BH15B is (-31.0 δ^{13}‰) PDB. The aromatic $\delta^{13}C$ compositions are (-26.5 δ^{13}‰) PDB and (29.2 δ^{13}‰) PDB respectively (Table 4.10). The coal sample is said to be higher or enriched in saturate and aromatic $\delta^{13}C$ than the shale. Generally, the *n*-alkanes become isotopically lighter or depleted with increasing chain length reflecting terrigenous input deposited in fluvial/deltaic depositional environment (Murray et al., 1994). The chain lengths of the coal and shale sample are C_{10}-C_{41} and C_9-C_{39} respectively. However, both samples are characterized by long chain aliphatic and it is expected that their $\delta^{13}C$ values should be depleted. The isotopic value of (-27.7 δ^{13}‰) PDB and (-31.0 δ^{13}‰) PDB for the

coal and shale respectively is comparable to value of (–32.19 to –27.15 δ^{13}‰) PDB obtained in Onyeama coal sourced from procaryotic organism and terrestrial organic matter. It is also comparable to value of (–30.6 to –25.8 δ^{13}‰) PDB in Awgu shales in the Lower Benue Trough which were characterized by plant wax derived n-alkanes (Schouten et al., 2000; Hu et al., 2002). Figure 4.52 reveals the coal and shale samples were derived from terrigenous sources. A wider range of saturate and aromatic δ^{13}C values would give more information on their enrichment/depletion.

Table 4.10: Isotope data for coal and shale samples of Maiganga, Gombe Formation

S/n	Sample code	Lithology	$\delta^{13}C$ Kerogen	$\delta^{13}C$ Saturate	$\delta^{13}C$ Aromatic
1	MG2H	Coal	-	-27.7	-26.5
2	MG2R	Shale	-25.9	-	-
3	MG3Z	Coal	-25.6	-	-
4	BH15B	Shale		-31.0	-29.2

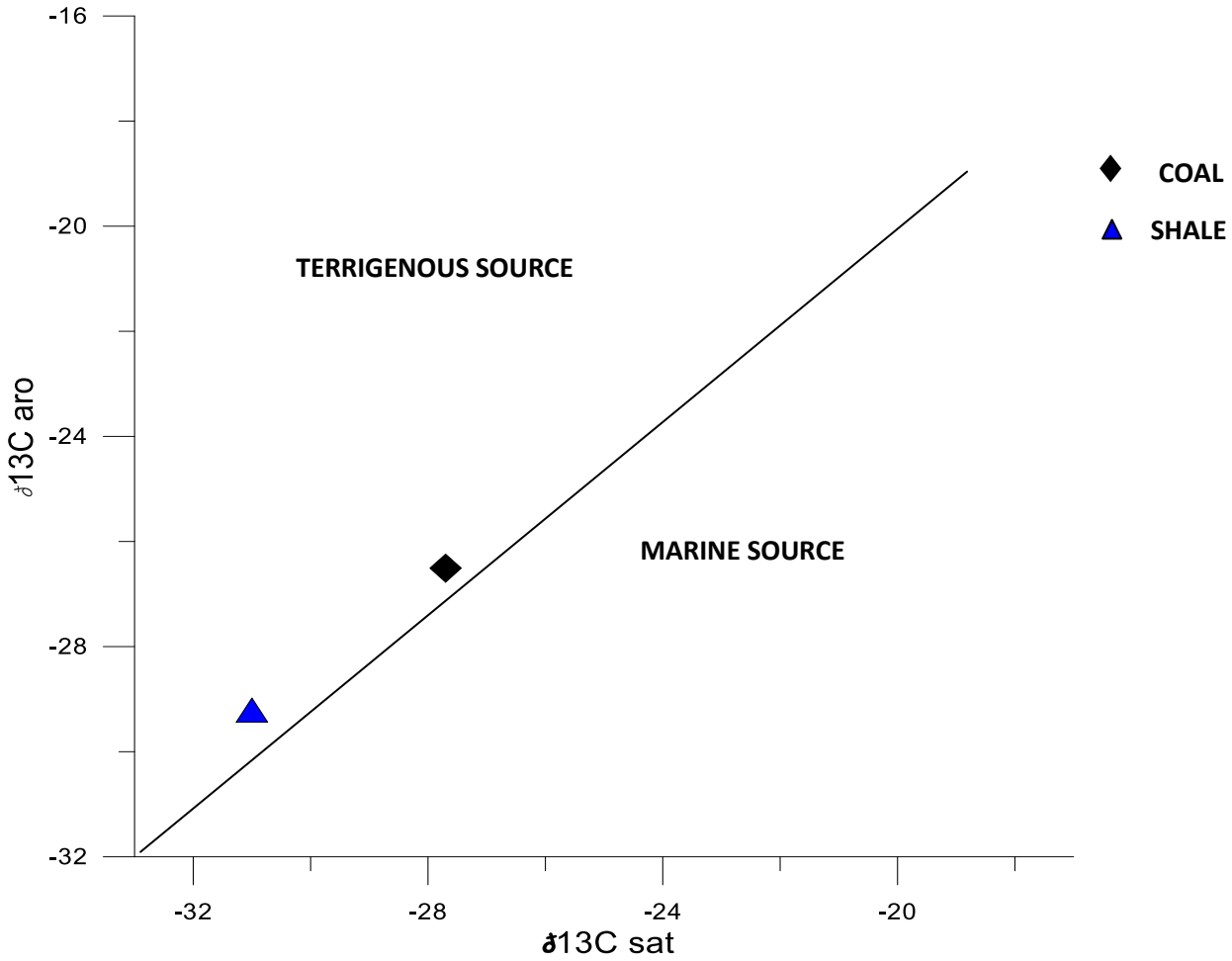


Figure 4.52: Plot of $\delta^{13}C$ saturate against $\delta^{13}C$ aromatic. The coal and shale plotted in terrigenous source (after Sofer, 1984).

4.7 Organic Petrography

Visual kerogen analyses of the shales and maceral studies for the coals samples were carried out to deduce the hydrocarbon potential of the source beds, depositional environments and maturity. Six samples (coals and shales) were investigated for visual kerogen while three coal samples were analysed for maceral study. The results of the petrographic analyses are presented in Table (4.11 and 4.12).

4.7.1 Maceral Composition and Hydrocarbon Potential

Figure 4.54(a-i) shows the proportion of different macerals of each sample on a pie-chart while (Figure 4.61) shows the photomicrographs of the coals. Petrographic examination revealed that organic matter in the coal and shale samples consists of opaque to non opaque biostructured phytoclasts and cuticles associated with common amounts of spores and pollen (Figure 4.55 – 4.60). The proportion of vitrinite is the most abundant in the samples, the vitrinite maceral in the coal ranges from 41.4%-70.1% while the shale ranges from 35%-45%. The inertinite content ranges from 25%-35% for the shale while the coal ranges from 23.5%-45% (Table 4.11 and 4.12). The high percentage of the vitrinite indicates gas prone and suggests they were deposited in close proximity to the source. The high percentages of the gas prone kerogenaceous debris and their low corresponding hydrogen index (HI) may be due to pre depositional or post depositional oxidation from the bulk of the sediments in the stratigraphic section or reworking of the organics.

According to (Hunt, 1996; Petersen and Nytoft, 2006) the generation of petroleum from coal source rocks and its type are basically dependent on the hydrogen content. Many authors have suggested that liptinite content is essential in estimating the potential of the coal to generate liquid hydrocarbon. (Hunt, 1991) has suggested 15-20% liptinite, (Snowdon, 1991) proposed 10% hydrogen rich maceral while Mukophadhyay and Hatcher (1993) suggest 15-20% liptinite content for a coal to generate oil. As indicated in (Table 4.11), the

percentage oil prone for the shale is about 30-40% with respect to the liptinite content up to 40% whereas the coals have low liptinite of about (5%) maximum indicating that the tendency to generate liquid hydrocarbon is minimal. Peterson and Nytoft (2006) has proven that humic coals dominated by huminite could generate oil, though liptinite macerals and are more oil prone than huminite because of its high paraffinicity in structure and its ability to generate long chain aliphatic component ($>C_{20}$-C_{25}) (Isaksen et al., 1998).

The ternary plot of vitrinite, liptinite and inertinite revealed the type of hydrocarbon the source beds can generate (Figure 4.53). Since vitrinite is the most abundant maceral in the coal samples analysed, it is logical to say that the coal has the potential to generate gaseous hydrocarbon (dry gas) while the shale has potential to generate wet gas (Fig. 4.53). All the samples are characterized by the absence of alginite and amorphous kerogen eliminating the presence of Type I kerogen typical of algae. The shales and coals are said to be dominated by Type III kerogen. In coals where the liptinite content is low, vitrinite is the main oil generator because the aliphatic character of vitrinite increases due to increase in HI of the humic coal up to the maximum HI (true generation potential) with increasing maturity.

4.7.2 Thermal Maturity

Palynofacies indicate the presence of trilete spore and pollen well preserved in all the samples and showed yellow-orange fluorescence (Table 4.11 and Figure 4.55 – 4.60). The vitrinite reflectance (Ro) of the coal ranges from 0.46-0.55 and 0.49-0.53 for the shale (Table 4.11 and 4.12). These values indicate immature to marginal maturity for the source beds. The thermal maturity (Tmax) for hydrocarbon generation for most source rock is between 430^{o}C - 435^{o}C corresponding to 0.70-0.81Ro whereas Tmax for Type (I and II) and Type III kerogen oil window is between 430^{o}C-470^{o}C and 465^{o}C-470^{o}C respectively (Tissot et al; 1987: Peters, 1986).

Most humic coals generate hydrocarbon at 0.50-0.60Ro and expel at 0.65Ro. These data indicates that the organic matter in the samples is yet to reach the generation stage of oil window**.** The thermal alteration index ranging from 2.4-2.6 (chevron scale) further corroborates late diagenetic stage for the organic matter maturation as supported by the spore colouration ranging from yellow to orange.

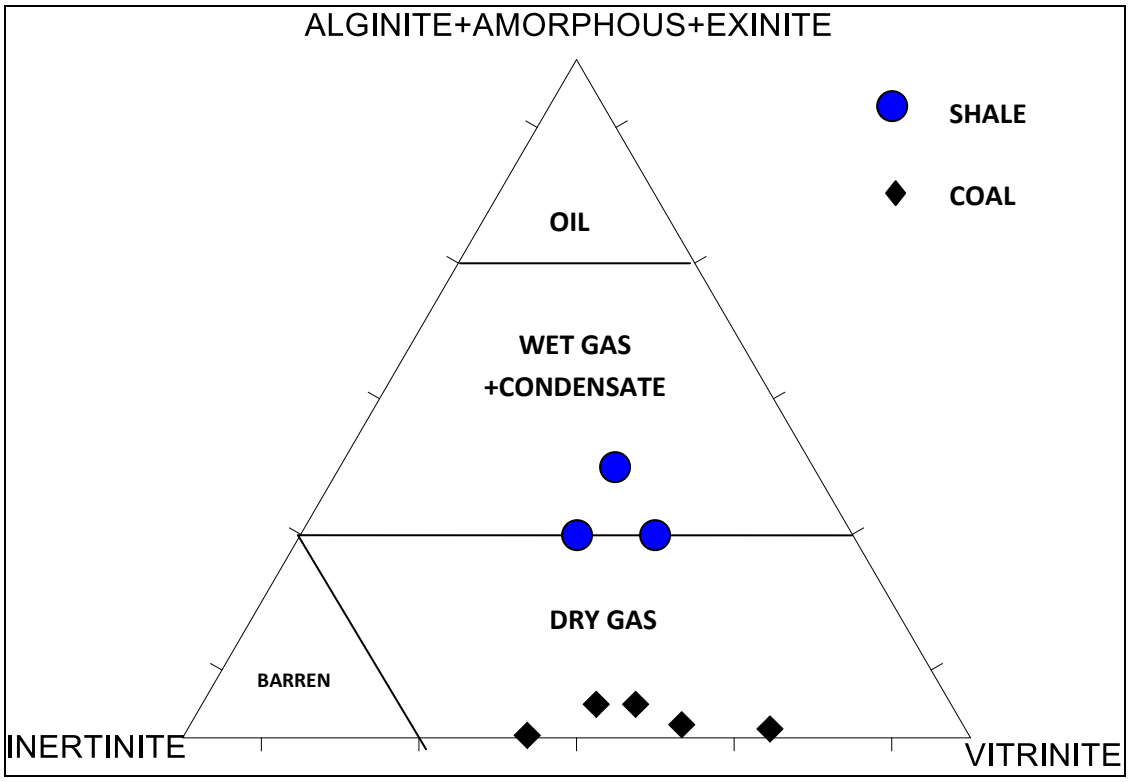


Figure 4.53: Ternary plot indicating the proportion of the vitrinite, inertinite and liptinite and the corresponding hydrocarbon compared with the reference diagram of Tissot and Welte (1978). Plot indicates that the coal and shales are gas prone.

4.7.3 Depositional Environments

Application of macerals group (Vitrinite, Liptinite and Inertinite) in coal facies based on the organic analysis was used to reconstruct the paleoenvironment of the coal. The origin of vitrinite maceral is from humified “woody” plant remains; inertinite is derived from oxidized and degraded plant remains having the same origin as vitrinite. A high proportion of vitrinite in the coal samples indicates good preservation of decayed plant material (Table 4.11 and 4.12) and suggests wet forest swamp facies mainly from arborescent vegetation (Teichmüller and Teichmüller, 1982; Bustin et al., 1983, Rimmer and Davis, 1988).

The high value of inertinites (up to 45%) and increasing fusinites (9.3%) (Table 4.12) also indicates change in high and low ground water tables as a result of periodic drainage of the peat surface condition and shift to drier condition. The relatively low mineral matter and high inertinite favours the oxidation of woody materials (vitrinite) under oxidizing condition due to high biochemical degradation (micrinite) and lack of formation of much mineral matter. Diessel (1986) has demonstrated an environmental model based on specific maceral combinations such as Tissue Preservation Index (TPI) and Gelification Index (GI) which can determine particular peat-forming environments.

High GI (>5) and TPI (>1) values indicate a wet condition of peat formation, while low GI (<5) and TPI (<1) tend towards a drier condition (Diessel, 1986). Lamberson et al. (1991) revealed that coals with high GI and TPI values in which vitrinite > inertinite and structured vitrinite > degraded vitrinite usually occur in wet forest swamp of telmatic zone with rapid burial. Microbial attack on coals precursor deposited in little influx of clastic materials will give high GI and low-moderate TPI values. The GI of the coals range from 0.78-2.98 with an average of 1.83 (Table 4.12) indicated drier condition of peat formation which may be influenced by level of ground water. The low GI of the coals suggest deposition in open-marsh marked by intense oxidation and desiccation as supported by the

absence of telinite and telocollinite and also disintegration of structured inertinite to form in-situ inertodetrinite commonly associated with ash increase.

The coals are likely to be deposited in open marsh to dry forest swamp of telmatic zone.

Table 4.11: Visual Kerogen Data for Coal and Shale samples of Maiganga, Gombe Formation

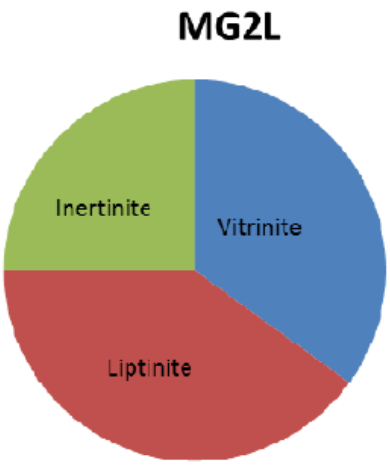
Sample code	Lithology	Alginite (%)	Liptinite (%)	Amorph -ous(%)	Vitrinite (%)	Inertinite (%)	Fluoresc -ence	% Oil prone	% Gas Prone	TAI	VR	Spore Colour	Age
MG2L	Shale	0	40	0	35	25	Good	40	35	2.4-2.5	0.49	Pale yellow-yellow	LC-T
MG2R	Shale	0	30	0	35	35	Good	30	35	2.5-2.6	0.50	Yellow-Orange	LC-T
MG3D	Coal	0	5	0	50	45	Good	5	50	2.5-2.6	0.50	Orange	M
MG3Z	Coal	0	5	0	55	40	Good	5	55	2.4-2.5	0.46	Pale yellow-yellow	M
MG4D	Shale	0	30	0	45	25	Good	30	45	2.5-2.6	0.53	Orange	M
BH15A	Shale	0	40	0	35	25	Good	40	35	2.5-2.6	0.50	Dark Orange	M

TAI- Thermal Alteration index, VR- Vitrinite Reflectance, LC-T: Late Cretaceous –Tertiary, M: Maastrichtian

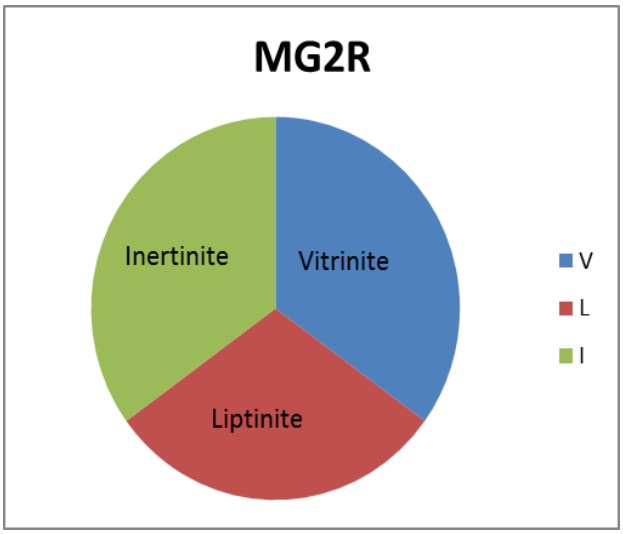
Table 4.12: Maceral and vitrinite reflectance data for Coal samples of Maiganga, Gombe Formation

code	Lithology	Romax (%)	R.R (%)	Reactive components (%)			Inert components (%)				m.m (%)	GI
				liptinite	vitrinite	R.semi-fusinite	I. semi-fusinite	fusinite	Inertodetrinite	Inertinite (%)		
MG2H	Coal	0.48	0.45	1.3	70.1	9.1	9.3	4.9	0.2	23.5	5.1	2.98
MG1W	Coal	0.49	0.46	1.9	59.3	13.9	13.9	5.9	0.2	33.9	4.9	1.75
MG1D	Coal	0.55	0.52	0.4	41.4	21.9	21.9	9.3	0.2	53.3	4.9	0.78

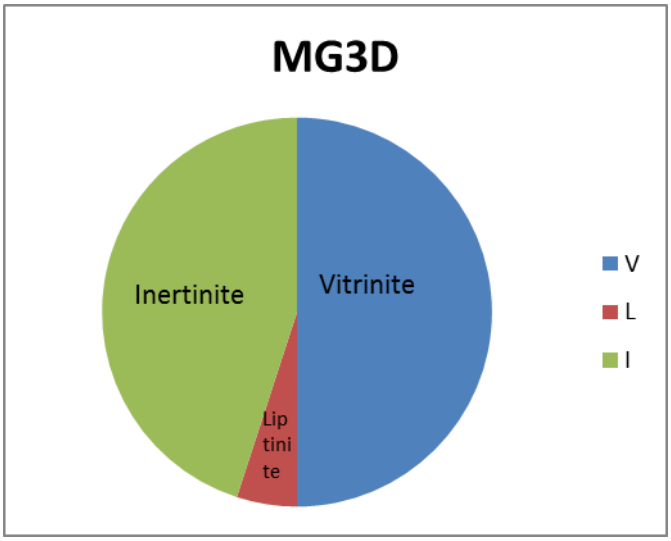
Romax: percent mean maximum vitrinite reflectance, R.R: Random reflectance, m.m: mineral matter.
GI: Gelification index = Vitrinite+Macrinite/Semifusinite +Fusinite+Inertodetrinite



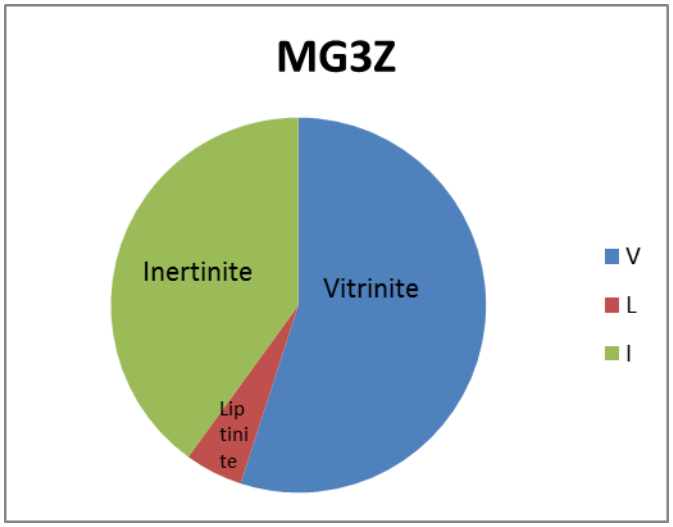
a): Maceral pie chart for sample MG2L



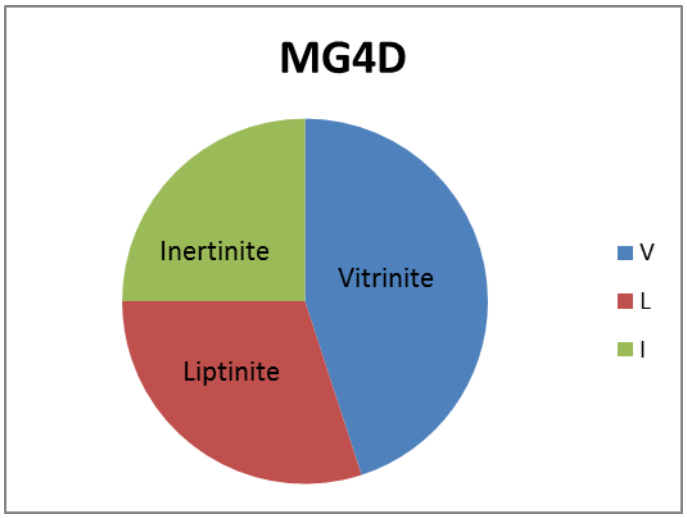
b): Maceral pie chart for sample MG2R



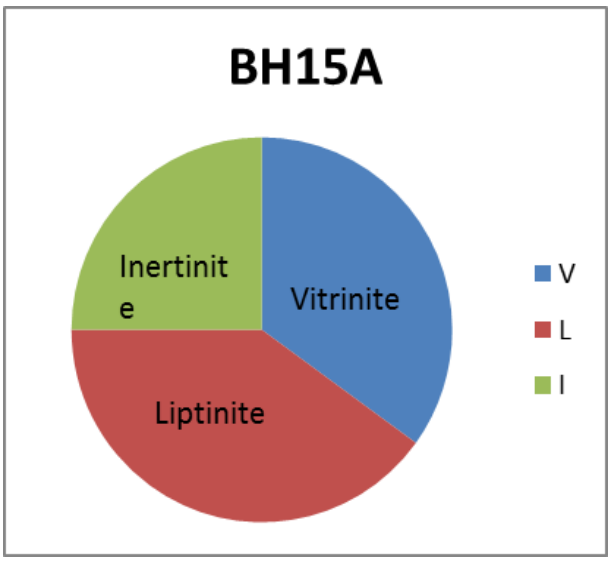
c): Maceral pie chart for sample MG3D



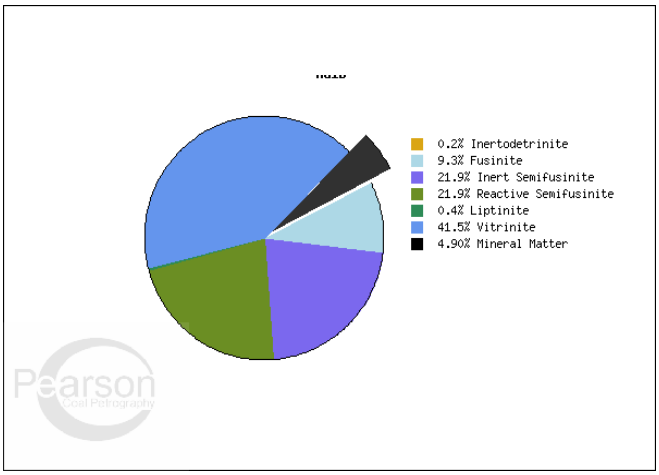
d): Maceral pie chart for sample MG3Z



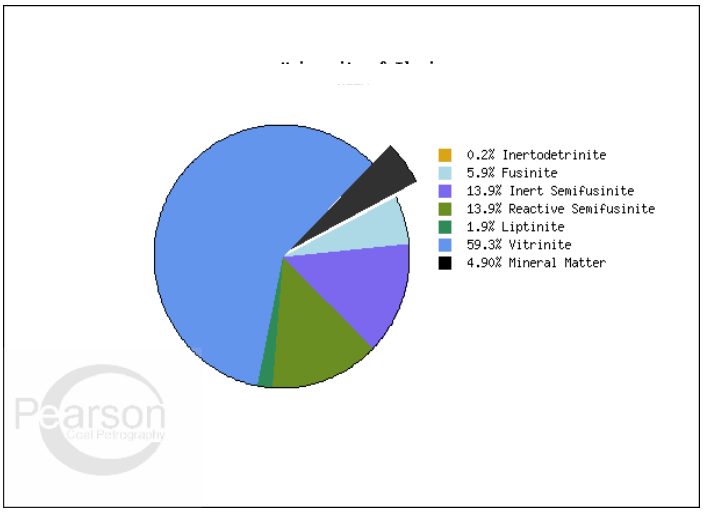
e): Maceral pie chart for sample MG4D



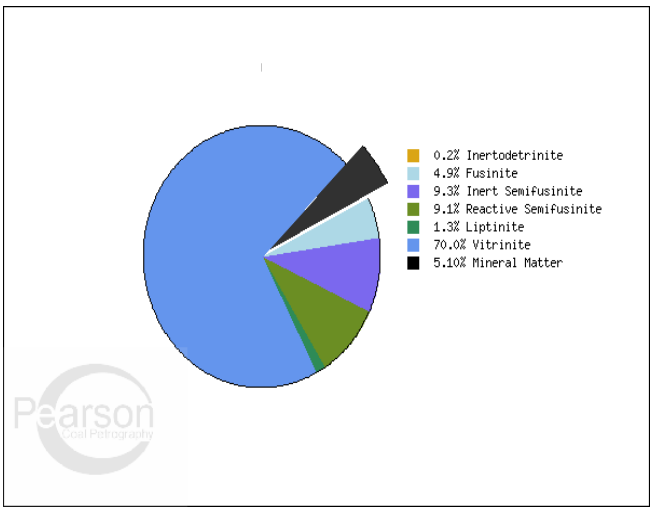
f): Maceral pie chart for sample BH15A



g): Maceral pie chart for sample MG1D



h): Maceral pie chart for sample MG1W



i): Maceral pie chart for sample MG2H

Figure 4.54: (a-i): Pie charts indicating the percentages composition of the macerals for coal and shale samples

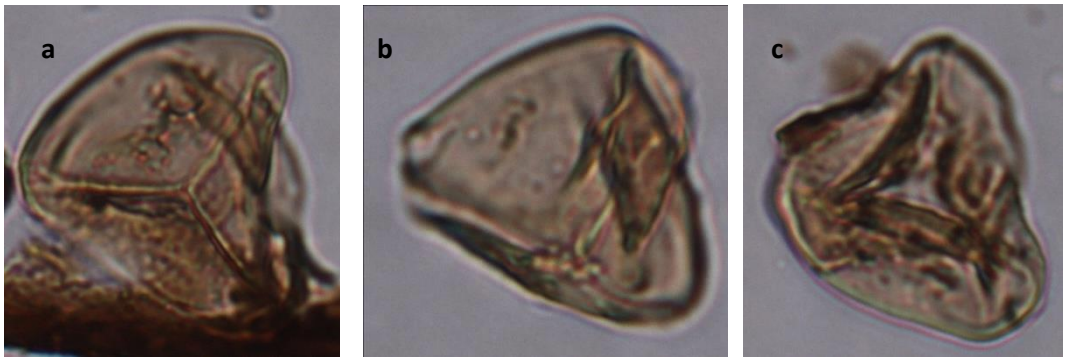


Figure 4.55: Photomicrographs of Palynomorphs observed in sample MG2L (Organic matter in this sample consists predominantly of large non-opaque phytoclasts (biostructured & cuticles) associated with very common amounts of pollen and spores (trilete spore).

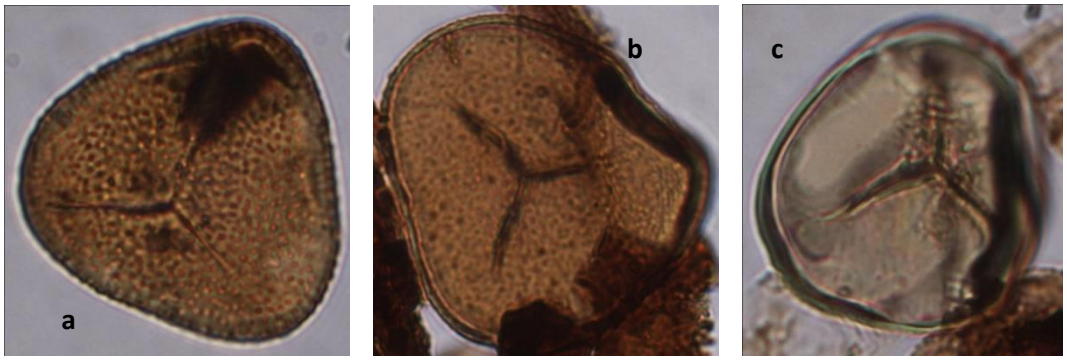


Figure 4.56: Photomicrographs of Palynomorphs observed in sample MG2R (Organic matter in this sample consists of predominant amount of phytoclasts (biostructured and cuticles) associated with common amounts of pollen and spores. (a-foveotriletes margaritae, b-Rugulatisporites caperatus).

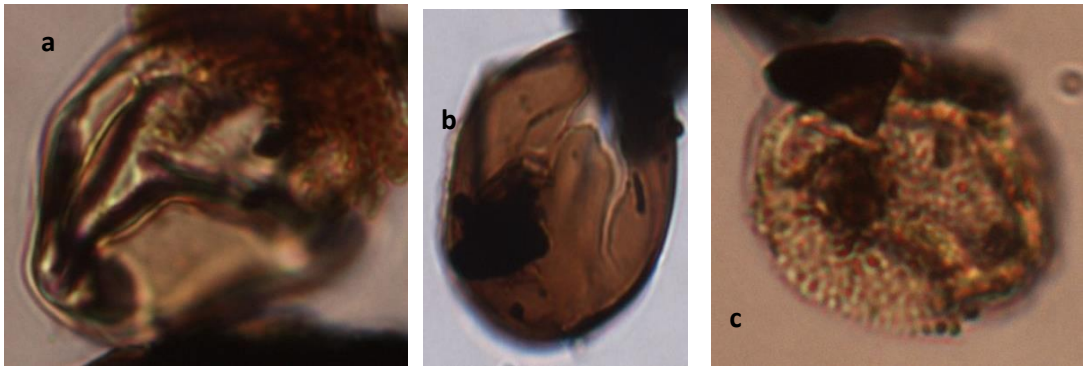


Figure 4.57: Photomicrographs of Palynomorphs observed in sample MG3D (Organic matter in this sample consists predominantly of opaque phytoclasts and rare amount of biostructured phytoclasts associated with rare amount of pollen grains. (C– Proxapertites sp.).

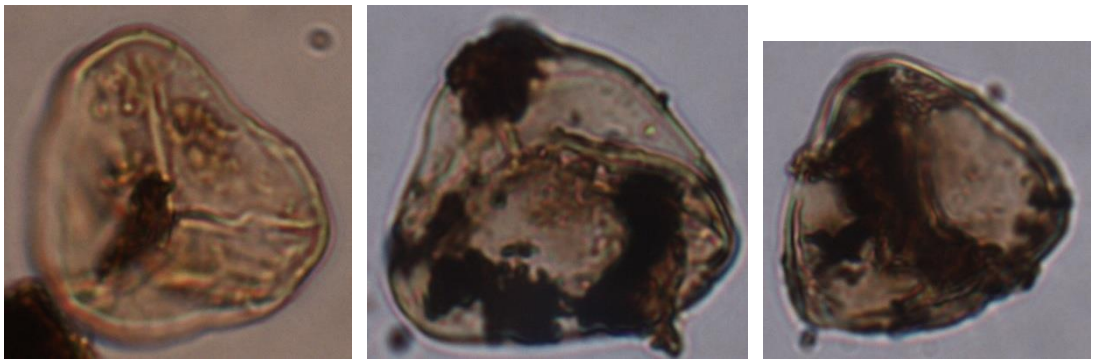


Figure 4.58: Photomicrographs of Palynomorphs observed in sample MG3Z (Organic matter in this sample consists of very common amount of opaque phytoclasts associated with rare amounts of biostructured phytoclasts and spores.

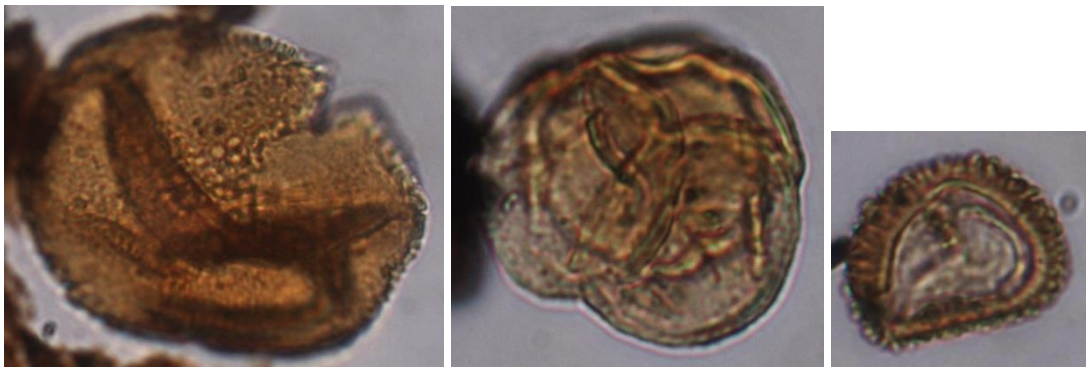


Figure 4.59: Photomicrographs of Palynomorphs observed in sample MG4D (Organic matter in this sample consists predominantly of biostructured phytoclasts and cuticles associated with a common amount of sporomorphs.

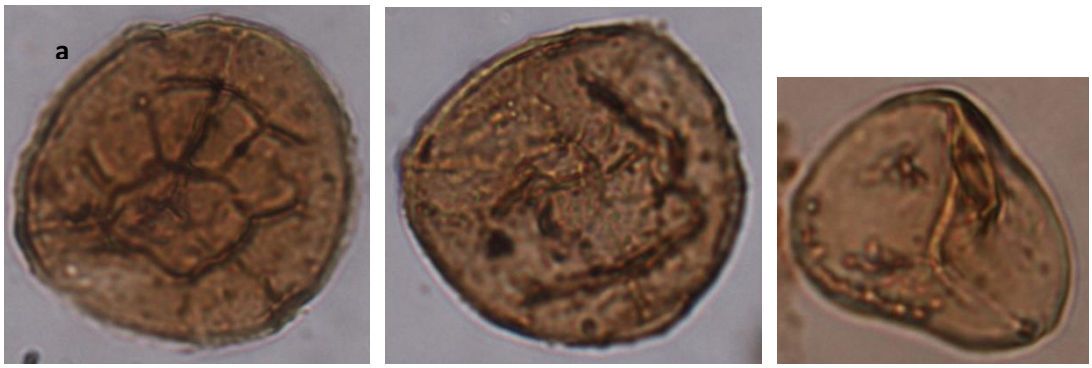


Figure 4.60: Photomicrographs of Palynomorphs observed in sample BH15A (Organic matter in this sample consists predominantly of biostructured phytoclasts associated with common amounts of spores and pollen, and a moderate amount of cuticles. (a-Zlivisporeites blanensis).

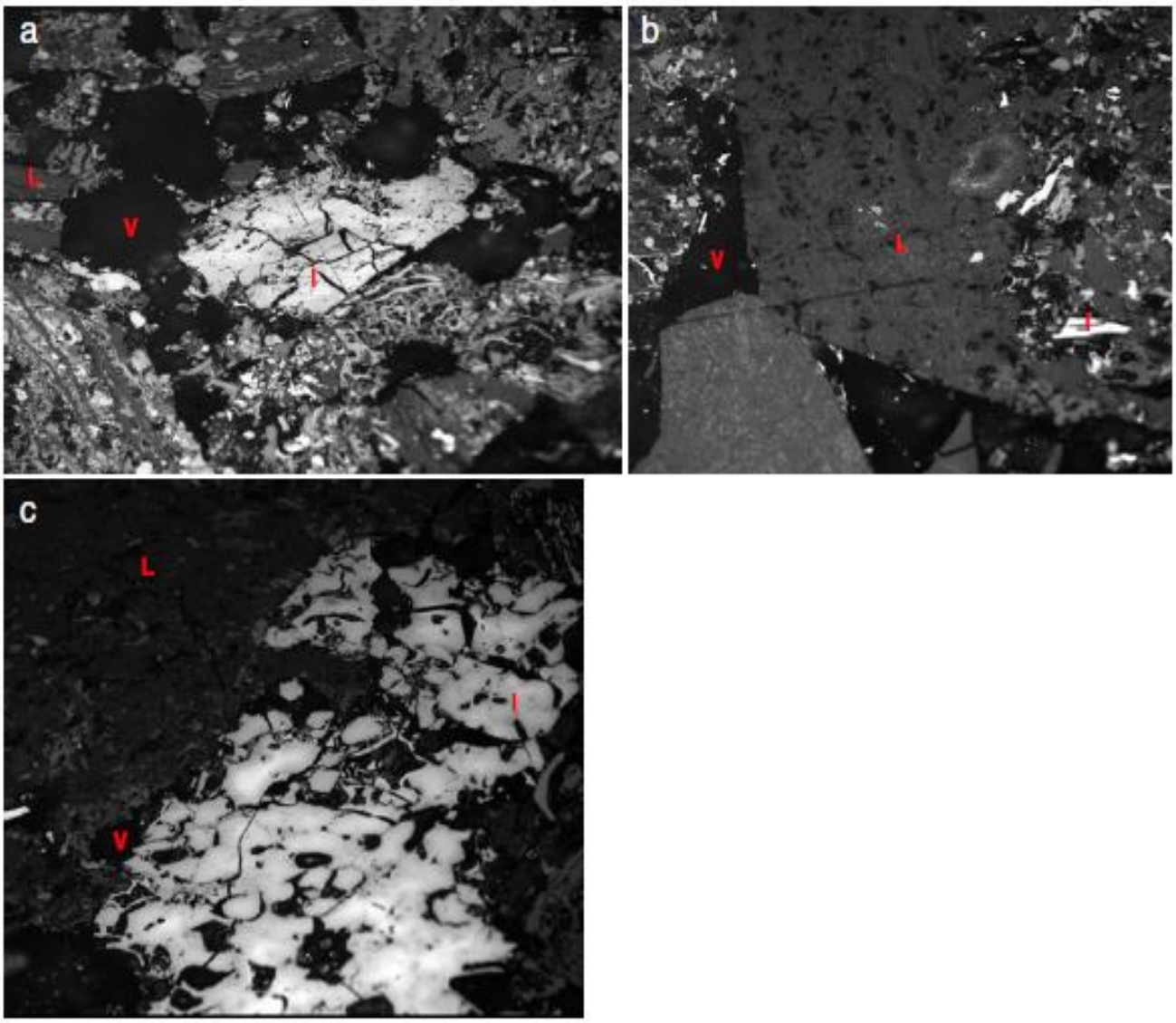


Figure 4.61: Photomicrograph of coal sample a) MG1D, b) MG1W and c) MG2H. (Liptinite shows grayish coloration, vitrinite is dark coloured and inertinite is white under reflected light. V: vitrinite, I: inertinite, L: liptinite,.

4.8 Palynology

Twenty two samples (coals, coaly shale and shales) from borehole 15 and phase I and II of Maiganga coal mine were analysed for palynomorphs (pollen, spores and dinocysts) at the Palynology Laboratory, Department of Archaeology and Anthropology, University of Ibadan. Twenty grams of each sample were analysed according to standard palynological procedure. Of the twenty two (22) samples, fourteen (14) (ten shales, three coals and 1 coaly shale) (Table 4.13) has considerable amount of palynomorphs. The shales yielded substantial amounts of palynomorphs (21-530); others were barren.

This analysis revealed a diverse assemblage of pollen and spores with a total count grain of 2426; a total of 100 palynomorph types. Some of the commonest palynomorphs found in the samples are *Arecipites* sp., *Ephedripites* sp., *Monocolpites marginatus, Cyathidites sp., Cercophora sp., Foveotriletes margaritae, Longapertites marginatus, Longapertites vaneendenburgi, Proxapertites cursus, Proxapertites operculatus, Cingulatisporites ornatus, Constructipollenites ineffectus, Retibrevitricolpites triangulatus, Echitriporites trianguliformis, Nyssapollenites sp., Araucariadites australis, Foveotriletes margaritae* and *Dictyophyllidites harrisii* (Table 4.13 and 4.14). Only one sample (BH15B) has a dinocyst. The palynomorphs data interpretation was used to deduce the age, paleoenvironments and paleoclimate of the organofacies in the study area. Photomicrographs of some of the palynomorphs observed are presented in plate (4.1-4.7).

Table 4.13: **List of Palynomorphs, abundance and count obtained from coal and shale samples of Gombe Formation**

Palynomorphs/ Samples	BH 15A	BH 15B	BH 15C	MG2F	MG10	MG1H	MG4D	MG4K	MG2R	MG3L	MG3D	MG1Z	MG3S	MG4S
2-celled spore				2					2		1			1
3-celled spore				2										2
4-celled fungal spore	2													
7-celled fungal spore		1	2	2										3
Alnus sp.													2	
Amaranthaceae					2									
Araucariadites australis	2	1	6						2			7		1
Arecipites sp 2	1									1				
Arecipites sp.	8	1	24	4	19	2	51	5	9	5	15	105	2	33
Baculate pollen			2						2					
Brachysporium sp.													1	
Caesalpiniaceae			2	1							1	6		
Canalisporium sp.									1					
Cercophora sp.	28			2			58		3	2			2	4
Cingulatisporites ornatus	4	1	21	1					5		5		2	
Constructipollenites ineffectus	6		1	1			8		3		7			5
Cyathidites sp.	14	1	21	2	15		11		3		10	8		9
Cycadopites sp.							1			1				1
Cyperacidites sp.					1									
Deltoidospora adriennis			5		2		1				2	1	3	2
Dictyophyllidites harrissii	13	1	24		8		83	7	6	2	8	91	7	8
Dinocyst		1												
Distaverrusporites simplex							1							
Drepanocarpus lunatus			1											
Echitricolporites baculatus			1											
Echitriporites trianguliformis	7	1	30	2	11		9		8	1	8	16	8	3
Ephedripites sp.	4	1	15	1	1		10				5	33		
Ericipites scabratus	14	4	15	1	6		17	2	6	1	13	22	9	7
Foveotriletes margaritae	8	1	1		2		1			1	1			11
Fusiformites sp.									1					
Gemmatricolpites cf. pergemmatus			4				31		2					1
Inaperturites sp.			1											

Ladakhipollenites lehmanii											2	1		1
Laevigatosporites ovatus	4	2	3				10				3	7		1
Liliacidites sp.	2		3						2			42		
Liliacidites sp.2			4											
Longapertites marginatus			12	2			18				1		2	
Longapertites vaneendeburgii			3	4	2		8		3			56		2
Lycopodiumsporites sp.				1			3		2		1	15	2	
Macaranga sp.	2		12											
Mauritiidites sp.	2	2	6								2			
Milforda sp.													1	
Mitragyna inermis													4	4
Monocolpites marginatus	31	1	33	2	12		65		2		11	1	6	1
Monocolpollenites sphaeroidites										1				
Monulcipollenites confossus			1											
Nothofagidites sp.							3							
Nymphaea sp.			2											
Nyssapollenites sp.	2		13	1				2	4	1	20		7	9
Papilionaceae	2		6											
Pluricellaesporites psilatus	4	5	6	6				2	7					
Pluricellaesporites scabiosus							31						7	3
Pluricellaesporites tamilensis														1
Pluricellaesporites. typicus					1									19
Podocarpidites sp.					1									
Polygonum sp. Type			2											
Polypodiaesisporites sp.					3									
Proteacidites dehaanni	2									2	4			
Proteacidites sp.											8	1	5	
Proxapertites cursus					2				2		3			
Proxapertites operculatus	8		1	1						2	2	1	6	9
Psilabrevitricolpites sp.												71	2	
Psilatricolpites sp.	2	1												
Psilatricolporites baculatus			6											
Psilatricolporites molinae			15	1			1					21		
Psilatricolporites sp.	16				13		22							
Psilatriporites annulatus			1		3									
Retibrevitricolpites triangulatus			1				1							
Retidiporites magdalenensis	10	2	2						3			18	2	

Retidiporites sp.			2											
Retimonoporites sp.									1					
Retistriatotricolporites sp.			1											
Retitricolpites sp.	2													
Retitricolporites sp.	4				2				2					
Retitricolporites sp. (ellip)	2													
Retitricolporites sp. (foveolate	1													1
Retitricolporites sp. (oval)	4													
Retitricolporites sp./Uapaca sp.										1	5			
Retitriporites sp.									2					
Rugulatisporites caperatus			4		4									
Sapindaceae, Psilatriporites	2		6											
Scabratriporites annellus	6						1					1		1
Scabratriporites simpliformis				2			3				2	1		
Scabratriporites sp.	2									1				
Steevesipollenites sp.			1				7						7	4
Striatricolporites sp.											2			
Syntricolporites sp. baculatus											1	1		
Syntriporites sp.	2													
Tricolpites sp.														1
Tricolporites sp. (Daniellia sp.)	2										2			
Triorites africaensis											1			21
Triporate v. small, triangle			28		3						5			
Triporate, microechinae	2	2	3	1	5		53	3		1				41
Triporites sp. (Celtis sp.)	1				3		1		2		2		2	3
Triporopollenites sp.	1	1					21							
Tubistephanocolpites cyclindricus													1	
Unidentified sp.									1					2
Verrucosisporites sp.	1													
Zizyphus sp.				1	1							1		
Zlivisporites cf. blanensis		1											1	
	230	30	353	43	122	2	530	21	86	23	153	527	91	215

Table 4.14: **Dominant palynomorphs in the the coal and shale samples of Gombe Formation**

SAMPLE NO	DEPTH (M)	LITHOLOGY	PALYNOMORPHS
MG1H	31	COAL	Arecipites sp.
MG1O	29	SHALE	Amaranthaceae, Cyperacidites sp. Arecipites sp., Cyathidites sp., Dictyophyllidites harrissii, Echitriporites trianguliformis, Ericipites scabratus, Foveotriletes margaritae, Monocolpites marginatus, Proxapertites cursus, Psilatricolporites sp., Longapertites vaneendeburgii, Polypodiaesisporites sp., Psilatriporites annulatus, Rugulatisporites caperatus, Triporate v. small, triangle, Triporate, microechinae, Triporites sp. (Celtis sp.)
MG1Z	25	SHALE	Araucariadites australis, Arecipites sp., Cyathidites sp, Dictyophyllidites harrissii, Echitriporites trianguliformis, Ericipites scabratus, Ladakhipollenites lehmanii, Laevigatosporites ovatus, Liliacidites sp., Longapertites vaneendeburgii, Lycopodiumsporites sp., Monocolpites marginatus, Proteacidites sp., Proxapertites operculatus, Psilabrevitricolpites sp., Psilatricolporites molinae, Retidiporites magdalenensis, Scabratriporites annellus, Syntricolporites sp. Baculatus, Zizyphus sp.
MG2F	22	SHALE	2 and 3-celled spore, 7-celled fungal spore, Arecipites sp., Cercophora sp., Longapertites marginatus, Longapertites vaneendeburgii, Cingulatisporites ornatus, Constructipollenites ineffectus, Cyathidites sp., Echitriporites trianguliformis, Ericipites scabratus, Monocolpites marginatus, Pluricellaesporites psilatus, Proxapertites operculatus, Scabratriporites simpliformis, Triporate, microechinae Zizyphus sp.
MG2R	16	SHALE	3-celled spore, Arecipites sp., Cercophora sp., Constructipollenites ineffectus, Cyathidites sp, Dictyophyllidites harrissii, Cingulatisporites ornatus, Echitriporites trianguliformis, Ericipites scabratus, Fusiformites sp. Canalisporium sp., Retimonoporites sp., Gemmatricolpites cf. Pergemmatus, Longapertites vaneendeburgii, Monocolpites marginatus, Nyssapollenites sp., Pluricellaesporites psilatus, Proxapertites cursus, Retidiporites magdalenensis, Retitricolporites sp., Retitriporites sp., Triporites sp. (Celtis sp.).
MG3D	23	COAL	2-celled spore, Arecipites sp., Constructipollenites ineffectus, Cyathidites, Cingulatisporites ornatus, Dictyophyllidites harrissii, Echitriporites trianguliformis, Ericipites scabratus, Foveotriletes

			margaritae, Ladakhipollenites lehmanii, Laevigatosporites ovatus, Longapertites marginatus, Monocolpites marginatus, Nyssapollenites sp. Proteacidites dehaanni, Proteacidites sp., Proxapertites cursus, Proxapertites operculatus, Retitricolporites sp./Uapaca sp., Scabratriporites simpliformis, Striatricolporites sp., Syntricolporites sp. baculatus, Tricolporites sp. (Daniellia sp.), Triorites africaensis, Triporate v. small, triangle.
MG3L	21	SHALE	Arecipites sp., Cercophora sp., Dictyophyllidites harrissii, Echitriporites trianguliformis, Ericipites scabratus, Foveotriletes margaritae, Monocolpollenites sphaeroidites, Proteacidites dehaanni, Proxapertites operculatus, Scabratriporites sp., Triporate microechinae.
MG3S	17	COALYSHALE	Alnus sp., Brachysporium sp., Milforda sp., Arecipites sp., Cercophora sp., Cingulatisporites ornatus, Deltoidospora adriennis, Dictyophyllidites harrissii, Echitriporites trianguliformis, Ericipites scabratus, Longapertites marginatus, Mitragyna inermis, Monocolpites marginatus, Nyssapollenites sp., Pluricellaesporites scabiosus, Proteacidites sp., Proxapertites operculatus, Psilabrevitricolpites sp., Retidiporites magdalenensis, Steevesipollenites sp., Triporites sp. (Celtis sp.), Zlivisporites cf. Blanensis.
MG4D	12	SHALE	Arecipites sp., Cercophora sp., Constructipollenites ineffectus, Cyathidites sp, Dictyophyllidites harrissii, Distaverrusporites simplex, Ephedripites sp., Ericipites scabratus, Echitriporites trianguliformis, Foveotriletes margaritae, Gemmatricolpites cf. Pergemmatus, Laevigatosporites ovatus, Longapertites marginatus, Longapertites vaneendeburgii, Monocolpites marginatus, Nothofagidites sp., Pluricellaesporites scabiosus, Psilatricolporites sp., Retibrevitricolpites triangulatus, Scabratriporites annellus, Steevesipollenites sp., Triporate microechinae, Triporopollenites sp.
MG4K	9	COAL	Arecipites sp., Dictyophyllidites harrissii, Ericipites scabratus, Nyssapollenites sp., Pluricellaesporites psilatus, Triporate, microechinae.
MG4S	6	SHALE	2 and 3-celled spore, 7-celled fungal spore, Arecipites sp., Cercophora sp., Constructipollenites ineffectus, Cyathidites sp., Cycadopites sp., Dictyophyllidites harrissii, Echitriporites trianguliformis, Ericipites scabratus, Foveotriletes margaritae, Gemmatricolpites cf. Pergemmatus, Ladakhipollenites lehmanii, Longapertites vaneendeburgii, Mitragyna inermis, Monocolpites marginatus, Nyssapollenites sp., Pluricellaesporites scabiosus, Pluricellaesporites tamilensis, Pluricellaesporites

			typicus, Proxapertites operculatus, Retitricolporites sp. (foveolate), Scabratriporites annellus, Steevesipollenites sp., Tricolpites sp., Triorites africaensis, Triporate microechinae, Triporites sp. (Celtis sp.)
BH15A	12	SHALE	4-celled fungal spore, Arecipites sp., Cercophora sp., Cyathidites sp., Dictyophyllidites harrissii, Echitriporites trianguliformis, Ericipites scabratus, Foveotriletes margaritae, Monocolpites marginatus, Proxapertites operculatus, Psilatricolporites sp., Retidiporites magdalenensis, Scabratriporites annellus, Cingulatisporites ornatus, Retitricolporites sp.
BH15B	20	SHALE	7-celled fungal spore, Arecipites sp., Cingulatisporites ornatus, Cyathidites sp., Dictyophyllidites harrissii, Echitriporites trianguliformis, Ericipites scabratus, Foveotriletes margaritae, Laevigatosporites ovatus, Pluricellaesporites psilatus, Retidiporites magdalenensis, Triporate, microechinae, Triporopollenites sp., Zlivisporites cf. Blanensis and Dinocyst.
BH15C	48	SHALE	7-celled fungal spore, Arecipites sp., Cingulatisporites ornatus, Cyathidites sp., Dictyophyllidites harrissii, Echitriporites trianguliformis, Ephedripites sp., Ericipites scabratus, Gemmatricolpites cf. Pergemmatus, Longapertites marginatus, Longapertites vaneendeburgii, Monocolpites marginatus, Macaranga sp., Nyssapollenites sp., Pluricellaesporites psilatus, Psilatricolporites molinae, Retidiporites magdalenensis, Triporate v. small triangle, Sapindaceae, Psilatriporites, Rugulatisporites caperatus, Triporate microechina, Baculate pollen, Drepanocarpus lunatus, Echitricolporites baculatus, Liliacidites sp.2, Retistriatotricolporites sp.

4.8.1 Palynostratigraphic Zonation and Age

The palynological results revealed a diverse assemblages and abundance (Table 4.13 and 4.14). The assemblage biozones are characterized by the abundance and assemblage of the coal facies from the two phases of the mine (MG1H, MG3D and MG4K) (Figure 4.62 and 4.63) have a total of 176 palynormophs with sample MG3D having the highest abundance (153) (Table 4.13) and characterised by abundance of *Dictyophyllidites harrisii*. The palynormorph *Arecipites sp* is the only pollen occurring in all the three coal samples (Table 4.13 and 4.14), other assemblages of palynomorphs found in the coals includes *Cyathidites sp, Nyssapollenites sp, Echitriporites trianguliformis, Ericipites scabratus, Monocolpites marginatus, Cingulatisporites ornatus, Constructipollenites ineffectus and Proteacidites sp.* (Table 4.13 and 4.14). On the basis of continuous occurrence of marker species and maximum development (Figure 4.65, 4.66) and abundance of species listed in (Table 4.14), and in line with the work of previous researchers such as Lawal and Moullade (1986), Ojo and Akande (2004) and Onoduku (2014), particularly in the Northern Benue Trough, much of the palynomorphs found in this facies have been reported by the above earlier workers and have dated the lower part of the Gombe Formation comprising of coal seams Early-Late Maastrichtian and accordingly, *Arecipites – Dictyophyllidites harrisii* zone is therefore assigned (Figure 4.65) between the interval of 31m-6m.

The shale facies comprising of shales and coaly shale from phase I (MG1O, MG1Z, MG2F, and MG2R) and (MG3L, MG3S, MG4D and MG4S) from phase II (Figure 4.62, 4.63) have about 778 and 859 palynomorphs respectively. The highest palynomorphs was recorded in sample MG1Z and MG4D making 65% and 60% of the total palynormorphs in phase I and II respectively (Table 4.13 and 4.14). The dominant marker species especially at the base of phase I (Figure 4.62) includes *Arecipites sp, Longapertites vaneendeburgii, Psilabrevitricolpites sp, Ephedripites sp, Dictyophyllidites harrisii, Echitriporites*

trianguliformis, Ericipites scabratus, Lilliacidites sp and Psilatricolpites molinae. Similar abundance of the palynomorphs was also recorded in phase II (Figure 4.63) with other notable assemblages such as *Cercophora sp, Germmatricolpites cf. Pergemmatus and Pluricellaesporites scabiosus.* Hence, based on the abundant occurrence of *Arecipites sp and Dictophyllidites harissi,* in the upper part, *Arecipites – Dictophyllidites harissi* assemblage zone has been assigned (Figure 4.65). The shale samples from borehole 15 between the interval of 20-48m (Figure 4.64) also consists of significant palynomorphs like 7-celled fungal spore, *Arecipites sp., Cingulatisporites ornatus, Cyathidites sp., Dictyophyllidites harrissii, Echitriporites trianguliformis, Ephedripites sp., Ericipites scabratus, Gemmatricolpites cf. Pergemmatus, Longapertites marginatus, Longapertites vaneendeburgii, Monocolpites marginatus, Macaranga sp., Nyssapollenites sp., Pluricellaesporites psilatus, Psilatricolporites molinae,* and *Retidiporites magdalenensi*s (Table 4.13, 4.14) (Figure 4.65).

The studied stratigraphic section (Phase I and II) (Figure 4.62 and 4.63) and borehole 15 (Figure 4.64) based on the palynormorphs have indicated stratigraphic age of Early-Late Maastrichtian. The marker species of palynomorphs includes *Monocolpites marginatus, Longapertites vaneendeburgii, Proxapertites cursus, Proxapertites operculatus, Cingulatisporites ornatus, Constructipollenites ineffectus, Echitriporites trianguliformis, Dictyophyllidites harrisii, Arecipites sp, Foveotrilete margaritae, Rugulatisporites caperatus, Zlivisporites blanensis, Retidiporites magdalensis and Proteacidites* indicates specifically late Maastrichtian. Furthermore, there was a fairly high diversity of fungal spores dominated by *Cercophora sp* and variant of the form *Pluricellaesporites* namely *P. psilatus, P. scabiosis, P. tamilensis and P.typicus.* These fungal spores are of late Cretaceous age; they corroborate the age provided by the pollen and pteridophyte (Edet and Nyong, 1994; Schrank, 1987). The palynomorphs mentioned above have been reported by various authors

particularly the Campanian – Maastrichtian sediments such as the Nkporo Formation in Southeastern Nigeria (Edet and Nyong, 1994), Tano Basin in Southwestern Ghana (Atta-Peters and Salami, 2004) and the Gombe Formation (Ojo and Akande, 2004). *E. trianguliformis, Proteacidites sp* and *Z. blanensis* all indicates Late Senonian (Hergreen, 1996). The Palmae forms which include the genera Longapertites, Proxapertites recovered in the samples indicate Palmae province of warm tropical – subtropical climate (Hergreen, 1981; Hergreen et al., 1996). The Palynomorphs observed in the samples suggest Early-Late Maastrichtian age for the coals and shales (Figure 4.66).

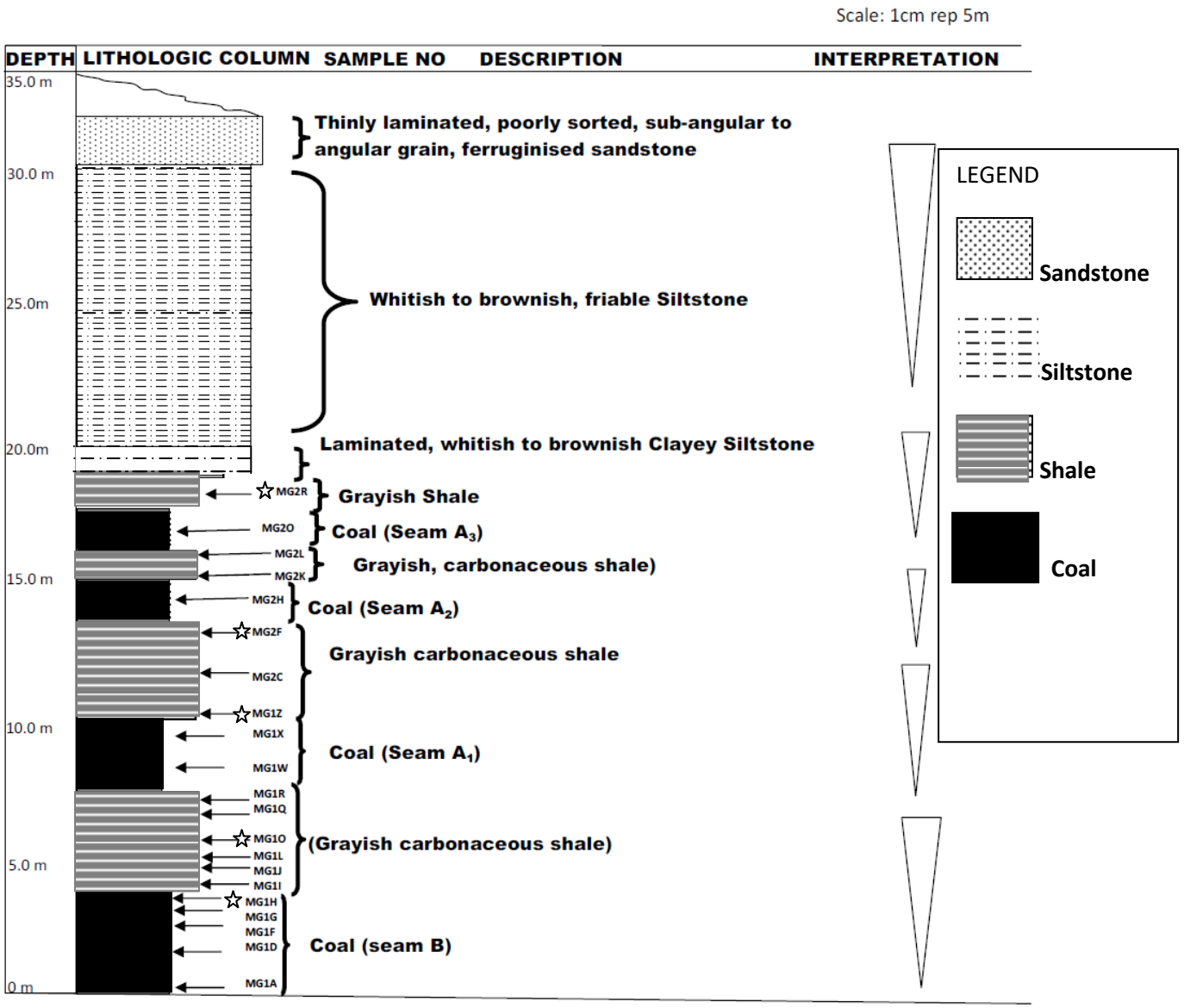


Figure 4.62: Lithologic succession of Gombe Formation exposed at the Maiganga mine. The coarse upward sequences from the base are coal, shale, siltstone to sandstone. The star symbol indicate samples in which palynomorphs were recovered at phase I (10^0 02^I 39^{II}N, 11^0 12^I 17^{II}E).

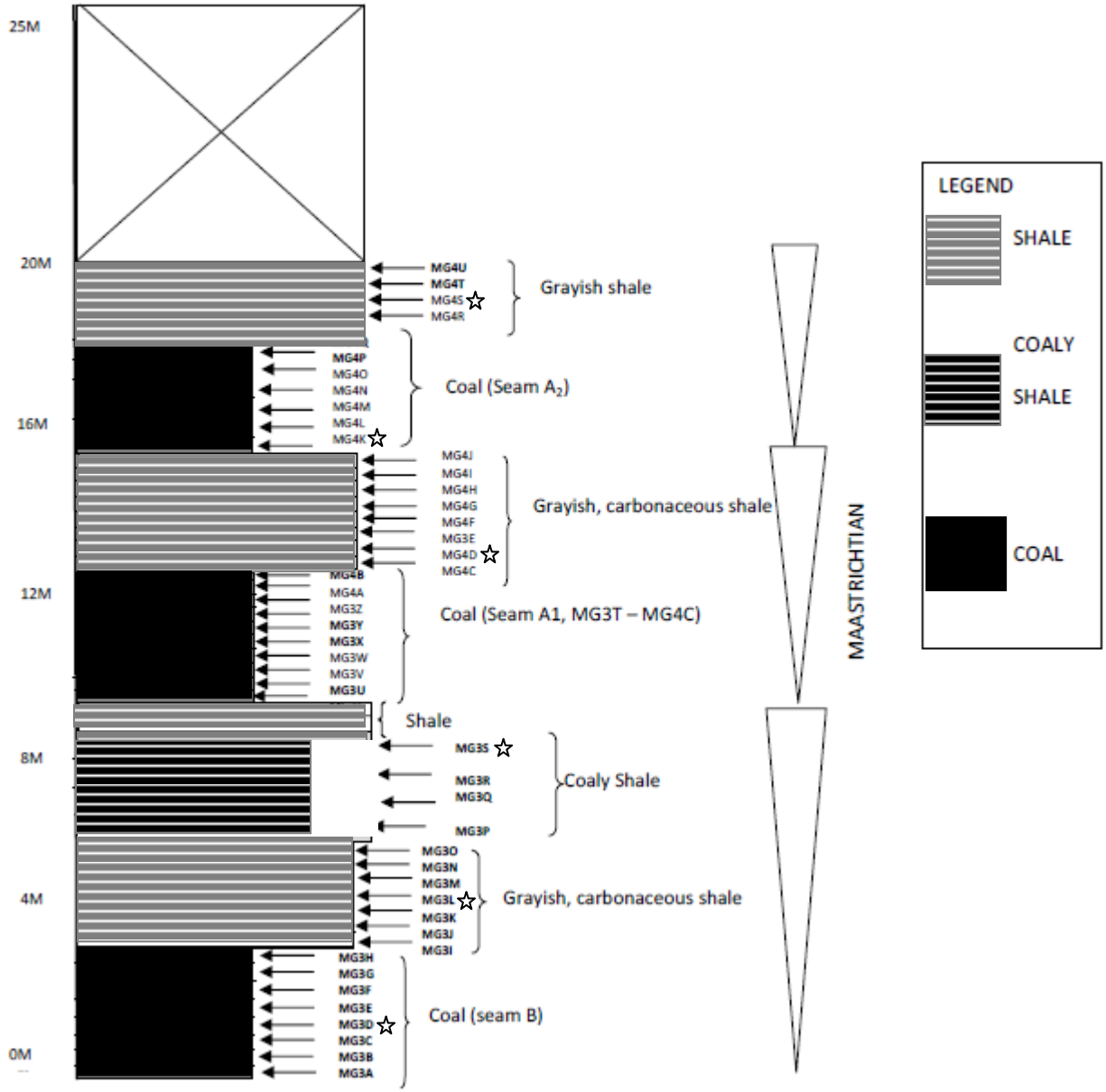


Figure 4.61: Lithologic succession of Gombe Formation exposed at the Maiganga mine. The succession consists of coal and shale interbeds. The star symbol indicate samples in which palynomorphs were recovered at phase II (10^{0} 04^{I} 46^{II}N, 11^{0} 12^{I} 23^{II}E).

meters			Lithology	Lithological description	
Depth from	Depth To	Thickness			
0.00	0.30	0.30		Top soil	
0.30	3.00	2.70		Clay reddish brown Sandstone	
3.00	6.50	3.50		Clayey Siltstone	
6.50	6.70	0.20		Indurated Ironstone	
6.70	9.00	2.30		Carbonaceous shale	
9.00	9.50	0.50		Indurated Ironstone	
9.50	12.00	2.50		Carbonaceous shale	☆ BH15A
12.00	12.50	0.50		Indurated Ironstone	
12.50	20.00	7.50		Carbonaceous shale	☆ BH15B
20.00	20.20	0.20		Well indurated Ironstone	
20.20	23.50	3.30		Yellowish Clayey siltstone	
23.50	27.00	3.50		Ironstone	
27.00	42.00	15.00		whitish-yellowish laminated friable siltstone	
42.00	50.00	8.00		grayish, well compacted carbonaceous shale	☆ BH15C

Figure 4.62: Litholog of Borehole (15) sampled at Maiganga. GPS: x = 734251, y = 1105749, z = 458. The log shows shale, siltstone and ironstone intercalation. The star symbol indicates samples in which palynomorphs were recovered.

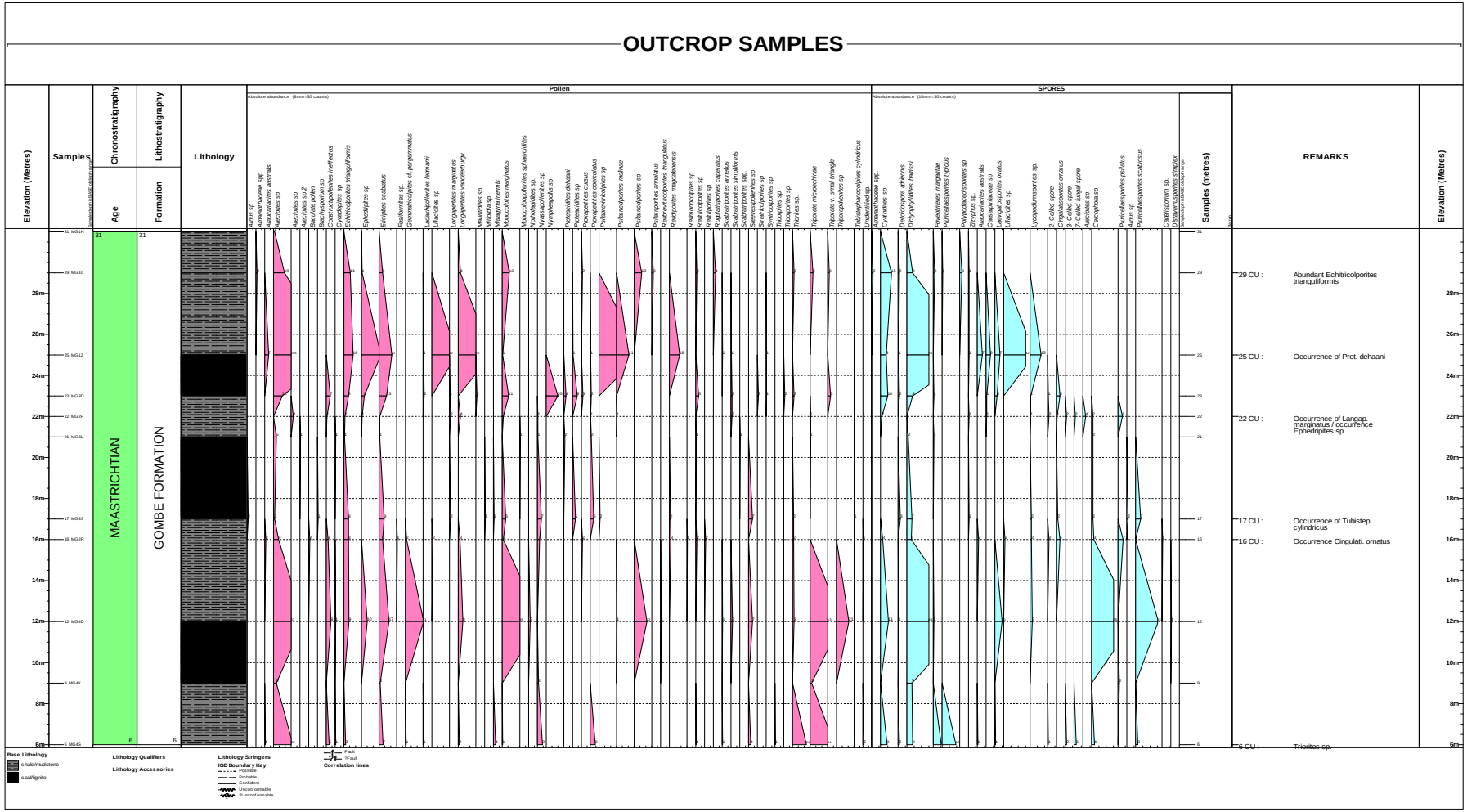


Figure 4.63: Palynomorph distribution charts of selected outcrop samples of Gombe

Palynological summary of selected outcrop samples

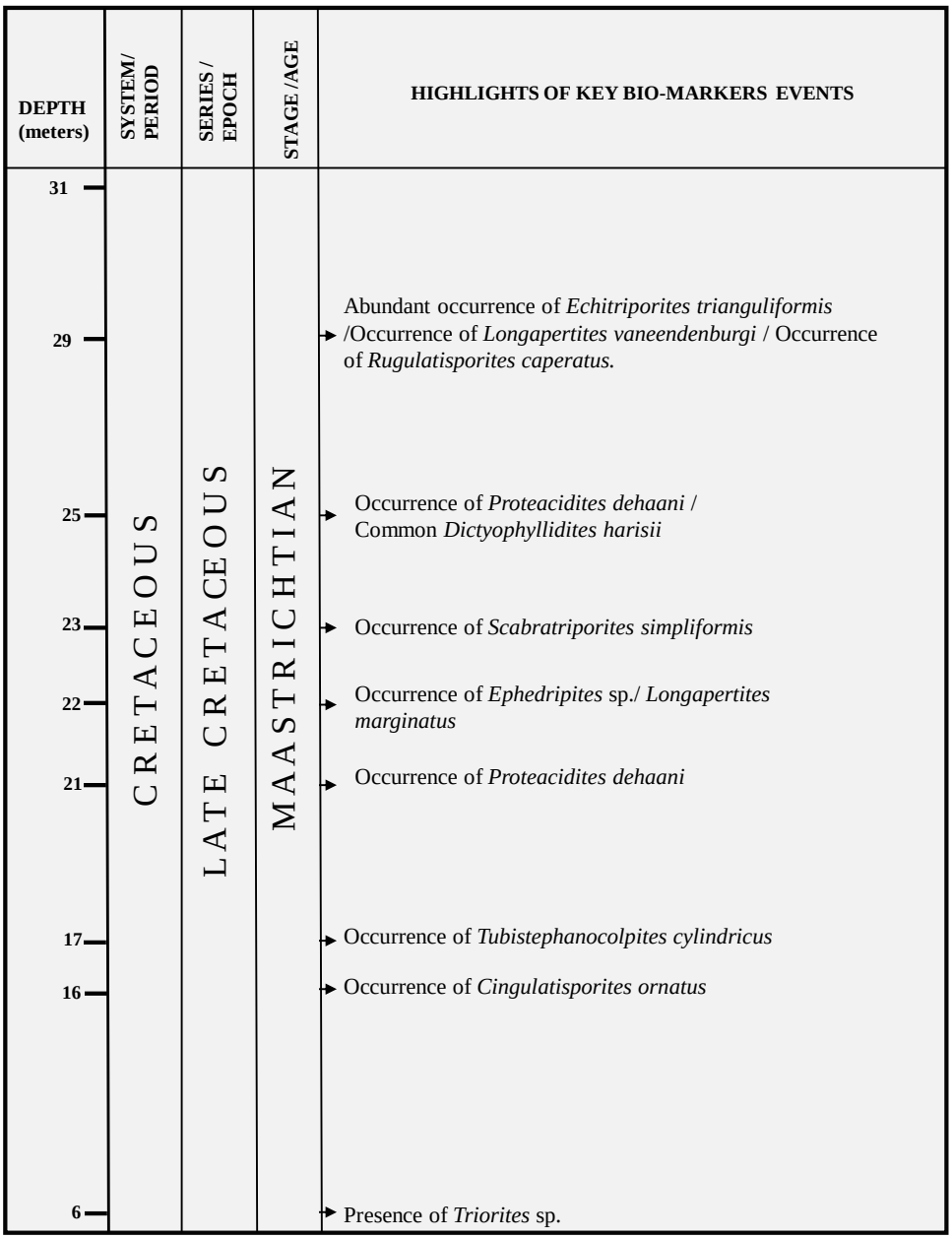


Figure 4.64: Highlight of key biomarker events at some depth from phase I and II. The occurrence of these marker species confirms the Maastrichtian age for the coal and shale samples.

4.8.2 Palynofacies, Paleoecology and Paleoclimate

Schrank (1987) has shown that palynormorphs assemblage with dominance of land derived spore and pollen indicates a terrestrial influence and vice – versa. In the samples analysed, most of the palynormorphs are land derived pollen and spores. The coal facies contains predominantly of opaque phytoclast and rare amounts of pollen and spores. The opaque phytoclasts (black debris) in the coal samples probably indicate oxidation of woody materials either during prolonged transport or post – depositional alteration. The presence of the black debris in the coals suggests oxidizing conditions and closeness to terrestrial sources or re-deposition of organic matter from fluvio-deltaic environment (Tyson, 1989).

The shale facies are essentially rich in large non opaque biostructured phytoclast with very common palynomorphs. The low amounts of opaques observed in the shale suggest low salinity in the water and proximity to active fluvio-deltaic sources (Carvalho et al., 2006a). The presence of poorly preserved phytoclasts and the low amounts of black debris suggest decomposition in a warm well oxygenated climatic condition. The presence of fungal spores confirms the abundance of land plants debris and therefore suggests ancient swamp, fluvio-deltaic or lacustrine with probable marine influence due to recovery of a dinocyst in a sample (Oboh, et al., 1992). However, based on the abundant occurrence of palm pollen (*Mauritiidites, Arecipites, Monocolpites marginatus, Proxapertites* and *Longapertites* sp.*)* and spores such as *Lycopodiumsporites fastiginoides, Foveotriletes margaritae* and *Cingulatisporites ornatus*, the inferred environment was generally warm. Many of the palms (*Arecipites* sp.) would have been predominant in swamps and similar marshy areas, and the occurrence of *Liliacidites* indicated the presence of some freshwater swamp (Herngreen, 1998). The occurrence of *Deltoidospora adriennis* (*Acrostichum aureum*) and absence of *Spinizonocolpites baculatus/echinatus* (*Nypa fruticans*), an early mangrove species in Nigeria indicated that the mangrove swamp forest was at its earliest development stage.

The climate would also have been occasionally hot accompanied by some wind activities on account of the recovery of *Ephedripites* sp., *Podocarpidites* sp. and *Nothofagidites* sp. In addition, the presence of diverse *Retitricolporites*, *Retitricolpites* sp, and *Monocolpollenites spaeroidites* many of the parent plants of which are presently found in the wetter/southern Guinea zone of Nigeria shows the presence of terrestrial vegetation. Majority of the fungal spores are saprophytes while other are associated with animal dung. In conclusion, the environment was dominated by vegetation adapted to swamps and marshy areas. The area was characterized by a tropical climate i.e. generally warm and dry due to the presence *Ephedripites* forms.

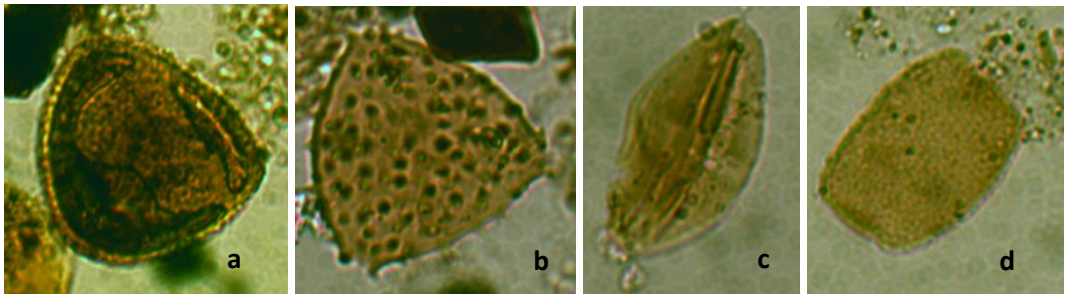


Plate 4.1

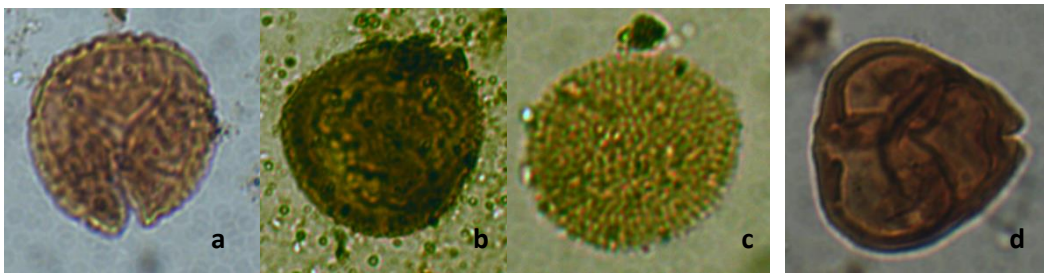


Plate 4.2

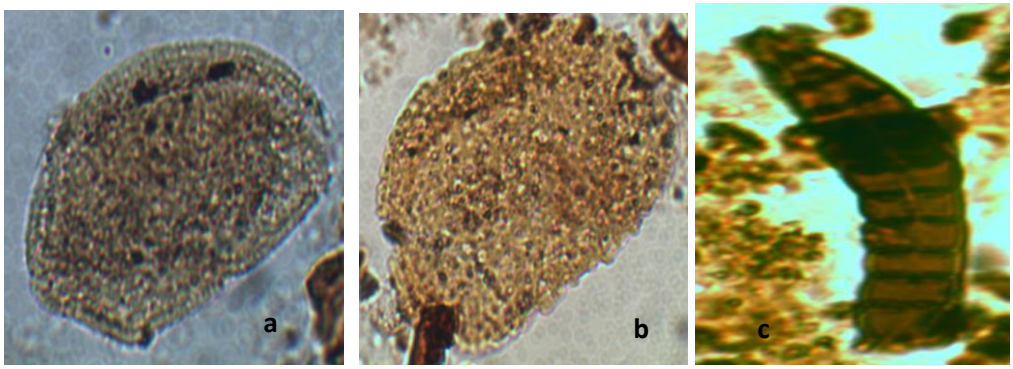


PLATE 4.3

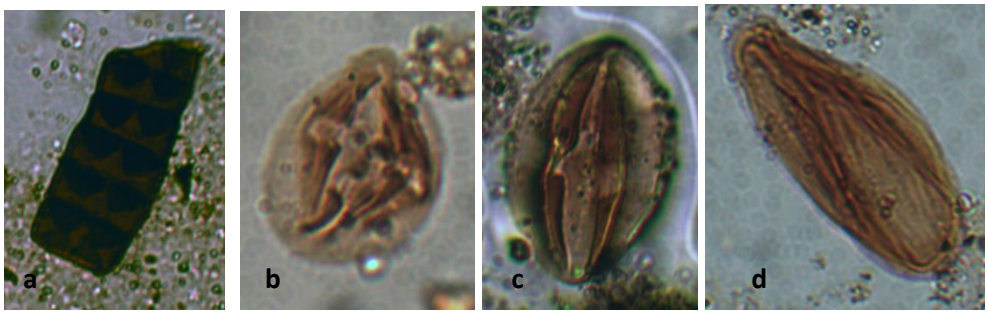


PLATE 4.4



PLATE 4.5

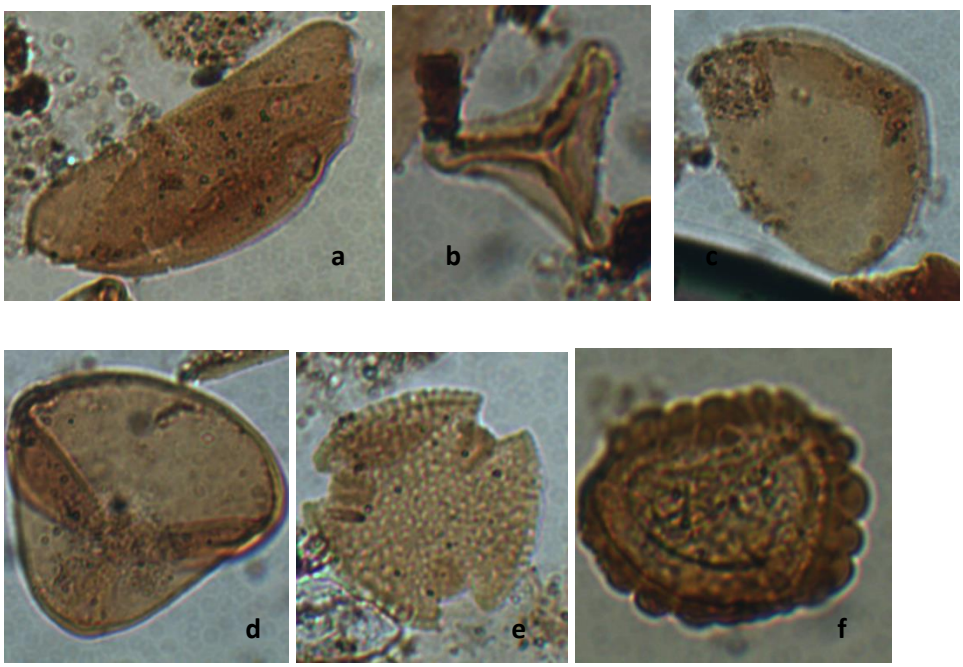


PLATE 4.6

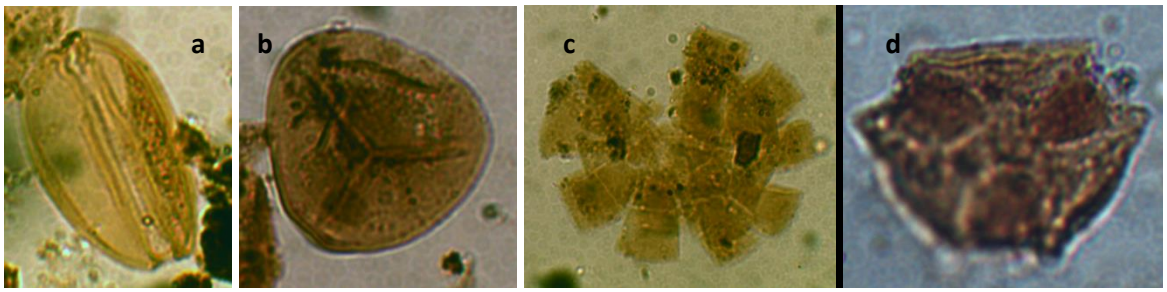


PLATE 4.7

PLATE 4.1
a=Foveotriletes margaritae (MG4D)
b=Echitriporites trianguliformis (BH15A)
c= Psilatricolporites sp (BH15A)
d=Retidiporites magdalenensis (BH15A)

PLATE 4.2
a=Lycopodiumsporites sp. (BH15C)
b=Zlivisporis blanensis (BH15B)
c=Constructipollenites ineffectus (BH15A)
d=Ericipites scabratus (BH15B)

PLATE 4.3
a=Longapertites vaneendeburgii (MG1Z)
b=Proxapertites cursus (MG2R)
c=Pluricellaesporites scabiosis (MG4D)

PLATE 4.4
a=Pluricellaesporites psilatus (BH15B)
b=Nyssapollenites sp.1 (BH15C)
c=Nyssapollenites sp.2 (BH15C)
d=Steevesipollensites sp. (BH15C)

PLATE 4.5
a=Cercophora sp. (MG4D)
b=Scabratriporites annellus (BH15A)
c=Cyathidites sp. (MG4S)
d=Scabratriporites sp. (BH15A)

PLATE 4.6

a=Longapertites marginatus (BH15C)

b=Dictyophyllidites harrisii (BH15C)

c=Proxapertites operculatus (BH15C)

d=Deltoidospora adriennis (BH15C)

e=Retibrevitricolpites triangulatus (BH15C)

f=Cingulatisporites ornatus (BH15C).

PLATE 4.7
a=Monocolpites marginatus (MG4D)
b=Distaverrusporites simplex (MG4D)
c=Nothofagidites sp. (MG4D)
d=Gemmatricolpites cf. Pergemmatus (MG1Z)

4.9 Coal Quality and Rank

The quality of the coals with respect to its usage for power generation, combustion and cokability was evaluated based on the interpretation of the proximate analysis obtained (Table 4.15) while the source of the plants that formed the coal, paleodepositional condition and acid generation potential of the coal were interpreted using the elemental composition of the coal (Table 4.16, 4.17 and 4.18).

The percentage of moisture (M), volatile matter (V.M) and ash content and the fixed carbon of all the samples (as received and air-dried) are shown in Table 4.15, Figures 4.67 and 4.68. Generally the moisture values varied from (8.43% – 14.24%). Coal sample MG2H has the highest moisture content (14.24%) and sample MG1W has the lowest (8.43%). The values suggest that coal sample MG2H will take more time to burn and will have lower calorific value (ASTM, 1974) due to the high moisture content, hence it will be consumed more during heating. Moisture content required for good coking coal is 1.5% but may range from 1-4% (Mackowsky, 1982). In the samples analyzed, the moisture content is higher probably due to oxidation and may not be suitable for coking (Chelgani et al, 2011). The results also indicated that other proximate parameters such as volatile matter, ash, fixed carbon and calorific values increases after the moisture content has been driven off (air-dried).

Volatile matter is the most important parameter used in determining coal rank, suitability and resource applicability (Mackowsky, 1982). Data obtained in this study showed that all the samples have high volatile matter which range from (36.79-40.44% as received) and (40.88-44.89% when air dried) (Table 4.15). As the volatile matter content of coal increases there is a relative decrease in the calorific value of coal from the older beds to the younger beds suggesting increased in level of coalification with burial. According to Mackowsky (1982), coals with high volatile matter content ignite easily and are highly

reactive in combustion applications. Weakly coking coals or high volatile non coking coals are known to have high volatile matter content of 36%. The investigated samples are therefore classified as non coking coal due to their relatively high volatile matter (> 36%) and high moisture content (Chelgani et al, 2011) (Table 4.15). Similar results were recorded for coals in Southern Benue Trough in Onyeama, Orukpa and Okaba coal (Fatoye and Gideon, 2013). Obaje and Hamza (2000) also reported that coal in the Central Benue Trough, the (Turonian – Coniacian Lafia - Obi coal) has low moisture content, low volatiles, high calorific value (7500-8500kcal/kg) and therefore classified as a coking coal.

The ash content of the investigated samples varies from (5.29-13.99%) when air dried. It is observed that as percentage of ash content increases, the heat value or calorific value decreases, i.e ash content is inversely proportional to the heat value. Low ash content (<10%) is essential requirement for coking coal (Mackowsky, 1982). In the studied samples, only coal sample MG2P has ash content greater than 10%. The low average value of the ash may be due to low amount of inorganic minerals present in the coal ash e.g quartz, (1.35%), kaolinite (1.83%) and sulphur (0.07%). Ash content reduces plasticity and may determine how slag reacts in a combustion chamber. The quartz and kaolinite contents were calculated using Raask's method (1985) by the following mathematical equations.

$$Q = SiO_2 - 1.5 \times Al_2O_3 \text{ ----------1}$$ (Q = quartz)

$$K = SiO_2 + Al_2O_3 + K_2O - Q + 9.1 \times K_2O \text{……...2}$$ (K = Kaolinite)

MG1A, Q=1.02- (1.5*0.53) **Q=0.225**

MG1W, Q=3.38-(1.5*0.79) **Q=2.195**

MG2H, Q=2.74-(1.5*0.75) **Q=1.615**

MG1A, K= (1.02+0.53+0.01) – 0.225+ (9.1*0.01) **K = 1.43**

MG1W, K= (3.38+0.79+0.01) – 2.195+ (9.1*0.01) **K = 2.08**

MG2H, K= (2.74+0.75+0.01) – 1.615+ (9.1*0.01) **K = 1.98**

Table 4.15: Results of Proximate analysis and the Calorific values of Maiganga coal

S/N	Sample Code	Lithology	Sample Type	Depth (m)	M (%)	V.M (%)	Ash (%)	F.C (%)	C.V (Kcal/kg)
1	MG1A*	Coal	Surface	35	11.13	38.89	4.70	44.28	5734
	MG1A^				-	44.89	5.29	49.83	6452
2	MG1G*	Coal	Surface	30	10.00	36.79	5.14	48.07	5748
	MG1G^				-	40.88	5.71	53.41	6387
3	MG1W*	Coal	Surface	25	8.43	39.44	7.97	44.16	5573
	MG1W^				-	43.07	8.70	48.23	6086
4	MG2H*	Coal	Surface	20	14.24	37.41	6.67	41.68	5397
	MG2H^				-	43.62	7.78	48.60	6294
5	MG2P*	Coal	Surface	17	9.55	40.44	12.65	37.36	4947
	MG2P^				-	44.71	13.99	41.30	5469

***= As received, ^= Dry, M - Moisture, V.M - Volatile matter, FC - Fixed carbon**

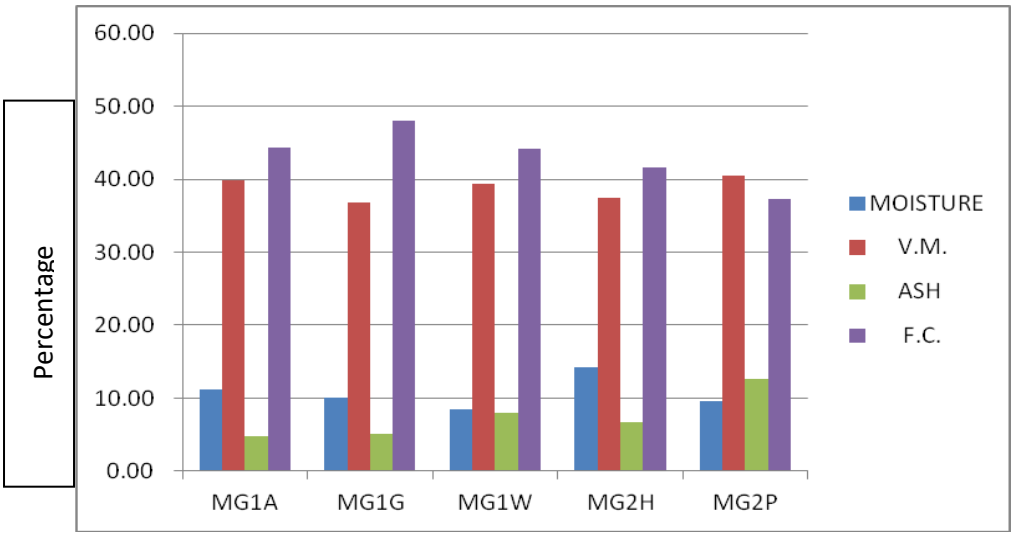


Figure 4.66: Bar chart showing the percentage of moisture, ash, volatile matter and fixed carbon of the coal samples (as received). The samples have low to medium moisture, high volatile matter with moderate ash content.

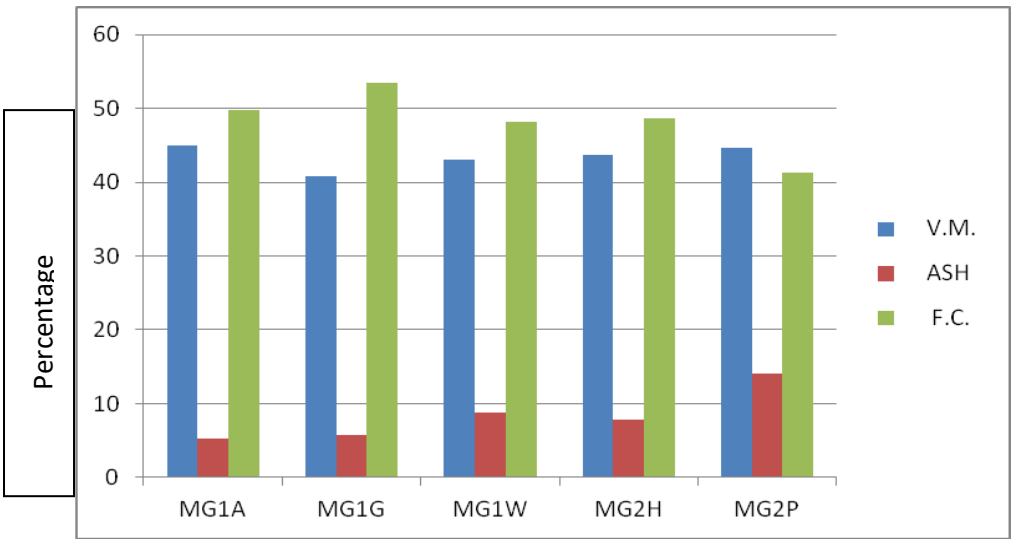


Figure 4.67: Bar chart showing the percentage of volatile matter, ash and fixed carbon of the coal samples (dry). The samples have high volatile matter with moderate ash content.

Table 4.16: Major elements of Maiganga coal, Gombe Formation

Sample no	Seam	SiO_2	Al_2O_3	Fe_2O_3	MgO	CaO	Na_2O	K_2O	TiO_2	P_2O_5	MnO	LOI	Total
							(%)						
MG1A	Seam A	1.02	0.53	0.43	0.34	1.02	<0.01	<0.01	0.046	<0.01	0.007	96.63	100
MG1W	Seam B	3.38	0.79	1.37	0.37	1.11	0.02	0.01	0.107	0.01	0.045	92.76	99.97
MG2H	Seam B	2.74	0.75	0.90	0.30	0.92	0.01	0.01	0.065	<0.01	0.025	92.26	99.99

Table 4.17: Trace elements of Maiganga coal, Gombe Formation

Sample no	Ba	Be	Co	Cs	Ga	Ge	Hf	Nb	Rb	Ni	Sc	Sn	Sr	Ta	Th	U	V	Y	W
									(ppm)										
MG1A	66	2	<1	<0.5	5	<1	<0.2	<1	<2	111	1.0	<1	52	<0.1	0.5	0.3	<5	5	2.89
MG1W	91	<1	3	<0.5	1	<1	0.7	2	<2	121	1.1	<1	65	0.2	1.1	0.2	<5	2	2.78
MG2H	65	<1	4	<0.5	2	<1	0.4	1	<2	205	1.1	<1	51	0.1	0.8	0.3	<5	2	2.63

Table 4.18: Rare earth elements of Maiganga coal, Gombe Formation

Sample no	La	Ce	Pr	Nd	Sm	Eu	Gd	Tb	Dy	Ho	Er	Tm	Yb	Lu
							(ppm)							
MG1A	1.1	2.9	0.39	1.7	0.4	0.1	0.4	<0.1	0.5	0.1	0.3	<0.05	0.3	0.05
MG1W	3.3	5.5	0.54	2.0	0.4	0.08	0.3	<0.1	0.3	<0.1	0.2	<0.05	0.2	<0.04
MG2H	2.7	5.5	0.61	2.3	0.4	0.09	0.4	<0.1	0.3	<0.1	0.2	<0.05	0.2	<0.04

Fixed carbon content is directly related to the calorific value. It varies between 41.30-53.41% (air dried) and (37.36-48.07% as received). Table 4.15, Figures 4.67, and 4.68 showed all the samples have high fixed carbon (above 40%) and it is reflected in the calorific value (up to 6452kcal/kg). The fixed carbon content can determine the yield of coke in coal samples because increase in fixed carbon increases the cokability of coal (Ryan et al., 1998) i.e high carbon content yield good coke and vice versa. However, the samples are not suitable for coking because of the high volatile matter. Calorific value varies from (5469-6452kcal/kg) indicating that all the samples have high calorific value which is reflected in the low ash content and high fixed carbon. The samples are better for fuel purposes than coking (Ryan et al., 1998). Figure 4.69 reveals a direct proportional relationship between the depth of the coal samples and its fixed carbon content, the fixed carbon content increases as the depth of burial increases with the exception of sample MG1A (Table 4.15).

This study shows that the coal samples contain medium moisture content, low ash and high volatile matter. The coals are high in volatiles and are sub-bituminous. Based on these results, the coals are suitable for combustion, power generation and fuel purposes. It is important to note that ash, fixed carbon, volatile matter and calorific value are all a function of original coal bed composition than rank.

4.9.1 Major Element Geochemistry

The major elements geochemistry of the coal samples analyzed were used to infer the depositional environment and acid generation potential of the coal ash using A-K-F ternary plot (Euglung and Jorgensen, 1973; Nesbitt et al., 1996) and the A –CNK-FM ternary plot (Huggins et al., 1981; Vincent, 1987) (Figures 4.70 and 4.71) respectively. Samples MG1A, MG1W and MG2H were analyzed for major elements (Si, Al, Mg, Ca, Na, Fe, Mn, K, Ti and P) and their oxides were recorded in percentages. The SiO_2 values ranges from 1.02-3.38%, while Al_2O_3 value ranges from 0.53-0.79%, the CaO and Fe_2O_3 averages 1.02 and 0.90%

respectively (Table 4.16). There is a significant positive correlation between the values of SiO_2 and Al_2O_3 with the Ash (r =1, 0.98) respectively suggesting that they are associated with aluminosilicate minerals and quartz. The low average value of Fe_2O_3 (0.90) suggest the absence or low content of iron bearing mineral like pyrite. The alkalis K_2O, Na_2O as well as CaO, MgO and MnO occur in relatively insignificant proportions (< 0.01 to 1.11%). The coal samples have extremely low SiO_2 contents of about 2.38% average and is primarily due to the fact that it consists basically of volatile constituents that were combusted as is evident from their average loss on ignition of (94.6%). The depositional environment deduced from AKF plots show a gradual transition from continental to transitional environments and to marine environments. However, the samples fall largely under transitional or paralic depositional setting **(**Figure 4.70).

The acid producing potential of the coal ash was inferred from the A –CNK-FM ternary plot (Huggins et al., 1981; Vincent, 1987) (Figure 4.71) which indicates the proportions of Al_2O_3, CaO + Na_2O + K_2O and Fe_2O_3 + MgO. This plot is used to determine the correlation between the composition of the coal ash grouped into basic, fluxing acidic and non-fluxing acidic oxides (Huggins et al., 1981; Vincent, 1987). The A-CNK –FM ternary plot of the three coal ash samples (Figure 4.71) indicates the samples have low proportion of base neutralizing cations (CNK). The chemical index of alteration (CIA) and sulphur content can also give clue on the potential of the ash to generate acid (Campbell et al, 2001). The CIA was calculated by the formula (Al_2O_3 / (Al_2O_3 + CaO + Na_2O + K_2O + MgO) x 100 (Nesbitt and Young, 1982). Coal ash producing acid tend to have CIA value greater than 20% (hence low base proportion in ash) and high reactive sulphur content (Campbell et al. 2001). However, the samples analyzed have CIA range from 40-44% indicating apparent acid generating potential. This is backed up by the moderate sulphur content of (0.05-0.1%) with an average of (0.07%).

4.9.2 Trace Element Geochemistry

The trace element geochemistry of the investigated coal samples were employed to decipher the environmental effect and impact on coal utilization via combustion and to determine the elements that were associated with the coal ash in organic matrix and in discrete (mineral) phase. Twenty (20) trace elements were analyzed namely Ba, Be, Co, Ta, Th, U, V, Y, Rb, Sn, Sr, W, Zr, Cs, Ga, Ge, Hf, Nb, Ni and Sc (Table 4.17). The concentrations of the trace elements are low except Nickel, Copper, Barium, Strontium and Zircon (Table 4.17). The release of some of these elements e.g Sb, As, F, Hg, Pb, Se, Th and U in to the environment may pose serious environmental problem if they occur in significant amounts (Skodras et al. 2002). It is important to consider the potential environmental impact of trace elements released during coal utilization. Several studies have indicated that trace elements from coal combustion and combustion residues increases the concentration of toxic elements in the biosphere, in some cases resulting in negative health impacts on animals, humans and plants (Panov et al. 1999; Zheng et al. 1999).

Nickel concentration of the investigated coal samples ranges from 111- 205ppm with an average of 146ppm, Cu (122-176ppm, avg 142ppm), Ba (65-91ppm, avg 74ppm), Sr (51-65ppm, avg 56ppm), Zr (8-28ppm, avg 18ppm) other trace elements has low values (Table 4.17). The average concentration of these elements is lower when compared to world coals and therefore have lesser negative impact to the environments (Table 4.19).

According to Spears and Zheng (1999), high concentrations of fluorine, chlorine and vanadium in the feed coal may cause corrosion of the combustion equipment. High vanadium coals may cause agglomeration in fluidised bed combustion boilers (Anthony and Jia, 2000). In this study, the concentrations of vanadium in the coals are low (< 5ppm). It has been suggested that sulphur from coal combustion can cause acid rain (Bouska and Pesek, 1999). Similarly chlorine and fluorine in coals can also cause acidic emissions. In the samples

analyzed, the low concentration of vanadium indicates low corrosion and agglomeration potential in combustion boilers (Anthony and Jia, 2000). Also the average concentration of trace elements like Zn (1.7ppm), Se (<3ppm), Hf (0.4ppm), Br (3.17ppm), Cr (<5ppm) and S (0.07%) are moderate in the samples. The utilization of these coals are said to be environmentally friendly.

Coal ash is dominated by either clastics (clays, quartz or zircon) high in Al and Si or by meteoric precipitate (pyrite) high in iron. A coal ash consisting of Al clay and clastic detritus could contain Hf bearing zircon and therefore would display a positive correlation between Hf/Zr and other bearing lithophile element (Chen et al., 2016). A low Al coal ash will tend to be high in iron indicating a far less detrital material including zircon. In this study, the significant positive correlation value (r=0.85) generated from plot of Hf/Zr (Figure 4.72) indicates that the coal samples from Maiganga consist of Al clay probably kaolinite and clastic detritus (quartz and zircon) (Chen et al., 2016). This is supported by the positive correlations of the trace elements such (Na, Ba, Th, and Co) with SiO_2 and Al_2O_3 suggesting primarily aluminosilicate affinities (Chen et al., 2016). Elemental cross plot may be used to determine whether elements exist in organic matrix of the coal or as discrete mineral phases. The element chlorine and vanadium are both thought to exist in inorganic matrix of the coal, but could however be derived from minerals halite and illite respectively. Cross plot of vanadium against coal ash (%) (Figure 4.73) with correlation value of (r=0.52) indicate that low vanadium is associated with low ash while high chlorine is present in low coal ash. This suggests an organic affinity for chlorine and a mineral affinity for vanadium.

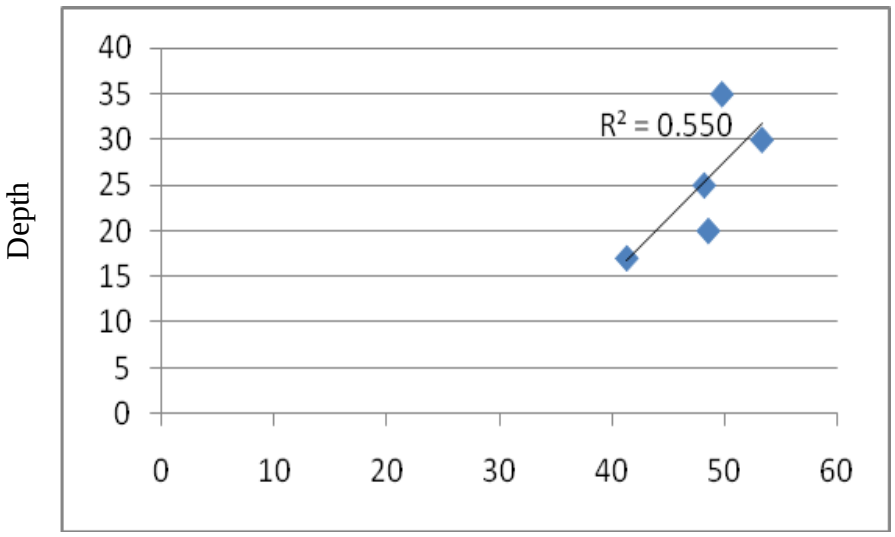


Figure 4.68: Correlation between stratigraphic depth and fixed carbon. The fixed carbon is directly proportional to the depth, the fixed carbon increases with stratigraphic depth.

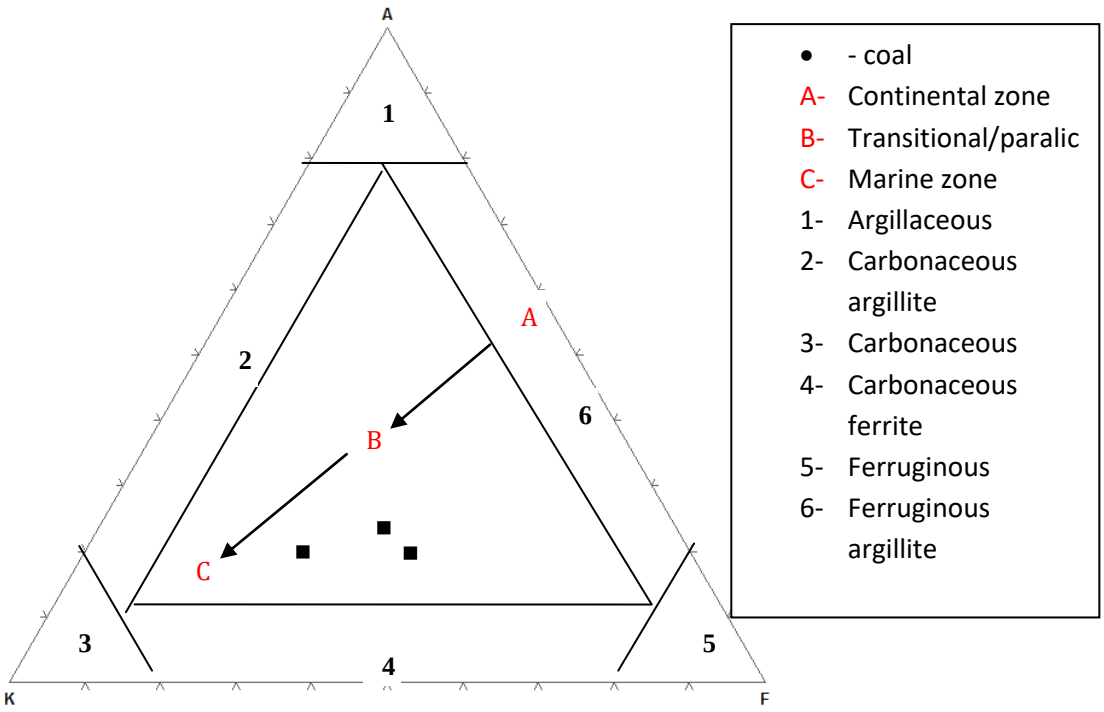


Figure 4.69: Al_2O_3 - (K_2O+CaO+MgO) - (Fe_2O_3+MgO) [AKF] Ternary plot of Maiganga coal samples. The coals plotted in the Transitional/ Paralic depositional environments (after Euglung and Jorgensen, 1973; Nesbitt et al., 1996).

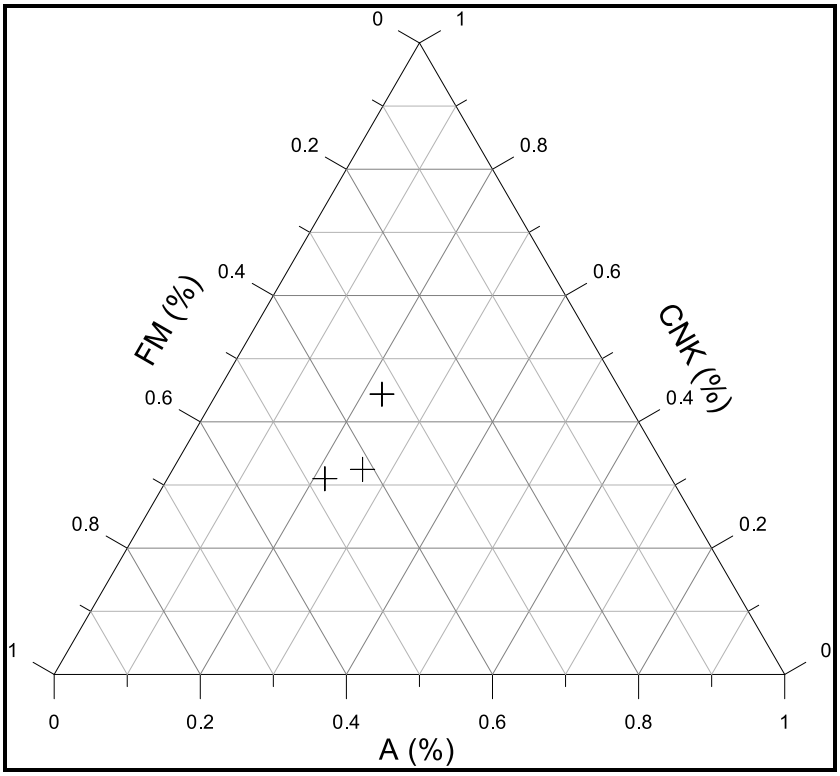


Figure 4.70: A-CNK-FM plot for the Maiganga coal samples which indicates low proportion of base neutralizing cation. A = Al_2O_3, CNK= CaO + Na_2O + K_2O and FM= Fe_2O_3 + MgO (after Huggins et al., 1981; Vincent, 1987).

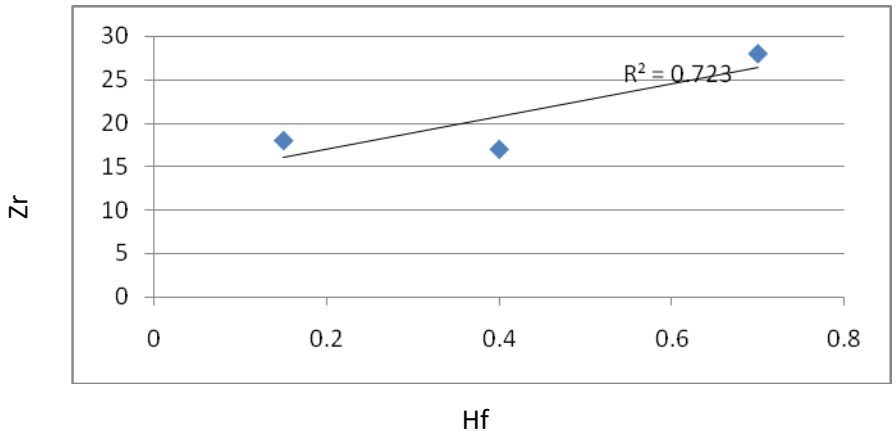


Figure 4.71: Plot of Hafnium (Hf) against Zirconium (Zr). The significant positive correlation value (r=0.85) indicates that the coal samples from Maiganga consist of Al clay probably kaolinite and clastic detritus.

Table 4.19: Average concentration of some trace elements in Maiganga coal compared with average world coals.

Elements	Present study (ppm)	World[c] (ppm)
Cr	<5	16
Hf	0.4	1.2
Se	<3	1.3
Zr	18	36
Zn	1.7	23
Sr	56	110
Ba	74	150

c From Ketris and Yudovich (2009).

The average trace elements concentration of Maiganga coal is lower compared to average world coals indicating that the coals will have lesser negative environmental impact in its utilization.

Table 4.20: Chondrite Normalized Values, Europium and Cerium Anomalies of Maiganga coal samples

Sample no	La	Ce	Pr	Nd	Sm	Eu	Gd	Tb	Dy	Ho	Er	Tm	Yb	Eu/Eu*	Ce/Ce*
MG1A	3.24	3.19	3.22	2.66	2.05	1.37	1.54	1.28	1.67	1.28	1.50	1.25	0.73	1.06	
MG1W	9.70	6.04	4.46	3.13	2.05	1.10	1.15	1.49	1.00	0.77	1.00	0.94	0.72	0.74	
MG2H	7.94	6.04	5.04	3.60	2.05	1.23	1.54	1.70	1.00	0.90	1.00	0.94	0.69	0.89	

$Eu/Eu^* = Eu_N/\sqrt{(Sm_N * Gd_N)}$

$Ce/Ce^* = 5Ce/(4La_N + Sm_N)$

Note: $_N$ and * indicate chondrite normalized elements.

4.9.3 Rare Earth Element Geochemistry

The Rare Earth Elements (REE) distribution in coal can provide information on the epigenetic changes, clastic provenance and depositional environment (Schatzel and Stewart, 2003; Liu et al., 2007). Rare earth element geochemistry was employed to determine the depositional condition and the vegetation type that form the coal bed. Liu et al., (2007) stated that during formation and depositional processes of coal, REE may be epigenetically modified particularly during weathering process. REE comprises of series of metals with atomic numbers 57 to 71 i.e La to Lu. The light rare earth elements (LREE) are the low atomic number members of the series (La-Pr) while the heavy rare earth elements (HREE) are those with the higher atomic numbers (Er-Lu). The middle rare earth elements (MREE) are the middle members of the group, Sm to Ho. REE concentrations in rocks and sediments are usually normalized to a standard which has the values for chondritic meteorites (Boynton, 1984). The standard used for this work is that of (Wakita et al. 1971).

The fractionation of the REE group relative to chondrite meteorites is usually done by normalization to eliminate the abundance variation between even and odd atomic elements (Boynton, 1984). The normalized REE (concentrations in ppm) were plotted against the atomic numbers of the REE to give a REE pattern (Figure 4.74) which could give a Europium anomaly. Europium anomalies may be calculated by comparing the measured concentration with an expected concentration obtained by interpolating between the normalized values of Sm and Gd. Thus, the ratio of Eu is a measure of the Europium anomaly and a value greater than 1.0 indicates a positive Europium anomaly while the value less than 1.0 is a negative anomaly. The chondrite normalized values, the Europium and Cerium anomalies value were calculated and the result presented in (Table 4.20).

Ce/Ce* is a geochemical proxy used for determining the paleoenvironmental conditions. Ce/Ce* values greater (>1.0) indicate an oxidizing condition (Milodowski and

Zalasiewicz, 1991; McDaniel et al. 1994). This study shows that there is enrichment of LREE over HREE and the europium anomaly (average of 0.71) is less than 1 indicating negative anomaly, this is supported by the REE pattern for the samples (Figure 4.74). The Cerium anomaly is also negative for the samples MG1W and MG2H (0.74 and 0.89) respectively indicating reducing condition while MG1A has Positive Ce anomaly with values (1.06) depicting oxidizing condition.

Identification of the original plants that formed a coal is sometimes a difficult process, it is generally thought that most coals originated from trees and peat, but also that some have originated from algae (Cross and Phillips, 1990). The trace elements in a coal can contain information on the origins of the coal and on the conditions of coalification, because the trace elements in coals principally come from the plants that formed the coal and from the surrounding environment. In particular, (REEs) in coal have been identified as a group of special significance (Mukhopadhyay et al. 1998; Schatzel and Stewart, 2003; Liu et al., 2007).

REEs in coals can originate from the original plants that formed the coal, from soil minerals, and from water. The percentage of REEs inherited from the original plants is dependent on the type of plants that formed the coals, and so can vary greatly, since different species of plants contain different levels of REEs (Akagi et al. 2002).

It has been previously reported that negative Ce anomalies are normally seen in soil-grown plants, and that the mineral fraction in soils either does not show a negative Ce anomaly, or shows a slightly positive Ce anomaly (Fu et al. 2001). REEs in terrestrial soil-grown plants originate from silicate minerals (Fu et al. 2001), whereas those in algae originate partly from water and partly from particles suspended in the water (Fu et al. 2000). Thus, the relative abundance of REEs in terrestrial soil-grown plants, peat vegetation, and algae are distinct from each other. Soil-grown plants and algae showed Ce anomalies in their

REE patterns, whereas peat vegetation showed no Ce anomaly (Akagi et al. 2002; Fu et al. 2000, 2001). In this study, the extent of the cerium anomaly (A_{Ce}) is expressed numerically by the formula A_{Ce} = log (Ce/Ce*). The value of A_{Ce} is quantified as the logarithm of Ce/ Ce*

MG1A= log (1.06)

= 0.025

MG1W = log (0.74)

= -0.130

MG2H= log (0.89)

= -0.050

REEs in sample MG1A (seam B) originated from peat vegetation with extent of Cerium anomaly being positive value A ($_{Ce)}$ of (0.02) with Ce anomaly in the REE pattern. This may be due to low PH value of the water in the peatland soil and redox potential to oxidize Ce^{3+} to Ce^{4+} (Akagi et al 2002). This is backed up by the Ce/Ce* value slightly greater than 1.0 (positive) (Table 4.20) indicating oxidizing condition and the original plant that form the peat is probably (*Sphagnum L*. 10cm or *Carex L*.). Coal seam A (MG1W and MG2H) has negative Ce anomaly value A ($_{Ce)}$ of (-0.13 and -0.05) respectively (Table 4.21) indicating mangrove and *Vicia villossa* for the soil grown plants.

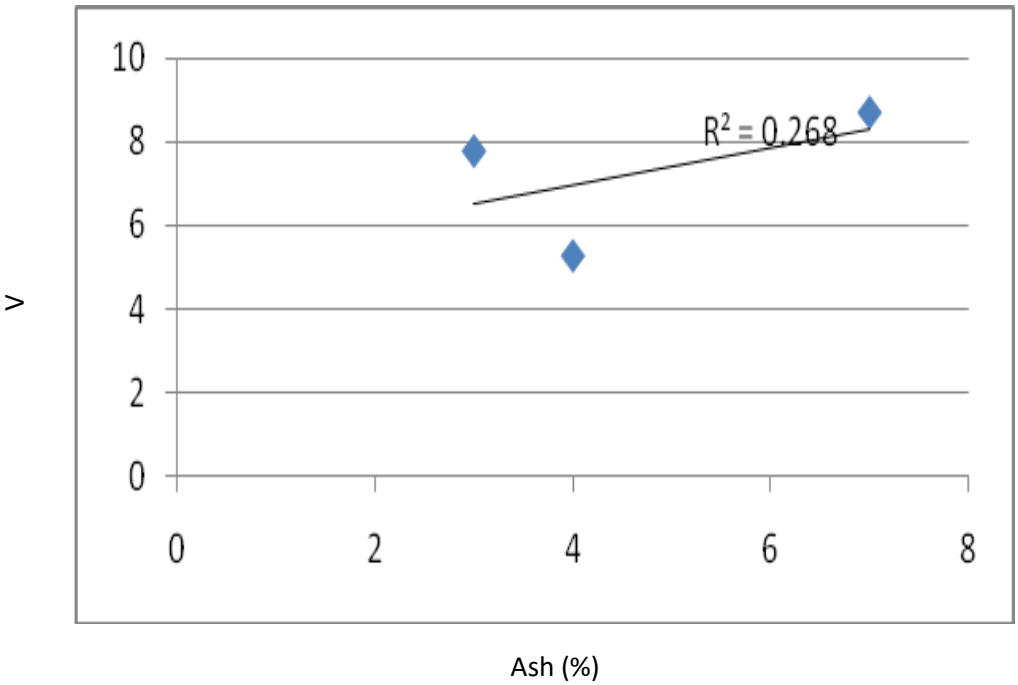


Figure 4.72: Plot of Vanadium (V) against Ash. Correlation value of (r=0.52) suggests an organic affinity for Chlorine and a mineral affinity for Vanadium.

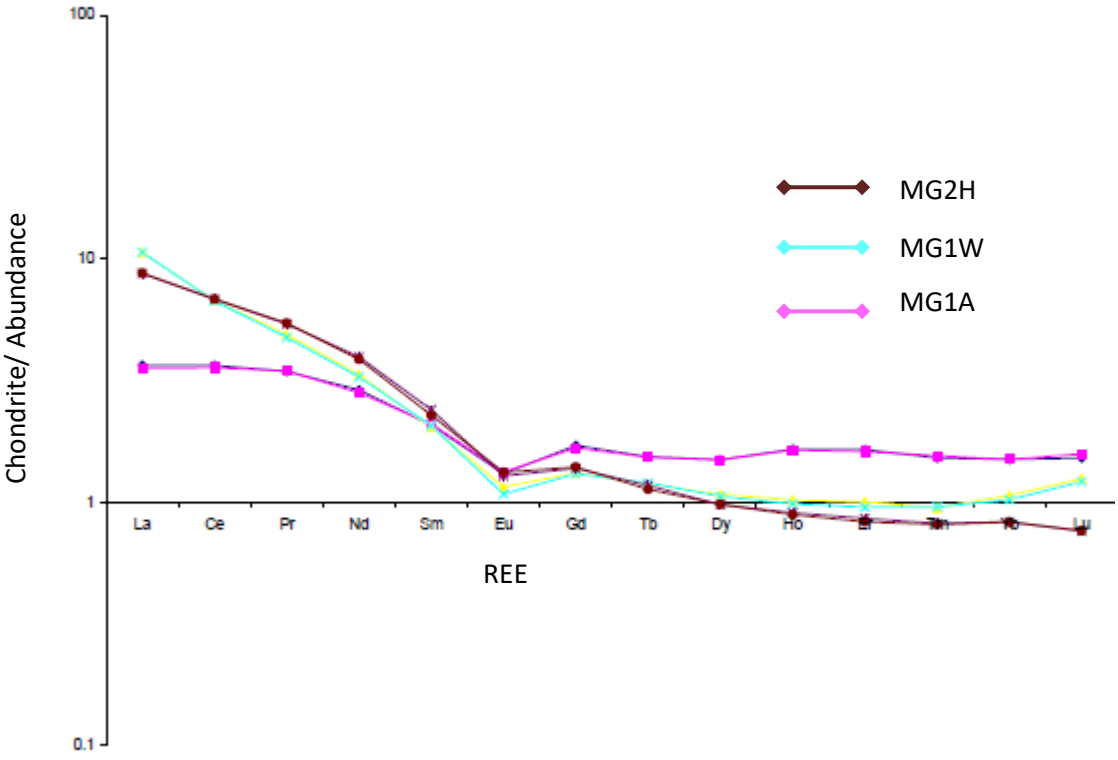


Figure 4.73: Rare earth elements (REE) Pattern for the coal samples. The pattern indicates negative europium anomaly for the coal samples.

Table 4.21: Ce anomalies with corresponding plant forming coal (modified after Fu et al. 2000, 2001 and Akagi et al. 2002).

Plants	Ce anomaly	$A_{(Ce)}$ anomaly (Present Study
Peat		
Vegetation*		
Sphagnum L. 10cm	0.01	0.02 (MG1A)
Sphagnum L. 30cm	0.01	
Carex L.	0.01	
Trunk of tree**		
Populous sieboldii	-0.6	
Mangrove	-0.15	-0.13 (MG1W)
Taxodium japonicum	-0.25	
Thea sinensis	-0.54	
Stem/ trunk of other soil grown plant!		
Matteuccia spp	-0.50	
Sasa nipponica	-0.16	
Vicia villosa	-0.08	-0.05 (MG2H)

CHAPTER FIVE

CONCLUSIONS AND RECOMMENDATION

5.1 Conclusions

Based on the field observations, source rock kinetics, isotopes, organic and inorganic geochemistry, organic petrography, palynology and proximate analyses carried out on the samples, the following conclusions were drawn;

i) The Gombe Formation was deposited in various sub environments swamp, fluvial/deltaic and lacustrine settings. The sandstone facies comprises of the fine grained and medium grained sandstone observed at Maiganga, Zange, Mallam Inna, Maiduku and Garin Magaji. The sandstones are brownish to reddish in colour, massive and poorly sorted consisting of sub angular to angular grains of quartz and feldspar. The clayey siltstones facies occur in all the study location and showed parallel lamination at some location. The siltstones are whitish to brownish in colour and moderately sorted. The carbonaceous shales are grayish in colour and rich in organic matter. The coal and shales represent nonmarine swamp/overbank deposit. The coal seams are about 3-4m thick occurring mainly at phase I and II of the mine. The coals are dark in colour, humic and are rich in organic matter. The occurrence of coal suggests development of incoaling condition in deltaic setting.

ii) The TOC values of the coaly and shaly source rocks exceed the minimal 0.5 wt% required for a potential source rock. The TOC of the coals ranges between (32.40-65.29 wt %) with an average of 38.03wt%, the shales ranges from (0.64-4.84 wt %) with an average of 3.14 wt% while coaly shales have an average of 12.1wt% indicating a good to excellent source rock. The hydrogen index for the coal ranges from (57-189mg/gTOC), (29-172mg/gTOC) for the shale and (84-140mg/gTOC) for coaly shale. HIs is generally less than 200mgHC/gTOC. The HIs indicated that the organic matter is Type III kerogen which

is capable of generating gas typical of terrestrial source, this is corroborated by the S2/S3 value which range from (1.6-7.4) a ratio indicative of Type III kerogen.

iii) The thermal maturity of the analysed samples represented by Tmax of (413–439°C). The coals range from (427-430°C) with an average of 428°C, the shale range between for shale, and (426-428°C), averaging 427°C for the coaly shale which indicates immature, this results also corroborated the vitrinite reflectance (Romax) values of the coals ranging from (0.48-0.55%) which implies that only one sample fall within the range of oil generation as most of the coal have vitrinite reflectance less than 0.5% and Tmax <430^{o}C. The low PI values recorded for all the samples also indicate that they are thermally immature (less than 0.1) indicating low level conversion to generate and expel oil. The thermal alteration index (TAI) of the samples (coals and shales) falls between (2.4-2.6) also corroborated other maturity indices such as the spore coloration which range between pale yellow –yellow, yellow-orange and dark orange also indicated that the organic matter is thermally immature.

iv) Kinetic study of the organofacies indicates broad distribution of the activation energy indicating heterogenous composition and terrigenous source. Based on the kinetics, the coal and shale facies are in early- late mature generation stage which probably has experienced a partial conversion of kerogen to oil and gas. The major phase and peak of hydrocarbon generation occurs at 460 – 465^{o}C for the coal and shale facies with a constant heating rate of 25^{o}C/min with peak hydrocarbon bond breaking at 54 and 55 kcal/mol defining up to 70% of the petroleum potential in which most of the kerogen has been converted to oil.

v) The high percentage of the NSO and Asphaltenes (heterocompounds) in the organofacies extract indicates organic matter originated from low maturity level of kerogen cracking. The biomarker maturity parameters (saturate and aromatic) further

validate the maturity level. The Carbon Preference Index (CPI) which measures the odd/even predominance (OEP) of the n-alkanes showed the samples to range from 2.74-3.76 and the CPI values (>>1) observed in the samples are characteristic of immature source rocks. Most of the saturate maturity parameters are lower compared to their corresponding Thermal Equilibrum Value (TEV) indicating low maturity status and hence have not reach onset of oil generation. The aromatic maturity indices also corroborate the maturity status of the organofacies. The calculated Methyl Phenanthrene index (MPI-1) and (MPI-2) are in close agreement with each other. Other indices such as TAS/(MAS+TAS), DNR and TDE confirms low level maturity.

vi) The *n*-alkanes distributions in the coaly source rocks ranges from C_{10}-C_{41} maximizing at C_{29} while the shale rock ranges from C_9-C_{41} maximizing at C_{16} and C_{29}. This pattern in coaly source rock indicates organic matter derived mainly from terrestrial organic matter and mixed source for the shale facies. Pr/Ph ratio for the coaly facies ranges from 2.15-3.51 (avg. 2.79) while the shaly facies ranges between 0.95-2.37 (avg. 1.82) indicating coastal swamp, fluvio/deltaic and lacustrine depositional environment in sub-oxic to oxic setting.

vii) The predominance of Pristane (n-C_{17}) over Phytane (n-C_{18}) support humic origin of the organic matter for the coaly source rocks in a mixed/transitional depositional environment and less reducing environmental condition. The coals are rich in C_{29} steranes (> 50%) an indication of significant land plant contribution. The shale facies has appreciable quantity of C_{27} and C_{28} αββS sterane (26% and 29%) and (34% and 24%) in C_{27}, C_{28}ααα R sterane confirming little marine contribution such as phytoplankton; algae and diatoms for the source. This is supported by the presence of C_{30} tetracyclic polyprenoids (TPP) a marker of lacustrine algae support fresh water lacustrine depositional conditions. The relatively low level of C_{23} tricyclic terpanes in m/z 191 of the

coal compared to other tricyclic terpane distribution is consistent with the tricyclic distribution seen in terrestrial organic matter. The C_{24}tetra/C_{26}tri(R+S) ratios range between 0.63-0.71 (avg, 0.68) for the coals probably reflects terrigenous organic matter input.

viii) The sterane/hopane ratio values range from 0.06-0.35) indicative of the incorporation of high level of bacterial inputs commonly associated with terrigenous organic matter in coals. The appreciable quantity of homohopanes (C_{31}-C_{35}) in all the samples, suggest that bacteriohopanetetrol and other polyfunctional C_{35} hopanoids and bacteriohopanepolyols commonly found in prokaryotic micro-organisms were significant contributors to the biomass. The low amounts of dibenzothiophene to phenanthrene (DBT/PH), 0.03 to 0.19 for the coal and 0.08-0.14 for the shaly source rocks indicate deposition of the organic matter predominantly in lacustrine and/or fluvial/deltaic environments.

ix) The predominance of C_{29} Triaromatic steroid (TAS) indicates a terrestrial source supported by the presence of appreciable amounts of *1,6-*, *1,7-*, and *2,6-*Dimethynaphthalene (DMN) in all the samples. The presence of *1,2,5-* and *1,2,7-*Trimethylnaphthalene (TMN) in the coal samples indicate both angiosperm and gymnosperms material contribution to the organic matter that formed the coals. The activation energy distributions observed in the samples are broad (41–65 kcal/mol) with associated fixed frequency factors of 2.00E+14/s reflecting heterogeneous compositions, which are typical of terrigenous organic matter derived from higher land plants.

x) Petrographic examination revealed that organic matter in the coal and shale samples consists of opaque to non opaque biostructured phytoclasts and cuticles associated with common amounts of spores and pollen. Vitrinite is the most abundant maceral in the coal followed by inertinite and liptinites. The high percentage of the vitrinite in the samples

indicates gas prone and suggests they were deposited in proximity to the source. All the samples are characterized by the absence of alginite and amorphous kerogen eliminating the presence of Type I kerogen typical of algae. The Palynomorphs observed in the samples includes Arecipites sp., Constructipollenites ineffectus, Cyathidites, Cingulatisporites ornatus, Dictyophyllidites harrissii, Echitriporites trianguliformis, Ericipites scabratus, Foveotriletes margaritae, Ladakhipollenites lehmanii, Laevigatosporites ovatus, Longapertites marginatus, Monocolpites marginatus, Nyssapollenites sp. Proteacidites dehaanni, Proteacidites sp., Proxapertites cursus, Proxapertites operculatus, Retitricolporites sp., Scabratriporites simpliformis, Striatricolporites sp., Syntricolporites sp. baculatus, Tricolporites sp. (Daniellia sp.), Triorites africaensis, Triporate v. suggesting late Cretaceous (Maastrichtian age) for the coals and the shales.

xi) The paleoenvironmental analysis of the coal deduced from the maceral suggests that the coal were deposited in wet forest swamp facies and that there was shift to drier condition from seam A to seam B. The proximate analysis of the coals revealed they are non coking but thermal coals of sub-bituminous rank that are easier to ignite and give greater flame stability due to the higher volatile matter content, suitable for combustion, fuelling and power generation as evidenced by the high calorific value and low ash content.

xii) The average concentrations of the trace elements are lower when compared to world coals and indicate lesser negative impact to the environments, plants, animals and humans. The positive correlations of the trace elements such (Na, Ba, Th, and Co) with SiO_2 and Al_2O_3 suggests primarily aluminosilicate affinities. The low ash and sulphur concentration of <1% of the coal suggest peat accumulation in a raised mire in a fluvial paralic/transitional depositional environment. The coals have association of inorganic

minerals like quartz, illite, kaolinite and little sulphur. Elemental analysis showed that the original plants that form the peat are *Sphagnum L or Carex L* for sample for (seam A) in oxidizing condition. Seam B coals are however characterized by trunk of soil grown mangrove plant and *Vicia villossa*.

5.2 Recommendations

The following recommendations are suggested;

1. Futher works such as burial and thermal history should be carried out in the study area.
2. The erosional level as well as the geothermal gradients in the basin should be carried out.
3. Geophysical tools should also be employed to unravel the ultimate petroleum system elements such as traps, reservoir and seal favorable for exploration of oil and gas.
4. There should be more collaboration between the industry and academic to bridge knowledge gap.

REFERENCES

Abbassi, S., Horsfield, B., George, S.C., Edwards, D.S., Volk, H., di Primio, R., (2014). Geochemical characterisation and predicted bulk chemical properties of pe- troleum generated from Jurassic and Cretaceous source rocks in the Vulcan Sub- basin, Bonaparte Basin, North West Shelf of Australia. *Org. Geochem*. 76, 82-103.

Abubakar, M.B. Obaje, N.G. Luterbacher, H.P. Dike, E.F.C. and Ashraf, A.R. (2006). A report on the occurrence of Albian-Cenomanian elater-bearing pollen in Nasara-1 well, Upper Benue Trough, Nigeria. Biostratigraphic and palaeoclimatological implications. *Journal of African Earth Sciences* 45, 347- 354.

Adegoke, A.K., Abdullah, W.H., Sarki, Y., Babangida, M. (2017). Provenance and paleoenvironment of organic matter within the Fika sediments in Chad (Bornu) Basin, northeastern Nigeria: An integrated organic geochemical and palynofacies approach. *International Journal of Coal Geology*.173: 94-109.

Akagi T, Fu, F.F, Yabuki S (2002). Absence of Ce anomaly in the REE patterns of peat moss and peat grass in the Ozegahara peatland. *Geochem. J.* 36, 113–119.

Akande S.O. Hoffknecht, A., Erdtman B.D. (1992a). Rank and Petrographic Composition of selected Upper Cretaceous and Tertiary Coals in the Southern Nigeria. *International journal of Coal Geology*, 20 (209-224)

Akande, S.O, Ogunmoyero, I.B. Petersen, H.I. and Nytoft, H.P (2007). Source Rock Evaluation of Coals from the Lower Maastrichtian Mamu Formation, SE Nigeria. *Journal of Petroleum Geology*, Vol. 30(4) pp 303-324

Akande, S.O. Erdtmann, B.D. (1998). Burial metamorphism (thermal maturation) in Cretaceous sediments of the southern Benue Trough and Anambra Basin, Nigeria, *AAPG Bulletin* 82, 1191-1206.

Akande, S.O. Lewan, M.D. Egenhoff, S. Adekeye, O. Ojo, O.J. Peterhansel, A. (2015). Source rock potential of lignite and interbedded coaly shale of the Ogwashi–Asaba Formation, Anambra basin as determined by sequential hydrous pyrolysis. *International Journal of Coal Geology*, 150–151 (2015) 224–237.

Akande. S.O., Egenhoff, S., Obaje, H.G., Ojo, O.J., Adekeye, O., Erdtmann, B.D. (2012). Hydrocarbon Potential of Cretaceous sediments in the Lower and Middle Benue Trough, Nigeria: Insights from a new source rock facies evaluation. *Journal of African Earth Sciences,* 64, 34-47.

American Society for Testing and Materials (1974). Standard specifications for classification of coals by rank, ASTM designation: D388-66, (reapproved 1972), in 1974, Annual book of ASTM standards, pt. 26; Philadelphia, PP., 54-58.

Anthony E.J, Jia L. (2000). Agglomeration and Strength Development of Deposits in CFBC Boilers Firing High-Sulphur Fuels. *Fuel*. 79, 1933-1942.

Arens, N.C., Jahren, A.H. and Amundson, R. (2000). Can C3 plants faithfully record the carbon isotopic composition of atmospheric carbon dioxide? *Paleobiology,* 261:137-164.

Atta-Peters, D. and Salami, M.B. (2004). Late Cretaceous to Early Tertiary pollen grains from offshore Tano basin, Southwestern Ghana. Revista Española de Micropaleontología, 36(3), 451-465.

Ayinla, H.A., Abdullah, W.H., Makeen, Y., Abubakar, M.B., Sarki, Y., Babangida, M., Mustapha, K., Zainal Abidin, S. (2017). Source rock characteristics, depositional setting and hydrocarbon generation potential of Cretaceous coals and organic rich mudstones from Gombe Formation, Gongola Sub-basin, Northern Benue Trough, NE Nigeria. *International Journal of Coal Geology*, 173, 212-216.

Balzerek, H., Fricke, W., Heinrich, J., Moldenhauer, K-M. a. Rosenberger, M. (2003). Man-made flood disaster in the Savanna town of Gombe / NE Nigeria. The natural hazard of gully erosion caused by urbanization dynamics and their peri-urban footprints. In: Erdkunde 57, 94-109.

Barker, C. (1974): Pyrolysis techniques for source-rock evaluation. *The American Association of Petroleum Geologists Bulletin*, 58 (11): 2349-2361.

Barker, C. (1979): Organic geochemistry in petroleum exploration. The American Association of Petroleum Geologists, Education Course Note Series No. 10, 159 pp.

Benkhelil, J. (1989). The Origin and Evolution of the Cretaceous Benue Trough (Nigeria). *J. Afr. Earth Sci.*, 8, 251-282. http://dx.doi.org/10.1016/S0899-5362(89)80028-4

Bertrand, P., (1984). Geochemical and petrographic characterization of humic coals considered as possible oil source rocks. *Organic Geochemistry,* 6, 481–488.

Boreham, C.J, Blevin, J.E, Radlinski, A.P. and Trigg, K.R. (2003). Coal as source of oil and gas, a case study from the Bass basin, Australia. *APPEA Journal*, 43.1:117-148.

Boreham, C.J, Horsfield, B., Schenk, H.J, (1999). Predicting the quantities of oil and gas generated from Australian Permian coals, Bowen Basin using pyrolytic methods. *Marine and Petroleum Geology,* 16, 165–188.

Boreham, C.J, Powell, T.G. (1993). Petroleum source rock potential of coal and associated sediments: qualitative and quantitative aspects. In: Law, B.E., Rice, D.D. (Eds.), Hydrocarbons in Coal. American Association of Petroleum Geologists Studies in Geol- ogy, vol. 38, pp. 133–157.

Bouska V, Pesek J. (1999). Quality Parameters of Lignite of the North Bohemian Basin in the Czech Republic in Comparison with the World Average Lignite. *International Journal of Coal Geology*, 40, 211-235

Boynton, W.V. (1984). Cosmochemistry of the rare earth elements: meteorite studies. In: Henderson P, editor. Rare earth element geochemistry. Amsterdam: Elsevier; p. 63–114.

Bustin, R.M., Cameron, A.R., Grive, A.D., and Kalkreuth, W.D., (1983). Coal Petrology-its principles, methods, and applications. Geological Association of Canada, 230p.

Campbell RN, Linndsay P, Clemens AH (2001). Acid Generating Potential of Waste Rock and Coal Ash in New Zealand Coal Mines. *Inter. Jour. of Coal Geol.*, 45, 163-179.

Carter, J. D., Barbar, W., Tait, E. A. and Jones, G. P. (1963). The geology of parts of Adamawa, Bauchi and Borno Provinces in northeastern Nigeria. Geological Survey of Nigeria Bulletin 30, 1–108.

Carvalho, M.A., Mendonça Filho, J.G., Menezes, T.R., (2006a). Palynofacies and sequence stratigraphy of the Aptian–Albian of the Sergipe Basin, Brazil. *Sedimentary Geology,* 192, 57–74.

Chabbi, A., Rumpel, C. and Kögel-Knabner, I. (2007). Stable carbon isotope signature and chemical composition of organic matter in lignite-containing mine soils and sediments are closely linked. *Organic Geochemistry*, 38.6:835-844.

Chelgani, S.C, Hower, J.C, Hart, B. (2011). Estimation of free-swelling index based on coal analysis using multivariable regression and artificial neural network. Fuel Process Technol; 92(3):349–55.

Chen, S., Wu, D., Liu, G., Sun, R., Fan, X., (2016). Geochemistry of major and trace elements in Permian coal: with an emphasis on no. 8 coal seam of Zhuji coal mine, Huainan Coalfield, China. Environmental Earth Sciences 75.

Clayton, J, King, J. (1987). Effects of weathering on biological marker and aromatic hydrocarbon composition of organic matter in phosphoria shale outcrop. geochim. cosmochim. acta, 51, 2153–2157.

Clayton, J.L, Law, E.B. (1993). Composition of crude oils generated from coals and coaly organic matter in shales. In: Rice, D.D. (Ed.), Hydrocarbons from Coal. American Association of Petroleum Geologist Studies in Geology 38. pp. 185–201.

Collister, J.W., Lichtfouse, E., Hiesshima, G. and Hayes, J.M. (1994). Partial resolution of sources of n-alkanes in the saline portion of the Parachute Creek Member, Green River Formation (Piceance Creek Basin, Colorado). *Organic Geochemistry,* 21:645-659.

Cook, A.C. and Kantsler, A.J., (1982). The origin and petrology of organic matter in coals, oil shales and petroleum source-rocks. The University of Wollongong, Wollongong, New South Wales, 35pp.

Coulon, C., P. Vida, C. Dupuy, P. Baudin, M. Popoff, H. Maluski and D. Hermite, (1996). The Mesozoic to early Cenozoic magmatism of the Benue trough (Nigeria); geochemical evidence for the involvement of the St Helena plume. *J. Petrol*., 37, 1341-1358.

Cross AT, Phillips TL (1990). Coal-forming plants through time in North America. *Int. J. of Coal Geology*, 16, 1–46.

Demaison, G. J., and G. T. Moore, (1980). Anoxic environments and oil source bed genesis: *AAPG Bulletin*, v. 64, p. 1179-1209

Dieckmann, V., (2005). Modelling petroleum formation from heterogeneous source rocks: the influence of frequency factors on activation energy distribution and geological prediction. Mar. *Petroleum Geol*. 22 (3), 375-390.

Diessel, C.F.K., (1986). On the correlation between coal facies and depositional environments. Proc., 8th Common. Min. Metall. Congr., 6, pp. 669–677.

Diessel, C.F.K., (1992). Coal-Bearing Depositional Systems. Springer-Verlag, Berlin, 721 p..

Dike, E.F.C. (1993). The Statigraphy and structure of the Kerri-Kerri Basin Northeastern Nigeria. *Journal Mining and Geology*, 29, 2, 77-93.

Durand, B., (1980). Kerogen, Insoluble Organic Matter from Sedimentary Rocks: Paris, Editions Technip, 519 p.

Edet, J.J, Nyong, E. E, (1994). Palynostratigraphy of Nkporo Shale exposures (Late Campanian-Maastrichtian) on the Calabar Flank, SE. Nigeria. Review of Paleobotany and Palynology, 80, 131-147.

EIA, International Energy Annual (2001). U.S. Department of Energy, Energy Information Administration, Washington, D.C., 2003, pp. 114–115.

Elizabeth, O.W. and Obaje, N.G. (2012). Petrographic Evaluation of the Ranks and Technological Applications of Some Coal Deposits in the Anambra Basin and Middle Benue Trough of Nigeria. *Journal of Earth Science and Engineering*, 2 (2012) 220-234

Englund JO, Jorgensen P (1973). A chemical classification system for argillaceous sediments and factors affecting their composition. *Geol. Stockholm Forh*. 95, 87-97.

Fatoye F.B, Gideon Y.B (2013). Appraisal of the Economic Geology of Nigerian Coal Resources. *Journal of Environment and Earth Sciences*. 3, 11, 25-31.

Ficken, K.J., Li, B., Swain, D.L. and Eglinton, G. (2000). An n-alkane proxy for the sedimentary input of submerged/floating fresh water aquatic macrophytes. *Organic Geochemistry*, 31.7-8:745-749.

Fu FF, Akagi T, Yabuki S, Iwaki M (2001). The variation of REE (rare earth elements) patterns in soil-grown plants: A new proxy for the source of rare earth elements and silicon in plants. *Plant and Soil* 235, 53–64.

Fu FF, Akagi T, Yabuki S, Iwaki M, Ogura N (2000). Distribution of rare earth elements in seaweed: Implication of two different sources of rare earth elements and silicon in seaweed. *J. Phycol*. 36, 62–70.

Genik, G.J., (1993). Petroleum geology of Cretaceous-tertiary rift basins in Niger, Chad, and Central African Republic. *Am. Assoc. Pet. Geol. Bull*. 77, 1405–1434.

Guiraud, M. (1990). Tectono-sedimentary framework of the Early Cretaceous continental Bima Formation (Upper Benue Trough, NE Nigeria). *Journal of African Earth Sciences*, 10, 341 353.

Hayes, J.M. (1993). Factors controlling 13C contents of sedimentary organic compounds: Principles and evidence. *Marine Geology*, 113:111-125.

Hergreen, G.F.W., Chlonova, A.F., (1981). Cretaceous Microfloral Provinces; *Pollen et Spores*, *23*, pp 441 – 556.

Hergreen G. F. W. (1981). *Microfloral relationships between Africa and South America in Middle and Upper Cretaceous time.* Proc. 4th Int. Palynol. Conf., Lucknow, (1976-77).

Hergreen G. F. W., Kedves M., Rovnina L. V., Smirnova S. B. (1996). *Cretaceous palynofloral provinces: a review*. In Jansonius, J. & McGregor, D.C. (Ed.), Palynology: Principles and applications; American Association of Stratigraphic Palynologists Foundation., 3: 1157-1188.

Holba, A.G., Dzoub, L.I., Wood, G.D., Ellisd, L., Adame, P., Schaeffere, P., Albrecht, P., Greenef, T., Hughes, W.B., (2003). Application of tetracyclic polyprenoids as indicators of input from fresh-brackish water environments. *Org. Geochem*. 34, 441–469.

Hood, A., Gutjahr, C.C.M., and Heacock, R. L. (1975). Organic metamorphism and the generation of petroleum. *The American Association of Petroleum Geologists Bulletin*, 59 (6): 986-996.

Hu, J., Peng, P., Jia, G., Fang, D., Zhang, G., Fu, J. and Wang, P. (2002). Biological markers and their carbon isotopes as an approach to the paleoenvironmental reconstruction of

Nansha area, South China Sea, during the last 30 ka. *Organic Geochemistry*, 33: 1197–1204.

Huggins, F.E. Kosmack and D.A. Huffman, G.P. (1981). Correlation between Ash Fusion Temperature and Ternary Equilibrium Phase Diagrams. Fuel, 60, 577-584.

Hughes, W.B. Holba, A.G. and Dzhou, L.I.P. (1995). The ratios of dibenzothiophene to phenanthrene and pristane to phytane as indicators of depositional environment and lithology of petroleum source rocks. Geochimica et Cosmochimica Acta 59:3581-3598.

Hunt J.H., (1991). Generation of gas and oil from coal and other terrestrial organic matter. *Organic Geochemistry*, 17(6): 673-680.

Hunt, J.H. (1996). Petroleum Geochemistry and Geology. Second Edition. Freeman, New York, 743 pp.

Hunt, J.M., (1995). Petroleum Geochemistry and Geology. W.H. Freeman and Company, New York, pp. 743.

Inaba, T. Suzuki, N. Hirai, A., Sekiguchi, K. and Watanabe, T. (2001). Source rock lithology prediction based on oil diacholestane abundance in the siliceousclastic Akita sedimentary basin, Japan. *Organic Geochemistry*. 32.7: 877-890.

Isaksen, G.H., Curry, D.J., Yeakel, J.D. and Jensen, A.I. (1998). Controls on the oil and gas potential of humic coals. *Organic geochemistry*, 29:23-44.

Ketris MP, Yudovich YE (2009). Estimations of Clarkes for carbonaceous biolithes: world average for trace element contents in black shales and coals. *International Journal of Coal Geology*. 78, 135–148.

Killops, S.D. and Killops, V.J. (1993). An introduction to organic geochemistry. UK: Longman Group Ltd.

Killops, S.D. and Killops, V.J. (2005). Introduction to organic geochemistry. Second edition.U.K: Blackwell Publishing Limited.

Killops, S.D., Funnell, R.H., Suggate, R.P., Sykes, R., Peters, K.E., Walters, C., Woolhouse, A.D., Weston, R.J., Boudou, J.-P., (1998). Predicting generation and expulsion of paraffinic oil from vitrinite-rich coals. *Organic Geochemistry*, 29, 1–21.

Killops, S.D., Woolhouse, A.D., Weston, R.J., Cook, R.A., (1994). A geochemical appraisal of oil generation in the Taranaki Basin, New Zealand. *American Association of Petroleum Geologists Bulletin*, 78, 1560–1585.

Kotarba, M.J., Clayton, J.L., Rice, D.D. and Wagner, M. (2002). Assesment of hydrocarbon source rock potential of Polish bituminous coals and carbonaceous shales. *Chemical Geology*, 184.1-2:11-35.

Langford, F.F, Blanc-Valleron, M.M (1990). Interpreting Rock Eval pyrolysis data using graphs of pyrolyzable hydrocarbons versus total organic carbon. *American Association of Petroleum Geologist Bulletin*, 74:799–804.

Lawal, O. and Moullade, M., (1986). Palynological biostratigraphy of Cretaceous sediments in the Upper Benue Basin N.E. Nigeria. *Revenue Micropaleotologie*, 29, 61-83

Levine, J.R., (1993). Coalification: the evolution of coal as source rock and reservoir rock for oil and gas. In: Law, B.E., Rice, D.D. (Eds.), Studies in Geology Series 39–77 Tulsa.

Liu, D.N, Zhou, A.C, Liu, J.Q. (2007). Geochemical characteristics of rare earth elements in Yan'an formation, Jurassic system, Dongsheng coalfield. Coal Geol China;19:20–2 (in Chinese with English abstract).

Lo, H, Cardott, B. (1995). Detection of natural weathering of upper mcalester coal and woodford shale, oklahoma, usa. org. geochem., 22, 73–83.

Mackenzie, A.S., Patience, R.L., Maxwell, J.R., Vandenbroucke, M., Durand, B., (1980). Molecular parameters of maturation in the Toarcian shales, Paris Basin, France. Changes in the configuration of acyclic isoprenoid alkanes, steranes and triterpanes. Geochimica et Cosmochimica Acta 44, 1709–1721.

Mackowsky, M.Th. (1982). The Application of Coal Petrography in Technical Processes. In: Stach's Textbook of Coal Petrology (Edited by Stach, E., Mackowsky, M.Th.,

Teichmuller, M., Taylir, G.H., Chandra, D., Teichmuller, R.), 413 – 483. Gebruder Borntraeger, Berlin.

Mahlstedt, N., Horsfield, B., (2012). Metagenetic methane generation in gas shales I. Screening protocols using immature samples. *Marine and Petroleum Geology*, 31, 1, p. 27-42.

Makeen, Y.M., Abdullah, W.H., Hakimi, M.H., Elhassana, O.M.A., (2015). Organic geochemical characteristics of the Lower Cretaceous Abu Gabra Formation in the great Moga oilfield, Muglad Basin Sudan: Implications for depositional environment and oil-generation potential. *J. African Earth Sci*. 103, 102–112.

Mccartney, J. T. and Teichmüller, M. (1972). Classification of coals according to the degree of coalification by reflectance of the vitrinite component. *Fuel*, 51: 64- 68.

McDaniel D.K, Hemming S.R, Mclennan S.M, Hanson G.N (1994). Resetting of neodymium isotopes and redistribution of REE'S during sedimentary processes: The early Proterozoic Chelmsford formation, Sudbury Basin, Ontario, Canada. *Geochima Cosmochimica Acta*. 58, 931 – 941.

Milodowski, A.E, Zalasiewkz, J.A (1991). Redistribution of rare earth elements during diagenesis of eurbidice /hemipelagic mudrock sequences and age from central wales. In: AC. Mortan, S.P., Todd and P.D.W. Houghton (Editors), Geological Society London Special Publications, 57, 101-124.

Miranda, A.C.M.L, Loureiro, M.R.B. and Cardoso, J.N. (1999). Aliphatic and Aromatic hydrocarbons in Candiota col samples: novel series of bicyclic compounds. *Organic Geochemistry*, 30:1027-1028.

Moldowan, J.M., Fago, F.J., Carlson, R.M.K., Young, D.C., Duvne, G.A., Clardy, J., Schoell, M., Pillinger, C.T., Watt, D.S., (1991). Rearranged hopanes in sediments and petroleum. Geochimica et Cosmochimica Acta 55, 3333–3353.

Moldowan, J.M., Seifert, W.K., Gallegos, E.J., (1985). Relationship between petroleum composition and depositional environment of petroleum source rocks. Am. Assoc. Pet. Geol. Bull. 69, 1255-1268.

Mukhopadhyay, P.K, Goodarzi, F, Crandlemire, A.L, Gillis, K.S, MacNeil, D.J, Smith, W.D (1998). Comparison of coal composition and elemental distribution in selected seams of the Sydney and Stellarton Basins, Nova Scotia, Eastern Canada. *Int. J. of Coal Geology*, 37, 113 141.

Mukhopadhyay, P.K., Hatcher, P.G., (1993). Composition of coal. In: Law, B.E., Rice, D.D. (Eds.), Hydrocarbons in Coal. American Association of Petroleum Geologists Studies in Geology, vol. 38, pp. 79–118.

Mukhopadhyay, P.K., Hatcher, P.G., Calder, J.H., (1991). Hydrocarbon generation from deltaic and intermontane fluviodeltaic coal and coaly shale from the Tertiary of Texas and Carboniferous of Nova Scotia. *Organic Geochemistry*, 17, 765–783.

Muktar, H. and Congjiao, X. (2012). Nigeria's inland basins: Investment opportunities and environment. *Journal of Petroleum and Gas Exploration Research* (ISSN 2276-6510) Vol. 2(11) pp. 202-211

Murray, A.P., Summons, R.E., Boreham, C.J., Dowling, L.M., (1994). Biomarker and normal alkane isotope profiles of Tertiary oils: relationship to source rock depositional setting. *Organic Geochemistry*, 22, 521–542.

Nesbitt, H.W, Young, G.M (1982). Early Proterozoic Climate and Plate motion inferred from major element chemistry of lutites, Nature 299, 715 – 717.

Nesbitt, H.W., Young, G.M., McLannan, S.M., Keays, R.R. (1996). Effects of Chemical Weathering and Sorting on the Petrogenesis of Siliclastic Sediments, with Implication for Provenance Studies. J. Geol., 104, 525-542.

Norgate, C.M., Boreham, C.J. and Wilkens, A.J. (1999). Changes in hydrocarbonmaturity indices with coal rank and type, Buller Coalfield, New Zealand. *Organic Geochemistry*, 30:985 1010.

Obaje, N.G, Hamza, H. (2000). Liquid Hydrocarbon Source-rock Potential of Mid-Cretaceous Coals and Coal Measures in the Middle Benue Trough of Nigeria. *International Journal Earth Science*s, 89:130–139.

Obaje, N.G. Wehner, H. Scheeder, O. Abubakar, M.B. and Jauro, H. (2004). Hydrocarbon prospectivity of Nigeria's inland basins: from the view point of organic geochemistry

and organic petrology. *American Association of Petroleum Geologists Bulletin*, 87:325-353.

Obaje, N.G., Ligouis, B. and Abaa, S.I. (1994). Petrographic Composition of Depositional Environment of Cretaceous Coals and Coal Measures in the Middle Benue Trough of Nigeria. *Int. J. of Coal Geology*, 26, 233-260

Oboh, F.E., Salami, M.B., Chapman, J.L., (1992). Palynological interpretation of the palaeoenvironments of miocene strata of the well igbomotoru-I, Niger Delta. *J. Micropalaeontol*., 2: 1-6.

Odebode, M. O. (2010). A Handout on the Geology of the Benue and Anambra Basins, Nigeria. Unpublished.

Offodile, M. E. (1976). The geology of the Middle Benue, Nigeria, Special Vol. 4. Palaeontological Institution of the University of Uppsala, Sweden

Ojo, O.J., Akande, S.O. (2009). Sedimentology and depositional environments of the Maastrichtian Patti Formation, southeastern Bida Basin, Nigeria. *Cretaceous Research*, 30(6), 1415-1425.

Ojo, O.J., Akande, S.O., (2004). Palynology and Paleoenvironmental studies of the Gombe Formation, Gongola Basin, Nigeria. *J. Min. Geol*. 40, 143–149.

Olade, M.A. (1975). Evolution of Nigerian Benue Trough (Aulacogen): A Tectonic Model. *Geol. Mag*. Vol. 112, pp. 575 – 583.

Onoduku, U.S. Okosun E.A. (2014). Palynology, Palynostratigraphy and Paleoenvironmental Analysis of Maiganga Coal Mine, Gombe Formation, Nigeria. *Universal Journal of Geoscience* 2(3): 93-103, 2014 DOI: 10.13189/ujg.2014.020302

Onoduku, U.S. Okosun, E.A and. Akande, W.G. (2013). An Assessment of the Hydrocarbon Potential of the Gombe Formation, Upper Benue Trough, Northeastern Nigeria: Organic Geochemical Point of View. *Earth Science Research*, Vol. 2, No. 2.

Panov, B.S, Dudik, A.M, Shevchenko, O.A, Matlak, E.S (1999). On Pollution of the Biosphere in Industrial Areas: the Example of the Donets Coal Basin. *International Journal of Coal Geology*. 40, 199-210.

Peters, K.E. and Moldowan, J.M. (1993). The Biomarker Guide.Interpreting Molecular Fossils in Petroleum and Ancient Sediments.New Jersey: Prentice-Hall, Englewood Cliffs.

Peters, K.E., (1986). Guidelines for evaluating petroleum source rock using programmed pyrolysis. *Am. Assoc. Petroleum Geol. Bull*. 70, 318-329.

Peters, K.E., Walters, C.C., Moldowan, J.M., (2005). The Biomarker Guide, second ed. Cambridge University Press.

Petersen, H., Rosenberg, P., (2000). The relationship between the composition and rank of humic coals and their activation energy distributions for the generation of bulk petroleum. Petroleum Geoscience 6, 137–149.

Petersen, H.I., Nytoft, H.P. (2006): Oil generation capacity of coals as a function of coal age and aliphatic structure. *Organic Geochemistry* 37:558-583.

Petters, S. W. (1982): Central West African Cretaceous – Tertiary Benthic Foraminifera and Stratigraphy, Palaeontographica Abteilung A 179, 1 – 104.

Petters, S.W and C.M. Ekweozor, (1982). Petroleum Geology of Benue Trough and South Eastern Chad Basin, Nigeria. *Am. Assoc. Petrol. Geol. Bull*., 66, 1141-1149.

Philip, R.P. and Gilbert, T.D. (1986). Biomarker distributions in Australian oils predominantly derived from terrigenous source material. *Organic Geochemistry* 10: 73-84.

Pusey, W. C. (1973a). The ESR method: A new technique of estimating the organic maturity of sedimentary rocks. Petroleum Times, January 12: 21-24, 32.

Pusey, W. C. (1973b). How to evaluate potential gas and oil source rocks. World Oil, 176 (5): 71-75

Raask, E. (1995). Mineral impurities in coal combustion behavior, problems and remedial measures, hemisphere publishing New York, 484 p

Requejo, A.G. (1994). Maturation of petroleum source rocks-II. Quantitative changes in extractable hydrocarbon content and composition associated with hydrocarbon generation. *Organic Geochemistry*, 21:91–105.

Rimmer, S. and Davis, A., (1988). The influence of depositional environments on coal petrographic composition of the Lower Kittanning Seam, western Pennsylvania. *Organic Geochemistry*, 12, p.375–387.

Rippen, D., Ralf, L., Bruns, B., Mahlstedt, N., (2013). Organic geochemistry and petrography of Lower Cretaceous Wealden black shales of the Lower Saxony Basin: the transition from lacustrine oil shales to gas shales. *Org. Geochem*. 63, 18-36.

Rohmer, M. (1987). The hopanoids, prokaryotic triterpenoids and sterol surrogates. In: Surface Structures of Microorganisms and their interactions with the Mammalian Host (Edited by E. Schriner et.al.). Proceeding of Eighteen Workshop Conference. Hocchst, Schloss Ringberg: 227 242.

Ryan, B, Leeder, R, Price, J.T, (1998). The effect of coal preparation on the quality of clean coal and coke. British Columbia Geological Survey Branch: Geological Fieldwork; 1998. p. 247–75.

Sabel, M., Bechtel, A., Püttmann, W. and Hoernes, S. (2005). Palaeoenvironment of the Eocene Eckfeld Maar lake (Germany): implications from geochemical analysis of the oil shale sequence. *Organic Geochemistry*, 36:873-891.

Sakurovs, R., He, L., Melnichenko, Y.B., Radlinski, A.P., Blach, T., Lemmel, H., Mildner, D.F., (2012). Pore size distribution and accessible pore size distribution in bituminous coals. *International Journal of Coal Geology*, 100, 51–64.

Sappal, K.K., (1986). Petrography of Collie Coal, Collie Basin, Western Australia. WAMPRI, 26, 202p.

Sari, A. and Bahtiyar, I. (1999). Geochemical evaluation of the Besikli oil field, Kahta, Adiyaman, Turkey. *Marine and Petroleum Geology*, 16:51-164.

Schatzel, S.J, Stewart, B.W. (2003). Rare earth element sources and modification in the Lower Kittanning coal bed, Pennsylvania: implications for the origin of coal mineral

matter and rare earth element exposure in underground mines. Int J Coal Geol; 54:223–51.

Schenk, H.J., Horsfield, B., (1997). Kinetics of petroleum generation. Applications and limitations. Zentralblatt fur Geologie und Pal- aontologie, Teil I, 1995 H. 11/12, 1113–1117.

Schenk, H.J., Horsfield, B., Krooss, B., Schaefer, R.G., Schwochau, K., (1997). Kinetics of petroleum formation and cracking. In: Welte, D.H., Horsfield, B., Backer, D.R. (Eds.), Petroleum and Basin Evolution; Insights from Petroleum Geochemistry, Geology and Basin Modeling. Springer, Berlin.

Schopf, J.M., (1956): Definitions of peat and coal and of graphite that terminates the coal series (graphocite). *Journal of Geology,* 74, 584–592.

Schouten, S., Hoefs, M.J.L. Sinninghe Damste, J.S. (2000). A molecular and stable carbon isotopic study of lipids in late Quartenary sediments from the Arabian Sea. Organic Geochemistry 31:509-521.

Schouten, S., Rijpstra, W.I.C., Kok, M., Hopmans, E.C., Summons, R.E., Volkman, J.K. and Sinninghe Damste, J.S. (2001). Molecular Organc tracers of biogeochemical processes in a saline meromictic lake (Ace Lake). Geochimica et Cosmochimica Acta 65,p.1629-1640.

Schrank, E. (1987). Palæozoic and Mesozoic palynomorphs from northeast Africa (Egypt and Sudan) with special reference to Late Cretaceous pollen and dinoflagellates. Berliner Geowissenschaftliche Abhandlungen, Reihe. 75 (1), 249–310.

Seifert, W.K. and Moldowan, J.M. (1986). Use of biological markers in petroleum exploration. In: Methods in Geochemistry and Geophysics vol.24 (R.B. Johns, ed.). Amsterdam: *Elsevier*. 261-290.

Shemang, E.M., C.O. Ajayi and W.R. Jacoby, (2001). A magmatic failed rift beneath the Gongola arm of the Upper Benue Trough, Nigeria?. *J. Geodyn.,* 32, 355-371.

Shibaoka, M., Bennett, A. J. R., and Gould, K. W. (1973). Diagenesis of organic matter and occurrence of hydrocarbons in some Australian sedimentary basins. *Australian Petroleum Exploration Association Journal*, 1973: 73-80.

Simoneit, B.R.T., Grimalt, J.O., Wang, T.G., Cox, R.E., Hatcher, P.G. and Nissenbaum, A. (1986). Cyclic terpenoids of contemporary resinous plant detritus and of fossil woods, amber and coal. *Organic Geochemistry*, 10:877- 889.

Sinninghe Damsté, J.S., Kenig, F., Koopmans, M.P., Koster, I., Schouten, S., Hayes, J.M. and De Leeum, J.W. (1995). Evidence for gammacerane as an indicator of water coloumn stratification. Geochim et Cosmochim Acta 59:1895-1900.

Skodras G, Orfanoudaki Th, Kakaras E, Sakellaropoulous GP (2002). Production of special activated carbon from lignite for environmental purposes. Elsevier journal: *Fuel Processing Technology*, 77-78, 75-87

Snowdon, L.R., (1991). Oil from Type III organic matter: resinite revisited. *Organic Geochemistry*, 17, 743–747.

Sofer, Z., (1984). Stable carbon isotope compositions of crude oils: application to source depositional environments and petroleum alteration. *AAPG Bull*. 68, 31-49.

Sonibare, O., Adedosu, T., Ekundayo, A.O., Jarvie, D. (2008). Hydrocarbon potential and Organic Geochemistry of Coals from Benue Trough, Nigeria. *Journal of Applied Sciences*, 4(11), 1511-1520.

Spears D.A, Zheng Y. (1999). Geochemistry and Origin of Elements in some UK Coals. *International Journal of Coal Geology*, 38, 161-179.

Stach, E.; Mackowski, M T.; Teichmuller, M.; Taylor, G.; Chandra, D.& Teichmuller, R. (1882). Stach's TextbookofCoal Petrology. 3ª ed., Berlin, Gebrüder Borntraeger, 535 p.

Standard Association of Australia (AS), (1977). Code of practice for preparation of hard coal samples for microscopical examination by reflected lights. AS 2061.

Staplin, F. L. (1969). Sedimentary organic matter, organic metamorphism, and oil and gas occurrence. *Canadian Petroleum Geology Bulletin*, 17: 47-66.

Stefanova, M., Markova, K., Marinov, S. and Simoneit, B.R.T. (2005). Molecular indicators for coal-forming vegetation of the Miocene Chukurovo lignite, Bulgaria. *Fuel* 84:1830–1838.

Struckmeyer, H.I.M. and Felton, E.A., (1990). The use of organic facies for refining palaeoenvironmental interpretations. A case study from the Otway Basin, Australia. *Australian Journal of Earth Sciences*, 37, p.351-364.

Suggate, R. P. (1959). New Zealand coals, their geological setting and its influence on their properties. New Zealand Department of Sciences, industry research bulletin, 134, 113 pp.

Sun, Y., Sheng, G., Peng, P., Fu, J., (2000). Compound-specific stable carbon isotope analysis as a tool for correlating coal-sourced oils and interbedded shale-sourced oils in coal measures: an example from Turpan basin, northwestern China. *Org. Geochem*. 31, 1349–1362

Sykes, R and L.R. Snowdon, (2002). Guidelines for assessing the petroleum potential of coaly source rocks using Rock Eval. Pyrolysis. *Organic Geochemistry*, 33: 1441-1455.

Sykes, R., (2001). Depositional and rank controls on the petroleum potential of coaly source rocks. Eastern Australasian Basins Symposium. Melbourne, 25–28 November, 2001. Australian Institute of Mining and Metallurgy, Carlton, Victoria, pp. 591– 601, for the Petroleum Exploration Society of Australia.

Sykes, R., Volk, H., George, S.C., Ahmed, M., Higgs, K.E., Johansen, P.E., Snowdon, L.R., (2014). Marine influence helps preserve the oil potential of coaly source rocks: Eocene Mangahewa Formation, Taranaki Basin, New Zealand. *Organic Geochemistry*, 66, 140–163

Taylor, G.H., Teichmuller, M., Davis, A., Diessel, C.F.K., Littke, R., Robert, P., (1998). Organic Petrology. Gebru der Borntraeger, Berlin (704 pp).

Teichmüller, M. and Teichmüller, R., (1982). Fundamental of coal petrology. In: Stach, E., Mackowsky, M-Th., Teichmüller, M., Taylor, G.H., Chandra, D., and Teichmüller, R. (eds.) Stach's Textbook of Coal Petrology. Gebrüder Borntraeger, Berlin, 3rd ed., 535p.

Tissot, B. P., Durand, B., Espitalié, J. and Combaz, A. (1974). Influence of nature and diagenesis of organic matter in formation of petroleum. *The American Association of Petroleum Geologists Bulletin,* 58: 499-506.

Tissot, B.P and D.H. Welte, (1984). Petroleum Formation and Occurrence. Belin Heidelberg, New York, Tokyo: Springer-Verlag.

Tissot, B.P., Espitalié, J., (1975). L'évolution thermique de la matière organique des sédiments: application d'une simulation mathématique. Revue de l'Institut Francais du Petrole 30, 743–777.

Tissot, B.P., Pelet, R., Ungerer, P.H., (1987). Thermal history of sedimentary basins, maturation indices, and kinetics of oil and gas generation. *American Association of Petroleum Geologists Bulletin* 71, 1445–1466.

Tissot, B.P., Welte, D.H., (1978). Petroleum Formation and Occurrence: a New Approach to Oil and Gas Exploration. Springer-Verlag, New York.

Tyson, R.V., (1989). Late Jurassic Palynofacies Trends, Piper and Kimmeridge Clay Formations, UK onshore and offshore: Northwest European Micropalaeontology and Palynology. British Micropalaeontological Society Series, Chichester, pp. 135–172.

Tyson, R.V., (1995). Sedimentary OrganicMatter–Organic Facies and Palynofacies. Chapman & Hall, London.

Van Krevelen, D.W. (1961). Coal: Typology-chemistry-physics-constitiution. Amsterdam: Elsevier Science.

Varma, A.K., Hazra, B., Mendhe, V.A., Chinara, I., Dayal, A.M., (2015). Assessment of organic richness and hydrocarbon generation potential of Raniganj basin shales, West Bengal, India. *Mar. Pet. Geol*. 59, 480- 490.

Vincent, R.G. (1987). Prediction of Ash Fusion Temperature from Ash Composition for some New Zealand coals, Fuel, 66, 1230-1239.

Volkman, J.K., Barrett, S.M., Blackburn, S.I., Mansour, M.P., Sikes, E.L. and Gelin, F. (1998). Microalgal biomarkers: a review of recent research developments. *Organic Geochemistry* 29:1163-1179.

Wakita H, Ray P, Schmitt RA (1971). Abundances of the 14 rare earth elements and 12 other trace elements in Apollo 12 samples: five igneous and one breccia rocks and four soils. Prov. 2nd Limar Sci. Cont. Perganon Press, Oxford, 1319 – 1329.

Wang, P., Li, M. and Larter, S.R. (1996). Extended hopanes beyond C40 in crude oils and source rocks extracts from Liaohe Basin, N.E. China. *Organic Geochemistry* 24.5:547-551.

Waples, D. W. (1979). Simple method for oil source bed evaluation. *The American Association of Petroleum Geologists Bulletin*, 63(2): 239-248.

Waples, D.W., Ramly, M., (2001). A statistical method for correcting log-derived temperatures: *Petroleum Geoscience*, volume. 7, no. 3, p. 231–240.

Whiteman, A. (1982). Nigeria: Its petroleum geology, resources and potential: London, Graham and Trotman, 381 p.

Wright, J.B. (1968). South Atlantic Continental Drift and the Benue Trough". Tectono – Physics. 6, 301 – 310.

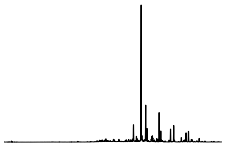
Yahaya, I., Adamu, S.J., (2016). Statistical Study of Rainfall Pattern in Gombe Metropolis, and its Implication on the Attainment of Sustainable Development Goals (SDGs). International Journal of Scientific and Research Publications, Volume 6, Issue 6, ISSN 2250-3153.

Yangming, Z., Huanxin, W., Aiguo, S., Digang, L. and Dehua, P. (2005). Geochemical characteristics of Tertiary saline lacustrine oils in the Western Qaidam Basin, northwest China. *Applied Geochemistry*, 33:1225-1240.

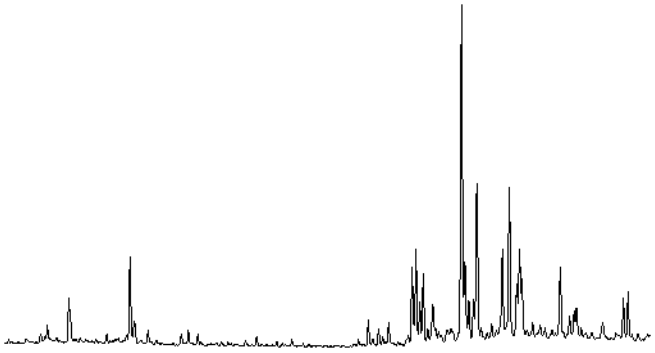
Zarboski, P., Ugodunlunwa, F. Idornigie, A., Nnabo, P and Ibe, K. (1997). Stratigraphy and structure of the Cretaceous Gongola basin, Northeastern Nigeria. Bulletin des Centres de Recherches Exploration-Production. ElF-Aquitaine 21, 153-185.

Zheng B, Ding Z, Huang R, Zhu J, Yu X, Wang A, Zhou D, Mao D, Su H (1999). Issues of Health and Disease Relating to Coal Use in Southwestern China. *International Journal of Coal Geology*. 40, 119-132.

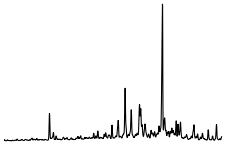
APPENDIX I



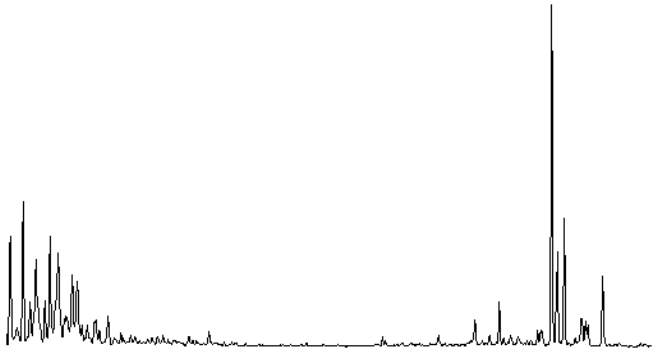
m/z 191: Tri- and Pentacyclics Terpanes for sample MG1G



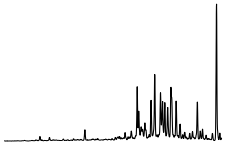
m/z 253: Monoaromatic steroid for sample MG1G



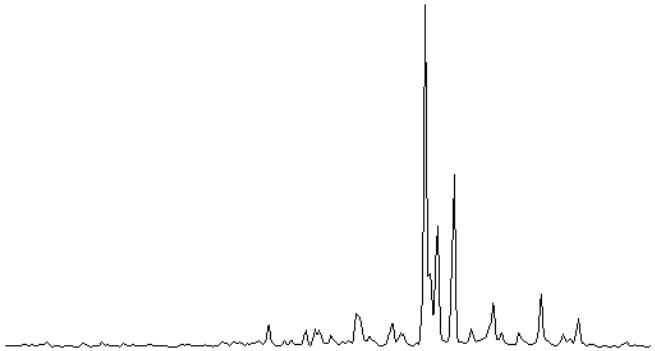
m/z 217: Sterane for sample MG1G



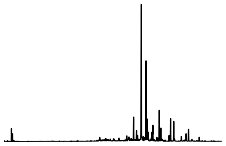
m/z 231: Triaromatic steroid for sample MG1G



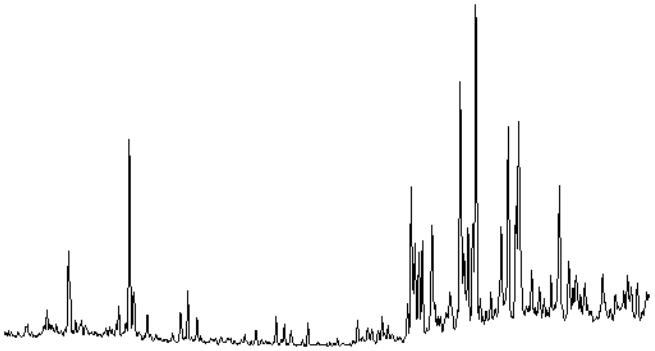
m/z 218: ββ Sterane for sample MG1G



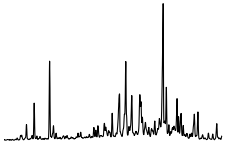
m/z 245: Triaromatic methylsteroid for sample MG1G



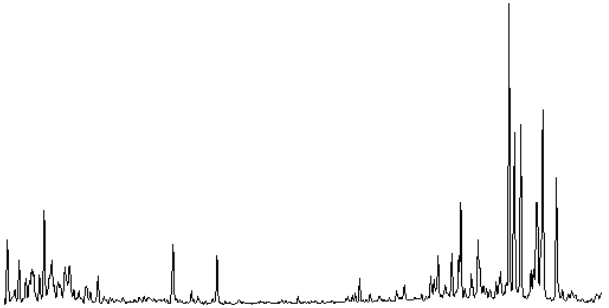
m/z 191: Tri- and Pentacyclics Terpanes for sample MG2H



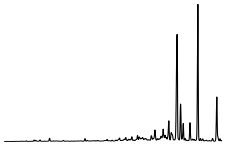
m/z 253: Monoaromatic steroid for sample MG2H



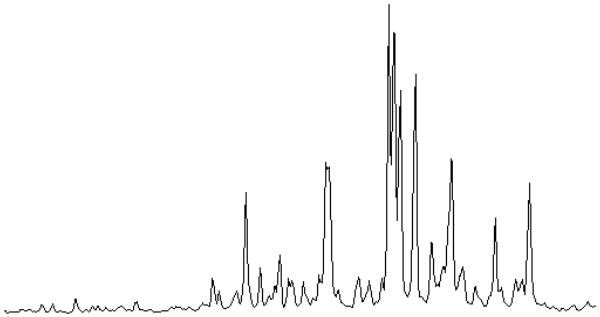
m/z 217: Sterane for sample MG2H



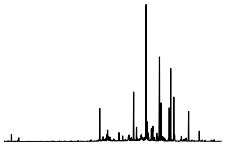
m/z 231: Triaromatic steroid for sample MG2H



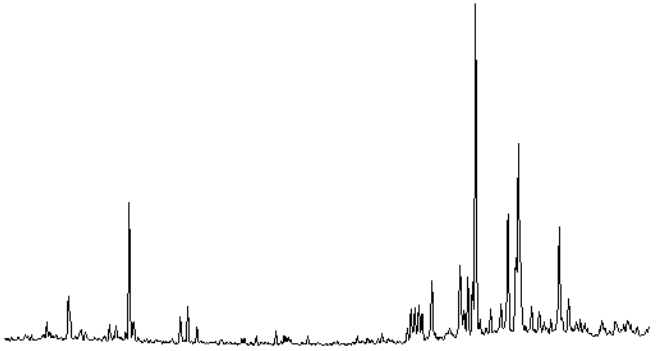
m/z 218: ββ Sterane for sample MG2H



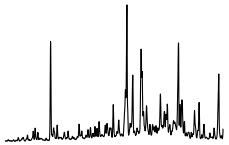
m/z 245: Triaromatic methylsteroid for sample MG2H



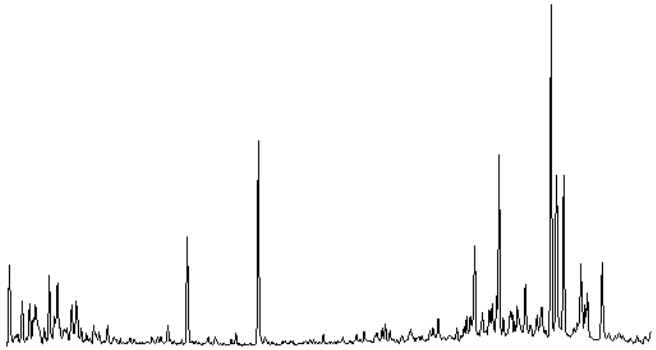
m/z 191: Tri- and Pentacyclics Terpanes for sample MG2O



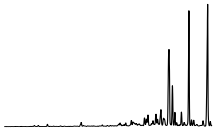
m/z 253: Monoaromatic steroid for sample MG2O



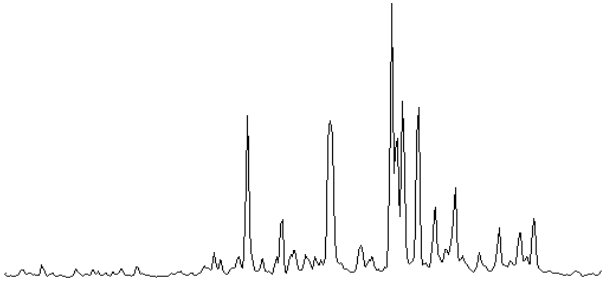
m/z 217: Sterane for sample MG2O



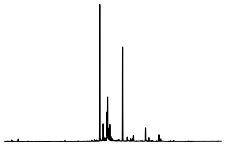
m/z 231: Triaromatic steroid for sample MG2O



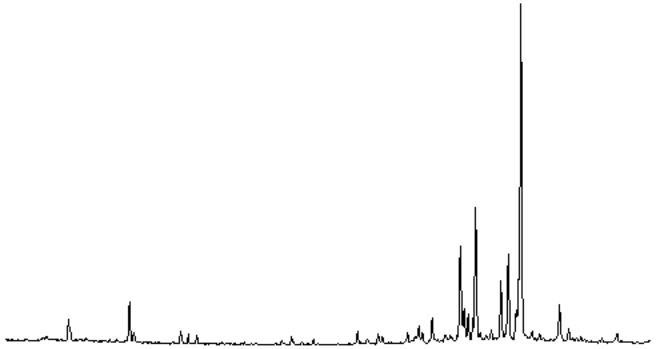
m/z 218: ββ Sterane for sample MG2O



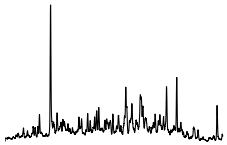
m/z 245: Triaromatic methylsteroid for sample MG2O



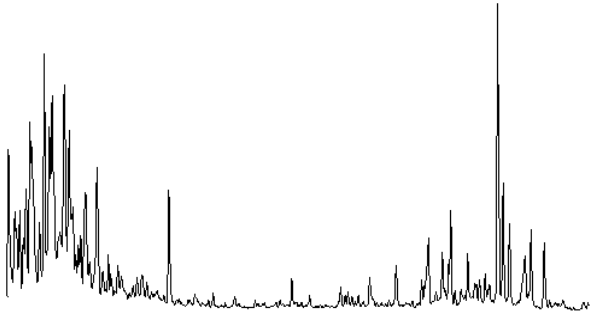
m/z 191: Tri- and Pentacyclics Terpanes for sample MG3S



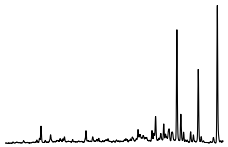
m/z 253: Monoaromatic steroid for sample MG3S



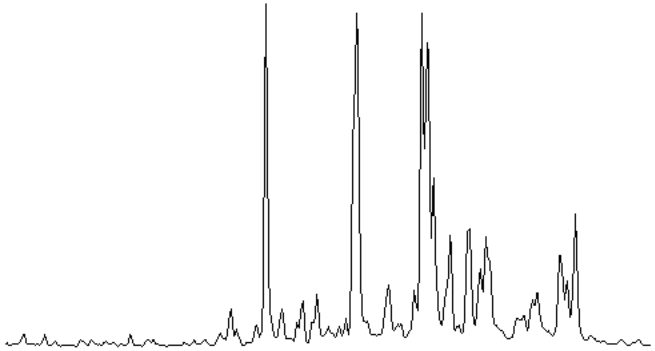
m/z 217: Sterane for sample MG3S



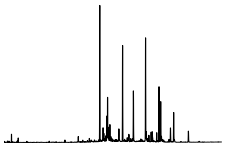
m/z 231: Triaromatic steroid for sample MG3S



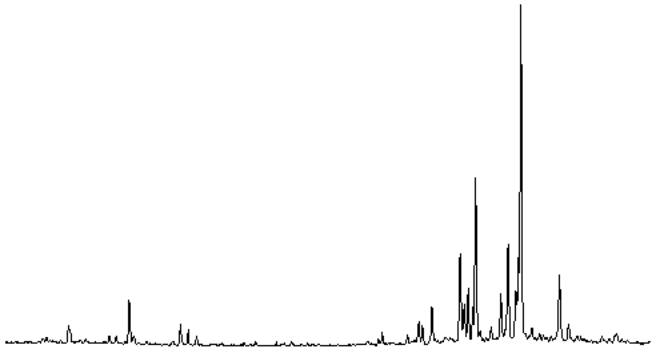
m/z 218: ββ Sterane for sample MG3S



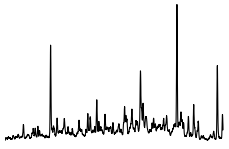
m/z 245: Triaromatic methylsteroid for sample MG3S



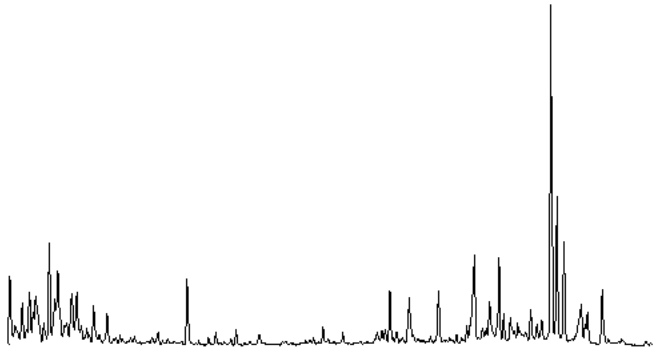
m/z 191: Tri- and Pentacyclics Terpanes for sample MG4D



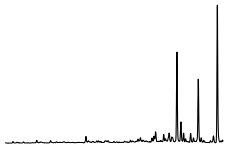
m/z 253: Monoaromatic steroid for sample MG4D



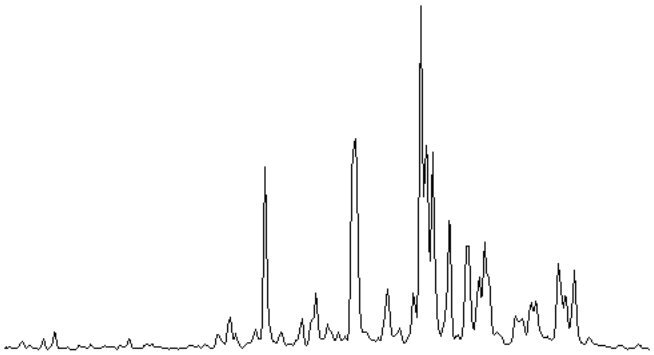
m/z 217: Sterane for sample MG4D



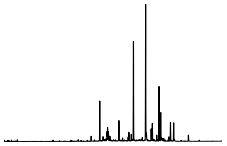
m/z 231: Triaromatic steroid for sample MG4D



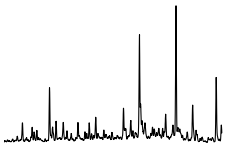
m/z 218: ββ Sterane for sample MG4D



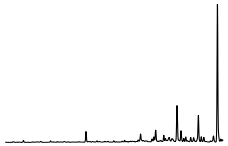
m/z 245: Triaromatic methylsteroid for sample MG3S



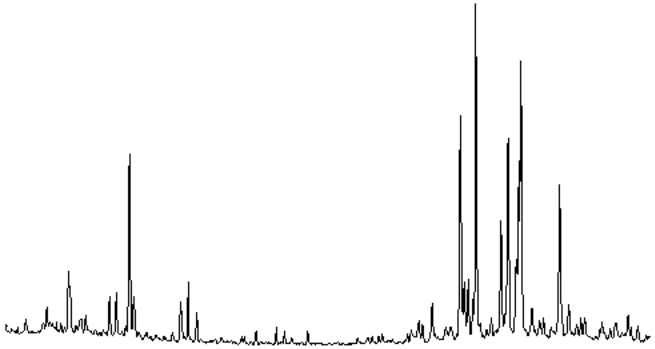
m/z 191: Tri- and Pentacyclics Terpanes for sample MG4K



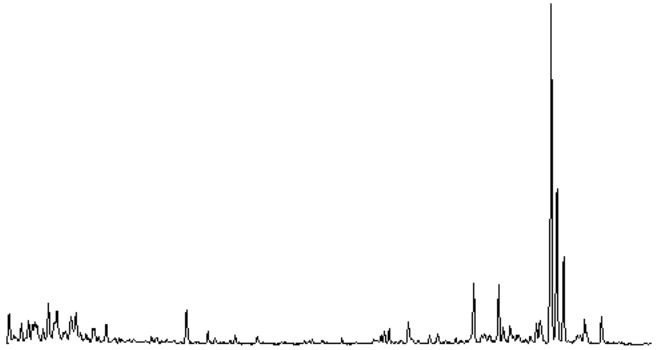
m/z 217: Sterane for sample MG4K



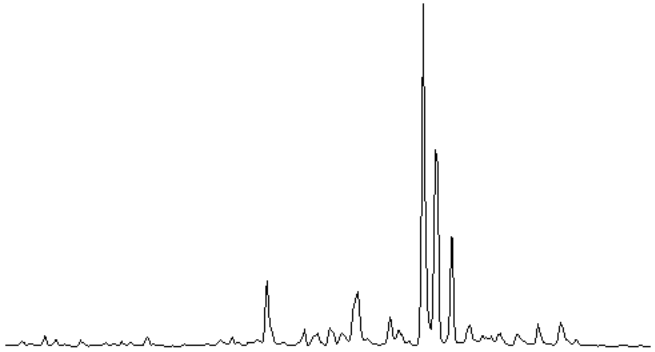
m/z 218: ββ Sterane for sample MG4K



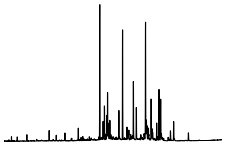
m/z 253: Monoaromatic steroid for sample MG4K



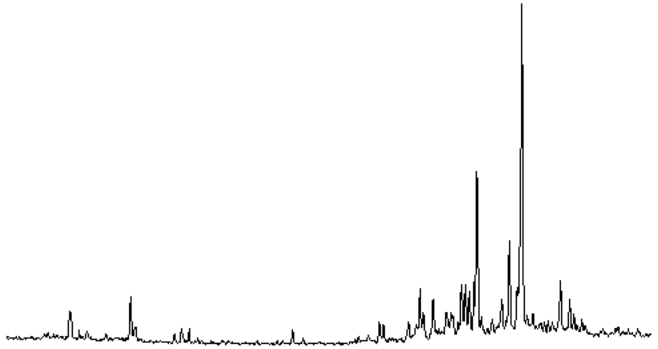
m/z 231: Triaromatic steroid for sample MG4K



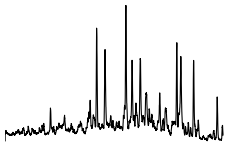
m/z 245: Triaromatic methylsteroid for sample MG3K



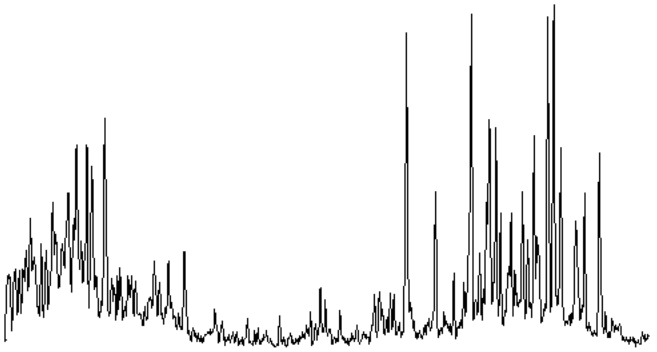
m/z 191: Tri- and Pentacyclics Terpanes for sample BH15B



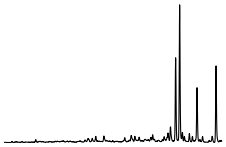
m/z 253: Monoaromatic steroid for sample BH15B



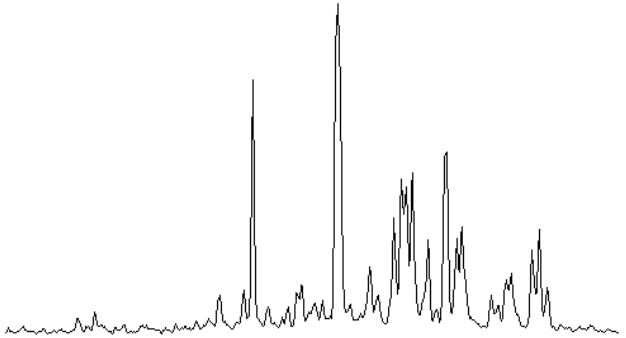
m/z 217: Sterane for sample BH15B



m/z 231: Triaromatic steroid for sample BH15B



m/z 218: ββ Sterane for sample BH15B



m/z 245: Triaromatic methylsteroid for sample BH15B

APPENDIX II

Ion	Peak Label	Compound Name	Ret. Time	Area	Height	ppm (Area)	ppm (Hght)
191	H31S	C31 22S 17α(H) hopane	72.814	1377587	188917	1921.1	1540.3
191	H31R	C31 22R 17α(H) hopane	73.331	4880833	713590	6806.5	5818.1
191	GAM	gammacerane	73.859	233802	18582	326.0	151.5
191	H32S	C32 22S 17α(H) hopane	76.111	146264	15135	204.0	123.4
191	H32R	C32 22R 17α(H) hopane	76.865	220627	31407	307.7	256.1
191	H33S	C33 22S 17α(H) hopane	80.173	80554	9183	112.3	74.9
191	H33R	C33 22R 17α(H) hopane	80.916	329528	28526	459.5	232.6
191	H34S	C34 22S 17α(H) hopane	83.998	34178	4651	47.7	37.9
191	H34R	C34 22R 17α(H) hopane	85.172	250499	27235	349.3	222.1
191	H35S	C35 22S 17α(H) hopane	87.952	144328	14426	201.3	117.6
191	H35R	C35 22R 17α(H) hopane	89.094	37847	5640	52.8	46.0
205	H31_2ME	C31- 2α-methylhopane	68.924	205491	22540	286.6	183.8
205	H31S_205	C31 22S 17α(H) hopane	72.814	400814	57596	559.0	469.6
205	H31R_205	C31 22R 17α(H) hopane	73.331	1475187	220229	2057.2	1795.6
205	H31_3ME	C31 3β-methylhopane	73.838	106710	12934	148.8	105.5
217	S21	C21 sterane	27.770	149309	27307	208.2	222.6
217	S22	C22 sterane	32.582	54452	5639	75.9	46.0
217	DIA27S	C27 βα 20S diasterane	47.559	205012	29247	285.9	238.5
217	DIA27R	C27 βα 20R diasterane	49.121	57357	6322	80.0	51.5
217	DIA28SA	C28 βα 20S diasterane a	51.709	16693	3870	23.3	31.6
217	DIA28SB	C28 βα 20S diasterane b	51.825	67170	6399	93.7	52.2
217	DIA28RA	C28 βα 20R diasterane a	53.485	83244	10934	116.1	89.1
217	DIA28RB	C28 βα 20R diasterane b	53.657	26851	4641	37.4	37.8
217	C27S	C27 αα 20S sterane	54.465	24605	3148	34.3	25.7
217	BB_D29S	C27 ββ 20R + C29 dia20S	55.306	136038	19395	189.7	158.1
217	C27BBS	C27 ββ 20S sterane	55.532	100102	14331	139.6	116.8
217	C27R	C27 αα 20R sterane	56.512	224215	26412	312.7	215.3
217	DIA29R	C29 βα 20R diasterane	56.997	159577	11973	222.5	97.6
217	C28S	C28 αα 20S sterane	58.969	1463847	139940	2041.4	1141.0
217	C28BBR	C28 ββ 20R sterane(+5 βαα)	59.648	685810	76726	956.4	625.6
217	C28BBS	C28 ββ 20S sterane	60.154	134538	10362	187.6	84.5
217	C28R	C28 αα 20R sterane	61.221	387231	26759	540.0	218.2
217	C29S	C29 αα 20S sterane	62.643	155469	15316	216.8	124.9
217	C29BBR	C29 ββ 20R sterane(+5 βαα)	63.440	247195	29036	344.7	236.7
217	C29BBS	C29 ββ 20S sterane	63.623	625047	91863	871.7	749.0
217	C29R	C29 αα 20R sterane	65.315	406953	43453	567.5	354.3
218	C27ABBR	C27 ββ 20R sterane	55.079	50101	4280	69.9	34.9
218	C27ABBS	C27 ββ 20S sterane	55.543	50128	5282	69.9	43.1
218	C28ABBR	C28 ββ 20R sterane	59.669	268035	34022	373.8	277.4
218	C28ABBS	C28 ββ 20S sterane	60.165	63844	10061	89.0	82.0
218	C29ABBR	C29 ββ 20R sterane	63.483	512524	46191	714.7	376.6
218	C29ABBS	C29 ββ 20S sterane	63.904	1342693	171242	1872.4	1396.2
218	C30ABBR	C30 ββ 20R sterane	66.662	135074	16618	188.4	135.5
218	C30ABBS	C30 ββ 20S sterane	66.845	100956	13217	140.8	107.8

Ion	Peak Label	Compound Name	Ret. Time	Area	Height	ppm (Area)	ppm (Hght)
259	D27S	C27 βα 20S diasterane	47.591	1159	329	1.6	2.7
259	D27R	C27 βα 20R diasterane	49.369	7588	1166	10.6	9.5
259	D28SA	C28 βα 20S diasterane a	51.675	9905	834	13.8	6.8
259	D28SB	C28 βα 20S diasterane b	51.847	6188	776	8.6	6.3
259	D28RA	C28 βα 20R diasterane a	53.517	6323	631	8.8	5.1
259	D28RB	C28 βα 20R diasterane b	53.668	10366	1480	14.5	12.1
259	D29S	C29 βα 20S diasterane	55.306	69781	8908	97.3	72.6
259	D29R	C29 βα 20R diasterane	57.126	7389	743	10.3	6.1
259	C30TP1	C30 tetracyclic polyprenoid	67.104	12782	2370	17.8	19.3
259	C30TP2	C30 tetracyclic polyprenoid	67.164	11078	6434	15.4	52.5

Saturate Peak label and compounds name for sample MG2O

Ion	Peak Label	Compound Name	Ret. Time	Area	Height	ppm (Area)	ppm (Hght)
217	CHOL	*5β cholane (internal standard)*	41.256	74488	12224	100.0	100.0
123	LABD	labdane					
123	RIMU	rimuane					
123	PIM	pimarane					
123	ENTBEY	ent-beyerane					
123	ISOPIM	isopimarane					
123	B_PHYLLO	β-phyllocladane					
123	B_KAUR	β-kaurane					
123	A_PHYLLO	α-phyllocladane					
125	BCAROT	β-carotane					
187	4MDIAM	4-methyldiamantane	8.507	1132	312	1.5	2.6
187	1MDIAM	1-methyldiamantane	9.098	934	879	1.3	7.2
187	3MDIAM	3-methyldiamantane	9.443	1396	397	1.9	3.2
188	DIAM	diamantane	8.354	846	429	1.1	3.5
191	TR19	C19 tricyclic terpane	17.714	19108	4024	25.7	32.9
191	TR20	C20 tricyclic terpane	20.564	154552	18717	207.5	153.1
191	TR21	C21 tricyclic terpane	23.801	37264	5240	50.0	42.9
191	TR22	C22 tricyclic terpane	27.189	39471	4515	53.0	36.9
191	TR23	C23 tricyclic terpane	31.429	51574	5112	69.2	41.8
191	TR24	C24 tricyclic terpane	33.929	26166	3036	35.1	24.8
191	DESAOL	des-A-oleanane					
191	DESALU	des-A-lupane					
191	TR25A	C25 tricyclic terpane (a)	38.971	57209	5119	76.8	41.9
191	TR25B	C25 tricyclic terpane (b)	39.262	122770	14929	164.8	122.1
191	DESEHOP	des-E-hopane	42.484	116174	10073	156.0	82.4
191	TR26A	C26 tricyclic terpane (a)	43.066	64480	6067	86.6	49.6
191	TR26B	C26 tricyclic terpane (b)	43.411	98969	7119	132.9	58.2
191	TR28A	C28 tricyclic terpane (a)	52.429	721900	105869	969.1	866.1
191	TR28B	C28 tricyclic terpane (b)	53.000	64981	7759	87.2	63.5
191	TR29A	C29 tricyclic terpane (a)	54.993	172961	12468	232.2	102.0
191	TR29B	C29 tricyclic terpane (b)	55.769	138028	13201	185.3	108.0
191	TR30A	C30 tricyclic terpane (a)	60.132	275722	35819	370.2	293.0
191	TR30B	C30 tricyclic terpane (b)	60.973	412753	35224	554.1	288.2
191	TS	Ts 18α(H)-trisnorhopane	57.202	119847	13057	160.9	106.8
191	TM	Tm 17α(H)-trisnorhopane	58.980	1588775	154327	2132.9	1262.5
191	H28	C28 17α18α21β(H)-bisnorhopane	63.128	1160807	128474	1558.4	1051.0
191	NOR25H	C29 Nor-25-hopane					
191	H29	C29 Tm 17α(H)21β(H)-norhopane	65.046	2239627	332322	3006.7	2718.6
191	C29TS	C29 Ts 18α(H)-norneohopane	65.315	3119442	460541	4187.8	3767.5
191	DH30	C30 17α(H)-diahopane	65.983	75065	11591	100.8	94.8
191	M29	C29 normoretane	67.114	2467809	369751	3313.0	3024.8
191	OL	oleanane					
191	H30	C30 17α(H)-hopane	68.601	1514813	201483	2033.6	1648.3
191	M30	C30 moretane	70.250	916504	118703	1230.4	971.1

Ion	Peak Label	Compound Name	Ret. Time	Area	Height	ppm (Area)	ppm (Hght)
191	H31S	C31 22S 17α(H) hopane	72.846	5873001	832789	7884.5	6812.7
191	H31R	C31 22R 17α(H) hopane	73.385	13011480	1813629	17467.9	14836.6
191	GAM	gammacerane	73.859	439323	40600	589.8	332.1
191	H32S	C32 22S 17α(H) hopane	76.111	177215	18797	237.9	153.8
191	H32R	C32 22R 17α(H) hopane	76.865	452529	53001	607.5	433.6
191	H33S	C33 22S 17α(H) hopane	80.141	165195	12271	221.8	100.4
191	H33R	C33 22R 17α(H) hopane	80.949	279241	21350	374.9	174.7
191	H34S	C34 22S 17α(H) hopane	84.181	368379	37525	494.5	307.0
191	H34R	C34 22R 17α(H) hopane	85.183	266846	31562	358.2	258.2
191	H35S	C35 22S 17α(H) hopane	87.952	242679	23858	325.8	195.2
191	H35R	C35 22R 17α(H) hopane	89.116	83077	4996	111.5	40.9
205	H31_2ME	C31- 2α-methylhopane	68.957	325048	36333	436.4	297.2
205	H31S_205	C31 22S 17α(H) hopane	72.846	1788561	250835	2401.1	2052.0
205	H31R_205	C31 22R 17α(H) hopane	73.385	4031209	569710	5411.9	4660.6
205	H31_3ME	C31 3β-methylhopane	73.859	289870	38190	389.2	312.4
217	S21	C21 sterane	27.770	83456	15628	112.0	127.8
217	S22	C22 sterane	32.647	37684	3690	50.6	30.2
217	DIA27S	C27 βα 20S diasterane	47.559	45741	6205	61.4	50.8
217	DIA27R	C27 βα 20R diasterane	49.186	31836	2414	42.7	19.7
217	DIA28SA	C28 βα 20S diasterane a	51.793	81663	7905	109.6	64.7
217	DIA28SB	C28 βα 20S diasterane b	52.052	18530	2738	24.9	22.4
217	DIA28RA	C28 βα 20R diasterane a	53.485	116703	15270	156.7	124.9
217	DIA28RB	C28 βα 20R diasterane b	53.776	64428	8285	86.5	67.8
217	C27S	C27 αα 20S sterane	54.508	67528	8902	90.7	72.8
217	BB_D29S	C27 ββ 20R + C29 dia20S	55.306	78913	11480	105.9	93.9
217	C27BBS	C27 ββ 20S sterane	55.543	72310	9648	97.1	78.9
217	C27R	C27 αα 20R sterane	56.491	101964	12663	136.9	103.6
217	DIA29R	C29 βα 20R diasterane	57.019	135227	9772	181.5	79.9
217	C28S	C28 αα 20S sterane	58.969	1004058	130852	1347.9	1070.5
217	C28BBR	C28 ββ 20R sterane(+5 βαα)	59.637	515322	60776	691.8	497.2
217	C28BBS	C28 ββ 20S sterane	60.143	66712	8033	89.6	65.7
217	C28R	C28 αα 20R sterane	61.221	320951	29693	430.9	242.9
217	C29S	C29 αα 20S sterane	62.524	52396	7745	70.3	63.4
217	C29BBR	C29 ββ 20R sterane(+5 βαα)	63.451	158330	21345	212.6	174.6
217	C29BBS	C29 ββ 20S sterane	63.602	236060	31611	316.9	258.6
217	C29R	C29 αα 20R sterane	65.283	394768	36075	530.0	295.1
218	C27ABBR	C27 ββ 20R sterane	55.079	66149	5666	88.8	46.4
218	C27ABBS	C27 ββ 20S sterane	55.564	47394	4964	63.6	40.6
218	C28ABBR	C28 ββ 20R sterane	59.648	214868	25900	288.5	211.9
218	C28ABBS	C28 ββ 20S sterane	60.316	398115	44382	534.5	363.1
218	C29ABBR	C29 ββ 20R sterane	63.289	716027	91424	961.3	747.9
218	C29ABBS	C29 ββ 20S sterane	63.473	455634	51267	611.7	419.4
218	C30ABBR	C30 ββ 20R sterane	66.673	242789	27749	325.9	227.0
218	C30ABBS	C30 ββ 20S sterane	66.877	57355	7361	77.0	60.2

Ion	Peak Label	Compound Name	Ret. Time	Area	Height	ppm (Area)	ppm (Hght)
259	D27S	C27 βα 20S diasterane	47.526	2486	466	3.3	3.8
259	D27R	C27 βα 20R diasterane	49.347	7428	794	10.0	6.5
259	D28SA	C28 βα 20S diasterane a	51.459	18633	1125	25.0	9.2
259	D28SB	C28 βα 20S diasterane b	52.095	19357	1166	26.0	9.5
259	D28RA	C28 βα 20R diasterane a	53.538	1755	452	2.4	3.7
259	D28RB	C28 βα 20R diasterane b	53.657	8956	1193	12.0	9.8
259	D29S	C29 βα 20S diasterane	55.413	9387	2245	12.6	18.4
259	D29R	C29 βα 20R diasterane	57.126	8540	1015	11.5	8.3
259	C30TP1	C30 tetracyclic polyprenoid	67.125	18309	3264	24.6	26.7
259	C30TP2	C30 tetracyclic polyprenoid	67.202	23170	10574	31.1	86.5

Saturate Peak label and compounds name for sample MG4K

187	4MDIAM	4-methyldiamantane	8.529	674	225	1.5	3.0
187	1MDIAM	1-methyldiamantane	9.110	796	182	1.7	2.5
187	3MDIAM	3-methyldiamantane	9.476	498	185	1.1	2.5
188	DIAM	diamantane	8.389	485	191	1.1	2.6
191	TR19	C19 tricyclic terpane					
191	H28	C28 17α18α21β(H)-bisnorhopane	63.085	6068675	904178	13294.2	12179.1
191	NOR25H	C29 Nor-25-hopane					
191	H29	C29 Tm 17α(H)21β(H)-norhopane	64.927	346726	43597	759.5	587.2
191	C29TS	C29 Ts 18α(H)-norneohopane	65.218	663731	89380	1454.0	1203.9
191	DH30	C30 17α(H)-diahopane	65.908	10411	1445	22.8	19.5
191	M29	C29 normoretane	67.039	172947	30040	378.9	404.6
191	OL	oleanane					
191	H30	C30 17α(H)-hopane	68.558	91205	10632	199.8	143.2
191	M30	C30 moretane	70.175	50296	5859	110.2	78.9
191	H31S	C31 22S 17α(H) hopane	72.782	74874	9001	164.0	121.2
191	H31R	C31 22R 17α(H) hopane	73.288	283168	36271	620.3	488.6
205	H31_2ME	C31- 2α-methylhopane	68.882	21942	1991	48.1	26.8
205	H31S_205	C31 22S 17α(H) hopane	72.782	21005	2672	46.0	36.0
205	H31R_205	C31 22R 17α(H) hopane	73.288	83512	11088	182.9	149.4
205	H31_3ME	C31 3β-methylhopane	73.795	4844	568	10.6	7.7

Saturate Peak label and compounds name for sample MG3S

187	4MDIAM	4-methyldiamantane	8.540	707	216	2.5	4.7
187	1MDIAM	1-methyldiamantane	9.121	861	217	3.0	4.8
187	3MDIAM	3-methyldiamantane	9.476	624	188	2.2	4.1
188	DIAM	diamantane	8.389	677	220	2.4	4.8
191	H28	C28 17α18α21β(H)-bisnorhopane	63.053	49717	5474	173.0	120.0
191	NOR25H	C29 Nor-25-hopane					
191	H29	C29 Tm 17α(H)21β(H)-norhopane	64.949	106912	10410	372.1	228.3
191	C29TS	C29 Ts 18α(H)-norneohopane	65.186	68219	7026	237.4	154.1
191	DH30	C30 17α(H)-diahopane	65.843	265856	36007	925.3	789.6
191	M29	C29 normoretane	67.029	54161	7651	188.5	167.8
191	OL	oleanane					
191	H30	C30 17α(H)-hopane	68.548	73806	7504	256.9	164.6
191	M30	C30 moretane	70.153	40241	4119	140.1	90.3
191	H31S	C31 22S 17α(H) hopane	72.782	21424	2446	74.6	53.6
191	H31R	C31 22R 17α(H) hopane	73.289	77138	7737	268.5	169.7
205	H31_2ME	C31- 2α-methylhopane	68.871	12509	1027	43.5	22.5
205	H31S_205	C31 22S 17α(H) hopane	72.782	4600	554	16.0	12.1
205	H31R_205	C31 22R 17α(H) hopane	73.299	17403	2206	60.6	48.4
205	H31_3ME	C31 3β-methylhopane	73.795	5751	647	20.0	14.2

Saturate Peak label and compounds name for sample MG4D

187	4MDIAM	4-methyldiamantane	8.529	1034	294	2.4	4.2
187	1MDIAM	1-methyldiamantane	9.132	1551	359	3.6	5.1
187	3MDIAM	3-methyldiamantane	9.465	694	205	1.6	2.9
188	DIAM	diamantane	8.389	790	267	1.8	3.8
191	TR19	C19 tricyclic terpane	17.736	5426	1299	12.6	18.4
191	TR20	C20 tricyclic terpane	20.521	34810	5735	80.6	81.1
191	TR21	C21 tricyclic terpane	23.823	24828	4683	57.5	66.2
191	TR22	C22 tricyclic terpane	27.211	11080	1541	25.6	21.8
191	TR23	C23 tricyclic terpane	31.505	31258	5050	72.4	71.4
191	TR24	C24 tricyclic terpane	33.951	18159	2768	42.0	39.1
191	H28	C28 17α18α21β(H)-bisnorhopane	63.064	92964	10890	215.2	154.0
191	NOR25H	C29 Nor-25-hopane					
191	H29	C29 Tm 17α(H)21β(H)-norhopane	64.960	344968	37672	798.5	532.7
191	C29TS	C29 Ts 18α(H)-norneohopane	65.197	83837	9570	194.1	135.3
191	DH30	C30 17α(H)-diahopane	65.854	175206	24777	405.6	350.4
191	M29	C29 normoretane	67.029	270456	37621	626.1	532.0
191	OL	oleanane					
191	H30	C30 17α(H)-hopane	68.548	262783	34490	608.3	487.7
191	M30	C30 moretane	70.175	178399	21606	413.0	305.5
191	H31S	C31 22S 17α(H) hopane	72.771	86403	10685	200.0	151.1
191	H31R	C31 22R 17α(H) hopane	73.288	385614	51572	892.6	729.2
191	GAM	gammacerane	73.806	31368	2524	72.6	35.7
205	H31_2ME	C31- 2α-methylhopane	68.860	30798	2809	71.3	39.7
205	H31S_205	C31 22S 17α(H) hopane	72.782	30149	3707	69.8	52.4
205	H31R_205	C31 22R 17α(H) hopane	73.288	122465	16251	283.5	229.8
205	H31_3ME	C31 3β-methylhopane	73.806	18794	2241	43.5	31.7
217	S21	C21 sterane	27.803	17348	2712	40.2	38.3
217	S22	C22 sterane	32.604	10274	1154	23.8	16.3

Saturate Peak label and compounds name for sample BH15B

Ion	Peak Label	Compound Name	Ret. Time	Area	Height	ppm (Area)	ppm (Hght)
217	CHOL	*5β cholane (internal standard)*	41.278	41640	6996	100.0	100.0
123	LABD	labdane					
123	RIMU	rimuane					
123	PIM	pimarane					
123	ENTBEY	ent-beyerane					
123	ISOPIM	isopimarane					
123	B_PHYLLO	β-phyllocladane					
123	B_KAUR	β-kaurane					
123	A_PHYLLO	α-phyllocladane					
125	BCAROT	β-carotane					
187	4MDIAM	4-methyldiamantane	8.529	865	268	2.1	3.8
187	1MDIAM	1-methyldiamantane	9.110	1039	311	2.5	4.4
187	3MDIAM	3-methyldiamantane	9.476	642	213	1.5	3.0
188	DIAM	diamantane	8.389	743	222	1.8	3.2
191	TR19	C19 tricyclic terpane	17.736	4852	1119	11.7	16.0
191	TR20	C20 tricyclic terpane	20.511	27396	5095	65.8	72.8
191	TR21	C21 tricyclic terpane	23.812	36957	7375	88.8	105.4
191	TR22	C22 tricyclic terpane	27.211	13355	2275	32.1	32.5
191	TR23	C23 tricyclic terpane	31.505	65563	11714	157.5	167.4
191	TR24	C24 tricyclic terpane	33.951	39176	6565	94.1	93.8
191	DESAOL	des-A-oleanane					
191	DESALU	des-A-lupane					
191	TR25A	C25 tricyclic terpane (a)	39.144	17527	2853	42.1	40.8
191	TR25B	C25 tricyclic terpane (b)	39.273	20686	3170	49.7	45.3
191	DESEHOP	des-E-hopane	42.495	29495	3981	70.8	56.9
191	TR26A	C26 tricyclic terpane (a)	43.077	45926	4941	110.3	70.6
191	TR26B	C26 tricyclic terpane (b)	43.465	16807	2423	40.4	34.6
191	TR28A	C28 tricyclic terpane (a)					
191	TR28B	C28 tricyclic terpane (b)					
191	TR29A	C29 tricyclic terpane (a)					
191	TR29B	C29 tricyclic terpane (b)					
191	TR30A	C30 tricyclic terpane (a)					
191	TR30B	C30 tricyclic terpane (b)					
191	TS	Ts 18α(H)-trisnorhopane					
191	TM	Tm 17α(H)-trisnorhopane					
191	H28	C28 17α18α21β(H)-bisnorhopane	63.064	73746	6181	177.1	88.4
191	NOR25H	C29 Nor-25-hopane					
191	H29	C29 Tm 17α(H)21β(H)-norhopane	64.981	247777	22199	595.0	317.3
191	C29TS	C29 Ts 18α(H)-norneohopane	65.175	146320	16061	351.4	229.6
191	DH30	C30 17α(H)-diahopane	65.963	15559	2000	37.4	28.6
191	M29	C29 normoretane	67.029	95750	12823	229.9	183.3
191	OL	oleanane					
191	H30	C30 17α(H)-hopane	68.548	145321	19379	349.0	277.0
191	M30	C30 moretane	70.175	61371	7699	147.4	110.0

Ion	Peak Label	Compound Name	Ret. Time	Area	Height	ppm (Area)	ppm (Hght)
191	H31S	C31 22S 17α(H) hopane	72.771	24211	2459	58.1	35.1
191	H31R	C31 22R 17α(H) hopane	73.288	98489	11334	236.5	162.0
191	GAM	gammacerane	73.730	18097	1135	43.5	16.2
191	H32S	C32 22S 17α(H) hopane					
191	H32R	C32 22R 17α(H) hopane					
191	H33S	C33 22S 17α(H) hopane					
191	H33R	C33 22R 17α(H) hopane					
191	H34S	C34 22S 17α(H) hopane					
191	H34R	C34 22R 17α(H) hopane					
191	H35S	C35 22S 17α(H) hopane					
191	H35R	C35 22R 17α(H) hopane					
205	H31_2ME	C31- 2α-methylhopane	68.882	11876	1021	28.5	14.6
205	H31S_205	C31 22S 17α(H) hopane	72.793	7582	904	18.2	12.9
205	H31R_205	C31 22R 17α(H) hopane	73.288	28539	3625	68.5	51.8
205	H31_3ME	C31 3β-methylhopane	73.795	5314	606	12.8	8.7
217	S21	C21 sterane	27.792	18837	2819	45.2	40.3
217	S22	C22 sterane	32.593	11061	1611	26.6	23.0
217	DIA27S	C27 βα 20S diasterane	47.645	3267	410	7.8	5.9
217	DIA27R	C27 βα 20R diasterane	49.261	2542	442	6.1	6.3
217	DIA28SA	C28 βα 20S diasterane a	51.696	4846	464	11.6	6.6
217	DIA28SB	C28 βα 20S diasterane b	51.815	8056	833	19.3	11.9
217	DIA28RA	C28 βα 20R diasterane a	53.377	2136	343	5.1	4.9
217	DIA28RB	C28 βα 20R diasterane b	53.636	3960	559	9.5	8.0
217	C27S	C27 αα 20S sterane	54.606	5265	916	12.6	13.1
217	BB_D29S	C27 ββ 20R + C29 dia20S	55.112	9896	730	23.8	10.4
217	C27BBS	C27 ββ 20S sterane	55.489	31410	4451	75.4	63.6
217	C27R	C27 αα 20R sterane	56.459	29479	3495	70.8	50.0
217	DIA29R	C29 βα 20R diasterane	57.105	6168	649	14.8	9.3
217	C28S	C28 αα 20S sterane	58.851	42551	5402	102.2	77.2
217	C28BBR	C28 ββ 20R sterane(+5 βαα)	59.562	24634	2977	59.2	42.6
217	C28BBS	C28 ββ 20S sterane	60.004	9819	1097	23.6	15.7
217	C28R	C28 αα 20R sterane	61.210	21000	1604	50.4	22.9
217	C29S	C29 αα 20S sterane	62.525	3912	447	9.4	6.4
217	C29BBR	C29 ββ 20R sterane(+5 βαα)	63.398	13316	1046	32.0	15.0
217	C29BBS	C29 ββ 20S sterane	63.678	1510	302	3.6	4.3
217	C29R	C29 αα 20R sterane	65.154	36087	3471	86.7	49.6
218	C27ABBR	C27 ββ 20R sterane	55.123	10723	1194	25.8	17.1
218	C27ABBS	C27 ββ 20S sterane	55.521	14841	1834	35.6	26.2
218	C28ABBR	C28 ββ 20R sterane	59.583	19085	2009	45.8	28.7
218	C28ABBS	C28 ββ 20S sterane	60.004	16359	1833	39.3	26.2
218	C29ABBR	C29 ββ 20R sterane	63.376	14524	1574	34.9	22.5
218	C29ABBS	C29 ββ 20S sterane	63.818	24516	2728	58.9	39.0
218	C30ABBR	C30 ββ 20R sterane					
218	C30ABBS	C30 ββ 20S sterane					

Ion	Peak Label	Compound Name	Ret. Time	Area	Height	ppm (Area)	ppm (Hght)
259	D27S	C27 βα 20S diasterane	47.656	1674	260	4.0	3.7
259	D27R	C27 βα 20R diasterane	49.240	1312	249	3.2	3.6
259	D28SA	C28 βα 20S diasterane a	51.664	2770	292	6.7	4.2
259	D28SB	C28 βα 20S diasterane b	51.890	2263	238	5.4	3.4
259	D28RA	C28 βα 20R diasterane a	53.366	832	115	2.0	1.6
259	D28RB	C28 βα 20R diasterane b	53.593	1272	220	3.1	3.1
259	D29S	C29 βα 20S diasterane	55.284	2253	325	5.4	4.6
259	D29R	C29 βα 20R diasterane	57.138	1483	168	3.6	2.4
259	C30TP1	C30 tetracyclic polyprenoid	67.018	779	171	1.9	2.4
259	C30TP2	C30 tetracyclic polyprenoid	67.136	3067	389	7.4	5.6

APPENDIX III

Aromatic peaks and compounds for sample MG1G

Ion	Peak Label	Compound Name	Ret. Time	Area	Height	ppm (Area)	ppm (Hght)
230	OTP	*Ortho-terphenyl* (internal standard)	75.031	28191160	6532897	300.0	300.0
128	NAPH	Naphthalene	28.894	12044280	2079826	128.2	95.5
142	2MN	2-Methylnaphthalene	37.985	16890430	2773613	179.7	127.4
142	1MN	1-Methylnaphthalene	39.213	11420770	1879560	121.5	86.3
154	BP	Biphenyl	44.700	4710751	758014	50.1	34.8
156	2EN	2-Ethylnaphthalene	46.163	2459374	377990	26.2	17.4
156	1EN	1-Ethylnaphthalene	46.241	1578632	279662	16.8	12.8
156	26DMN	2,6-Dimethylnaphthalene	47.051	7503433	1274272	79.8	58.5
156	27DMN	2,7-Dimethylnaphthalene	47.208	8554495	1324357	91.0	60.8
156	1317DMN	1,3 & 1,7-Dimethylnaphthalenes	48.200	31088970	4293330	330.8	197.2
156	16DMN	1,6-Dimethylnaphthalene	48.462	23738130	3797609	252.6	174.4
156	23DMN	2,3-Dimethylnaphthalene	49.637	4291253	763252	45.7	35.1
156	14DMN	1,4-Dimethylnaphthalene	49.742	7944696	1265799	84.5	58.1
156	15DMN	1,5-Dimethylnaphthalene	49.846	5954406	1020226	63.4	46.9
156	12DMN	1,2-Dimethylnaphthalene	50.787	5490238	814851	58.4	37.4
168	2MBP	2-Methylbiphenyl					
168	DPM	Diphenylmethane					
168	3MBP	3-Methylbiphenyl					
168	4MBP	4-Methylbiphenyl					
168	DBF	Dibenzofuran					
170	BB_EMN	Ethyl-methyl-Naphthalene	55.123	7657865	918577	81.5	42.2
170	AB_EMN	Ethyl-methyl-Naphthalene	56.325	4829154	721773	51.4	33.1
170	137TMN	1,3,7-Trimethylnaphthalene	56.769	14518090	2471393	154.5	113.5
170	136TMN	1,3,6-Trimethylnaphthalene	57.161	51516590	8636790	548.2	396.6
170	146135T	(1,4,6+1,3,5)-Trimethylnaphthalenes	58.206	22235240	3308459	236.6	151.9
170	236TMN	2,3,6-Trimethylnaphthalene	58.494	12783840	2204265	136.0	101.2
170	127TMN	1,2,7-Trimethylnaphthalene	59.225	8634131	1533452	91.9	70.4
170	167126T	(1,6,7+1,2,6)-Trimethylnaphthalenes	59.408	31552930	5056479	335.8	232.2
170	124TMN	1,2,4-Trimethylnaphthalene	60.322	3449351	532083	36.7	24.4
170	125TMN	1,2,5-Trimethylnaphthalene	60.767	17585880	3094469	187.1	142.1
178	PHEN	Phenanthrene	70.302	232184300	51147060	2470.8	2348.7
184	1357	1,3,5,7-Tetramethylnaphthalene	64.738	12424060	2150209	132.2	98.7
184	1367	1,3,6,7-Tetramethylnaphthalene	65.887	46926320	10026160	499.4	460.4
184	1247	(1,2,4,7+1,2,4,6+1,4,6,7)-Tetramethylnaphthalenes	66.645	20102810	3610387	213.9	165.8
184	1257	1,2,5,7-Tetramethylnaphthalene	66.828	14201180	1956949	151.1	89.9
184	2367	2,3,6,7-Tetramethylnaphthalene	67.193	9540110	1824603	101.5	83.8
184	1267	1,2,6,7-Tetramethylnaphthalene	67.637	8390971	1680905	89.3	77.2
184	1237	1,2,3,7-Tetramethylnaphthalene	67.820	4834453	1022424	51.4	47.0
184	1236	1,2,3,6-Tetramethylnaphthalene	68.082	12060040	2262321	128.3	103.9
184	1256	1,2,5,6-Tetramethylnaphthalene	68.813	25247090	5394041	268.7	247.7
184	DBT	Dibenzothiophene	69.022	6975191	935553	74.2	43.0
191	BH32	C32 Benzohopane	118.139	21795530	2662473	231.9	122.3
191	BH33	C33 Benzohopane	120.386	23267340	2842125	247.6	130.5
191	BH34	C34 Benzohopane	122.371	8191537	899275	87.2	41.3
191	BH35	C35 Benzohopane	124.644	30048090	3210977	319.8	147.5
192	3MP	3-Methylphenanthrene	75.240	19629040	4480475	208.9	205.8
192	2MP	2-Methylphenanthrene	75.423	78122180	18843190	831.3	865.3
192	9MP	9-Methylphenanthrene	76.128	160849400	35402050	1711.7	1625.7
192	1MP	1-Methylphenanthrene	76.311	78615720	16019990	836.6	735.7

198	CAD	*(Cadalene)*	66.180	371763	419198	4.0	19.3
198	4MDBT	4 Methyl Dibenzothiophene	73.568	5328662	1033539	56.7	47.5
198	23MDBT	2 & 3 Methyl Dibenzothiophenes	74.404	10949400	1866509	116.5	85.7
198	1MDBT	1 Methyl Dibenzothiophene	75.162	8022914	1409197	85.4	64.7
206	36DMP	3,6-Dimethylphenanthrene	79.417	8099633	1990332	86.2	91.4
206	26DMP	2,6-Dimethylphenanthrene	79.761	11969640	2251986	127.4	103.4
206	27DMP	2,7-Dimethylphenanthrene	79.865	25580060	4677944	272.2	214.8
206	39DMP	(3,9+3,10+2,10+1,3)-Dimethylphenanthrenes	80.362	30787400	6571084	327.6	301.8
206	29DMP	(2,9+1,6)-Dimethylphenanthrenes	80.597	39154360	8200029	416.7	376.6
206	17DMP	1,7-Dimethylphenanthrene	80.727	93400540	19313990	993.9	886.9
206	23DMP	2,3-Dimethylphenanthrene	81.015	24042840	5247438	255.9	241.0
206	19DMP	1,9-Dimethylphenanthrene	81.172	67801080	8926333	721.5	409.9
206	18DMP	1,8-Dimethylphenanthrene	81.537	22678440	3125027	241.3	143.5
206	12DMP	1,2-Dimethylphenanthrene	82.034	10770300	1851643	114.6	85.0
231	231A20	C20 Triaromatic Steroid	92.484	12877220	1553705	137.0	71.3
231	231B21	C21 Triaromatic	94.861	3653449	539620	38.9	24.8
231	231C26	C26 20S Triaromatic	104.162	708065	119359	7.5	5.5
231	231D26	C27 20S & C26 20R Triaromatic	105.782	4650398	620842	49.5	28.5
231	TADMD1	C28 23,24-Cholestane Triaromatic	106.382	297547	72508	3.2	3.3
231	TADMD2	C28 23,24-Cholestane Triaromatic	106.950	911181	188372	9.7	8.7
231	231E28	C28 20S Triaromatic	107.009	1806990	333196	19.2	15.3
231	231F27	C27 20R Triaromatic	107.767	2646325	563325	28.2	25.9
231	TADMD3	C28 23,24-Cholestane Triaromatic	107.794	648242	345489	6.9	15.9
231	C29TA1	C29 Triaromatic	108.028	626015	178951	6.7	8.2
231	C29TA2	C29 Triaromatic	108.133	10260740	2621562	109.2	120.4
231	TADMD4	C28 23,24-Cholestane Triaromatic	109.100	651265	127070	6.9	5.8
231	231G28	C28 20R Triaromatic	109.204	1412754	285074	15.0	13.1
231	TADMD5	C28 23,24-Cholestane Triaromatic	109.361	1439986	278345	15.3	12.8
231	C29TA3	C29 Triaromatic	110.667	31273530	7773503	332.8	357.0
245	C3S	C27 20S 3-Methyl Triaromatic Steroid	106.905	1011455	172881	10.8	7.9
245	C4S	C27 20S 4-Methyl Triaromatic Steroid	107.506	4871051	922296	51.8	42.4
245	E2S	C28 20S 2-Methyl Triaromatic Steroid	108.028	374219	99813	4.0	4.6
245	E3SC3R	C28 20S 3-Methyl & C27 20R 3-Methyl TAS	108.368	3868801	665155	41.2	30.5
245	E4SC4R	C28 20S 4-Methyl & C27 20R 4-Methyl TAS	108.995	11624870	1391678	123.7	63.9
245	S2S	C29 20S 2-Methyl Triaromatic Steroid	109.204	2579026	387568	27.4	17.8
245	DA	Triaromatic Dinosteroid a	109.296	640296	194423	6.8	8.9
245	S3S	C29 20S 3-Methyl Triaromatic Steroid	109.596	5961273	941198	63.4	43.2
245	DB	Triaromatic Dinosteroid b	110.040	601225	126827	6.4	5.8
245	S4SE2R	C29 20S 4-Methyl & C28 20R 2-Methyl TAS	110.171	55983790	14533080	595.8	667.4
245	E3R	C28 20R 3-Methyl Triaromatic Steroid	110.380	22880100	5116057	243.5	234.9
245	E4R	C28 20R 4-Methyl Triaromatic Steroid	110.954	3935581	716513	41.9	32.9
245	DC	Triaromatic Dinosteroid c	111.163	2492895	352405	26.5	16.2
245	DD	Triaromatic Dinosteroid d	111.320	11655620	1811432	124.0	83.2
245	S2R	C29 20R 2-Methyl Triaromatic Steroid	111.764	3017017	535497	32.1	24.6
245	S3R	C29 20R 3-Methyl Triaromatic Steroid	111.848	1015978	199671	10.8	9.2
245	DE	Triaromatic Dinosteroid e	112.156	10786550	2218282	114.8	101.9
245	S4R	C29 20R 4-Methyl Triaromatic Steroid	112.522	2865474	508613	30.5	23.4
245	DF	Triaromatic Dinosteroid f	112.653	1571400	315896	16.7	14.5
253	S253A	*C21 Ring-C Monoaromatic Steroid*	84.594	6225337	1328345	66.2	61.0
253	S253B	C22 Monoaromatic steroid	87.076	11816070	2559518	125.7	117.5
253	S253C	C27 Reg 5β(H),10β(CH3) 20S	97.082	2731677	507977	29.1	23.3
253	S253D	C27 Dia 10β(H),5β(CH3) 20S	97.265	1441160	293804	15.3	13.5
253	S253E	C27 Dia10βH,5βCH3 20R+Reg5βH,10βCH3 20R	98.754	5731195	1242331	61.0	57.1
253	S253F	C27 Reg 5α(H),10β(CH3) 20S	98.885	10128080	2072589	107.8	95.2
253	S253G	C28 Dia 10αH,5αCH3 20s+Reg5βH,10βCH3 20S	99.276	7440421	1139262	79.2	52.3
253	S253H	C27 Reg 5α(H),10β(CH3) 20R	100.557	12902130	2301454	137.3	105.7
253	S253I	C28 Reg 5α(H),10β(CH3) 20S	100.713	5920717	1158918	63.0	53.2
253	S253J	C28 Dia 10αH,5αCH3 20R+Reg5βH,10βCH3 20R	100.922	6215956	1197169	66.1	55.0
253	S253K	C29 Dia 10βH,5βCH3 20S+Reg5βH,10βCH3 20S	101.053	24800710	4561657	263.9	209.5
253	S253L	C29 Reg 5α(H),10β(CH3) 20S	102.359	26436760	4434851	281.3	203.7
253	S253M	C28 Reg 5α(H),10β(CH3) 20R	102.647	8268276	1626057	88.0	74.7
253	S253N	C29 Dia 10βH,5βCH3 20R+Reg5βH,10βCH3 20R	102.777	14534420	2625700	154.7	120.6
253	S253O	C29 Reg 5α(H),10β(CH3) 20R	104.397	11747190	2087180	125.0	95.8
365	SH29	C29 8,14-secohopanoids	104.136	872741	100761	9.3	4.6
365	SH30	C30 8,14-secohopanoids	106.252	2579526	377504	27.5	17.3

Aromatic peaks and compounds for sample MG2H

Ion	Peak Label	Compound Name	Ret. Time	Area	Height	ppm (Area)	ppm (Hght)
230	OTP	*Ortho-terphenyl* (internal standard)	75.031	28191160	6532897	300.0	300.0
128	NAPH	Naphthalene	28.894	12044280	2079826	128.2	95.5
142	2MN	2-Methylnaphthalene	37.985	16890430	2773613	179.7	127.4
142	1MN	1-Methylnaphthalene	39.213	11420770	1879560	121.5	86.3
154	BP	Biphenyl	44.700	4710751	758014	50.1	34.8
156	2EN	2-Ethylnaphthalene	46.163	2459374	377990	26.2	17.4
156	1EN	1-Ethylnaphthalene	46.241	1578632	279662	16.8	12.8
156	26DMN	2,6-Dimethylnaphthalene	47.051	7503433	1274272	79.8	58.5
156	27DMN	2,7-Dimethylnaphthalene	47.208	8554495	1324357	91.0	60.8
156	1317DMN	1,3 & 1,7-Dimethylnaphthalenes	48.200	31088970	4293330	330.8	197.2
156	16DMN	1,6-Dimethylnaphthalene	48.462	23738130	3797609	252.6	174.4
156	23DMN	2,3-Dimethylnaphthalene	49.637	4291253	763252	45.7	35.1
156	14DMN	1,4-Dimethylnaphthalene	49.742	7944696	1265799	84.5	58.1
156	15DMN	1,5-Dimethylnaphthalene	49.846	5954406	1020226	63.4	46.9
156	12DMN	1,2-Dimethylnaphthalene	50.787	5490238	814851	58.4	37.4
168	2MBP	2-Methylbiphenyl					
168	DPM	Diphenylmethane					
168	3MBP	3-Methylbiphenyl					
168	4MBP	4-Methylbiphenyl					
168	DBF	Dibenzofuran					
170	BB_EMN	Ethyl-methyl-Naphthalene	55.123	7657865	918577	81.5	42.2
170	AB_EMN	Ethyl-methyl-Naphthalene	56.325	4829154	721773	51.4	33.1
170	137TMN	1,3,7-Trimethylnaphthalene	56.769	14518090	2471393	154.5	113.5
170	136TMN	1,3,6-Trimethylnaphthalene	57.161	51516590	8636790	548.2	396.6
170	146135T	(1,4,6+1,3,5)-Trimethylnaphthalenes	58.206	22235240	3308459	236.6	151.9
170	236TMN	2,3,6-Trimethylnaphthalene	58.494	12783840	2204265	136.0	101.2
170	127TMN	1,2,7-Trimethylnaphthalene	59.225	8634131	1533452	91.9	70.4
170	167126T	(1,6,7+1,2,6)-Trimethylnaphthalenes	59.408	31552930	5056479	335.8	232.2
170	124TMN	1,2,4-Trimethylnaphthalene	60.322	3449351	532083	36.7	24.4
170	125TMN	1,2,5-Trimethylnaphthalene	60.767	17585880	3094469	187.1	142.1
178	PHEN	Phenanthrene	70.302	232184300	51147060	2470.8	2348.7
184	1357	1,3,5,7-Tetramethylnaphthalene	64.738	12424060	2150209	132.2	98.7
184	1367	1,3,6,7-Tetramethylnaphthalene	65.887	46926320	10026160	499.4	460.4
184	1247	(1,2,4,7+1,2,4,6+1,4,6,7)-Tetramethylnaphthalenes	66.645	20102810	3610387	213.9	165.8
184	1257	1,2,5,7-Tetramethylnaphthalene	66.828	14201180	1956949	151.1	89.9
184	2367	2,3,6,7-Tetramethylnaphthalene	67.193	9540110	1824603	101.5	83.8
184	1267	1,2,6,7-Tetramethylnaphthalene	67.637	8390971	1680905	89.3	77.2
184	1237	1,2,3,7-Tetramethylnaphthalene	67.820	4834453	1022424	51.4	47.0
184	1236	1,2,3,6-Tetramethylnaphthalene	68.082	12060040	2262321	128.3	103.9
184	1256	1,2,5,6-Tetramethylnaphthalene	68.813	25247090	5394041	268.7	247.7
184	DBT	Dibenzothiophene	69.022	6975191	935553	74.2	43.0
191	BH32	C32 Benzohopane	118.139	21795530	2662473	231.9	122.3
191	BH33	C33 Benzohopane	120.386	23267340	2842125	247.6	130.5
191	BH34	C34 Benzohopane	122.371	8191537	899275	87.2	41.3
191	BH35	C35 Benzohopane	124.644	30048090	3210977	319.8	147.5
192	3MP	3-Methylphenanthrene	75.240	19629040	4480475	208.9	205.8
192	2MP	2-Methylphenanthrene	75.423	78122180	18843190	831.3	865.3
192	9MP	9-Methylphenanthrene	76.128	160849400	35402050	1711.7	1625.7
192	1MP	1-Methylphenanthrene	76.311	78615720	16019990	836.6	735.7

Ion	Peak Label	Compound Name	Ret. Time	Area	Height	ppm (Area)	ppm (Hght)
198	CAD	*(Cadalene)*	66.180	3435589	3951758	37.1	167.5
198	4MDBT	4 Methyl Dibenzothiophene	73.568	4518368	925698	48.7	39.2
198	23MDBT	2 & 3 Methyl Dibenzothiophenes	74.388	2856196	687337	30.8	29.1
198	1MDBT	1 Methyl Dibenzothiophene	75.135	5853599	1250184	63.1	53.0
206	36DMP	3,6-Dimethylphenanthrene	79.447	2938452	629982	31.7	26.7
206	26DMP	2,6-Dimethylphenanthrene	79.734	5527136	1257749	59.6	53.3
206	27DMP	2,7-Dimethylphenanthrene	79.891	10312110	1498056	111.2	63.5
206	39DMP	(3,9+3,10+2,10+1,3)-Dimethylphenanthrenes	80.361	17495830	3527473	188.7	149.5
206	29DMP	(2,9+1,6)-Dimethylphenanthrenes	80.570	18935680	3870989	204.3	164.1
206	17DMP	1,7-Dimethylphenanthrene	80.701	35387960	6869467	381.8	291.2
206	23DMP	2,3-Dimethylphenanthrene	81.010	5778226	1332635	62.3	56.5
206	19DMP	1,9-Dimethylphenanthrene	81.067	11646000	2047793	125.6	86.8
206	18DMP	1,8-Dimethylphenanthrene	81.511	9858463	1648213	106.4	69.9
206	12DMP	1,2-Dimethylphenanthrene	82.033	4473154	1000130	48.3	42.4
231	231A20	C20 Triaromatic Steroid	92.457	4799120	558653	51.8	23.7
231	231B21	C21 Triaromatic	94.861	1482785	229644	16.0	9.7
231	231C26	C26 20S Triaromatic	104.162	457585	87790	4.9	3.7
231	231D26	C27 20S & C26 20R Triaromatic	105.781	3279766	524127	35.4	22.2
231	TADMD1	C28 23,24-Cholestane Triaromatic	106.278	761369	96036	8.2	4.1
231	TADMD2	C28 23,24-Cholestane Triaromatic	106.879	3709333	801690	40.0	34.0
231	231E28	C28 20S Triaromatic	107.009	2904311	682124	31.3	28.9
231	231F27	C27 20R Triaromatic	107.767	7390454	1504771	79.7	63.8
231	TADMD3	C28 23,24-Cholestane Triaromatic	107.833	424732	307983	4.6	13.1
231	C29TA1	C29 Triaromatic	108.054	6011498	1399104	64.9	59.3
231	C29TA2	C29 Triaromatic	108.133	13285040	3080877	143.3	130.6
231	TADMD4	C28 23,24-Cholestane Triaromatic	109.099	2852733	447962	30.8	19.0
231	231G28	C28 20R Triaromatic	109.230	1586109	377828	17.1	16.0
231	TADMD5	C28 23,24-Cholestane Triaromatic	109.361	1648966	313827	17.8	13.3
231	C29TA3	C29 Triaromatic	110.667	24945580	5530775	269.1	234.5
245	C3S	C27 20S 3-Methyl Triaromatic Steroid	106.879	2983782	668078	32.2	28.3
245	C4S	C27 20S 4-Methyl Triaromatic Steroid	107.506	12099800	2479818	130.5	105.1
245	E2S	C28 20S 2-Methyl Triaromatic Steroid	108.028	2046167	459455	22.1	19.5
245	E3SC3R	C28 20S 3-Methyl & C27 20R 3-Methyl TAS	108.368	2559464	578695	27.6	24.5
245	E4SC4R	C28 20S 4-Methyl & C27 20R 4-Methyl TAS	108.995	26955710	3117811	290.8	132.2
245	S2S	C29 20S 2-Methyl Triaromatic Steroid	109.230	1993339	402473	21.5	17.1
245	DA	Triaromatic Dinosteroid a	109.301	496694	102537	5.4	4.3
245	S3S	C29 20S 3-Methyl Triaromatic Steroid	109.596	4268865	666969	46.1	28.3
245	DB	Triaromatic Dinosteroid b	110.040	3278610	636688	35.4	27.0
245	S4SE2R	C29 20S 4-Methyl & C28 20R 2-Methyl TAS	110.170	28356000	6521432	305.9	276.5
245	E3R	C28 20R 3-Methyl Triaromatic Steroid	110.379	20678490	4673357	223.1	198.1
245	E4R	C28 20R 4-Methyl Triaromatic Steroid	110.954	8026304	1422700	86.6	60.3
245	DC	Triaromatic Dinosteroid c	111.189	7128438	889880	76.9	37.7
245	DD	Triaromatic Dinosteroid d	111.320	21710180	3196123	234.2	135.5
245	S2R	C29 20R 2-Methyl Triaromatic Steroid	111.790	2429464	463923	26.2	19.7
245	S3R	C29 20R 3-Methyl Triaromatic Steroid	111.834	1227338	250569	13.2	10.6
245	DE	Triaromatic Dinosteroid e	112.156	9886246	1939291	106.7	82.2
245	S4R	C29 20R 4-Methyl Triaromatic Steroid	112.522	3334976	620394	36.0	26.3
245	DF	Triaromatic Dinosteroid f	112.652	3723638	622574	40.2	26.4
253	S253A	*C21 Ring-C Monoaromatic Steroid*	84.594	2834172	609139	30.6	25.8
253	S253B	C22 Monoaromatic steroid	87.050	6536718	1396350	70.5	59.2
253	S253C	C27 Reg 5β(H),10β(CH3) 20S	97.108	643896	108479	6.9	4.6
253	S253D	C27 Dia 10β(H),5β(CH3) 20S	97.265	1005732	198525	10.9	8.4
253	S253E	C27 Dia10βH,5βCH3 20R+Reg5βH,10βCH3 20R	98.728	3141605	598473	33.9	25.4
253	S253F	C27 Reg 5α(H),10β(CH3) 20S	98.884	3067393	667462	33.1	28.3
253	S253G	C28 Dia 10αH,5αCH3 20s+Reg5βH,10βCH3 20S	99.276	4653333	757452	50.2	32.1
253	S253H	C27 Reg 5α(H),10β(CH3) 20R	100.556	3310322	525246	35.7	22.3
253	S253I	C28 Reg 5α(H),10β(CH3) 20S	100.713	3255706	697219	35.1	29.6
253	S253J	C28 Dia 10αH,5αCH3 20R+Reg5βH,10βCH3 20R	100.896	4091561	723765	44.1	30.7
253	S253K	C29 Dia 10βH,5βCH3 20S+Reg5βH,10βCH3 20S	101.027	11784360	2249283	127.1	95.4
253	S253L	C29 Reg 5α(H),10β(CH3) 20S	102.333	8121409	1378955	87.6	58.5
253	S253M	C28 Reg 5α(H),10β(CH3) 20R	102.646	4361877	825388	47.1	35.0
253	S253N	C29 Dia 10βH,5βCH3 20R+Reg5βH,10βCH3 20R	102.751	10303420	1417670	111.2	60.1
253	S253O	C29 Reg 5α(H),10β(CH3) 20R	104.397	6832837	960641	73.7	40.7
365	SH29	C29 8,14-secohopanoids	104.135	821856	58735	8.9	2.5
365	SH30	C30 8,14-secohopanoids	106.252	1412096	272659	15.2	11.6

Aromatic peaks and compounds for sample MG2O

Ion	Peak Label	Compound Name	Ret. Time	Area	Height	ppm (Area)	ppm (Hght)
230	OTP	*Ortho-terphenyl* (internal standard)	75.031	28059860	6882049	300.0	300.0
128	NAPH	Naphthalene	28.868	19809120	3535140	211.8	154.1
142	2MN	2-Methylnaphthalene	37.959	13592710	2216148	145.3	96.6
142	1MN	1-Methylnaphthalene	39.187	9226518	1484286	98.6	64.7
154	BP	Biphenyl	44.673	4156712	671193	44.4	29.3
156	2EN	2-Ethylnaphthalene	46.110	1193362	189260	12.8	8.3
156	1EN	1-Ethylnaphthalene	46.215	702617	110379	7.5	4.8
156	26DMN	2,6-Dimethylnaphthalene	47.025	3650980	607122	39.0	26.5
156	27DMN	2,7-Dimethylnaphthalene	47.181	5613432	873484	60.0	38.1
156	1317DMN	1,3 & 1,7-Dimethylnaphthalenes	48.174	11676790	1565747	124.8	68.3
156	16DMN	1,6-Dimethylnaphthalene	48.435	17823460	2821436	190.6	123.0
156	23DMN	2,3-Dimethylnaphthalene	49.585	2102584	345764	22.5	15.1
156	14DMN	1,4-Dimethylnaphthalene	49.716	2813680	474426	30.1	20.7
156	15DMN	1,5-Dimethylnaphthalene	49.754	2252000	344039	24.1	15.0
156	12DMN	1,2-Dimethylnaphthalene	50.761	2239181	303897	23.9	13.2
168	2MBP	2-Methylbiphenyl					
168	DPM	Diphenylmethane					
168	3MBP	3-Methylbiphenyl					
168	4MBP	4-Methylbiphenyl					
168	DBF	Dibenzofuran					
170	BB_EMN	Ethyl-methyl-Naphthalene	55.097	1810994	214168	19.4	9.3
170	AB_EMN	Ethyl-methyl-Naphthalene	56.299	1526312	227401	16.3	9.9
170	137TMN	1,3,7-Trimethylnaphthalene	56.743	3960923	660760	42.3	28.8
170	136TMN	1,3,6-Trimethylnaphthalene	57.135	13027570	2044901	139.3	89.1
170	146135T	(1,4,6+1,3,5)-Trimethylnaphthalenes	58.206	6145314	910080	65.7	39.7
170	236TMN	2,3,6-Trimethylnaphthalene	58.468	4230577	748966	45.2	32.6
170	127TMN	1,2,7-Trimethylnaphthalene	59.199	4637343	837174	49.6	36.5
170	167126T	(1,6,7+1,2,6)-Trimethylnaphthalenes	59.382	11681280	1824295	124.9	79.5
170	124TMN	1,2,4-Trimethylnaphthalene	60.296	893034	127658	9.5	5.6
170	125TMN	1,2,5-Trimethylnaphthalene	60.767	8427934	1422437	90.1	62.0
178	PHEN	Phenanthrene	70.276	26734440	5771476	285.8	251.6
184	1357	1,3,5,7-Tetramethylnaphthalene	64.738	2771967	389813	29.6	17.0
184	1367	1,3,6,7-Tetramethylnaphthalene	65.887	8968652	1811639	95.9	79.0
184	1247	(1,2,4,7+1,2,4,6+1,4,6,7)-Tetramethylnaphthalenes	66.619	6595471	1153342	70.5	50.3
184	1257	1,2,5,7-Tetramethylnaphthalene	66.802	3201913	572936	34.2	25.0
184	2367	2,3,6,7-Tetramethylnaphthalene	67.193	1389162	230276	14.9	10.0
184	1267	1,2,6,7-Tetramethylnaphthalene	67.611	2254529	407268	24.1	17.8
184	1237	1,2,3,7-Tetramethylnaphthalene	67.794	1274651	206702	13.6	9.0
184	1236	1,2,3,6-Tetramethylnaphthalene	68.082	3899770	719117	41.7	31.3
184	1256	1,2,5,6-Tetramethylnaphthalene	68.787	12659260	2725985	135.3	118.8
184	DBT	Dibenzothiophene	68.996	2608247	439245	27.9	19.1
191	BH32	C32 Benzohopane	118.113	30098480	4123463	321.8	179.7
191	BH33	C33 Benzohopane	120.386	36875300	4249924	394.3	185.3
191	BH34	C34 Benzohopane	122.371	13062250	1650765	139.7	72.0
191	BH35	C35 Benzohopane	124.670	11173700	1043398	119.5	45.5
192	3MP	3-Methylphenanthrene	75.214	2769863	584145	29.6	25.5
192	2MP	2-Methylphenanthrene	75.397	5270522	1160184	56.3	50.6
192	9MP	9-Methylphenanthrene	76.102	13776490	2937992	147.3	128.1
192	1MP	1-Methylphenanthrene	76.285	11156760	2034846	119.3	88.7

Ion	Peak Label	Compound Name	Ret. Time	Area	Height	ppm (Area)	ppm (Hght)
198	CAD	*(Cadalene)*	66.180	3931779	4007727	42.0	174.7
198	4MDBT	4 Methyl Dibenzothiophene	73.568	1801750	331317	19.3	14.4
198	23MDBT	2 & 3 Methyl Dibenzothiophenes	74.404	2935471	399347	31.4	17.4
198	1MDBT	1 Methyl Dibenzothiophene	75.135	4279648	887583	45.8	38.7
206	36DMP	3,6-Dimethylphenanthrene	79.421	1407055	226649	15.0	9.9
206	26DMP	2,6-Dimethylphenanthrene	79.735	2129599	465828	22.8	20.3
206	27DMP	2,7-Dimethylphenanthrene	79.892	4400151	694991	47.0	30.3
206	39DMP	(3,9+3,10+2,10+1,3)-Dimethylphenanthrenes	80.336	8622752	1659599	92.2	72.3
206	29DMP	(2,9+1,6)-Dimethylphenanthrenes	80.571	6193476	1513125	66.2	66.0
206	17DMP	1,7-Dimethylphenanthrene	80.702	13600200	1920052	145.4	83.7
206	23DMP	2,3-Dimethylphenanthrene	81.020	2438106	570796	26.1	24.9
206	19DMP	1,9-Dimethylphenanthrene	81.093	4399107	885621	47.0	38.6
206	18DMP	1,8-Dimethylphenanthrene	81.511	2916885	655681	31.2	28.6
206	12DMP	1,2-Dimethylphenanthrene	82.034	1624003	331028	17.4	14.4
231	231A20	C20 Triaromatic Steroid	92.380	1954869	296347	20.9	12.9
231	231B21	C21 Triaromatic	94.861	773477	124289	8.3	5.4
231	231C26	C26 20S Triaromatic	104.162	281528	55312	3.0	2.4
231	231D26	C27 20S & C26 20R Triaromatic	105.782	2142512	352278	22.9	15.4
231	TADMD1	C28 23,24-Cholestane Triaromatic	106.487	882102	212505	9.4	9.3
231	TADMD2	C28 23,24-Cholestane Triaromatic	106.879	1433289	357491	15.3	15.6
231	231E28	C28 20S Triaromatic	107.010	1859295	347730	19.9	15.2
231	231F27	C27 20R Triaromatic	107.741	1814915	414072	19.4	18.1
231	TADMD3	C28 23,24-Cholestane Triaromatic	107.783	498296	287775	5.3	12.5
231	C29TA1	C29 Triaromatic	108.029	2340190	641157	25.0	27.9
231	C29TA2	C29 Triaromatic	108.133	11431770	2921992	122.2	127.4
231	TADMD4	C28 23,24-Cholestane Triaromatic	109.152	3708142	839656	39.6	36.6
231	231G28	C28 20R Triaromatic	109.185	954238	392714	10.2	17.1
231	TADMD5	C28 23,24-Cholestane Triaromatic	109.361	981849	195292	10.5	8.5
231	C29TA3	C29 Triaromatic	110.641	11775880	2636650	125.9	114.9
245	C3S	C27 20S 3-Methyl Triaromatic Steroid	106.879	1882500	382478	20.1	16.7
245	C4S	C27 20S 4-Methyl Triaromatic Steroid	107.480	11637810	2363281	124.4	103.0
245	E2S	C28 20S 2-Methyl Triaromatic Steroid	108.029	1104981	275630	11.8	12.0
245	E3SC3R	C28 20S 3-Methyl & C27 20R 3-Methyl TAS	108.342	2341251	379436	25.0	16.5
245	E4SC4R	C28 20S 4-Methyl & C27 20R 4-Methyl TAS	109.021	18918820	2266898	202.3	98.8
245	S2S	C29 20S 2-Methyl Triaromatic Steroid	109.204	1253326	195792	13.4	8.5
245	DA	Triaromatic Dinosteroid a	109.325	633765	95558	6.8	4.2
245	S3S	C29 20S 3-Methyl Triaromatic Steroid	109.570	3266934	439121	34.9	19.1
245	DB	Triaromatic Dinosteroid b	110.014	477120	125125	5.1	5.5
245	S4SE2R	C29 20S 4-Methyl & C28 20R 2-Methyl TAS	110.249	9778761	2003782	104.5	87.3
245	E3R	C28 20R 3-Methyl Triaromatic Steroid	110.354	11476730	2546228	122.7	111.0
245	E4R	C28 20R 4-Methyl Triaromatic Steroid	110.955	6674224	998824	71.4	43.5
245	DC	Triaromatic Dinosteroid c	111.138	2331594	378246	24.9	16.5
245	DD	Triaromatic Dinosteroid d	111.320	8009604	1286496	85.6	56.1
245	S2R	C29 20R 2-Methyl Triaromatic Steroid	111.765	2181733	336269	23.3	14.7
245	S3R	C29 20R 3-Methyl Triaromatic Steroid	111.848	694183	146610	7.4	6.4
245	DE	Triaromatic Dinosteroid e	112.073	897169	231942	9.6	10.1
245	S4R	C29 20R 4-Methyl Triaromatic Steroid	112.522	4144243	635547	44.3	27.7
245	DF	Triaromatic Dinosteroid f	112.627	1182035	287322	12.6	12.5
253	S253A	*C21 Ring-C Monoaromatic Steroid*	84.594	2723608	638866	29.1	27.8
253	S253B	C22 Monoaromatic steroid	87.050	8172092	1968783	87.4	85.8
253	S253C	C27 Reg 5β(H),10β(CH3) 20S	97.082	381705	68764	4.1	3.0
253	S253D	C27 Dia 10β(H),5β(CH3) 20S	97.265	910545	145636	9.7	6.3
253	S253E	C27 Dia10βH,5βCH3 20R+Reg5βH,10βCH3 20R	98.728	2715618	488189	29.0	21.3
253	S253F	C27 Reg 5α(H),10β(CH3) 20S	98.859	1780575	367758	19.0	16.0
253	S253G	C28 Dia 10αH,5αCH3 20s+Reg5βH,10βCH3 20S	99.277	4738585	834906	50.7	36.4
253	S253H	C27 Reg 5α(H),10β(CH3) 20R	100.557	1986579	377977	21.2	16.5
253	S253I	C28 Reg 5α(H),10β(CH3) 20S	100.714	3694083	849280	39.5	37.0
253	S253J	C28 Dia 10αH,5αCH3 20R+Reg5βH,10βCH3 20R	100.896	3421785	772340	36.6	33.7
253	S253K	C29 Dia 10βH,5βCH3 20S+Reg5βH,10βCH3 20S	101.027	21144340	4675985	226.1	203.8
253	S253L	C29 Reg 5α(H),10β(CH3) 20S	102.333	9829942	1706083	105.1	74.4
253	S253M	C28 Reg 5α(H),10β(CH3) 20R	102.647	6355352	1092348	67.9	47.6
253	S253N	C29 Dia 10βH,5βCH3 20R+Reg5βH,10βCH3 20R	102.751	12899650	2694954	137.9	117.5
253	S253O	C29 Reg 5α(H),10β(CH3) 20R	104.397	8301236	1539612	88.8	67.1
365	SH29	C29 8,14-secohopanoids	104.214	667165	121860	7.1	5.3
365	SH30	C30 8,14-secohopanoids	106.226	1431269	275465	15.3	12.0

Aromatic peaks and compounds for sample MG4K

Ion	Peak Label	Compound Name	Ret. Time	Area	Height	ppm (Area)	ppm (Hght)
230	OTP	*Ortho-terphenyl* (internal standard)	74.979	20227290	5184611	300.0	300.0
128	NAPH	Naphthalene	28.815	2087694	325196	31.0	18.8
142	2MN	2-Methylnaphthalene	37.907	5583019	840708	82.8	48.6
142	1MN	1-Methylnaphthalene	39.109	3668355	539800	54.4	31.2
154	BP	Biphenyl	44.621	2678326	360097	39.7	20.8
156	2EN	2-Ethylnaphthalene	46.058	1042432	147967	15.5	8.6
156	1EN	1-Ethylnaphthalene	46.146	394430	83478	5.9	4.8
156	26DMN	2,6-Dimethylnaphthalene	46.973	3362810	533465	49.9	30.9
156	27DMN	2,7-Dimethylnaphthalene	47.129	3945821	574737	58.5	33.3
156	1317DMN	1,3 & 1,7-Dimethylnaphthalenes	48.096	9014882	1215001	133.7	70.3
156	16DMN	1,6-Dimethylnaphthalene	48.357	10476710	1665117	155.4	96.4
156	23DMN	2,3-Dimethylnaphthalene	49.533	1251548	239528	18.6	13.9
156	14DMN	1,4-Dimethylnaphthalene	49.637	2792343	369995	41.4	21.4
156	15DMN	1,5-Dimethylnaphthalene	49.742	1620536	307295	24.0	17.8
156	12DMN	1,2-Dimethylnaphthalene	50.708	1776622	227667	26.4	13.2
168	2MBP	2-Methylbiphenyl					
168	DPM	Diphenylmethane					
168	3MBP	3-Methylbiphenyl					
168	4MBP	4-Methylbiphenyl					
168	DBF	Dibenzofuran					
170	BB_EMN	Ethyl-methyl-Naphthalene	55.019	2485930	292979	36.9	17.0
170	AB_EMN	Ethyl-methyl-Naphthalene	56.247	1522847	203537	22.6	11.8
170	137TMN	1,3,7-Trimethylnaphthalene	56.691	6229993	1016752	92.4	58.8
170	136TMN	1,3,6-Trimethylnaphthalene	57.057	17582920	2947753	260.8	170.6
170	146135T	(1,4,6+1,3,5)-Trimethylnaphthalenes	58.128	6801885	1013112	100.9	58.6
170	236TMN	2,3,6-Trimethylnaphthalene	58.415	5685396	894114	84.3	51.7
170	127TMN	1,2,7-Trimethylnaphthalene	59.147	4020635	674651	59.6	39.0
170	167126T	(1,6,7+1,2,6)-Trimethylnaphthalenes	59.330	10846200	1608413	160.9	93.1
170	124TMN	1,2,4-Trimethylnaphthalene	60.244	1234568	158377	18.3	9.2
170	125TMN	1,2,5-Trimethylnaphthalene	60.688	6700715	1062435	99.4	61.5
178	PHEN	Phenanthrene	70.224	12037240	2329389	178.5	134.8
184	1357	1,3,5,7-Tetramethylnaphthalene	64.659	3901787	559737	57.9	32.4
184	1367	1,3,6,7-Tetramethylnaphthalene	65.835	21797530	4397231	323.3	254.4
184	1247	(1,2,4,7+1,2,4,6+1,4,6,7)-Tetramethylnaphthalenes	66.593	8451045	1527601	125.3	88.4
184	1257	1,2,5,7-Tetramethylnaphthalene	66.749	7582670	814416	112.5	47.1
184	2367	2,3,6,7-Tetramethylnaphthalene	67.141	2121770	372047	31.5	21.5
184	1267	1,2,6,7-Tetramethylnaphthalene	67.559	3047041	540522	45.2	31.3
184	1237	1,2,3,7-Tetramethylnaphthalene	67.768	1481784	275353	22.0	15.9
184	1236	1,2,3,6-Tetramethylnaphthalene	68.029	5027471	975209	74.6	56.4
184	1256	1,2,5,6-Tetramethylnaphthalene	68.735	6884320	1357093	102.1	78.5
184	DBT	Dibenzothiophene	69.037	2257933	248902	33.5	14.4
191	BH32	C32 Benzohopane	118.087	41226080	6455823	611.4	373.6
191	BH33	C33 Benzohopane	120.360	45857620	6064606	680.1	350.9
191	BH34	C34 Benzohopane	122.319	15943930	2159810	236.5	125.0
191	BH35	C35 Benzohopane	124.827	3705565	412689	55.0	23.9
192	3MP	3-Methylphenanthrene	75.188	3638482	839556	54.0	48.6
192	2MP	2-Methylphenanthrene	75.371	7198901	1530173	106.8	88.5
192	9MP	9-Methylphenanthrene	76.050	17295890	3717469	256.5	215.1
192	1MP	1-Methylphenanthrene	76.233	18159050	3576167	269.3	206.9

Ion	Peak Label	Compound Name	Ret. Time	Area	Height	ppm (Area)	ppm (Hght)
198	CAD	*(Cadalene)*	65.966	338882	78152	5.0	4.5
198	4MDBT	4 Methyl Dibenzothiophene	73.516	2263828	403729	33.6	23.4
198	23MDBT	2 & 3 Methyl Dibenzothiophenes	74.352	4027173	594798	59.7	34.4
198	1MDBT	1 Methyl Dibenzothiophene	75.083	5968609	1065756	88.5	61.7
206	36DMP	3,6-Dimethylphenanthrene	79.369	2166569	345807	32.1	20.0
206	26DMP	2,6-Dimethylphenanthrene	79.709	3391141	681673	50.3	39.4
206	27DMP	2,7-Dimethylphenanthrene	79.839	6140277	1035217	91.1	59.9
206	39DMP	(3,9+3,10+2,10+1,3)-Dimethylphenanthrenes	80.310	14398880	3091373	213.6	178.9
206	29DMP	(2,9+1,6)-Dimethylphenanthrenes	80.519	13548580	2399237	200.9	138.8
206	17DMP	1,7-Dimethylphenanthrene	80.675	18952240	4028390	281.1	233.1
206	23DMP	2,3-Dimethylphenanthrene	80.982	4182606	833670	62.0	48.2
206	19DMP	1,9-Dimethylphenanthrene	81.067	9127535	1531851	135.4	88.6
206	18DMP	1,8-Dimethylphenanthrene	81.485	7377773	1359167	109.4	78.6
206	12DMP	1,2-Dimethylphenanthrene	81.982	2968282	654963	44.0	37.9
231	231A20	C20 Triaromatic Steroid					
231	231B21	C21 Triaromatic					
231	231C26	C26 20S Triaromatic					
231	231D26	C27 20S & C26 20R Triaromatic					
231	TADMD1	C28 23,24-Cholestane Triaromatic					
231	TADMD2	C28 23,24-Cholestane Triaromatic					
231	231E28	C28 20S Triaromatic					
231	231F27	C27 20R Triaromatic					
231	TADMD3	C28 23,24-Cholestane Triaromatic					
231	C29TA1	C29 Triaromatic					
231	C29TA2	C29 Triaromatic					
231	TADMD4	C28 23,24-Cholestane Triaromatic					
231	231G28	C28 20R Triaromatic					
231	TADMD5	C28 23,24-Cholestane Triaromatic					
231	C29TA3	C29 Triaromatic					
245	C3S	C27 20S 3-Methyl Triaromatic Steroid					
245	C4S	C27 20S 4-Methyl Triaromatic Steroid					
245	E2S	C28 20S 2-Methyl Triaromatic Steroid					
245	E3SC3R	C28 20S 3-Methyl & C27 20R 3-Methyl TAS					
245	E4SC4R	C28 20S 4-Methyl & C27 20R 4-Methyl TAS					
245	S2S	C29 20S 2-Methyl Triaromatic Steroid					
245	DA	Triaromatic Dinosteroid a					
245	S3S	C29 20S 3-Methyl Triaromatic Steroid					
245	DB	Triaromatic Dinosteroid b					
245	S4SE2R	C29 20S 4-Methyl & C28 20R 2-Methyl TAS					
245	E3R	C28 20R 3-Methyl Triaromatic Steroid					
245	E4R	C28 20R 4-Methyl Triaromatic Steroid					
245	DC	Triaromatic Dinosteroid c					
245	DD	Triaromatic Dinosteroid d					
245	S2R	C29 20R 2-Methyl Triaromatic Steroid					
245	S3R	C29 20R 3-Methyl Triaromatic Steroid					
245	DE	Triaromatic Dinosteroid e					
245	S4R	C29 20R 4-Methyl Triaromatic Steroid					
245	DF	Triaromatic Dinosteroid f					
253	S253A	*C21 Ring-C Monoaromatic Steroid*	84.542	3161613	669302	46.9	38.7
253	S253B	C22 Monoaromatic steroid	87.024	8650424	1905723	128.3	110.3
253	S253C	C27 Reg 5β(H),10β(CH3) 20S	97.056	428245	81465	6.4	4.7
253	S253D	C27 Dia 10β(H),5β(CH3) 20S	97.213	500992	104333	7.4	6.0
253	S253E	C27 Dia10βH,5βCH3 20R+Reg5βH,10βCH3 20R	98.702	1596217	233214	23.7	13.5
253	S253F	C27 Reg 5α(H),10β(CH3) 20S	98.833	956854	187377	14.2	10.8
253	S253G	C28 Dia 10αH,5αCH3 20s+Reg5βH,10βCH3 20S	99.251	2525024	393204	37.5	22.8
253	S253H	C27 Reg 5α(H),10β(CH3) 20R	100.531	2883962	590570	42.8	34.2
253	S253I	C28 Reg 5α(H),10β(CH3) 20S	100.687	2903295	609055	43.1	35.2
253	S253J	C28 Dia 10αH,5αCH3 20R+Reg5βH,10βCH3 20R	100.870	2025733	411606	30.0	23.8
253	S253K	C29 Dia 10βH,5βCH3 20S+Reg5βH,10βCH3 20S	101.001	16807720	3452331	249.3	199.8
253	S253L	C29 Reg 5α(H),10β(CH3) 20S	102.307	10978010	2063604	162.8	119.4
253	S253M	C28 Reg 5α(H),10β(CH3) 20R	102.621	4821567	819663	71.5	47.4
253	S253N	C29 Dia 10βH,5βCH3 20R+Reg5βH,10βCH3 20R	102.725	8626183	1834374	127.9	106.1
253	S253O	C29 Reg 5α(H),10β(CH3) 20R	104.371	8675154	1595204	128.7	92.3
365	SH29	C29 8,14-secohopanoids	104.188	941306	195510	14.0	11.3
365	SH30	C30 8,14-secohopanoids	106.226	2377827	446944	35.3	25.9

Aromatic peaks and compounds for sample MG3S

Ion	Peak Label	Compound Name	Ret. Time	Area	Height	ppm (Area)	ppm (Hght)
230	OTP	*Ortho-terphenyl* (internal standard)	74.979	8625591	2098208	300.0	300.0
128	NAPH	Naphthalene	28.841	726236	110650	25.3	15.8
142	2MN	2-Methylnaphthalene	37.933	3440970	504091	119.7	72.1
142	1MN	1-Methylnaphthalene	39.135	2216024	349811	77.1	50.0
154	BP	Biphenyl	44.647	1788381	230200	62.2	32.9
156	2EN	2-Ethylnaphthalene	46.084	656823	114583	22.8	16.4
156	1EN	1-Ethylnaphthalene	46.128	432428	80836	15.0	11.6
156	26DMN	2,6-Dimethylnaphthalene	46.972	2718696	438851	94.6	62.7
156	27DMN	2,7-Dimethylnaphthalene	47.129	3305513	461993	115.0	66.1
156	1317DMN	1,3 & 1,7-Dimethylnaphthalenes	48.122	8467418	1162674	294.5	166.2
156	16DMN	1,6-Dimethylnaphthalene	48.383	10744290	1652830	373.7	236.3
156	23DMN	2,3-Dimethylnaphthalene	49.559	1317145	231019	45.8	33.0
156	14DMN	1,4-Dimethylnaphthalene	49.663	2559382	399218	89.0	57.1
156	15DMN	1,5-Dimethylnaphthalene	49.768	2014566	324080	70.1	46.3
156	12DMN	1,2-Dimethylnaphthalene	50.708	1542655	221995	53.7	31.7
168	2MBP	2-Methylbiphenyl					
168	DPM	Diphenylmethane					
168	3MBP	3-Methylbiphenyl					
168	4MBP	4-Methylbiphenyl					
168	DBF	Dibenzofuran					
170	BB_EMN	Ethyl-methyl-Naphthalene	55.045	2337640	290158	81.3	41.5
170	AB_EMN	Ethyl-methyl-Naphthalene	56.247	1666087	244732	57.9	35.0
170	137TMN	1,3,7-Trimethylnaphthalene	56.691	7081773	1142485	246.3	163.4
170	136TMN	1,3,6-Trimethylnaphthalene	57.083	22965220	3673951	798.7	525.3
170	146135T	(1,4,6+1,3,5)-Trimethylnaphthalenes	58.154	8666833	1287993	301.4	184.2
170	236TMN	2,3,6-Trimethylnaphthalene	58.415	6829511	1114727	237.5	159.4
170	127TMN	1,2,7-Trimethylnaphthalene	59.173	4776173	837291	166.1	119.7
170	167126T	(1,6,7+1,2,6)-Trimethylnaphthalenes	59.329	18452190	2804219	641.8	400.9
170	124TMN	1,2,4-Trimethylnaphthalene	60.244	1022011	152756	35.5	21.8
170	125TMN	1,2,5-Trimethylnaphthalene	60.714	8386193	1446427	291.7	206.8
178	PHEN	Phenanthrene	70.250	18531720	3655920	644.5	522.7
184	1357	1,3,5,7-Tetramethylnaphthalene	64.685	2715938	406948	94.5	58.2
184	1367	1,3,6,7-Tetramethylnaphthalene	65.835	17789230	3785269	618.7	541.2
184	1247	(1,2,4,7+1,2,4,6+1,4,6,7)-Tetramethylnaphthalenes	66.592	5599338	1024643	194.7	146.5
184	1257	1,2,5,7-Tetramethylnaphthalene	66.775	3963452	573866	137.9	82.1
184	2367	2,3,6,7-Tetramethylnaphthalene	67.141	1474977	297275	51.3	42.5
184	1267	1,2,6,7-Tetramethylnaphthalene	67.585	2272194	438996	79.0	62.8
184	1237	1,2,3,7-Tetramethylnaphthalene	67.768	962632	197800	33.5	28.3
184	1236	1,2,3,6-Tetramethylnaphthalene	68.029	3414916	690770	118.8	98.8
184	1256	1,2,5,6-Tetramethylnaphthalene	68.735	8753955	1781947	304.5	254.8
184	DBT	Dibenzothiophene	68.970	2093240	273463	72.8	39.1
191	BH32	C32 Benzohopane	118.087	3377263	518668	117.5	74.2
191	BH33	C33 Benzohopane	120.333	4409518	579024	153.4	82.8
191	BH34	C34 Benzohopane	122.319	1951068	254787	67.9	36.4
191	BH35	C35 Benzohopane	124.827	663238	62607	23.1	9.0
192	3MP	3-Methylphenanthrene	75.188	3331511	721514	115.9	103.2
192	2MP	2-Methylphenanthrene	75.370	7193241	1585470	250.2	226.7
192	9MP	9-Methylphenanthrene	76.050	12410210	2564146	431.6	366.6
192	1MP	1-Methylphenanthrene	76.233	12211970	2345249	424.7	335.3

198	CAD	*(Cadalene)*	65.991	37689	9518	1.3	1.4
198	4MDBT	4 Methyl Dibenzothiophene	73.515	1566757	316860	54.5	45.3
198	23MDBT	2 & 3 Methyl Dibenzothiophenes	74.352	1808840	242669	62.9	34.7
198	1MDBT	1 Methyl Dibenzothiophene	75.109	2345059	450388	81.6	64.4
206	36DMP	3,6-Dimethylphenanthrene	79.447	1179893	202188	41.0	28.9
206	26DMP	2,6-Dimethylphenanthrene	79.709	2030391	498943	70.6	71.3
206	27DMP	2,7-Dimethylphenanthrene	79.813	3885173	642329	135.1	91.8
206	39DMP	(3,9+3,10+2,10+1,3)-Dimethylphenanthrenes	80.309	6582114	1428741	228.9	204.3
206	29DMP	(2,9+1,6)-Dimethylphenanthrenes	80.518	5975787	1025111	207.8	146.6
206	17DMP	1,7-Dimethylphenanthrene	80.675	12666010	2346603	440.5	335.5
206	23DMP	2,3-Dimethylphenanthrene	80.936	2293236	459083	79.8	65.6
206	19DMP	1,9-Dimethylphenanthrene	81.041	3104683	547648	108.0	78.3
206	18DMP	1,8-Dimethylphenanthrene	81.485	2651517	423233	92.2	60.5
206	12DMP	1,2-Dimethylphenanthrene	81.981	1385411	279348	48.2	39.9
231	231A20	C20 Triaromatic Steroid					
231	231B21	C21 Triaromatic					
231	231C26	C26 20S Triaromatic					
231	231D26	C27 20S & C26 20R Triaromatic					
231	TADMD1	C28 23,24-Cholestane Triaromatic					
231	TADMD2	C28 23,24-Cholestane Triaromatic					
231	231E28	C28 20S Triaromatic					
231	231F27	C27 20R Triaromatic					
231	TADMD3	C28 23,24-Cholestane Triaromatic					
231	C29TA1	C29 Triaromatic					
231	C29TA2	C29 Triaromatic					
231	TADMD4	C28 23,24-Cholestane Triaromatic					
231	231G28	C28 20R Triaromatic					
231	TADMD5	C28 23,24-Cholestane Triaromatic					
231	C29TA3	C29 Triaromatic					
245	C3S	C27 20S 3-Methyl Triaromatic Steroid					
245	C4S	C27 20S 4-Methyl Triaromatic Steroid					
245	E2S	C28 20S 2-Methyl Triaromatic Steroid					
245	E3SC3R	C28 20S 3-Methyl & C27 20R 3-Methyl TAS					
245	E4SC4R	C28 20S 4-Methyl & C27 20R 4-Methyl TAS					
245	S2S	C29 20S 2-Methyl Triaromatic Steroid					
245	DA	Triaromatic Dinosteroid a					
245	S3S	C29 20S 3-Methyl Triaromatic Steroid					
245	DB	Triaromatic Dinosteroid b					
245	S4SE2R	C29 20S 4-Methyl & C28 20R 2-Methyl TAS					
245	E3R	C28 20R 3-Methyl Triaromatic Steroid					
245	E4R	C28 20R 4-Methyl Triaromatic Steroid					
245	DC	Triaromatic Dinosteroid c					
245	DD	Triaromatic Dinosteroid d					
245	S2R	C29 20R 2-Methyl Triaromatic Steroid					
245	S3R	C29 20R 3-Methyl Triaromatic Steroid					
245	DE	Triaromatic Dinosteroid e					
245	S4R	C29 20R 4-Methyl Triaromatic Steroid					
245	DF	Triaromatic Dinosteroid f					
253	S253A	*C21 Ring-C Monoaromatic Steroid*	84.542	1162430	289881	40.4	41.4
253	S253B	C22 Monoaromatic steroid	87.024	2529818	547163	88.0	78.2
253	S253C	C27 Reg 5β(H),10β(CH3) 20S	97.056	750386	131715	26.1	18.8
253	S253D	C27 Dia 10β(H),5β(CH3) 20S	97.213	486297	104133	16.9	14.9
253	S253E	C27 Dia10βH,5βCH3 20R+Reg5βH,10βCH3 20R	98.702	1369407	223063	47.6	31.9
253	S253F	C27 Reg 5α(H),10β(CH3) 20S	98.832	699150	133137	24.3	19.0
253	S253G	C28 Dia 10αH,5αCH3 20s+Reg5βH,10βCH3 20S	99.250	1781334	329383	62.0	47.1
253	S253H	C27 Reg 5α(H),10β(CH3) 20R	100.530	1963866	411385	68.3	58.8
253	S253I	C28 Reg 5α(H),10β(CH3) 20S	100.687	1463490	336585	50.9	48.1
253	S253J	C28 Dia 10αH,5αCH3 20R+Reg5βH,10βCH3 20R	100.870	1106681	253738	38.5	36.3
253	S253K	C29 Dia 10βH,5βCH3 20S+Reg5βH,10βCH3 20S	101.001	7903940	1695366	274.9	242.4
253	S253L	C29 Reg 5α(H),10β(CH3) 20S	102.307	5832481	1125315	202.9	160.9
253	S253M	C28 Reg 5α(H),10β(CH3) 20R	102.620	1806898	389300	62.8	55.7
253	S253N	C29 Dia 10βH,5βCH3 20R+Reg5βH,10βCH3 20R	102.725	3966991	964211	138.0	137.9
253	S253O	C29 Reg 5α(H),10β(CH3) 20R	104.371	2536460	482525	88.2	69.0
365	SH29	C29 8,14-secohopanoids	104.188	251205	44440	8.7	6.4
365	SH30	C30 8,14-secohopanoids	106.200	480160	93972	16.7	13.4

Aromatic peaks and compounds for sample MG4D

230	OTP	*Ortho-terphenyl* (internal standard)	74.978	14712690	3566096	300.0	300.0
128	NAPH	Naphthalene	28.815	1929533	292425	39.3	24.6
142	2MN	2-Methylnaphthalene	37.907	7348033	1144839	149.8	96.3
142	1MN	1-Methylnaphthalene	39.135	5116186	787538	104.3	66.3
154	BP	Biphenyl	44.621	3748911	514542	76.4	43.3
156	2EN	2-Ethylnaphthalene	46.058	1744093	269527	35.6	22.7
156	1EN	1-Ethylnaphthalene	46.128	984103	180309	20.1	15.2
156	26DMN	2,6-Dimethylnaphthalene	46.972	6789224	1088765	138.4	91.6
156	27DMN	2,7-Dimethylnaphthalene	47.129	7574435	1167434	154.4	98.2
156	1317DMN	1,3 & 1,7-Dimethylnaphthalenes	48.096	24153600	3212507	492.5	270.3
156	16DMN	1,6-Dimethylnaphthalene	48.357	30781270	4976631	627.6	418.7
156	23DMN	2,3-Dimethylnaphthalene	49.532	3530208	713432	72.0	60.0
156	14DMN	1,4-Dimethylnaphthalene	49.637	8666065	1164883	176.7	98.0
156	15DMN	1,5-Dimethylnaphthalene	49.741	4982176	966297	101.6	81.3
156	12DMN	1,2-Dimethylnaphthalene	50.708	4330398	628141	88.3	52.8
168	2MBP	2-Methylbiphenyl					
168	DPM	Diphenylmethane					
168	3MBP	3-Methylbiphenyl					
168	4MBP	4-Methylbiphenyl					
168	DBF	Dibenzofuran					
170	BB_EMN	Ethyl-methyl-Naphthalene	55.019	6489643	759531	132.3	63.9
170	AB_EMN	Ethyl-methyl-Naphthalene	56.247	5266900	767401	107.4	64.6
170	137TMN	1,3,7-Trimethylnaphthalene	56.691	22624430	3828139	461.3	322.0
170	136TMN	1,3,6-Trimethylnaphthalene	57.057	78178870	12987110	1594.1	1092.5
170	146135T	(1,4,6+1,3,5)-Trimethylnaphthalenes	58.128	29199530	4475608	595.4	376.5
170	236TMN	2,3,6-Trimethylnaphthalene	58.415	21705050	3702748	442.6	311.5
170	127TMN	1,2,7-Trimethylnaphthalene	59.147	18041100	3147418	367.9	264.8
170	167126T	(1,6,7+1,2,6)-Trimethylnaphthalenes	59.329	60946280	9578711	1242.7	805.8
170	124TMN	1,2,4-Trimethylnaphthalene	60.244	3775603	634338	77.0	53.4
170	125TMN	1,2,5-Trimethylnaphthalene	60.714	31797850	5282813	648.4	444.4
178	PHEN	Phenanthrene	70.224	70071150	14044510	1428.8	1181.5
184	1357	1,3,5,7-Tetramethylnaphthalene	64.659	10791440	1615971	220.0	135.9
184	1367	1,3,6,7-Tetramethylnaphthalene	65.835	67862520	14589760	1383.8	1227.4
184	1247	(1,2,4,7+1,2,4,6+1,4,6,7)-Tetramethylnaphthalenes	66.592	25308760	4933871	516.1	415.1
184	1257	1,2,5,7-Tetramethylnaphthalene	66.775	17226680	2636578	351.3	221.8
184	2367	2,3,6,7-Tetramethylnaphthalene	67.141	5401096	1104729	110.1	92.9
184	1267	1,2,6,7-Tetramethylnaphthalene	67.559	8223569	1647356	167.7	138.6
184	1237	1,2,3,7-Tetramethylnaphthalene	67.768	4322816	862838	88.1	72.6
184	1236	1,2,3,6-Tetramethylnaphthalene	68.029	13668560	2817005	278.7	237.0
184	1256	1,2,5,6-Tetramethylnaphthalene	68.734	33920580	7015088	691.7	590.1
184	DBT	Dibenzothiophene	68.944	5826722	721247	118.8	60.7
191	BH32	C32 Benzohopane	118.086	15143570	2579249	308.8	217.0
191	BH33	C33 Benzohopane	120.333	15120310	2073020	308.3	174.4
191	BH34	C34 Benzohopane	122.319	9031769	1206249	184.2	101.5
191	BH35	C35 Benzohopane	124.801	2203935	213616	44.9	18.0
192	3MP	3-Methylphenanthrene	75.187	12125670	2802928	247.2	235.8
192	2MP	2-Methylphenanthrene	75.370	24692940	5446853	503.5	458.2
192	9MP	9-Methylphenanthrene	76.050	48324840	10399320	985.4	874.8
192	1MP	1-Methylphenanthrene	76.232	47583110	10338660	970.2	869.7

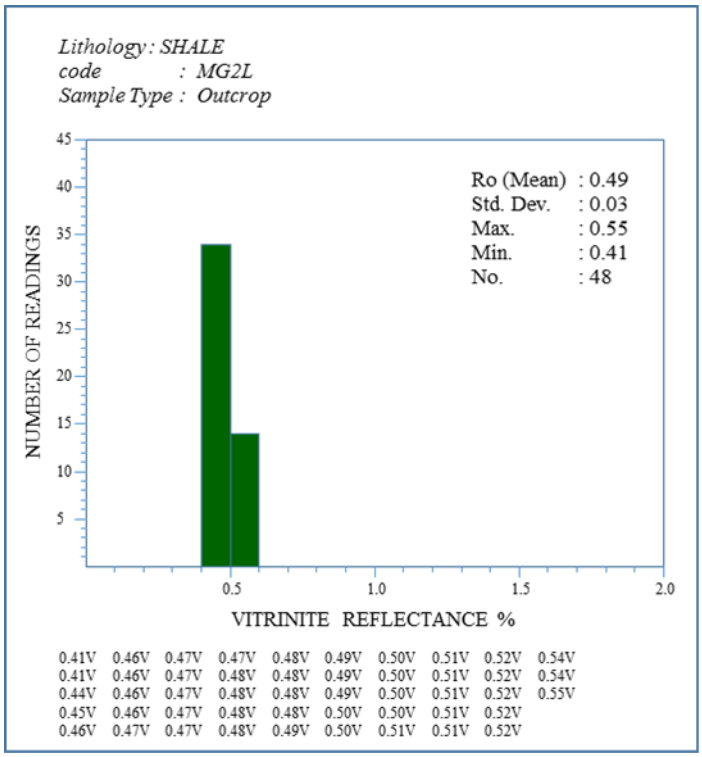
198	CAD	*(Cadalene)*	65.991	445611	76903	9.1	6.5
198	4MDBT	4 Methyl Dibenzothiophene	73.515	4544495	935172	92.7	78.7
198	23MDBT	2 & 3 Methyl Dibenzothiophenes	74.351	6365692	895605	129.8	75.3
198	1MDBT	1 Methyl Dibenzothiophene	75.083	11684820	2366614	238.3	199.1
206	36DMP	3,6-Dimethylphenanthrene	79.447	1809826	395100	36.9	33.2
206	26DMP	2,6-Dimethylphenanthrene	79.682	5220042	1069712	106.4	90.0
206	27DMP	2,7-Dimethylphenanthrene	79.813	5524664	1050654	112.7	88.4
206	39DMP	(3,9+3,10+2,10+1,3)-Dimethylphenanthrenes	80.309	18076920	3966290	368.6	333.7
206	29DMP	(2,9+1,6)-Dimethylphenanthrenes	80.518	20160610	3322561	411.1	279.5
206	17DMP	1,7-Dimethylphenanthrene	80.675	35091640	7993468	715.5	672.5
206	23DMP	2,3-Dimethylphenanthrene	80.936	4875553	1027393	99.4	86.4
206	19DMP	1,9-Dimethylphenanthrene	81.067	9371815	1654208	191.1	139.2
206	18DMP	1,8-Dimethylphenanthrene	81.485	8055318	1553216	164.3	130.7
206	12DMP	1,2-Dimethylphenanthrene	81.981	4442193	970994	90.6	81.7
231	231A20	C20 Triaromatic Steroid					
231	231B21	C21 Triaromatic					
231	231C26	C26 20S Triaromatic					
231	231D26	C27 20S & C26 20R Triaromatic					
231	TADMD1	C28 23,24-Cholestane Triaromatic					
231	TADMD2	C28 23,24-Cholestane Triaromatic					
231	231E28	C28 20S Triaromatic					
231	231F27	C27 20R Triaromatic					
231	TADMD3	C28 23,24-Cholestane Triaromatic					
231	C29TA1	C29 Triaromatic					
231	C29TA2	C29 Triaromatic					
231	TADMD4	C28 23,24-Cholestane Triaromatic					
231	231G28	C28 20R Triaromatic					
231	TADMD5	C28 23,24-Cholestane Triaromatic					
231	C29TA3	C29 Triaromatic					
245	C3S	C27 20S 3-Methyl Triaromatic Steroid					
245	C4S	C27 20S 4-Methyl Triaromatic Steroid					
245	E2S	C28 20S 2-Methyl Triaromatic Steroid					
245	E3SC3R	C28 20S 3-Methyl & C27 20R 3-Methyl TAS					
245	E4SC4R	C28 20S 4-Methyl & C27 20R 4-Methyl TAS					
245	S2S	C29 20S 2-Methyl Triaromatic Steroid					
245	DA	Triaromatic Dinosteroid a					
245	S3S	C29 20S 3-Methyl Triaromatic Steroid					
245	DB	Triaromatic Dinosteroid b					
245	S4SE2R	C29 20S 4-Methyl & C28 20R 2-Methyl TAS					
245	E3R	C28 20R 3-Methyl Triaromatic Steroid					
245	E4R	C28 20R 4-Methyl Triaromatic Steroid					
245	DC	Triaromatic Dinosteroid c					
245	DD	Triaromatic Dinosteroid d					
245	S2R	C29 20R 2-Methyl Triaromatic Steroid					
245	S3R	C29 20R 3-Methyl Triaromatic Steroid					
245	DE	Triaromatic Dinosteroid e					
245	S4R	C29 20R 4-Methyl Triaromatic Steroid					
245	DF	Triaromatic Dinosteroid f					
253	S253A	*C21 Ring-C Monoaromatic Steroid*	84.541	1404520	313954	28.6	26.4
253	S253B	C22 Monoaromatic steroid	86.997	3678787	762667	75.0	64.2
253	S253C	C27 Reg 5β(H),10β(CH3) 20S	97.056	573009	111628	11.7	9.4
253	S253D	C27 Dia 10β(H),5β(CH3) 20S	97.212	953376	213901	19.4	18.0
253	S253E	C27 Dia10βH,5βCH3 20R+Reg5βH,10βCH3 20R	98.701	2083431	394391	42.5	33.2
253	S253F	C27 Reg 5α(H),10β(CH3) 20S	98.832	1280140	307768	26.1	25.9
253	S253G	C28 Dia 10αH,5αCH3 20s+Reg5βH,10βCH3 20S	99.224	3700705	620265	75.5	52.2
253	S253H	C27 Reg 5α(H),10β(CH3) 20R	100.530	3356460	633614	68.4	53.3
253	S253I	C28 Reg 5α(H),10β(CH3) 20S	100.687	4064324	911981	82.9	76.7
253	S253J	C28 Dia 10αH,5αCH3 20R+Reg5βH,10βCH3 20R	100.870	2831410	599238	57.7	50.4
253	S253K	C29 Dia 10βH,5βCH3 20S+Reg5βH,10βCH3 20S	101.000	13410830	2791272	273.5	234.8
253	S253L	C29 Reg 5α(H),10β(CH3) 20S	102.307	8470256	1651860	172.7	139.0
253	S253M	C28 Reg 5α(H),10β(CH3) 20R	102.594	4382568	858221	89.4	72.2
253	S253N	C29 Dia 10βH,5βCH3 20R+Reg5βH,10βCH3 20R	102.725	7170017	1554221	146.2	130.8
253	S253O	C29 Reg 5α(H),10β(CH3) 20R	104.371	5735154	1147362	116.9	96.5
365	SH29	C29 8,14-secohopanoids	104.188	1074526	198255	21.9	16.7
365	SH30	C30 8,14-secohopanoids	106.199	1836239	352845	37.4	29.7

Aromatic peaks and compounds for sample BH15B

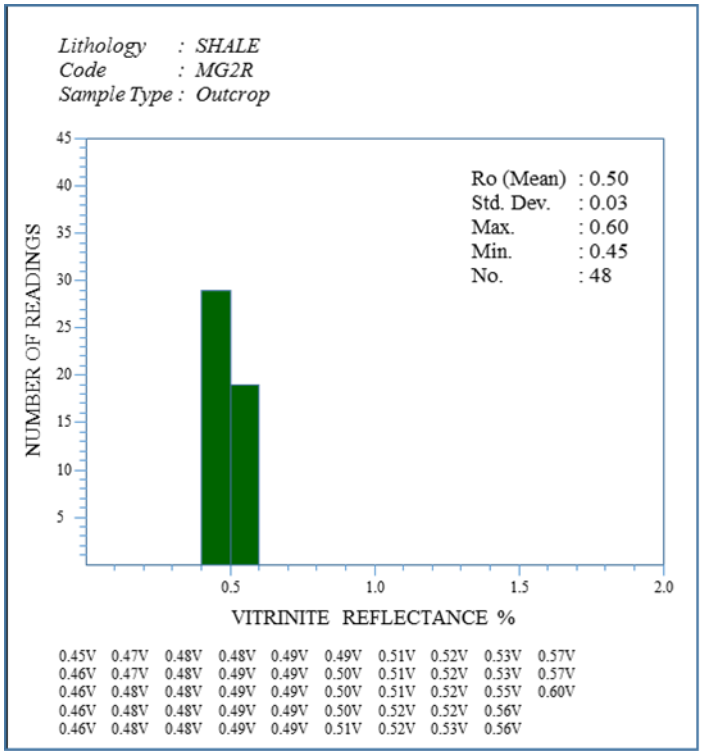
Ion	Peak Label	Compound Name	Ret. Time	Area	Height	ppm (Area)	ppm (Hght)
230	OTP	*Ortho-terphenyl* (internal standard)	74.978	7132789	1729082	300.0	300.0
128	NAPH	Naphthalene	28.789	31850	4148	1.3	0.7
142	2MN	2-Methylnaphthalene	37.907	365463	49504	15.4	8.6
142	1MN	1-Methylnaphthalene	39.135	301661	44245	12.7	7.7
154	BP	Biphenyl	44.621	533746	68315	22.4	11.9
156	2EN	2-Ethylnaphthalene	46.084	199399	27172	8.4	4.7
156	1EN	1-Ethylnaphthalene	46.170	52104	15048	2.2	2.6
156	26DMN	2,6-Dimethylnaphthalene	46.998	675383	106116	28.4	18.4
156	27DMN	2,7-Dimethylnaphthalene	47.129	802996	110728	33.8	19.2
156	1317DMN	1,3 & 1,7-Dimethylnaphthalenes	48.122	1611710	213478	67.8	37.0
156	16DMN	1,6-Dimethylnaphthalene	48.383	1734838	255350	73.0	44.3
156	23DMN	2,3-Dimethylnaphthalene	49.558	231592	41955	9.7	7.3
156	14DMN	1,4-Dimethylnaphthalene	49.663	532370	86615	22.4	15.0
156	15DMN	1,5-Dimethylnaphthalene	49.741	435353	71634	18.3	12.4
156	12DMN	1,2-Dimethylnaphthalene	50.708	445940	65397	18.8	11.3
168	2MBP	2-Methylbiphenyl					
168	DPM	Diphenylmethane					
168	3MBP	3-Methylbiphenyl					
168	4MBP	4-Methylbiphenyl					
168	DBF	Dibenzofuran					
170	BB_EMN	Ethyl-methyl-Naphthalene	55.045	1010659	126925	42.5	22.0
170	AB_EMN	Ethyl-methyl-Naphthalene	56.247	479625	70654	20.2	12.3
170	137TMN	1,3,7-Trimethylnaphthalene	56.691	1674281	261635	70.4	45.4
170	136TMN	1,3,6-Trimethylnaphthalene	57.083	2880024	454643	121.1	78.9
170	146135T	(1,4,6+1,3,5)-Trimethylnaphthalenes	58.154	2244283	335802	94.4	58.3
170	236TMN	2,3,6-Trimethylnaphthalene	58.415	2161449	353689	90.9	61.4
170	127TMN	1,2,7-Trimethylnaphthalene	59.173	1134481	189136	47.7	32.8
170	167126T	(1,6,7+1,2,6)-Trimethylnaphthalenes	59.355	2981589	413128	125.4	71.7
170	124TMN	1,2,4-Trimethylnaphthalene	60.270	455114	71867	19.1	12.5
170	125TMN	1,2,5-Trimethylnaphthalene	60.714	2181446	373605	91.8	64.8
178	PHEN	Phenanthrene	70.250	11014720	2203000	463.3	382.2
184	1357	1,3,5,7-Tetramethylnaphthalene	64.685	1051704	166713	44.2	28.9
184	1367	1,3,6,7-Tetramethylnaphthalene	65.835	1458962	303252	61.4	52.6
184	1247	(1,2,4,7+1,2,4,6+1,4,6,7)-Tetramethylnaphthalenes	66.592	1897871	351981	79.8	61.1
184	1257	1,2,5,7-Tetramethylnaphthalene	66.775	1132619	217651	47.6	37.8
184	2367	2,3,6,7-Tetramethylnaphthalene	67.141	452005	88448	19.0	15.3
184	1267	1,2,6,7-Tetramethylnaphthalene	67.585	687794	140878	28.9	24.4
184	1237	1,2,3,7-Tetramethylnaphthalene	67.768	346629	71373	14.6	12.4
184	1236	1,2,3,6-Tetramethylnaphthalene	68.029	650156	128079	27.3	22.2
184	1256	1,2,5,6-Tetramethylnaphthalene	68.761	2722125	534941	114.5	92.8
184	DBT	Dibenzothiophene	68.970	1533373	185660	64.5	32.2
191	BH32	C32 Benzohopane	118.086	1386588	204894	58.3	35.6
191	BH33	C33 Benzohopane	120.333	1391236	190811	58.5	33.1
191	BH34	C34 Benzohopane	122.345	933595	111461	39.3	19.3
191	BH35	C35 Benzohopane	124.827	458126	54572	19.3	9.5
192	3MP	3-Methylphenanthrene	75.187	2350180	508074	98.8	88.2
192	2MP	2-Methylphenanthrene	75.370	2905845	612475	122.2	106.3
192	9MP	9-Methylphenanthrene	76.049	2218880	443839	93.3	77.0
192	1MP	1-Methylphenanthrene	76.258	2229243	405219	93.8	70.3

Ion	Peak Label	Compound Name	Ret. Time	Area	Height	ppm (Area)	ppm (Hght)
198	CAD	*(Cadalene)*	65.991	37702	7487	1.6	1.3
198	4MDBT	4 Methyl Dibenzothiophene	73.515	1038526	205331	43.7	35.6
198	23MDBT	2 & 3 Methyl Dibenzothiophenes	74.325	930010	122135	39.1	21.2
198	1MDBT	1 Methyl Dibenzothiophene	75.109	1278525	242782	53.8	42.1
206	36DMP	3,6-Dimethylphenanthrene	79.447	585172	126685	24.6	22.0
206	26DMP	2,6-Dimethylphenanthrene	79.708	1279940	287578	53.8	49.9
206	27DMP	2,7-Dimethylphenanthrene	79.813	942739	196393	39.7	34.1
206	39DMP	(3,9+3,10+2,10+1,3)-Dimethylphenanthrenes	80.309	3244685	607509	136.5	105.4
206	29DMP	(2,9+1,6)-Dimethylphenanthrenes	80.518	2079591	321904	87.5	55.9
206	17DMP	1,7-Dimethylphenanthrene	80.675	1842885	391378	77.5	67.9
206	23DMP	2,3-Dimethylphenanthrene	80.936	766840	169632	32.3	29.4
206	19DMP	1,9-Dimethylphenanthrene	81.067	1002576	182260	42.2	31.6
206	18DMP	1,8-Dimethylphenanthrene	81.485	622611	94122	26.2	16.3
206	12DMP	1,2-Dimethylphenanthrene	81.981	266017	52390	11.2	9.1
231	231A20	C20 Triaromatic Steroid	92.405	497239	65412	20.9	11.3
231	231B21	C21 Triaromatic	94.809	219576	28611	9.2	5.0
231	231C26	C26 20S Triaromatic	104.136	105123	19984	4.4	3.5
231	231D26	C27 20S & C26 20R Triaromatic	105.729	343359	61466	14.4	10.7
231	TADMD1	C28 23,24-Cholestane Triaromatic	106.304	27987	6335	1.2	1.1
231	TADMD2	C28 23,24-Cholestane Triaromatic	106.853	77798	18849	3.3	3.3
231	231E28	C28 20S Triaromatic	107.086	258978	55069	10.9	9.6
231	231F27	C27 20R Triaromatic	107.715	296541	51372	12.5	8.9
231	TADMD3	C28 23,24-Cholestane Triaromatic	107.819	471977	86066	19.9	14.9
231	C29TA1	C29 Triaromatic	108.080	353402	82362	14.9	14.3
231	C29TA2	C29 Triaromatic	108.263	182737	46347	7.7	8.0
231	TADMD4	C28 23,24-Cholestane Triaromatic	109.125	293019	56474	12.3	9.8
231	231G28	C28 20R Triaromatic	109.334	195232	36529	8.2	6.3
231	TADMD5	C28 23,24-Cholestane Triaromatic	109.439	49721	10679	2.1	1.9
231	C29TA3	C29 Triaromatic	110.589	457827	75872	19.3	13.2
245	C3S	C27 20S 3-Methyl Triaromatic Steroid	106.853	146394	28508	6.2	4.9
245	C4S	C27 20S 4-Methyl Triaromatic Steroid	107.453	891736	203438	37.5	35.3
245	E2S	C28 20S 2-Methyl Triaromatic Steroid	108.080	59414	16220	2.5	2.8
245	E3SC3R	C28 20S 3-Methyl & C27 20R 3-Methyl TAS	108.316	163554	33908	6.9	5.9
245	E4SC4R	C28 20S 4-Methyl & C27 20R 4-Methyl TAS	108.969	1932929	264701	81.3	45.9
245	S2S	C29 20S 2-Methyl Triaromatic Steroid	109.204	121982	18767	5.1	3.3
245	DA	Triaromatic Dinosteroid a	109.387	79361	11317	3.3	2.0
245	S3S	C29 20S 3-Methyl Triaromatic Steroid	109.543	318597	49991	13.4	8.7
245	DB	Triaromatic Dinosteroid b	109.988	454831	89497	19.1	15.5
245	S4SE2R	C29 20S 4-Methyl & C28 20R 2-Methyl TAS	110.118	1087661	121291	45.7	21.0
245	E3R	C28 20R 3-Methyl Triaromatic Steroid	110.327	687439	127550	28.9	22.1
245	E4R	C28 20R 4-Methyl Triaromatic Steroid	110.928	841573	144651	35.4	25.1
245	DC	Triaromatic Dinosteroid c	111.111	366869	73565	15.4	12.8
245	DD	Triaromatic Dinosteroid d	111.216	493854	82942	20.8	14.4
245	S2R	C29 20R 2-Methyl Triaromatic Steroid	111.372	70191	10018	3.0	1.7
245	S3R	C29 20R 3-Methyl Triaromatic Steroid	111.738	138558	27339	5.8	4.7
245	DE	Triaromatic Dinosteroid e	111.999	212511	40837	8.9	7.1
245	S4R	C29 20R 4-Methyl Triaromatic Steroid	112.470	313564	65102	13.2	11.3
245	DF	Triaromatic Dinosteroid f	112.600	418021	82101	17.6	14.2
253	S253A	*C21 Ring-C Monoaromatic Steroid*	84.568	442843	65193	18.6	11.3
253	S253B	C22 Monoaromatic steroid	87.024	501874	98491	21.1	17.1
253	S253C	C27 Reg 5β(H),10β(CH3) 20S	97.056	256804	45346	10.8	7.9
253	S253D	C27 Dia 10β(H),5β(CH3) 20S	97.212	201030	41766	8.5	7.2
253	S253E	C27 Dia10βH,5βCH3 20R+Reg5βH,10βCH3 20R	98.702	536298	111591	22.6	19.4
253	S253F	C27 Reg 5α(H),10β(CH3) 20S	98.832	342946	60895	14.4	10.6
253	S253G	C28 Dia 10αH,5αCH3 20s+Reg5βH,10βCH3 20S	99.250	557020	84684	23.4	14.7
253	S253H	C27 Reg 5α(H),10β(CH3) 20R	100.530	515309	108516	21.7	18.8
253	S253I	C28 Reg 5α(H),10β(CH3) 20S	100.687	503508	95654	21.2	16.6
253	S253J	C28 Dia 10αH,5αCH3 20R+Reg5βH,10βCH3 20R	100.870	523287	114674	22.0	19.9
253	S253K	C29 Dia 10βH,5βCH3 20S+Reg5βH,10βCH3 20S	101.001	2049261	355839	86.2	61.7
253	S253L	C29 Reg 5α(H),10β(CH3) 20S	102.307	1050496	207018	44.2	35.9
253	S253M	C28 Reg 5α(H),10β(CH3) 20R	102.620	483705	103273	20.3	17.9
253	S253N	C29 Dia 10βH,5βCH3 20R+Reg5βH,10βCH3 20R	102.725	985454	220334	41.4	38.2
253	S253O	C29 Reg 5α(H),10β(CH3) 20R	104.371	634425	121336	26.7	21.1
365	SH29	C29 8,14-secohopanoids	104.214	194018	27773	8.2	4.8
365	SH30	C30 8,14-secohopanoids	106.199	233740	44372	9.8	7.7

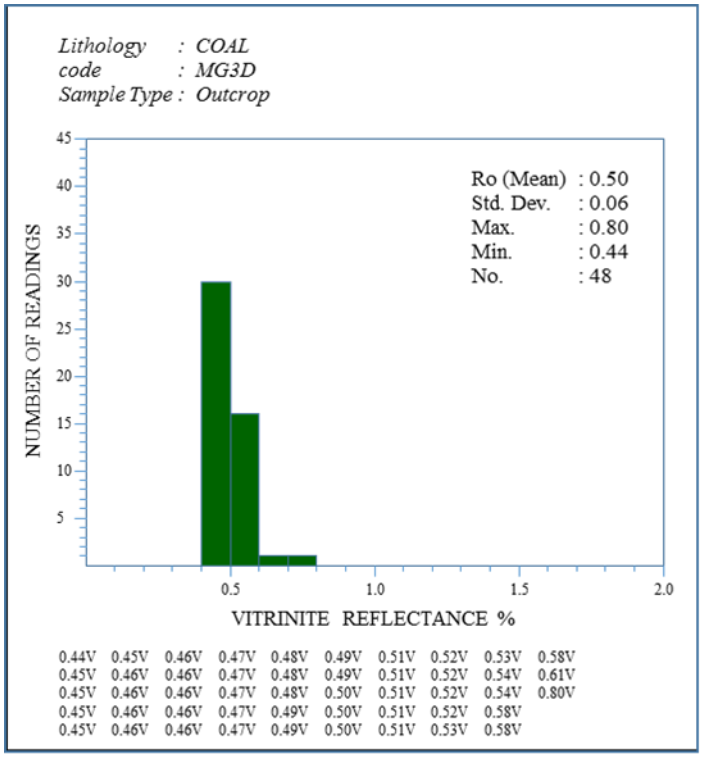
APPENDIX IV



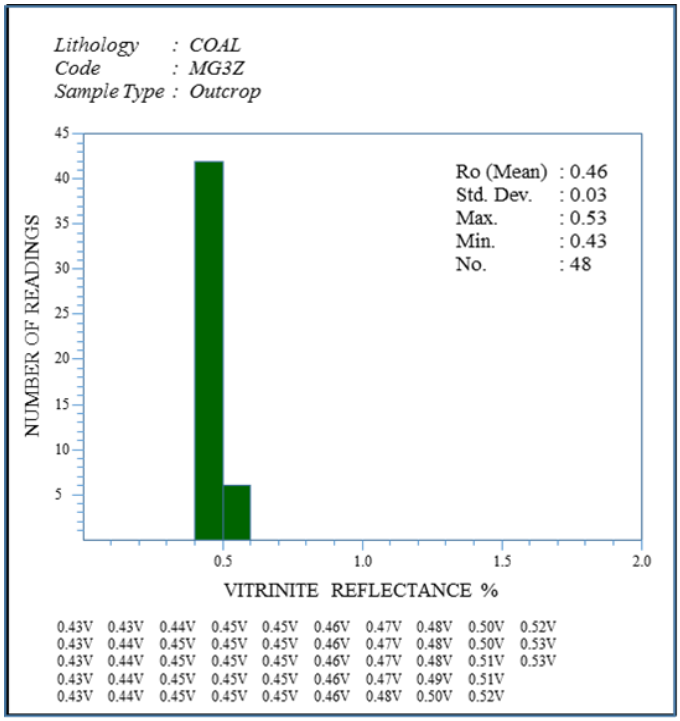
a): Vitrinite Graph for Sample MG2L



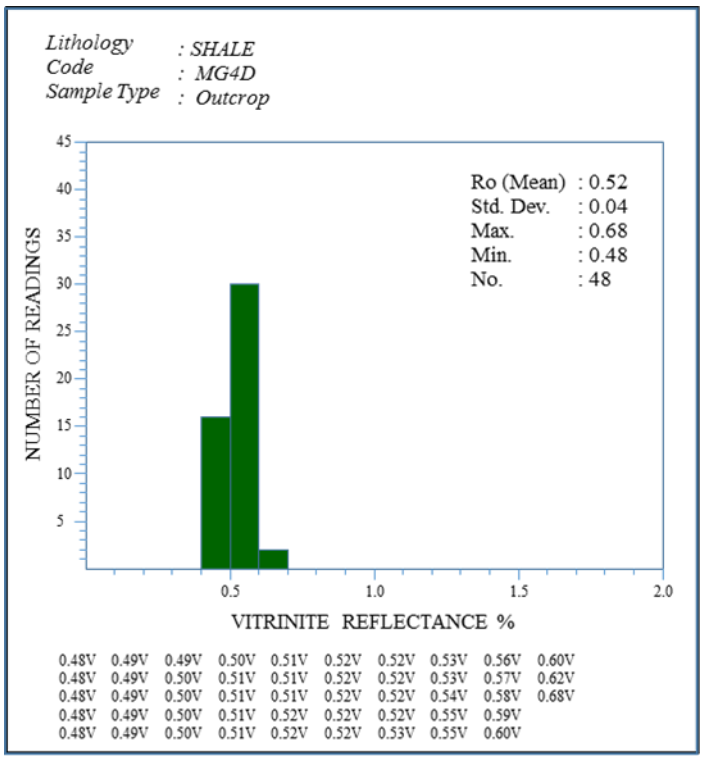
b): Vitrinite Graph for Sample MG2R



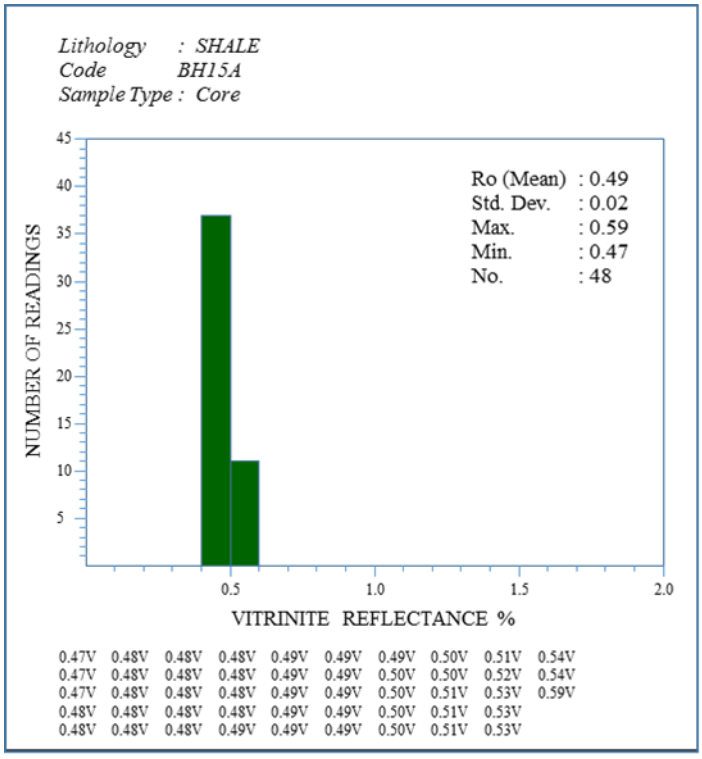
c): Vitrinite Graph for Sample MG3D



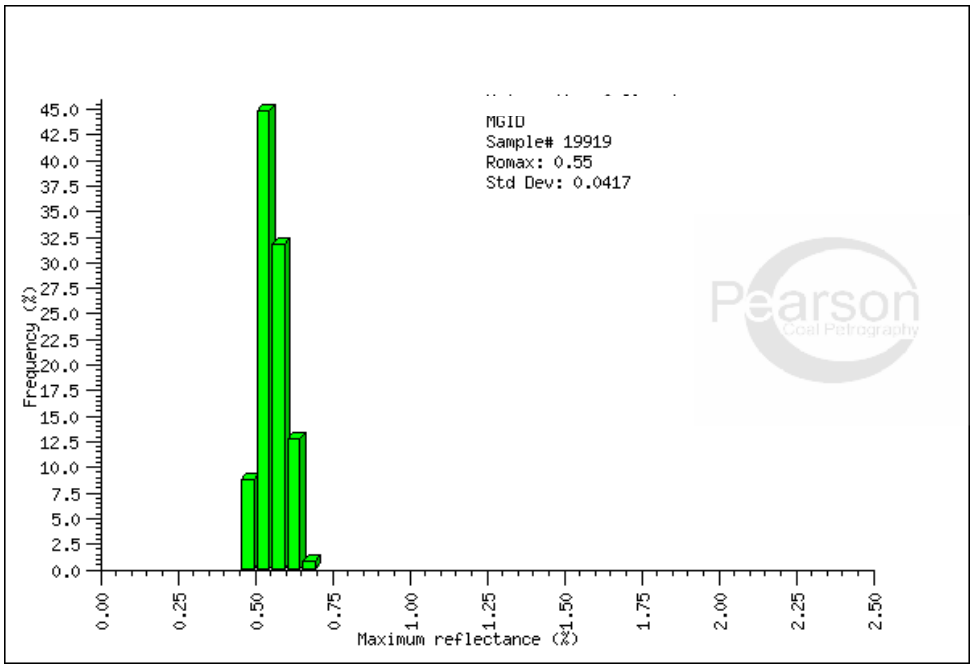
d): Vitrinite Graph for Sample MG3Z



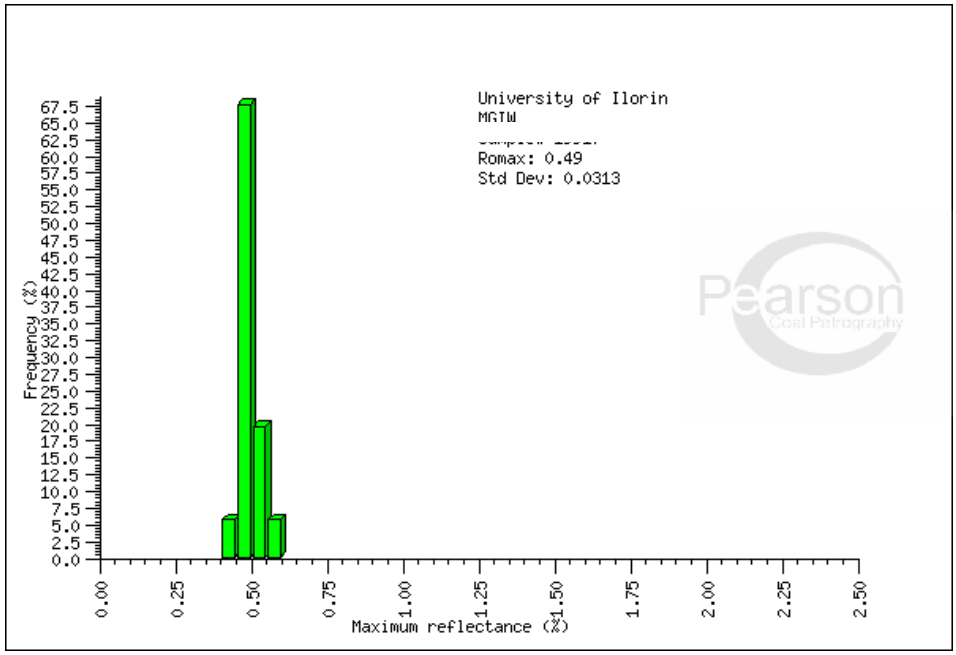
e): Vitrinite Graph for Sample MG4D



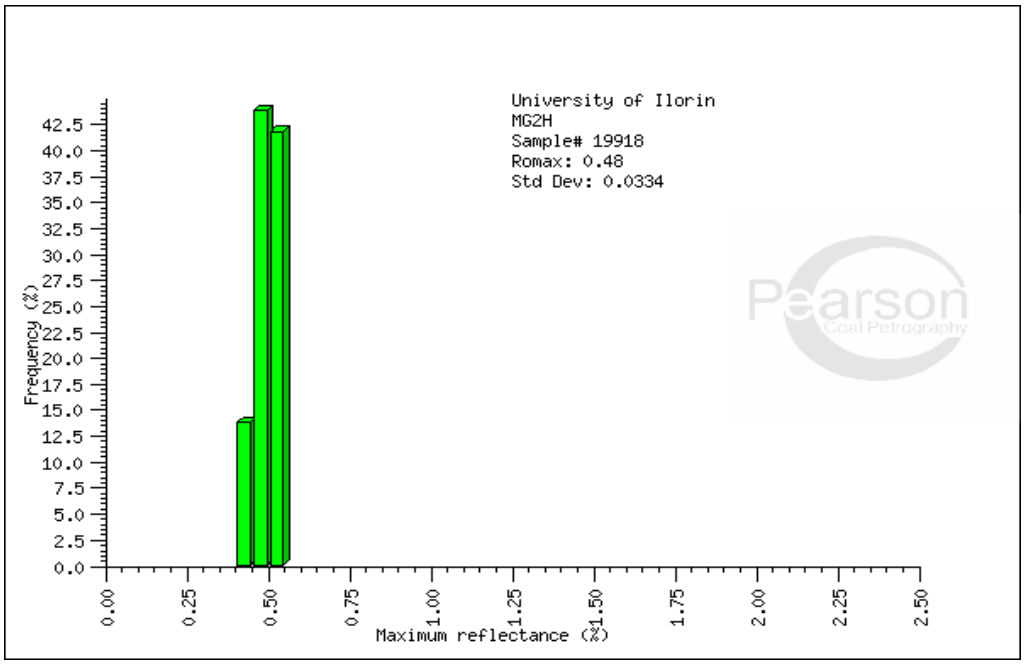
f): Vitrinite Graph for Sample BH15A



g): Vitrinite Graph for Sample MG1D



h): Vitrinite Graph for Sample MG1W



i): Vitrinite Graph for Sample MG2H

(a-i): Vitrinite graphs show maximum vitrinite reflectances (%) against frequency (number of readings) for coal and shale samples analysed.